Proceeding of

ISFT2018

Update version

February 2019

7th International Symposium on the Fusion of Science & Technologies

16 - 20 December, 2018

Bangkok, ***Thailand***

Proceeding of

ISFT2018

Update version

February 2019

7th International Symposium on the

Fusion of Science & Technologies

16 - 20 December, 2018

Bangkok, ***Thailand***

Proceeding of ISFT2018

7th International Symposium on the Fusion of Science & Technologies

16 - 20 December, 2018

Bangkok, Thailand

Publication name

Proceeding of ISFT2018

Edition 1 / **Year** 2018

Website

www.isft365.org

Publisher by

Research and Development Institute

Rajamangala University of Technology Suvarnabhumi

60 Moo 3 Asian Highway, Phranakhon Si Ayutthaya 13000, Thailand

ISBN 978-974-625-830-2 (e-book)

Table of Contents

Welcome message from the President of RUS

Rajamangala University of Technology Suvarnabhumi or RUS is the host of the 1st RUSiCON and the 7th ISFT 2018. Our students, faculty, alumni, administrators, and staff stand out for their commitment to academic excellence, diversity, and creative innovation. We would like to welcome more 80 participants from 10 countries to Bangkok, Thailand.

The International Symposium on the Fusion of the Science and Technologies or ISFT was established on 2012 by the former dean of engineering (Assoc. Prof. Napat Watjanatepin) of RUS and a former dean of engineering of GNU (Prof. Dr. Hanshik Chung). Until now, the strong cooperative on the research and academic was showed by the seven years of the long story of ISFT conference at Korea, Thailand and India. ISFT 2018 and the 1st RUSiCON is the joint conference between Korea and Thailand. I would like to express appreciate on to Prof. Dr. Hanshik Chung, from Gyeongsang National University of Korea and Dr. Chulsu Kim the CEO of KTENG, Korea who helped make the conference between the RUSiCON and ISFT possible.

RUS is reimagining what it is to be a university in the 21st century: pioneering research, outstanding teaching, and a presence across the global that move to the international, interconnected perspective so necessary in our modern world.

I welcome you to joy with the academic activities and culture activities at the ISFT 2018 and the 1st RUSiCON. We hope this time will be a fantastic opportunities of your time in RUS and also in Bangkok, Thailand.

Lastly, I would like to bless all of you comeback home by comfortable and safe.

Asst. Prof. Paisal Burinwattana

President of RUS, Thailand

Honorary Chairman of ISFT 2018

Message from the Organizing Chairman

Welcome to 1st RUSiCON and ISFT2018

I would like to welcome all of you to the 1st Rajamangala University of Technology Suvarnabhumi International Conference, and the 7th International Symposium on the Fusion of the Science and Technologies or ISFT2018 which is held in Bangkok, Thailand from the 16 to 20 of December, 2018.

First of all, I would like to express appreciate on to Asst. Prof. Paisal Burinwattana the president of RUS of Thailand, Prof. Dr. Hanshik Chung, from Gyeongsang National University of Korea and Dr. Chulsu Kim the CEO of KTENG, Korea who helped make the joint conference between the RUSiCON and ISFT 2018 possible.

Also, to the plenary speakers, Prof. Dr. Min Soo Kim, Seoul National University, Prof. Dr. Shengqiang Shen, Dalian University of Technology, Prof. Dr. Ganefri, Padang State University of Indonesia, Prof. Dr. Hideaki Ohgaki, Kyoto University and Keynote speakers, Prof. Dr. Noureddine Takorabet, University de Lorraine, France, and also Prof. Dr. Naveen Kumar from Delhi Technological University, India who will all present wonderful speeches, you have my sincerest thanks and gratitude.

Lastly, I would like to extend my thanks to all participants including professors, students, researchers, and everyone who helped us makes the RUSiCON and ISFT 2018 possible.

The RUSiCON and ISFT 2018 as a cooperated international conference dealing extensively with machinery and energy, civil engineering and architecture, agricultural technology, electrical engineering, and so on, has exchanged and shared groundbreaking research about the fusion of science & technology with influential experts from countries all over the world.

Also, the RUSiCON and ISFT have provided each country with the opportunity for interchanging the ideas and subjects of interest about the fusion of science & technology from passionate announcements and debates by each territory's experts. These countries include Poland, France, South Korea, China, India, Thailand, Singapore, Myanmar, Indonesia, Japan, Bangladesh, Vietnam, etc. Following this significant movement, the ISFT 2018 offers the opportunity to exchange a broad range of expertise for the fusion of science and technology to many categories of industrial experts, technicians, and scientists. All of this is being done as they are breaking the limits of existing scientific technologies as well as developing new technology for the new territories that go with them. These are all based on the creative and innovative ideas from scientists and technicians from all over the world.

Bangkok is the best city in the world and it is the capital city of Thailand, Bangkok is the most popular City For International Tourists In 2017, CNN give Bangkok are the World's best cuisine, the real cities have longest names in the world, the best little movie poster shop in the East, best all-night food counter, the market to end all markets with the perfect of the fusion between culture, science & technology.

Assoc. Prof. Napat Watjanatepin

Organizing Chairman of RUSiCON and ISFT2018

Associate Professor, Rajamangala University of Technology Suvarnabhumi, Thailand

Message from Honorary Chairman

Congratulation on successfully hosting the 7th International Symposium on the Fusion of Science and Technologies (ISFT 2018) in Bangkok, Thailand! I deeply appreciate Paisal Burinwatthana, the President of Rajamangala University of Technology Suvarnabhumi (RUS) for his support of this conference. ISFT 2018 would not have been possible without sustained efforts by Prof. Napat Watjanatepin and organizers. After the rigorous screening process, about 80 papers have been published. I look forward to this year's in-depth discussion and research exchange among researchers from diverse disciplines.

The Fourth Industrial Revolution has created the new era where traditional disciplines converge and diverse technologies complement each other. In this respect, ISFT 2018 is likely to play a critical role. A pursuit of fusion and interdisciplinary research over the last six years has become a foundation for the flowering of this year's conference. The results of these multi-year efforts have already led to joint research and educational exchanges across countries. As a key conference for research cooperation in our region, ISFT 2018 will continue to encourage and facilitate joint research projects, visiting scholar programs, and educational exchange programs among students.

As a result of the aforementioned efforts, I have been a visiting scholar at RUS during the year 2018. Here, I visit various universities and companies in Thailand to promote mutual cooperation. Thailand has been an attractive place as a hub for international cooperation. I have been enjoying this year's fruitful research activities, as well as building new friendships in Thailand. Thailand is a country with an enormous amount of cultural resources. During ISFT 2018, I hope that participants will the opportunity to fully enjoy Thai culture and cuisine. Through such social and cultural activities, we will become friends and become important partners in our cooperation.

I sincerely wish for the prosperous development of RUS. I again extend thanks the committee chairs, organizers and staff members for their efforts and time.

Prof. Hanshik Chung

Gyeongsang National University, Republic of Korea

Honorary Chairman of ISFT 2018

Message from ISFT Korea Chairman

Welcome to ISFT 2018!

I would like to welcome all of you to the 7th ISFT, (International Symposium on the Fusion of the Science and Technologies) being held in Bangkok, Thailand from the 16th to the 21st of December, 2018.

First of all, I would like to express my appreciation to Prof. Hanshik Chung, from Gyeongsang National University of Korea and Prof. Napat Watjanatepin, RMUTSB of Thailand who helped make the ISFT 2018 possible.

Also, I would like to extend my thanks to all participants including professors, students, researchers, and everyone who helped us makes the ISFT 2018 possible.

The ISFT is an international conference dealing extensively with machinery and energy, civil engineering and architecture, agricultural technology, electrical engineering, and so on, and has exchanged and shared groundbreaking research about the fusion of science & technology with influential experts from countries around the world.

The ISFT provides countries with opportunities to collaborate with ideas and subjects of interest about the fusion of science & technology from passionate announcements and debates by each territory's experts. These countries include America, South Korea, China, India, Thailand, Singapore, Malaysia, Indonesia, Japan, Bangladesh, Iran, Iraq, Vietnam, etc. Together, we exchange our vast knowledge while breaking the limits of existing scientific technologies as well as developing new technology for the new territories that go with them.

I hope you enjoy the culture of Thailand and have a safe and wonderful time.

Dr. Chulsu Kim

Korea Chairman of ISFT2018

CEO of KTENG Co., LTd. Korea

Conference Committees

Honorary Chair

Asst. Prof. Paisal Burinwattana RUS, Thailand
Prof. Hanshik Chung Gyeongsang National University, Korea

Organizing Committee Chair

Assoc. Prof. Napat Watjanatepin RUS, Thailand

Secretariat technical program ISFT2018

Ms. Patcharanun Srithanauthaikorn RUS, Thailand
Asst. Prof. Warunee Srisongkram RUS, Thailand

Sponsorship

-Platinum Sponsors

KTENG Co., Ltd, Korea

-Gold Sponsors

ELWE (Thailand)
Primacy Supply
G-Tech Collage (Chuenchom-Thai German collage of Technology)
Thai Auto Tool and Dies (TAT)
RUS Nonthaburi Alumni Association
RUS Nonthaburi Parents and Teacher Association

International Advisory Committee

-International Advisory Committee Chairman

Prof. Dr. Prayoot Akkaraekthalin, KMUTNB, Thailand
Dr.Manoon Chuenchom, ELWE (Thailand)

-International Advisory Committee member

Prof. Min Soo Kim, Seoul National University
Prof. Byung Ha Kang, Kookmin University

International Technical Committees

-Bangladesh

Prof. M. Sq. Rahman, Hajee Mohammad Danesh Science and Technology University

-China

Prof. Shengqiang Shen, Dalian University of Technology
Prof. Xingsen Mu, Dalian University of Technology

-France

Prof. Dr. Noureddine Takorabet, University de Lorraine
Assoc. Prof. Dr. Damien Gilbert, University de Lorraine

-Indonesia

Prof. H. Ganefri, Padang State University

-India

Prof. Dr. Naveen Kumar, Delhi Technological University

-Iran

Prof. Mohammad Pazouki, Materials and Energy Research Institute
Prof. Ghasem D. Najafpour, Babol Noshirvani University of Technology

-Japan

Prof. Hideaki Ohgaki, Kyoto University
Prof. Tsutomu Ito, Kagawa College

-Korea

Prof. Min soo Kim, Seoul National University
Prof. Byung Ha Kang, Kookmin University
Prof. Byung Ki Kim, Ulsan University
Dr. Joon Young Choi, Korea Testing Laboratory
Prof. Sun Hyeng Jo, Deajeon Campus of Korea Polytechnic
Prof. Seung Il Choi, Kimje Campus of Korea Polytechnic

-Poland

Prof. Dr.Neo Christopher CHUNG, University of Warsaw

-Vietnam

Dr.Tran Hoang Hai, Hanoi University of Science and Technology

Thailand

-Thailand Committee Chairman

Assco.Prof. Napat Watjanatepin, Rajamangala University of Technology Suvarnabhumi

-Thailand Committee member

Pathumwan Institute of Technology
Assco.Prof. Dr.Satean Thanyasrirat
Assco.Prof. Dr.Santi Wangnipparnto

Rajamangala University of Technology Suvarabhumi
Asst. Prof. Dr. Paiboon Kiatsookkanatorn,
Asst. Prof. Dr. Chaiyant Boonmee
Asst. Prof. Dr. Danupon Kampanya
Dr. Nuttawut Intaboot
Asst. Prof. Chollada Taweekoon
Dr. Sompong Piriyayon
Dr.Wanich Nilnont
Asst. Prof. Surachai Am-ugsorn
Asst. Prof. Dr.Laddawan Someran
Asst. Prof. Warunee Srisongkram
Asst. Prof. Thaveesak Srichanin
Ms.Waraporn Luejai

Rajamangala University of Technology Isan
Dr. Aniwat Hasook
Asst. Prof. Araya Uengpaiboonkit

Rajamangala University of Technology Lanna
Asst. Prof. Dr. Nopporn Patcharaprakiti
Dr. Anon Naminn

Rajamangala University of Technology Srivijaya
Asst. Prof. Dr. Apirak Songrak

Siam Technology College
Dr. Kosart Thawichsri

Maejo University
Asst. Prof. Dr. Jeerawan Saelao

Thammasart University
Dr.Choompol Boonmee

Financial Chair

Asst. Prof. Thaveesak Srichanin

Publication Chair

Assit.Prof. Dr. Chaiyant Boonmee
Asst. Prof. Warunee Srisongkram
Asst. Prof. Dr. Panida Lorwongtrakul
Ms.Waraporn Luejai

Secretariat General

Ms. Patcharanun Srithanauthaikorn, RUS, Thailand
Asst. Prof. Warunee Srisongkram RUS, Thailand

Secretariat staff

Ms. Jindaporn Kongdhet , RUS, Thailand
Ms.Waraporn Luejai, RUS, Thailand

Location

IFST 2018 will be held at seminar halls of Rajamangala University of Technology Suvarnabhumi (Nonthaburi campus) 7/1 Nonthaburi 1 Suan-Yai Muang Nonthaburi 11000, Thailand.

FUSION of Science & Technologies

RUS_Map

Venue

Rajamangala University of Technology Suvarnabhumi (Nonthaburi campus) /1 Nonthaburi 1 Suan-Yai Muang Nonthaburi 11000, Thailand.

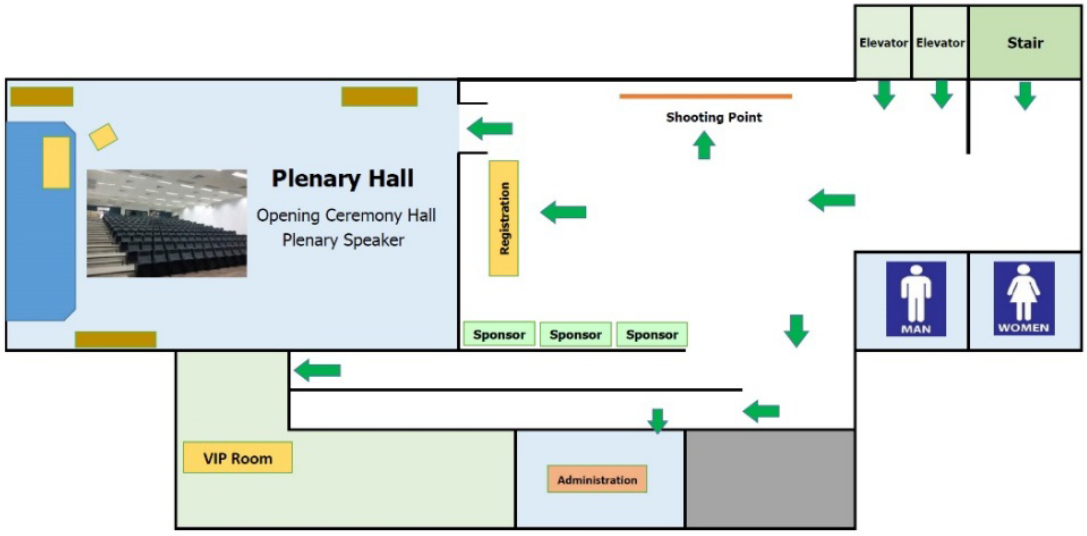

Building 21 Floor 3

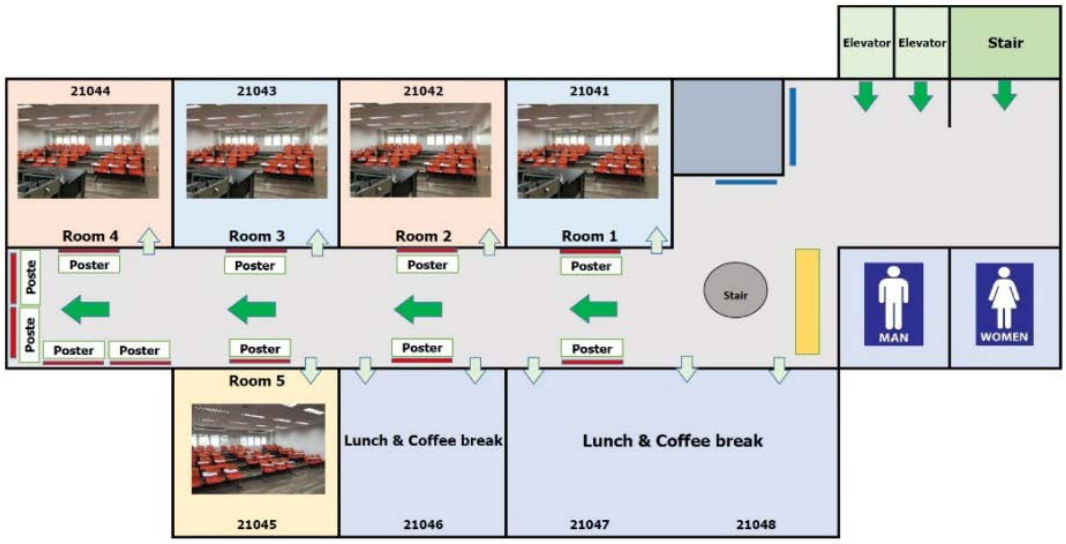

Building 21 Floor 4

The Role of Ichneumonidae as Pollinator in Arabica Coffee Plantation

Duangthip Kantha[1)], Wissarut Sukhaket[2)] and Phawini Khetnon[3)]
[1)] *School of Information Technology, King Mongkut's University of Technology Thonburi, Bangkok, Thailand*

[1)]*Department of Entomology, Kasetsart University, NakhonPathom, Thailand*
[2),3)]*Lamtakhong Research Station, Thailand Institute of Scientific and Technological Research, Nakhon Ratchasima, Thailand*
Email: agrdtk@ku.ac.th

ABSTRACT: The occurrence of Ichneumonidae; Hymenoptera is comprised of three species, Pimpla rufipes, Ichneumon xanthorious and Rhyzsa persuasoria, in arabica coffee plantation with organic agroforestry management. This study was aimed to focus on the parasitic Hymenoptera which visiting coffee flower. This experiment was investigated in tree shred-grow arabica coffee at blooming season during April 2017, Ban Khun Lao, Chiang Rai Province, the north of Thailand. T hree species of Ichneumonidae were collected by transect net-sweeping and colour pan traps operating. All number of three species of Ichneumonidae, P. rufipes, I. xanthorious and R. persuasoria were compared with the number of main pollinators, honey bee for 7.33+ 2.88 and 16.00+ 8.65, respectively. There were not significant overall between the population densities of three species of Ichneumonidae and honeybee ($p > 0.05$).

Keywords: Ichneumonidae, pollinator, arabica coffee

1. INTRODUCTION

Ichnuemonidae are known as the efficient parasitoid of common pests, Coleoptera, Lepidoptera and Hymenoptera. These hosts are infected in larval and pupal stage of key pests. The ichneumornid that genus Ichneumon Linnaeus, 1758 (Hymenoptera: Ichneumonidae) consists mainly of endoparasitoids that attack the pupal stage of the macro-lepidopteran hosts [1] Moreover, In the pollination the ichnuemornid were The mainly pollen vectors furthermore the male of Ichneumonidae were on average over three times as frequent as females and carried 81% of the pollinia in the observation that was conducted in Öland and in Uppland, Sweden, during 1974–1980 [2]. Also, the advances in organic agroecoforestry management for arabica plantation have incorporated the both specification of Ichneumonidae, the biological control agents and pollinators into the organic coffee plantation to be considerate. This investigation we focused on the role of Ichnuemonidae as pollinators in the organic coffee plantation at blooming season during April 2017, Ban Khun Lao, Chiang Rai Province, the north of Thailand. for increase the arabica coffee production and moreover, the role of biological control agents in ichneumornid group to be interested in the beneficial insects.

2. RESEARCH METHODOLOGY

2.1 Study site

The experiment was done in arabica coffee at blooming season during April 2017, Ban Khun Lao, Chiang Rai Province, the north of Thailand at altitude of 1,221 – 1,312 meters above sea level, covering into three sites; untouched forest, middle close to untouched forest, and really touched forest. These Arabica coffee trees were part of the organic plantation forest with the organic agroforesty management and 100 square meters plots were conducted per each area for data sampling.

2.2 Study species

We collected all pollinators that found visiting flower with using sweep net and color traps. All collections in the field were done during 07:30–17:30 hours. The color traps with odorless of detergent mixed water were placed randomly in each site using with color yellow, white, red and blue. The samples of pollinators from sweep net and color traps were collected and preserved in ethyl alcohol for counting and identification.

2.3 Statistical analyses

Various outputs were requested from the Paired-Samples T-Test analysis of GNU PSPP. We counted the number of all pollinators and performed Paired-Samples T-Test to compare two dependent variables from two groups or treatments, i.e. parasitic pollinators, (Ichneumonidae; P. rufipes, I. xanthorious and R. persuasoria) were compared with the number of main pollinators (Apidae; honey bee).

3. RESULT AND DISCUSSION

All pollinators from transect net-sweeping and color traps from 07:30–17:30 o'clock daily to separate group; Parasitic pollinators, (Ichneumonidae; P. rufipes, I. xanthorious and R. persuasoria) and main pollinators (Apidae; honey bee). The specimens were indentified to species level: Ichneumonidae; Pimpla rufipes, Ichneumon xanthorious and Rhyzsa persuasoria, Apidae; Tetragonula sapiens, Tetragonula cabonaria, Apis cerana, Bombus ruderatus and Apis florae (Fig. 1). The population density of pollinators between parasitic pollinators or ichneumnid and main pollinators or honey bee were 7.33+ 2.88 and 16.00+ 8.65 (mean+ SE), respectively (Fig. 2). The correlation of these group, $r = 0.759$, Sig (2-tailed) = 0.08 ($p > 0.05$). There were not significant overall between the population densities of three species of Ichneumonidae and honeybee, $t = 1.287$, Sig (2-tailed) = 0.255 ($p > 0.05$).

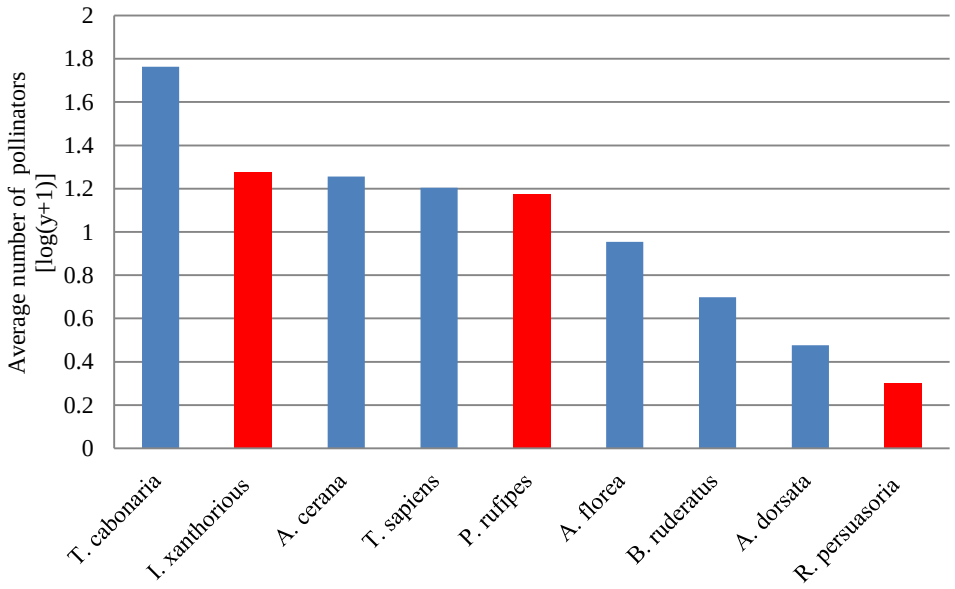

Fig. 1. *The population density of pollinators between parasitic pollinators or ichneumnid and main pollinators or honey bee (Ichneumonidae; P. rufipes, I. xanthorious and R. persuasoria, Apidae; T. sapiens, T. cabonaria, A. cerana, B. ruderatus and A. florae) in arabica coffee at blooming season during April 2017, Ban Khun Lao, Chiang Rai Province*

The parasitic pollinators, Ichneumonidae; P. rufipes, I. xanthorious and R. persuasoria were found for high visiting density of the pollination in blooming season of arabica coffee plantation. These group of the parasitic are the pollinator besides honey bee visit blooming flowers. The adult stage of Ichneumonidae is free-living that feed on pollen and nectar from flower which bloom [3]. Moreover, Ichneumonid include consideration to use as the biocontrol agents in the organic agroecosystem plantation that the specification of these family can be used to control the common pests. They are internal and external parasitiod of Lepidoptera, Coleoptera, Diptera and Hymenoptera [4].

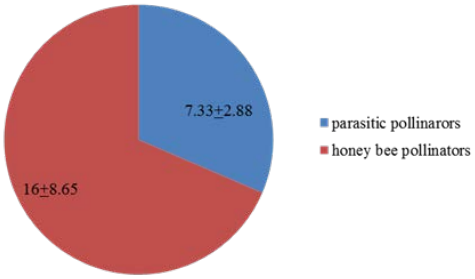

Fig. 2. *Proportion of parasitic pollinators or ichneumnid and main pollinators or honey bee were 7.33± 2.88 and 16.00± 8.65 (mean± SE), respectively, during April 2017, Ban Khun Lao, Chiang, Rai Province*

4. CONCLUSION

The role of Ichneumonidae in arabica coffee plantation not only are the pollinators but also the biocontrol agents protected. The application of the ichneumonid to use for biological control practices for coffee production can be considered which aims to manage organic coffee plantation for sustainability of food production.

5. ACKNOWLEDGEMENTS

I truthfully thank to the villagers at Ban Khun Lao for their support in field experiments.

6. REFERENCE

[1] Hilpert H. Zur Systematik der Gattung Ichneumon Linnaeus, 1758 in der Westpalaearktis (Hyemnoptera, Ichneumonidae, Ichneumoninae) Entomofauna. 1992;13 (Suppl. 6):1–389.
[2] Nilsson L. A., 1981, The pollination ecology of Listera ovata (Orchidaceae),Volume1, Issue4November 1981, Pages 461-480.
[3] The Manitoba museum, 2014, Ichneumonid Wasp, PrairiePollination,http://www.prairiepollination.ca/plan_du_site-site_map/.
[4] Pinto, J. D.,2009,Hypermetomorphosis, Encyclopedia of Insects (Second Edition), Pages 484-486.

Effects of Temperature and Relative Humidity on Growth rate of Melon in the Greenhouse

Pirun Chomsri [1] *, Chaloemkwan Ariyawong [1], Amnuaypos Thongkam [1], and Chaiyan Chansiri [2]

[1]* *Department of Agricultural Technology, Faculty of Agriculture and Agro-Industry, Rajamangala University of Technology Suvarnabhumi , Ayutthaya 13000*

[2] *Department of Agricultural Engineering, Faculty of Engineering, Khonkaen University, Khon Kaen 40002*

ABSTRACT: The aims of these studied was compared the growth rate of melon under difference system in the greenhouse which systems were the temperature and relative humidity control system and without temperature and relative humidity control system. The control system was controlled temperature and relative humidity in the greenhouse less than 30 ○C and 86 %, recpective. The experiments that was used 24 melon trees per experiment. The data were collected incuding height of tree, stem size, number of leaves and stamens. The melon tree under the control of temperature and relative humidity was showed data higher than without temperature control system including height of tree, average stem size, number of leaves and stamens were 144.6 cm, average stem size 4.2 cm, 24 leaves, 15 flowers and 103 cm, average stem size 3.8 cm, 22 leaves and 10 flowers, respective. The melon tree under temperature and relative humidity control system in greenhouse was showed the pollen is faster than without temperature and relative humidity control system that it was grew similar and comfortable for culture. Therefore, the data from these experiment was showed high efficiency production of melon from the temperature and relative humidity control system that It is possible to use a temperature and relative humidity control systemin the greenhouse to increase the efficiency of production and reduce the time of cultivation.

Keywords: melon, Temperature control, greenhouse.

1. INTRODUCTION

It is often difficult for commercial growers melon of many important horticultural crops to select planting dates that result in desired harvest date windows; this is due mainly to temperature differences among growing seasons. Temperature is a major environmental variable in seedling crop development. Ideal temperature for planting The average season for growing in Thailand is 25 - 30 degrees Celsius during daytime and 18 - 20 degrees Celsius at night. Late in the rainy season or cold in the cold [1] Growing under light conditions is not enough. The sky is clouded or rainy for several days. High growth and high temperature hindrances. Pollination problems [2] Responding to the rising temperatures on the type and stage of development of crops such as wheat [3] Green beans[4] was the temperature during the development and the size of the seed. The effect of germination. The strength of the seed fell.

Therefore, this study aimed to study. Comparing growth rates under different melons in greenhouses which controls temperature and humidity and no temperature control and humidity in the greenhouse to. Used as a basis for the production of melon in the right temperature conditions.

2. MATERIALS AND METHODS

The Experimental process consists of two factors. Factor 1 the temperature of Melon received two levels: 1) normal hygiene in the greenhouse. 2) a greenhouse that controls the temperature at 18-25 degrees Celsius by means of fogging to relative humidity in the range of 85-86 percent. and the Factor 2 is the development of the flower. There are 2 different levels. 1) Melon grows at normal temperatures in the greenhouse. 2) Melon grown by controlling the greenhouse. The experiment was carried out with 3 replications at 4 plants. Growing melon varieties yabariking into pots with coconut planting materials mixed with coconut husk. Until melon grows until flowering. Experimented at the Department of Agricultural Technology, Faculty of Agriculture and Agro-Industry, Rajamangala University of Technology Suvarnabhumi, Ayutthaya.

3. RESULTS AND DISCUSSION

Day and night temperatures. the recording of the temperature. Data logger found that in normal internal temperature conditions Greenhouse. The temperature is in the range of 29-37 degrees Celsius. And in greenhouses with controlled temperatures with daily temperatures in the range of 22-23 degrees Celsius, the temperature of the two buildings will have different temperatures around 6 degrees Celsius (Fig. 1).

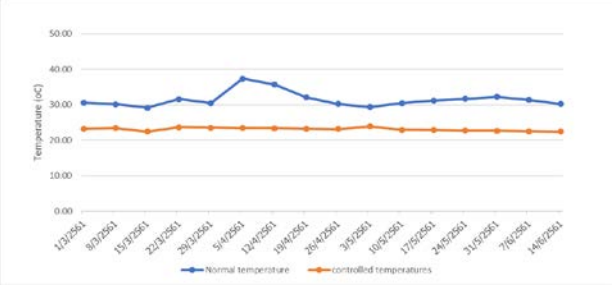

Fig. 1 Temperature used Melon cultivation experiment

The Relative humidity is in the range of 53-70 percent. And in greenhouses with controlled relative humidity with daily relative humidity in the range of 85-86 percent, Relative humidity of the two greenhouses will have different relative humidity around 15 percent (Fig. 2).

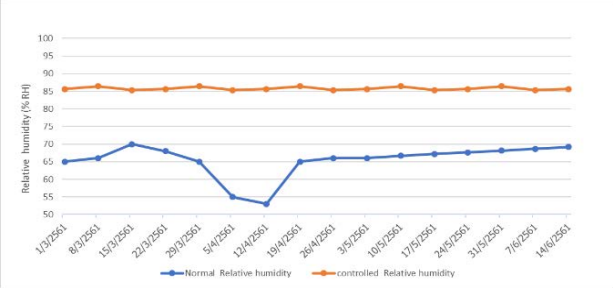

Fig. 2 Relative Humidity used Melon cultivation experiment

When considering the effect of temperature on the seed germination of melon Grown in greenhouses at room temperature showed a growth of melon seedlings [5]. Lower melon grown in greenhouses with controlled temperatures. The effect of inadequate fertilizer makes seeds less strong. May be the result of Physiological degradation of seeds As reported in Tomato [6].

Growth of Melon The temperature control and non-temperature control systems showed different growth within 5 weeks after seedling emergence. The average height was 144.6 cm, the average stem size was 4.2 cm, the average number of leaves was 24 and the average was 15 females. In the absence of climate control and relative humidity control The average stem size was 103 cm, the average stem size was 3.8 cm, the average number of leaves was 22, and the average was 10 females. The growth of melon with temperature control and relative humidity was better. No temperature control system and relative humidity (Table1).

TABLE 1. The growth of the melon 1-5 weeks**.**

Temperature and Relative Humidity control				
Average Factor	height (cm)	Stem size (cm)	Number of leaves(leaves)	pollen
Week 1	12.0	1.5	5	-
Week 2	25.4	2.1	12	3
Week 3	40.5	2.6	15	7
Week 4	80.0	3.5	21	10
Week 5	144.6	4.2	24	15
Non Temperature and Relative Humidity control				
Average Factor	height (cm)	Stem size (cm)	Number of leaves(leaves)	pollen
Week 1	9.2	1.5	5	-
Week 2	17.3	1.9	9	2
Week 3	35.5	2.4	15	5
Week 4	74.6	3.2	20	7
Week 5	103.0	3.8	22	10

4. SUMMARY AND CONCLUSIONS

High temperatures affect the germination, growth were reduced. The results of the study on growth of melon trees. Greenhouses with temperature control and relative humidity have better growth of melon trees. The Greenhouse has no temperature and relative humidity control system because of high temperature. It should have a control system to suit the cultivation of melon.

5. REFERENCES

[1] Preecha Wangpitak.2016. *Planting melon festival*, pp. 1-12, Printed by the Ministry of Agriculture and Rural Development, Bangkok, Thailand.

[2] Nipon ChaiMongkol .1907. Plant of Melon. Field of Vegetable. Department of Plant Technology. Maejo Agricultural Technology Institute, Chiangmai ,Thailand.

[3] Hasan, M.A., J.U. Ahmed, T. Hossain, M.A.K. Mian and M.M. Haque. 2013. Evaluation of the Physiological Quality of Wheat Seed as Influenced by High Parent Plant Growth Temperature. J. Crop Sci. Biotech. 16(1): 69-74

[4] Egli, D.B., D.M. TeKrony, J.J. Heitholt and J. Rupe. 2005.Air Temperature During Seed Filling and Soybean Seed Germination and Vigor. Crop Sci. 45: 1329-1335.

[5] ISTA. 2012. International Rules for Seed Testing. Bassersdorf , Switzerland.

[6] Ibrahim, D., M. Anna, Ashirow and M. Kazim. 2008. Effect of seed production environment and time of harvest on tomato seedling growth. Research Journal of Seed Science. 1(1): 1-10

Effect of photosynthetic bacteria on Moina macrocopa production

Matthura Labaiden[1)], Songwut Phatkaew[2)] and Sataporn Direkbusrakom[2)]
[1)] *Faculty of Agricultural Technology And Agro-Industry,*
Rajamangala University of Technology Suvarnabhumi, Phra Nakhon Si Ayutthaya, Thailand
[2)]*Research Center of Excellence in Shrimp, School of Agricultural Technology, Walailak University,*
Nakhon Si Thammarat, Thailand
Email: matthura@hotmail.com

ABSTRACT: In this study, effect of photosynthetic bacteria on *Moina macrocopa* production was investigated. *M. macrocopa* were cultured by using *Chlorella* sp., photosynthetic bacteria and *Chlorella* sp. mixed with photosynthetic bacteria for 3 days. Three replications of each trial were performed. After cultivation for 3 days, the production of *M. macrocopa* was collection. The results indicated that the production of *M. macrocopa* cultured by using *Chlorella* sp. mixed with photosynthetic bacteria was significantly ($P < 0.05$) higher than cultured using *Chlorella* sp. or photosynthetic bacteria. Moreover, total carotenoid in *M. macrocopa* cultured using *Chlorella* sp. mixed with photosynthetic bacteria were higher than other treatments. These findings demonstrate that cultivation of *M. macrocopa* using *Chlorella* sp. mixed with photosynthetic bacteria can be applied to enhance nutrition and production of *M. macrocopa*.

Keywords: *Moina macrocopa*, *photosynthetic bacteria*, carotenoid

1. INTRODUCTION

Moina macrocopa or water flea is a zooplankton with has an excellent potential as a live feed for fish and crustaceans larvae (Alam *et al*., 1993; Kang *et al*., 2006; Islam *et al*., 2017). It has a high nutritional value than commercially available newly hatched *Artemia nauplii* (He *et al*., 2001). The protein content of *M. macrocopa* is 50 to 60% (dry weight) and the total amount of fat per dry weight is 20-27% (Islam *et al*., 2017). *M. macrocopa* can be easily mass cultivated under varying conditions including low dissolved oxygen (DO) level and high ammonium concentration (Loh *et al*., 2013 Mubarak *et al*., 2017). *M. macrocopa* can be cultured using wide variety of tiny organisms such as microalgae, yeast and bacteria as feed (Siddque *et al*., 2004). The freshwater microalgae *Chlorella* spp. is known to use as food source to culture *M. macrocopa* in the large scale (Rani *et al*., 2008). However, the production of *M. macrocopa* by using *Chlorella* spp. in the commercial scale is limited because the variations in temperature, both diurnal and seasonal especially in the rain season. The enrichment should be done in order to produce the mass culture production of *M. macrocopa*.

Photosynthetic bacteria are widely distributed in nature. These bacteria are found in freshwater, seawater, aquaculture and wastewater pond. They are dominant in polluted areas because they are very efficient in converting wastes into useful products (Kobayashi, 1982; Sasikala et al., 1993; Banerjee et al., 1999). Photosynthetic bacteria cells are rich in proteins, carotenoids, biological cofactors and vitamins (Kobayashi and Kutara, 1978; Kim and Lee, 2000). Photosynthetic bacteria almost contained high levels of total carotenoids which play other important functions as pro-vitamin A, antioxidants, immunoregulators and they are mobilized from muscle to ovaries which suggest a function in reproduction (Nakano et al., 1999; Bell et al., 2000; Chavarria and Flores, 2013). It has also observed that fishes with a high level of carotenoids are more resistant to bacterial and fungal diseases (Chavarria and Flores, 2013) and were also enhanced the survival rate of fish larvae, and improved the production of scallop seed (Huang et al., 1990; Wang et al., 1994). Moreover, It was report that addition of photosynthetic bacteria as food source could enhanced the growth of zooplankton more than green algae and are very useful for growth of brine shrimp (Kobayashi, 1995) and increase the population growth rate of live food such as *Brachionus plicatilis* (Xu et al., 1992). So, this study is aim to investigate effect of photosynthetic bacteria on enhance nutrition and production of *M. macrocopa*

2. RESEARCH METHODOLOGY

Microorganism

Photosynthetic bacteria was obtained from Research Center of Excellence in Shrimp, School of Agricultural Technology, Walailak University and was grown in glutamate acetate medium (Suwansaard, 2010). After cultivation for 5 days, this bacterial was use as food source to culture *M. macrocopa*.

Experimental design

The completely randomized experimental design was applied in three treatments. *M. macrocopa* (initial weight 0.2 g/L) was cultured using *Chlorella* sp. (10^6 cell/ml), photosynthetic bacteria and *Chlorella* sp. mixed with photosynthetic bacteria (1:1). Three replications of each trial were performed. After cultivation for 3 days, the total production of *M. macrocopa* was harvested for proximate analysis and wet weight was recorded.

Proximate analysis

Proximate analysis of *M. macrocopa* was carried out using standard methods (AOAC, 1995). Total carotenoids content was following the method modified from Hirayama (1974). Sample was centrifugation at 10,000 rpm for 15 min, the cell pellet was washed with 0.9 % NaCl and then extracted with methanol: acetone solution (2:3 v/v), centrifuged and the supernatant was collected from each strain. Re-extraction of the cell was repeated until the

pigment was not observed in the supernatant. The volume of extraction liquid was adjusted to have an appropriate optical density at OD 480 and OD 770 for calculating the carotenoids content

$$\text{Total carotenoid content (mg/g dry weight)} = \frac{(OD_{480}-0.10\times OD_{770})\times 3.85\times B}{Z\qquad A}$$

A = Volume of liquid before extraction (ml)
B = Volume of liquid after extraction (ml)
Z = Dry cell weight of photosynthetic bacteria (g/liter)

Statistical analysis

Data was analyzed using SPSS v13.0 (Statistical Package for the Social Sciences, Chicago, IL, USA). Significant differences (p<0.05) between mean values were determined using Duncan's multiple range tests.

3. RESULTS

The results indicated that the production of *M. macrocopa* cultured by using *Chlorella* sp. mixed with photosynthetic bacteria was significantly (P < 0.05) higher than cultured using *Chlorella* sp. or photosynthetic bacteria (Figure 1). According to Kobayashi (1995) reported that addition of photosynthetic bacteria as food source could enhanced the growth of zooplankton more than green algae and are very useful for growth of brine shrimp. Similar results were also obtained in *Brachionus plicatilis* (Xu et al., 1992).

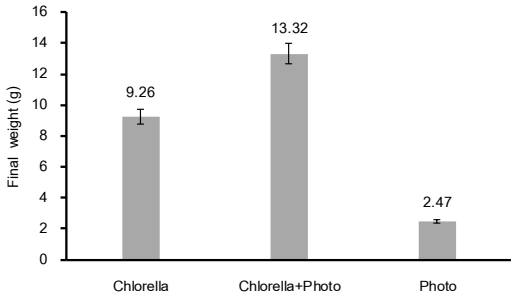

Figure 1 Final weight of *Moina macrocopa* in experimental treatment (Chlorella, *Chlorella* sp.; Chlorella+Photo, *Chlorella* sp. mixed with photosynthetic bacteria; Photo, photosynthetic bacteria)

The contents of protein, lipid, and total carotenoids in *M. macrocopa* at different treatments are listed in Table 1. Total carotenoid in *M. macrocopa* cultured using *Chlorella* sp. mixed with photosynthetic bacteria were higher than other treatments. A source of carotenoids, various groups of microorganisms, including carotene-producing yeast, often attract attention. The expediency of their use as a source of carotenoids for a live feed is based not only on their high carotenosynthetic activity but also on their dimensional characteristics, which makes it possible for zooplankton to ingest them. The use of yeast as a fodder substrate for *M. macrocopa* is also appropriate due to the similarity of the amino acid composition of yeast and *Moina* (Khudyi et al., 2018).

Table 1 The nutritional composition of *Moina macrocopa* while using *Chlorella* sp. , photosynthetic bacteria and *Chlorella* sp. mixed with photosynthetic bacteria as feed

Treatment	Parameters		
	Proteins (%)	Lipids (%)	Total carotenoids (mg/g)
Chlorella sp	4.65 ± 0.14^{a}	0.55 ± 0.02^{a}	10.10 ± 1.43^{a}
Chlorella+ photosynthetic bacteria	4.80 ± 0.03^{a}	0.57 ± 0.02^{a}	11.23 ± 0.82^{a}
photosynthetic bacteria	4.83 ± 0.03^{a}	0.50 ± 0.01^{a}	9.17 ± 1.26^{b}

*The different superscripts in the same column indicate significant differences between treatments by DMRT (p<0.05).

There are many reports that photosynthetic bacterial cells are enriched with high quality proteins and other physiologically active substances for inclusion in animal feeds (Kobayashi, 1995, Shipman et al., 1975). Phototrophic bacteria are reported to contain 40-69% (w/w) protein, 0.09-0.08 mg carotenoids per gram dry cell weight, 30-79 mg vitamin B12 per kg dry cell weight and essential amino acid composition comparable with egg, algae and soybean (Kobayashi and Kurata, 1978; Vrati, et al.,;Banerjee et al., 2000).

However, Proteins and Lipids contents of *Moina macrocopa* in this study are not significantly difference but *M. macrocopa* fed *Chlorella* sp. mixed with photosynthetic bacteria is tend to higher than other treatment. So, the suitable concentration of *Chlorella* sp. mixed with photosynthetic bacteria should be investigation in further study.

4. CONCLUSION

The present study demonstrated that cultivation of *M. macrocopa* using *Chlorella* sp. mixed with photosynthetic bacteria can be applied to enhance nutrition and production of *M. macrocopa*.

5. REFERENCES

[1]Alam M.J., K.J. Ang and S.H. Cheah. 1993. Use of Moina micrura (Kurz) as an Artemia substitute in the production of Macrobrachium rosenbergii (de Man) post larvae, Aquaculture 109: 337-349.
[2]AOAC. 1995. Official Methods of Analysis of AOAC International. Arlington Virginia USA: AOAC International 16th edition II.
[3] Atlantic salmon (Salmo salar) affects autoxidative defense and fatty acid metabolism. American Society for Nutritional Sciences, 1800-1807.
[4]Chavarría M.G. and M.L. Flores.2013. The use of carotenoid in aquaculture. Research Journal of Fisheries and Hydrobiology. 8(2):38-49
[5]He Z.H, J.G Qin, Y. Wang, H. Jing and Z. Wen. 2001. 'biology of *Moina mongolica* (Moinidae, Cladocera) and perspective as live food for marine fish larvae: review, Hydrobiologia 457: 25-37
[6]Hirayama, O., Ando E., Wamori K. and Hara N. 1974. Colorimetric method to measure bacterial pigment. Journal of the Agricultural Chemical Society of Japan 48:97
[7]Huang H, Z. Yao and J. Zheng. 1990. The study of the applications of photosynthetic bacteria to aquaculture (3)-The value of using photosynthetic bacteria as the initial feed for fish larvae. J of Zhanjiang Fish Coll 10: 58-61. (in Chinese, Abstract in English).

[8]Islam M.R., M.R. Hassan, M.Begum, N.J. Punom, M.K. Begum, N. Sultana and M.S. Rahman. 2017. Effect of feeding zooplankton, Moina macrocopa (Straus, 1820) on the growth of Nile tilapia Oreochromis niloticus L. Bangladesh J. Sci. Ind. Res. 52(2), 81-88
[9]Kang C.K., H.Y. Park, M.C. Kim and W.J. Lee. 2006. Use of marine yeasts as an available diet for mass cultures of Moina macrocopa. Aquaculture Research. 37:1227-1237
[10]Khudyia O., O. Kushnirykb , L. Khudac and M. Marchenkod. 2018. Differences in Nutritional Value and Amino Acid Composition of Moina macrocopa (Straus) Using Yeast Saccharomyces cerevisiae and Rhodotorula glutinis as Fodder Substrates. International Letters of Natural Sciences. 68:27-34
[11]Kim J.K. and B.K. Lee. 2000. Mass production of Rhodopseudomonas palustris as diet for aquaculture. Aquaculture Engineering 23:281-293
[12]Kobayashi, M. and S.I. Kurata. 1978. The mass culture and cell utilization of photosynthetic bacteria. Process Biochem. 13:27-30
[13]Kobayashi, M. 1982. The role of phototrophic bacteria in nature and their utilization. In: Advances in Agricultural Microbiology (Ed. N.S.S. Rao). Butterworth Scientific, London. 643-651 pp.
[14]Kobayashi, M. 1995. Waste remediation and treatment using anoxygenic phototrophic bacteria. In: Blenkenship, R.E., Madigan, M.T., Bauer, C,E. (Eds.), Anamoxygenic phototrosynthetic bacteria. Kluwer Academic, Dordrecht, 1272-1274 pp.
[15]Loh J.Y., H.K. Alan Ong, Y.S. Hii, T.J. Smith, M.M. Lock, G. Khoo. 2013. Impact of Potential Food Sources on the Life Table of the Cladoceran, *Moina macrocopa*. The Israeli Journal of Aquaculture – Bamidgeh. 65:820-828
[16]Mubarak A.S., D. Jusadi, M.Z. Junior, M.A. Suprayudi. 2017. The population growth and the nutritional status of Moina macrocopa feed with rice bran and cassava bran suspensions. Jurnal Akuakultur Indonesia. 16(2):223-233
[17]Nakano, T., T. Kanmuri, M. Sato and M. Takeuchi, 1999. Effect of astaxanthin rich red yeast (Phaffia rhodozyma) on oxidative stress in rainbow trout. Biochimica et Biophysica Acta, 1426: 119-125.
[18]Rani V., S. Palaniichamy and N. Neethiselvan. Mass production of Moina, *Moina brachiate* with microalgal species Chlorella vulgaris as feed and preservation of its dormant cysts. Aquaculture 9(2):239-243
[19]Sasikala, K., C.V. Ramana, P.R. Rao and K. L. Kovacs. 1993. Anoxygenic phototrophic bacteria: physiology and advance in hydrogen production technology. Advances in Applied Microbiology. 38:211-295
[20]Shipman, R.H., I.C. Kao and L.T. Fan. 1975. Single cell protein production by photosynthetic bacteria cultivation in agricultural by-product. Biotechnology and Bio-engineering. 17:1561-1570
[21]Siddque N., M.M Hassan, M.G.Q. Khan, M.A. Hassanat and M.Z. Rahman. 2004. Laboratory culture of Moina with organic and inorganic fertilizers. Bangladesh J. Fish. Res., 8(2), 87-93
[22]Suwansaard M. 2010. Production of hydrogen and 5 aminolevulinic acid by photosynthetic bacteria from palm oil mill effluent, PhD thesis. Prince of Songkla University.
[23]Vrati, S. 1994. Single cell protein production by photosynthetic bacteria grown on the clarified effluents of biogas plant. Applied Microbiology and Biotechnology 19:199-202
[24]Wang X, Z. Sun, X. Liu, J. Ma, B. Wang, X. Song, Z. Zhu, J. Shi and F. Wang. 1994. Application of photosynthetic bacteria in scallop artificial seed breeding. J Fish China 18: 65-68. (in Chinese, Abstract in English).
[25]Xu B, M. Ding, J. Mao and H.S. Xu. 1992. The food value of *Phodopseudomonas spheroides* for *Brachionus plicatilis*. T Oceanol Limnol 2: 17-22. (in Chinese, Abstract in English).

INVESTIGATION OF AREA RATIO EFFECT OF INLET TO OUTLET FOR NATURAL VENTILATION

Dong-Hun Han[1)], Yeong Sik Kim[2)], Hanshik Chung[3)] , Hyomin Jeong[3)] , Soon-Ho Choi[3)] *

[1)]Masan Technical High School, Masan City, 51353, Republic of Korea
[2)] DAE SUNG AIR TECH., Kimhae City, Republic of Korea
[3)] Department of Energy and Mechanical Engineering, Institute of Marine Industry, Gyeongsang National University, Tongyeong City, 53064, Republic of Korea

ABSTRACT: Unlike in the past, in response to the demands of the sustainable growth in modern society, interest in natural ventilation is increasing at present. As well known, the driving forces for natural ventilation are the outdoor wind and the indoor-outdoor temperature difference. However, natural ventilation generally does not occur only with one of these two factors, but with two factors coupled. Although the wind-induced natural ventilation was qualitatively and quantitatively investigated in many other studies, thermal buoyancy-induced natural ventilation was rarely done. In this study, the fundamental theories of thermal buoyancy-induced natural ventilation and some experimental results were introduced, which were referred from the authors' previous works. In addition to it, it was shown that the area ratio of the inlet opening to the outlet opening for natural ventilation is a key factor to effect on natural ventilation. In conclusion, it will be introduced that natural ventilation flowrate increases exponentially when the area ratio increases.

1. INTRODUCTION

Due to the improvement of living standard, it cannot be denied at present that the proper ventilation designs for buildings and houses is essential in the civil engineering [1,2]. Ventilation is classified into the mecha-nical type and natural type. In the past, the mechanical type was popular in the past, however natural type has been preferred due to the sustainable society at present. Although many types of natural ventilators are used for buildings and houses as shown in Fig.1, the wind turbine was investigated in this study.

This experimental study was concerned the effect of an area ratio for natural ventilation, in which the area ratio means the inlet area to the outlet area for natural ventila-tion [3,4,5]. In addition to it, from the experiments of this study, the thermal buoyancy induced driving force and the wind induced driving force can be compared to the equi-valent driving force and it was confirmed that there is a minimum temperature difference and a minimum wind speed to drive a wind turbine (This paper is not the origin-nal one for ISFT-2018 because the materials of this paper is the summary of the earlier reported paper [6] of the authors, which means that this paper is for introducing the authors' previous study).

2. EXPEIMENTAL APPARATUS

Fig. 2 shows the experimental apparatus used in this study. The left schematic diagram is the whole experi-mental system that consists of four axial fans, the flow rectifier screen and the chamber, which is simulate the room. The electrical heater as shown in the right photo is placed in the chamber to control the room temperature.

The outdoor wind is simulated by operating the fans and it was controlled the velocities ranged from 0.5 to 4.0 m/s and the indoor temperatures were controlled

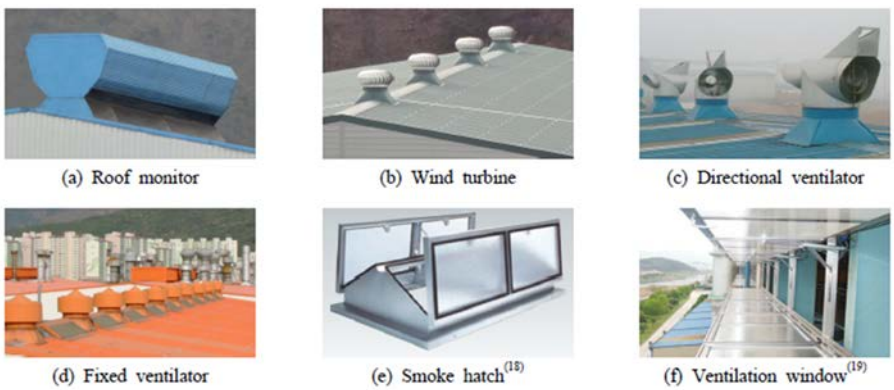

Fig. 1 Various types of the natural ventilators. In this study, the wind turbine of (b) was evaluated. This figure was copied from Ref. [6].

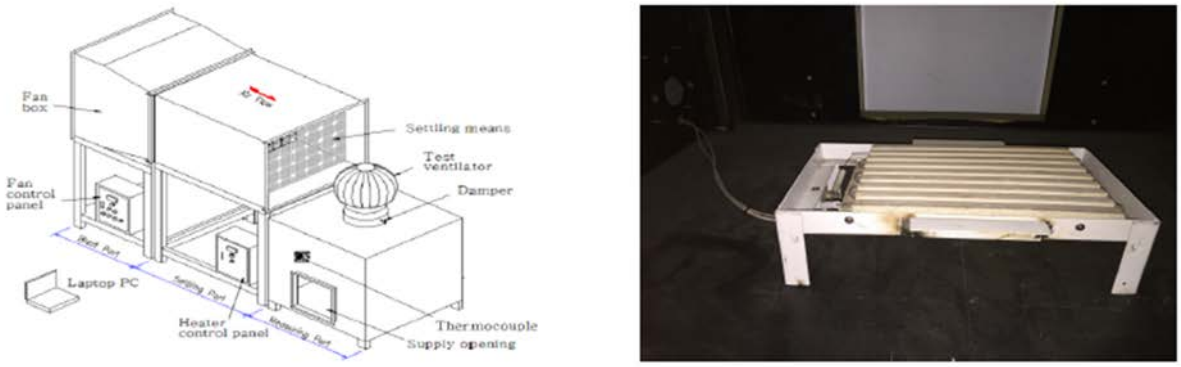

Fig. 2 Schematic diagram of the experimental apparatus. The right photo is the electrical heater placed into the chamber, which enables to maintain the indoor-outdoor temperature difference. This figure was copied from Ref. [6].

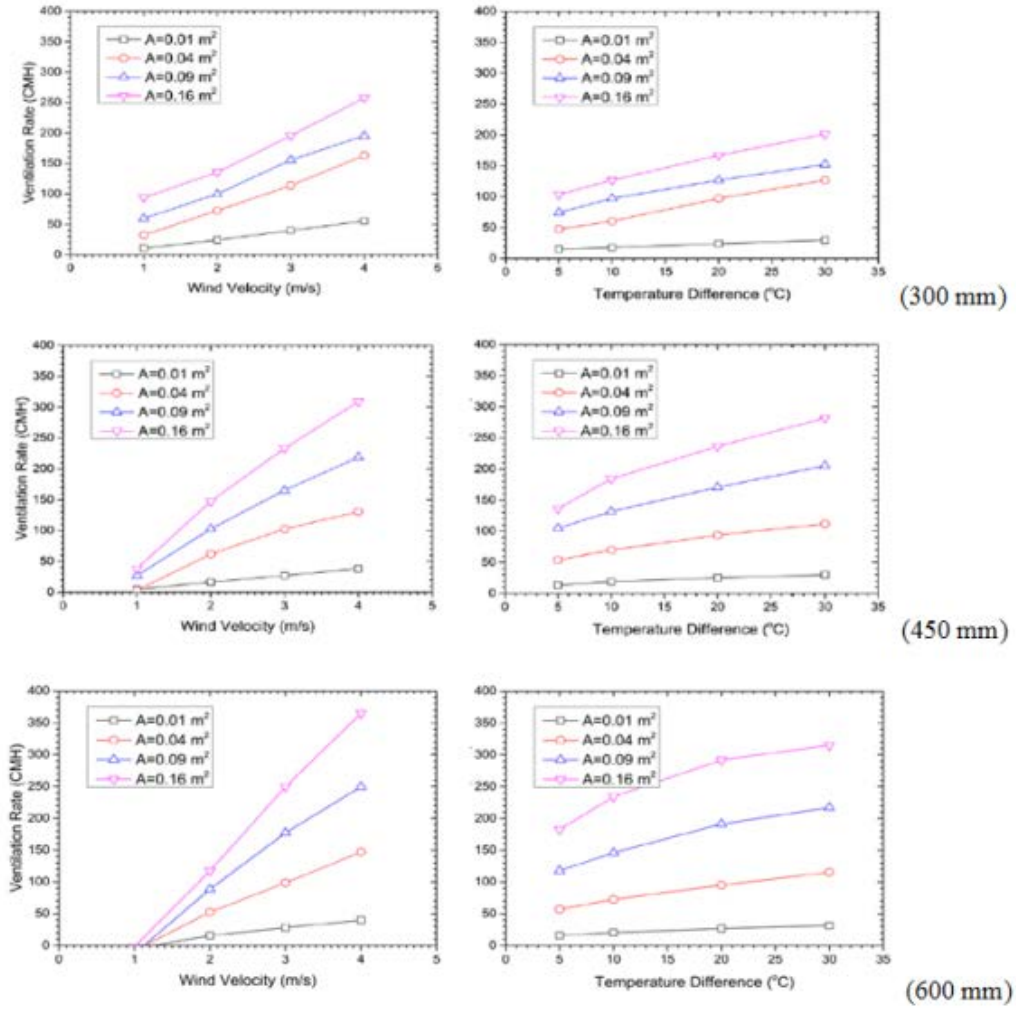

Fig. 3 Ventilation characteristics of the wind turbine. The tested wind turbines are the sizes of 300, 450 and 600 mm inlet diameter. This figure was copied from Ref. [6].

from 5 to 30 °C. To investigate the influence by the area ratio, the area ratio were set to 0.01, 0.04, 0.09 and 0.16, respective-ly. The ventilated flowrates were measured at the entrance area by using a hot wire anemometer and the indoor and outdoor temperatures were measured by using TESTO digital thermometer (174H).

3. EXPERIMENTAL RESULTS AND DISCUSSION

The ventilated air flowrates were measured by changing the wind speed and the indoor-outdoor temperature difference. Figs. 3 shows the experimental results; the left ones are the ventilated air flowrates vs. the outdoor wind speeds and the right ones are the ventilated air flowrates vs. the indoor-outdoor temperature differences. Three sized wind turbines were tested and their inlet diameters are 300, 450 and 600 mm, respectively.

As seen in Fig. 3, it can be confirmed that the ventilated air flowrates were increased when the outdoor wind speed and the indoor-outdoor temperature difference increases. However, a minimum outdoor wind speed is required to rotate the wind turbine. However, whenever there exists the indoor-outdoor temperature difference, the thermal buoyancy induced natural ventilation is occurred. Furthermore, it was seen that the ventilated air flowrates were increased as the inlet area is larger than the outlet area.

4. CONCLUSION

From this experimental study, the following observations were obtained;

- The ventilated air flowrate due to the outdoor wind speed is linearly increased while the ventilated air flowrate due to the indoor-outdoor temperature difference is exponentially increased.
- As the area ratio is increased, the ventilated air flowrate is certainly increased whatever the natural ventilation mechanism is the wind induced or the thern=mal buoyancy induced. However, the ventilated air flowrate is converged when the area ratio is over any value.
- As the size of the wind turbine is larger, the minimum outdoor wind speed is increased to rotate it. In other words, if the wind speed is not over any threshold speed, the wind turbine is not rotated and the ventilation is not occurred.
- In the case of a wind turbine, the indoor-outdoor temperature difference of 5 ^{o}C corresponds to the outdoor wind speed of 1.0 m/s for natural ventilation when the size of wind turbine is 300 and 450 mm.

REFERENCES

[1] Su-Mi Lee, Jae-Hoon Jin, and Doo-Sam Song 2010, Feasibility Study on Natural Ventilation Design and Performance Evaluation Standard for Apartment Building in Korea, *Proc. SAREK*, pp. 28-33.

[2] Jae-Hoon Jin and Doo-Sam Song 2010, A Feasibility of the Natural Ventilation System in Multi-residential Building, *Proc. SAREK*, pp. 568-575.

[3] Dong-Hun Han, Sedong Kim, Jae Hyuk Choi, Yeong Sik Kim, HanShik Chung, Hyomin Jeong, Napat Watjanatepin, Chalermpol Ruangpattanawiwat, Soon-Ho Choi, 2018, Experimental study on thermal buoyancy-induced natural ventilation, *Energy and Buildings*, Vol. 177, pp. 1-11.

[4] Yeong Sik Kim, Dong Hun Han, Hanshik Chung, Hyomin Jeong and Soon-Ho Choi, 2017, Experimental study on Venturi-type natural ventilator, *Energy and Buildings*, Vol. 139, pp. 232-241.

[5] Yeong Sik Kim, Hanshik Chung, Hyomin Jeong, Sung-Ki Song, Chungseob Yi and Soon-Ho Choi, 2016, Experimental study on a Fixed Type Natural Ventilator, *Int. J. of Air-Cond. & Refri.*, Vol. 24, No. 3, pp. 1650016(1-12).

[6] Dong-Hun Han, Yeong-Sik Kim, HanShik Chung, Hyomin Jeong, Soon-Ho Choi, 2017, An experimental study on the ventilation characteristics of the wind turbine natural ventilator by the outdoor wind velocity and the indoor-outdoor temperature difference, *Kor. J. Air-Cond. & Refri. Eng*., Vol. 29, No. 4, pp. 175-184.

DESIGN AND DEVELOPMENT OF "SUVARNABHUMI SUSTAINABLE HOUSE" BY USING THAI-HOUSE STYLE

Thaveesak Srichanin[1)], Natthawut Boonpho[1)], Jumnien Faydee[1)], Narongsak Yenprasert[1)]
Nattaya Art-Ong[1)], Atima Duangchan[1)], Panya Lukplub[2)]
[1)] *Department of Civil Engineering, Faculty of Engineering and Architecture,Rajamangala University of Technology Suvarnabhumi, Nonthaburi Campus,Thailand*
[2)] *Faculty of Engineering and Architecture,Rajamangala University of Technology Suvarnabhumi, Nonthaburi Campus,Thailand*

ABSTRACT : The objective of this research is to design and construct with the concept comfort and convenience by the combination of Thai wisdom to fit and suitable for a small 2-3 people family. The outstanding of the house is one story house, with high gable roof, usage space is 31 m^2, which consisting of living room, kitchen, balcony, bedroom and restroom. The main idea for the house is designed for comfortable living, not too hot and also can use natural sunlight in some area. The roof have a good heating resistance at the thermal coefficient 0.836 W/m.K. The roof has a gable roof vents and ceiling vents are installed around the house to reduce heat by natural mechanism. The interior ceiling is installed with heat resistance gypsums board which can reflect the heat radiation up to 86 %, in addition, there is a tree to shade over the house in order to reduce the sunlight from the west of the house. The lightweight brick is suitable for construction, which its potential in 0.13 W/m.K of the heat transfers, better than ordinary brick which its potential in 1.15 W/m.K. Suvarnabhumi Sustainable House must use the light and bright for both interior and exterior in order to reflect the sunlight and solar radiation. Beside, the area around Suvarnabhumi Sustainable House should have a moist glass ground cover and watering throughout the day that will make the surrounding around Suvarnabhumi Sustainable House cool down and cover ground surface not to dry. This is the house which will make you to stay feel comfortable, convenience and safe.

1. INTRODUCTION

Housing is the most important human factor. However, at present, the problem of climate change which is caused by the use of energy from combustion; the challenge of energy shortage; and the challenge of energy prices are rising. Suvarnabhumi Rajamangala University of Technology has initiated the research and develop "Suvarnabhumi Sustainable House" to respond to such problems and challenges, and also to respond to the future housing needs. Suvarnabhumi Sustainable House is a prototype house that uses technology to effectively manage energy. This project is designed and built for Suvarnabhumi Sustainable House which based on the concept of comfortable house by using the combination of the Thai wisdom that make house is not too hot and able to use natural light in some areas. Suvarnabhumi Sustainable House is designed to fit for a small 2-3 people family.

2. PROCEDURE

1.To design and build a Suvarnabhumi Sustainable Home based on the combination of the Thai wisdom to fit for a small 2-3 people family. The design takes into consideration of the surroundings of the house and the most effective way to save energy. The following will be considered:

1.1 Roof design will take into consideration of heat protection from the sun, that is ventilated into the house by conduction of heat by using materials with good heat resistance.

1.2 Ventilation of the roof is a way to reduce the heat transferred into the house. The roof will be built in a high gable roof with gaps under the roof likewise heat insulation and also increasing ventilation under the roof.

1.3 Reduce the exposure area or avoid direct exposure by using the cover from the outside, planting shade tree, or using of two-story roofs, for instance. These will reduce the difference of temperature surface of the outer and inner roofs.

1.4 The wall is a part of the house frame where the heat from the sun is transferred into the house by the heat conduction. The smaller houses are more affected by the heat conduction through the house walls than the larger house, therefore, should select materials with high thermal resistance to the wall. These will reduce the amount of heat transferred into the house.

1.5 Select the light or bright colors such as white, light yellow, and polished reflective materials that will reflect the sun-ray.

2. Sketch Suvarnabhumi Sustainable Homes

3. Specify materials for Suvarnabhumi Sustainable Homes

3.1The whole house structure is reinforced concrete;

3.2 Roof structure is steel shaped;

3.3 Light weight 7.5 mm mortar wall;

3.4 Floor coverings with glazed tile;

3.5 Interior ceilings use gypsum board 9 mm thick, seamless glaze, galvanized steel frame;

3.6 External ceiling, prefabricated and ventilate eaves, internal pad with mosquito net, Galvanized steel frame;

3.7 Roofing materials use for concrete tiles;

4. Construct a prototype house according to the blueprint at Rajamangala University of Technology Suvarnabhumi, Phranakhon Si Ayutthaya, Hantra, approximately 2 months construction schedule.

3. OPERATIONS RESEARCH

1. Design and construction of Suvarnabhumi Sustainable House is the combination of the Thai wisdom which is not too hot, uses natural light in some areas, and uses a good heat shield. It is suitable for a small 2-3 people family. The house is constructed with 1 story floor, with total area 31 sq.m, consisting of 1 bedroom, 1 bathroom, living room and kitchen area. Each rooms and spaces are as follows;

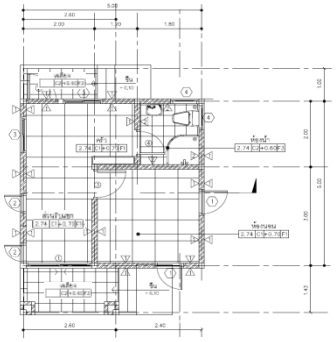

Fig.1 Usage Area of Suvarnabhumi Sustainable House

Fig.2 Suvarnabhumi Sustainable House

2. The Characteristics of Suvarnabhumi Sustainable House Construction

2.1Roof protects the heat from the sun to be vented into the house by conduction of heat. The material used was a concrete tile with a thermal conductivity (kinetic coefficient) of 0.836W / K. The lower the K value, the lower conduction of heat, the higher the K value, the higher conduction of heat

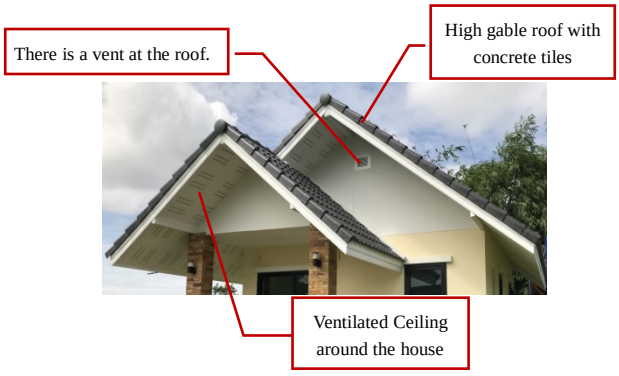

Fig. 3 The Roof of Sustainable Suvarnabhumi House

2.2 Ventilation under the roof, the design is gable roof in order to let the hot air under the roof float up. There is a vent at the gable roof and ventilated ceiling around the house to reduce the heat by natural mechanisms. In addition, the ceiling is installed with a heat-resistant gypsum board that can reflect heat radiation up to 86%

2.3 There is a tree to shade the roof in order to reduce exposure area or avoid direct exposure from the west of the house

2.4 The characteristic of Sustainable Suvarnabhumi House is designed with a small and cozy house, and the living space of the house is very close to the wall, therefore, it necessary to choose a high heat resistance material, lightweight brick walls will improve the effective heat resistance into to the house. The lightweight brick wall have more thermal conductivity qualification than the ordinary brick, as shown in Table .2

Fig.5 Reduction Exposure Area of Sustainable Suvarnabhumi House

Table 2 Comparison between the Lightweight Brick and the Ordinary Brick

Qualification		Lightweight Bricks	Ordinary Bricks
Weight	(Kg / Sq.m)	45	130
Weight with 2-side plaster	(Kg / Sq.m)	90	180
Compressive Strength Rate	(Kg / Sq.cm)	55	27
Thermal Conduction Rate	(W·m-1·K-1)	0.13	1.15
Overall Thermal Transfer V alue (OTTV)	(Watt/m^2)	37	64
Soundproofing Rate	(Decibel)	43	38
Fireproof Rate	(Hour)	4	1-2

2.5 Using light or bright colour for Sustainable Suvarnabhumi House both interior and exterior in order to reflect solar radiation.

Fig. 6 Selection of Soft Colors of Sustainable Suvarnabhumi House

4. SUMMARY

This research project is designed and built for Sustainable Suvarnabhumi House with the concept of comfortable and cozy, which is not too hot, and also able to use natural light in some areas. Using wall and heat protection materials. The blend of Thai home wisdom to fit and suitable for 2-3 small families. It can be summarized as follows:

1. The Sustainable Suvarnabhumi House is located at Rajamangala University of Technology, Phranakhon Si Ayutthaya Center, Hantra. The characteristics is a single story house, with two-level gable roof and 31 square meters of living space which including 1 bedroom, 1 bathroom, living room and kitchen area, kitchen and preparing food space, with front and back porch. The coefficient of thermal

conductivity is 0.836 W / m K;

2. Ventilation under the roof of the gable. There is a vent at the gable roof and the ceiling is ventilated around the house in order to reduce the heat by natural mechanisms. In addition, the ceiling is installed with a heat-resistant gypsum board that can reflect heat radiation up to 86%;

3. There is tree to shade roof in order to reduce exposure or avoid direct exposure from the west of the house.

4. Wall of Sustainable Suvarnabhumi House should choose materials with high heat resistance. This will reduce the amount of heat transferred into the house. By using lightweight brick walls will improves the heat resistance of the house. The lightweight brick wall has a thermal conductivity of 0.13 W / m K. which is better than ordinary bricks with a thermal conductivity of 1.15 W / K.

5. Using light and bright for Sustainable Suvarnaphumi House both interior and exterior in order to reflect the sun radiator;

6. The area around Sustainable Suvarnabhumi House Suvarnabhumi have moist grass mulching with good watering and maintenance throughout the day, in addition, there is a big tree shade behind the house in the west, which will help to make the house more comfortable.

12. REFERENCES

[1] Jinda Kaewkiew and team, *"Knowledge about energy conservation."* Board of Directors National Energy Policy, Thailand" Energy Conservation Center(Online),source: http://www.selectcon.com/ba.1asp.

[2] Sirinuch Jindaraksa, "Small Solar Home" Journal of Naresuan University, Vol.(2) 11, Naresuan University, .2003

[3] Supawadee Rattanamas, *"Research project on solar biogas in Thailand"*. Faculty of Architecture King Mongkut's Institute of Technology Ladkrabang, 2013 (Online), source: http://www.silpathai.net (03 November 2015)

[4] House and Garden. Prohibition for building a Thai style house.(online.(source http://www.homedecorthai.com/articles/Restrictions_for the_house-83-493-p8.html (03 November 2015)

[5] Thai local architecture. (online) .source: http://52011112031.blogspot.com/2012/05/blog-post_2450.html (03 November 2015

THE DEVELOPMENT STRENGTH OF A BRICK BUILDING WITHOUT BURN WITH LOCAL MATERIALS

Natapong Janpetch[1)], Supakorn Limkhunthammo[2)], Sasiwan Phoolsawat[2)], Pornthep Kaewchur[2)], Kobchai Mekdee[2)], and Rossukon Yamthongkam[2)]
[1)] *Department of Civil Engineering, Faculty of Engineering Architecture Rajamangala University of Technology Suvarnabhumi, Nonthaburi Campus, Thailand, Nonthaburi Thailand*
[2)] *Faculty of Business Administration and Information Technology, Rajamangala University of Technology Suvarnabhumi, Wasukri Campus, Thailand Phranakhon Si Ayutthaya Thailand*
Email: jnatapong@hotmail.com

ABSTRACT: This research aims to create wealth for other entrepreneurs by using the cement criteria: Dirt: Sand is 1: 6: 0, 1: 5: 1, 1: 4: 2, 1: 3: 3, 1: 2: 4 by weight And tested in accordance with the standard brick construction Mon. The test results showed that the ratio of 1: 3: 3 is the ratio of ordinary brick construction without burning. The optimum amount of dirt soil per sand. Which volume It can make ordinary brick construction do not need to burn the best compressive strength and qualification standards. This improved non-combustible brick construction can reduce the amount of soil that is imported from foreign countries. And the local sand can be used as substitutes to reduce the cost of production as well

Keywords: *Brick Building, Without Burn, Local Materials*

1. INTRODUCTION

Nowadays, sand is utilized as material in construction works and industry largely. When there is increasing need of sand, the amount of natural sand is used vastly beyond the limitation that the nature can supply. In Thailand there are sources of natural sand found in every region and the utilization of sand is dramatically huge. The management of sand utilization is controlled by the government sector and separated to private sector to responsible for the extraction of sand. Therefore, sand from natural sources may not meet required standards or specification. The information of comparison between mechanical and physical properties of sand used in this construction can help provide sand for the construction so that its quality shall meet required specification.

This research aimed to make a comparison between mechanical property and physical property of sand from Phra Nakhon Si Ayutthaya province so as to respond to the benefits of construction works and be able to utilize sand appropriately according to sand property.

2. RESEARCH METHODOLOGY

The researcher designed new ratio of unburned masonries from local materials; 5 ratios. The ratio of cement: gravel: sand is 1: 6: 0, 1: 5: 1, 1:4:2,1: 3: 3, 1: 2: 4. Bring the samples of sand to test mechanical and physical properties. The samples of sand are from Phra Nakhon Si Ayutthaya province from 2 sources; S.Saithong 8888 and Aor.Thipjinda sand pits. Sieve ordinary Portland cement type 1, weigh the ordinary Portland cement, gravel, sand. Use clean water at the amount as designed. Mix all materials well. Bring all the mixture into a compression molding to form a shape of masonry. Bring the samples of masonry to cure at room temperature.

Wherever Times is specified, Times Roman or Times New Roman may be used. If neither is available on your word processor, please use the font closest in appearance to Times. Avoid using bit-mapped fonts if possible. True-Type 1 or Open Type fonts are preferred. Please embed symbol fonts, as well, for math, etc.

3. TESTING PLAN

1. Test the physical and mechanical properties of the sand.
2. Test physical and mechanical properties of the masonries.

4. PROCEDURES OF IMPLEMENTATION AND TEST METHODS

Sand

1. Test to find density of sand; 5 samples are tested
2. Test to find natural moisture content in 5 samples
3. Test to find size and mineral composition in sand; 5 samples.
4. Test to find organic matter in fine aggregate; 5 samples.
5. Test to find specific gravity of sand; 5 samples.

Brick

1. Compressive strength test at a specific curing time.
2. Test to find water absorption property.

5. TEST AND ANALYSIS RESULTS

1. Comparison of the test result of physical and mechanical properties of sand from local sources in Phra Nakhon Si Ayutthaya province; S.Saithong 8888 and Aor.Thipjinda sand pits.
2. Comparison of average compressive strength of unburned masonries made from local materials according to the specified ratio of mixture that mixed with sand from local sources in Phra Nakhon Si Ayutthaya province; S.Saithong 8888 and Aor.Thipjinda sand pits with different curing period.

6. RESULTS

For sand, it was found that sand from the 2 sources had similar density to each other. With regard to the amount of natural moisture content, sand from Aor.Thipjinda had more moisture content than that of S.Saithong 8888. Sand from S.Saithong 8888 had similar specific gravity to sand from Aor.Thipjinda. In relation to the test to find organic matter in sand, it was found that the color of solution reacted with the sand from two sources matched the number 3 of the standard color shade.

For unburned masonries, it was found that the samples made from S.Saithong 8888 sand had the highest compressive strength based on the ratio of gravel to sand at 1:3:3, followed by the samples made from Aor.Thipjinda sand; 148and 159 kg/m^3 respectively. For water absorption property test, the masonries made from the mixture of sand to gravel based on the 5 ratios had average water absorption property (from Aor.Thipjinda) = 7.64, 7.44, 7.19, 6.82, and 7.93 percent, (from S.Saithong 8888) = 7.83, 7.65, 7.71, 7.27, and 8.09 percent.

7. CONCLUSION

With regard to the operational performance of the project, the conclusion can be as follows:

1. Development of compressive strength of unburned masonries with local materials can be made with the mixtures; the mixture of cement to gravel, the well mixed mixture, compression molding to form a shape of masonries so as to obtain unburned masonries that are full of strength and durability.

2. The ratio or suitable amount of the mixture of cement to gravel for producing unburned masonries is 1:3:3 with the reference of the test methods and standard test results. The tests are done in 3 aspects; dimension test, compressive strength test, and water absorption property test. It is found that all of the test results meet the standard.

3. The research results show that a role model of unburned masonry product that meets the standard of masonry is obtained and can be used for commercial purposes.

4. The research results show that unburned masonries increase potential for people to make use of massive amount of local sand and add more value to

8. REFERENCES

[1]Natapong janpetch et al., 2010, "Prismatic Compression Block CementedThe formula," Proceedings at the 15th National Convention on Civil Engineering, Ubon Ratchathani University.

[2]Natapong janpetch et al. "Compaction of Prismatic Blocks" Proceedings at the Proceedings 17th National Convention on Civil Engineering (NCCE 17) May 9-11, 2012, Udon Thani

[3]Natapong janpetch et al. "The capacity to compress the production block. From the waste of the industry. " Proceedings at the 19th National Convention on Civil Engineering (NCCE 19) 14-16 May 2014, Khon Kaen

[4]ACECOMS, 2000. Use of Interlocking Cement Blocks as Load Bearing Walls Laboratory Test Report. Final Report for Habitech Center.SERD,AIT

THE STUDY OF THE GINGERBREAD HOUSE PATTERN THE THAI HANDICRAFT: BANGKOK, VICINITIES AND PHRAE PROVINCE

Patravadee Siriwan[1)] and Rungpassorn Sattathanapat[2)]
1) Department Architecture, Rajamangala University of Technology Suvarnabhumi,, Nonthaburi, Thailand
2) Faculty of Liberal Arts, Ramkhamhaeng University, Bangkok, Thailand
Email: pla012@windowslive.com

ABSTRACT: This research is to collect and study gingerbread fretworks of artisan clans in Bangkok, vicinities and Phrae Province. The research is a consequence of the study on Gingerbread House Architecture in Thailand, Case Study: Bangkok, Vicinities and Phrae Province. The objectives of this research are to study buildings decorated by fretworks and collect, copy, analyze and categorize gingerbread designs found in Bangkok, Vicinities and Phrae Province, so that the local art and culture in central and northern regions can be preserved before they are demolished or deteriorated. The study can be used as learning and teaching materials for architecture or building improvement and decoration and so on. This study uses data received from the study result of Gingerbread House Architecture in Thailand, Case Study: Bangkok, Vicinities and Phrae Province as a main field of study in actual places. The places include 12 buildings decorated by gingerbread fretworks with 156 designs. According to the study, the buildings decorated with gingerbread fretwork were popular during the reigns of King Rama V and King Rama VI. However, the popularity decreased during the reign of King Rama VII. Most of the buildings are located in Phra Nakhon District of Bangkok, Mueang District of Nakhon Pathom Province and Mueang District of Phrae Province. These buildings were influenced by Western culture before the influence spread to Bangkok. For the buildings decorated by gingerbread designs, there is no information about the artisans. However, the only information shows that most of the artisans were local and Chinese artisans. Meanwhile, some fretworks were purchased from the capital city. The buildings were popularly decorated by gingerbread designs. The decorations were in the areas beyond accordion doors, windows and supporters. Also, the decorations were beneath ceilings, eaves ornamental fringes, splashboard ornamental fringes, window ornamental fringes, balustrade bars and splashboard skids. Gingerbread designs include wood patterns, and most of the wood patterns are vertical, horizontal, transparent, delicate, curved and smooth. In addition, some patterns are twisted. The uniqueness of the pattern is vine pattern by having branches, clusters and glumes. Meanwhile, tulip pattern is the original pattern of gingerbread design. Another characteristic is a pattern derived from gaps, and most of them are vertical by being perforated into a variety of closed and opened gaps linked with the same style of perforated wood plates. The pattern of perforated gaps is caused from wood with two opened gaps by similarly having left and right perforations. Additionally, the left perforation is different, or it is on single wood plates consistently placed in array. The popular patterns of perforated gaps include larvae, leaves, flowers and petals. After the patterns are produced, the patterns will possess the same characteristics as those of a variety of clusters.

Keywords: Gingerbread House Pattern, Thai Handicraft, Bangkok Vicinities and Phrae Province

1. INTRODUCTION

Bangkok is a capital city with advanced technology, and the city is rich in arts, culture and architecture, as the city is the home of Vimanmek Mansion, Abhisek Dusit Throne Hall, Phaya Thai Palace in the area of Phramongkutklao Hospital, Golden Teak Museum, Thewarat Kunchorn Temple, Baan Ekkanak and Diamond Hall in Boworn Niwet Temple. Gorgeous Gingerbread fretworks are found in these places, and the Gingerbread fretworks blend well with buildings. Also, buildings in Nakhon Pathom Province are decorated with Gingerbread patterns, including Ruean Phra Thanesuan and Sanam Chan Palace. In addition, houses are beautifully ornamented with Gingerbread patterns. These Gingerbread patterns were very popular in Bangkok and in Phrae Province of Northern region. Houses of wealthy people were built with teak, employing Thai, Chinese and Vietnamese artisans. Gingerbread fretworks blend well with buildings and houses of people in Bangkok and its vicinity and Phrae Province.

Thus, this research aims to gather Gingerbread fretworks of artisan clans in Bangkok and its vicintiy and Phrae Province. The study is to collect patterns of Gingerbread fretworks to allow interested people to make use of them. Besides, evidences have been gathered prior to deterioration of buildings, aiming to preserve arts and culture.

2. RESEARCH METHODOLOGY

Research on the Study and the Collection of Patterns of Gingerbread Fretworks, Artisan Clans of Bangkok and Its Vicinity and Phrae Province: The research methodology is as follows:

1. Collection of Data and Documents and Study of Documents and Related Research: The researchers have collected and verified the documents, including academic documents, books, aerial photographs, other related historical evidences, etc.

2. Approaches in documents have been studied. Complete draft has been produced. Field data have been collected. To collect field data, actual locations have been surveyed.

3. Creation of Questionaires

4. Survey of Actual Locations (Collection of Field Data): The researchers have studied and prepared collection of field data of Gingerbread houses at the following locations.

1. Vimanmek Mansion, Bangkok
2. Abhisek Dusit Throne Hall, Bangkok
3. Gingerbread Monks' Cells, Suan Plu Temple, Bangkok

4. Golden Teak Museum, Thewarat Kunchorn Temple, Bangkok
5. Diamond Hall
6. Baan Ekkanak, Bangkok
7. Ruean Phra Thanesuan in Sanam Chan Palace, Nakhon Pathom Province
8. Khum Chao Luang Mueang Phrae, Phrae Province
9. Baan Wong Buri, Phrae Province

5. Interview has been used as a tool for verifying survey evidences and data of documents to make sure whether data reliability is sufficient.

6. Data Synthesis: Data received from field study have been used and classified into groups for data analysis.

7. Data Analysis: Data of object arts, patterns of fretworks and decoration of buildings and architecture with fretworks have been emphasized. In addition, study has been reported by means of analytical description.

8. Conclusion, Discussion and Suggestions

3. RESULTS

According to the study of 11 buildings decorated with Gingerbread patterns in Bangkok and its vicinity and Phrae Province, there are 62 patterns of fretworks. These patterns of fretworks were popular during the reigns of King Rama V and King Rama VI. However, the popularity was reduced during the reign of King Rama VII. The decoration of buildings with Gingerbread patterns was influenced by western design, arriving in Bangkok, Thailand and spreading to other cities. The results of the study are as follows:

1. Types of Constructions in Bangkok, Decorated with Gingerbread Patterns

Gingerbread patterns were arriving in Bangkok while the characteritsics of accommodations of the Thai people were changing. The popularity of Thai style houses was decreased, but brick masonry houses, half-cement-half-wood houses, wooden houses, hip roof houses1, gable-roof houses2or houses with combination of the two styles became popular, replacing Gingerbread patterns. These housing styles were found in centers of administration, communities, religious sites, houses of government officials, houses of wealthy people and commercial buildings on main streets in the past. According to surveys of both registered and non-registered archaeological sites, the most ancient Gingerbread patterns are found at throne halls in Suan Dusit Palace and inner court. The evidences can be found in photos at National Archives of Thailand, and the Gingerbread patterns can be seen nowadays. However, some palaces remain in photos only.

Some ancient buildings were docorated with Gingerbread patterns in some parts. In general, to consider whether buildings are decorated with Gingerbread patterns, porches must be first taken into account, as the porches are the forefront of buildings, showing splendor. Meanwhile, the porches are beautifully docorated. On the other hand, some buildings were made of wood, so porches were not decorated. Decorations are found in other parts, such as eaves and supporters above doors and windows. These decorations are mostly found in Nakhon Pathom Province, and for most of lined designs, designers focus on Gingerbread patterns clearly. Meanwhile, in appendix, Gingerbread patterns are found in some parts of buildings, and splendor is shown. Gingerbread patterns in Bangkok are shown in the following areas (Fine Arts Department; 2017: 11).

1.1 Palaces

When King Rama V returned from Europe in 1897, His Majesty the King ordered to build Suan Dusit Palace, aiming to be used as a throne for relaxation after royal duties. The palace was equipped with exercise facilities. Meanwhile, Dr. Reiter, a court physician explained to His Majesty the King that there were several thrones and houses in the palace, there was no good air ventilation, so His Majesty the King and royal family members were always ill. Later, His Majesty the King visited Chang Hee Field and saw that the field was shady, as there were a lot of trees. Air in the area was cool and pleasant. Thus, His Majesty the King bought this land with private money and named the place as “Suan Dusit” (In the reign of King Rama VI, the place was called “Dusit Palace”.) Several throne halls were built in western style, and royal residences were divided, referring to ancient royal traditions. The royal residences were divided into outer court (Males) and inner court (females). The throne hall was the place where the white tiered umbrella of kingship was located, and His Majesty the King attended the meeting at the throne hall. In addition, the throne hall was used as a venue for royal ceremonies. Within the palace were His Majesty the King’s throne hall and royal family members’ residences. Throne halls and residences in Dusit Palace were decorated with Gingerbread patterns, including Vimanmek Mansion3 and inner court (Suan Hong Mansion and Four Seasons Mansion5, etc.).

1.2 Religious Sites

Most of Buddhist constructions were monks’ cells or pavilions built later by Buddhist laymen. These monks’ cells or pavilions were not constructed when temples were first built. Temples in Bangkok built prior to the reigns of King Rama V and King Rama VI include Boworn Niwet Temple, Thewarat Kunchorn Temple, Suan Plu Temple, etc. (Fine Arts Department, 2017: 12-23).

1.3 Houses of Government Officials

Houses of government officials in the reigns of King Rama V and King Rama VI were built with different styles. The houses were beautifully decorated, showing tastes, wealthiness and titles. The houses of government officials built with Gingerbread patterns include Baan Ekkanak (house of Pol. Col. Phraya Prasong Sanpakorn).

1.4 Houses of Wealthy People

In Phrae Province, Gingerbread patterns are found in Baan Wong Buri. The house has fretworks on its gables, ornamental fringes, supporters, doors and windows. The house was popular in the reign of King Rama V. Apart from Baan Wong Buri, Khum Chao Luang Mueang Phrae built in the reign of King Rama V was also decorated with Gingerbread patterns (Fine Arts Department, 1987: 25-26).

Fig 1 Gable of Baan Wong Buri

Fig 2 Eaves of Khum Chao Luang Mueang Phrae

Fig 3 Supporter of Ruean Phra Thanesuan

Fig 4 Window of Baan Wong Buri

Fig 5 Pulp Remain above Door of Baan Wong Buri

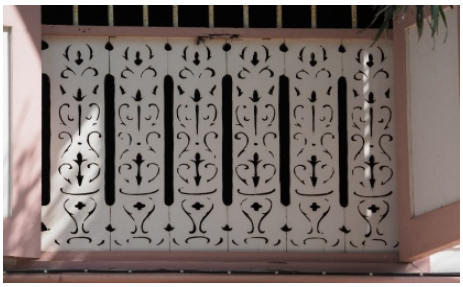

Fig 6 Patterns on Window of Baan Wong Buri

Fig 7 Balustrade of Baan Wong Buri

Fig 8 Low Door of Baan Wong Buri

6. DISCUSSION

Buildings were built with Gingerbread patterns of artisan clans of Bangkok and its vicinity and Phrae Province. The buildings show social and economic statuses and modernity in Bangkok and its vicinity and Phrae Province as well as cities of administration centers, aiming to decrease foreign influences. Also, Gingerbread patterns are found in Bangkok and its vicinity and Phrae Province, showing artisan skills, fretworks and designs of local artisans. Thai design combined with western design was popular at the time, applying Thai and Chinese artisans' concepts and skills. Additionally, some fretworks are fashionably carved, the patterns of which are harmonious, concave and deep. The fretworks are a good combination of Gingerbread patterns of Bangkok and its vicinity and Phrae Province.

Types of Gingerbread Patterns

1. Western Design
2. Thai Design
3. Geometric Design

Characteristics of Western Design
1. Vines
2. Tulip
3. Lacework and Crochet

Results and Discussion

Most of gingerbread patterns in Bangkok are inspired by and duplicated from nature. Especially, vine design is generally found. The main characteristics of Gingerbread patterns include vines, stems, branches, treetops, blossoms and burgeons. These Gingerbread patterns are decorated on gables, skylights, vents, semicircles above doors and curves. The decorations are a good combination.

Apart from the Gingerbread patterns mentioned above, alphabets are designed in the centers. These designs can be found at Boworn Niwet Temple, Pathum Khongkha Temple, Anong Kharam Temple and Baan Ekkanak, aiming to provide information about donors and periods of time for further generation and characteristics of patterns and buildings in each period (Fine Arts Department, 2017: 39).

7. CONCLUSION

Gingerbread patterns come from fretworks with appropriate designs and materials. Thickness of the wood must be between one and two centimeters. The patterns found are small, deliberate, narrow and thin. Difficulty of wood carving must be taken into account, and arrangement of patterns must relate to designing space. For examples, gables must be designed by having triangles and semicircles above doors and windows. Meanwhile, supporters and skylights above doors and windows must be vertical, such as balcony balustrades, etc.

Wood Carving: Patterns are carved by two methods.

1. Pulp Remain: After wood is carved for pictures or patterns, pulp still remains. This pattern is decorated on gables and supporters above doors and windows, as the pattern is suitable for large space, showing splendor, softness and delicacy, aiming to improve stability and prevent removal, damages or fragility (Fine Arts Department, 2017: 43).

Characteristics of Thai Design
1. Kanok Pattern
2. Krajang Pattern
3. Four Petals Pattern

Characteristics of Geometric Pattern
1. Circle
2. Arrow
3. Sun
4. Number
5. Vertical and Horizontal Patterns

Characteristics of Gingerbread Fretwork
1. Space above Accordion Door
2. Door Panel
3. Space above Window Panel
4. Supporter under Ceiling
5. Space at Eaves and Window Splashboard
6. Pillar Supporting Eaves

8. ACKNOWLEDGEMENT

This research is successful, and the researcher would like to thank for providing fund for the research received from Financial Budget 2018. Rajamangala University of Technology Suvarnabhumi Nonthaburi would like to thank Mr. Sahayot Wongburi, owner of Baan Wong Buri, officials of Khum Chao Luang Mueang Phrae and officials of all agencies for providing research data, including Diamond Hall, Boworn Niwet Temple, Golden Teak Museum, Thewarat Kunchorn Temple, Baan Ekkanak, Ruean Phra Thanesuan, Sanam Chan Palace in Nakhon Pathom Province and Suan Plu Temple. The data received are useful for the research and students of architecture of Rajamangala University of Technology Suvarnabhumi Nonthaburi and all concerned. The researcher would like to thank all concerned.

9. REFERENCES

[1] Department of Archaeology, Fine Arts Department, Ministry of Culture. 2017. Gingerbread Fretwork, Aesthetics of Rattanakosin. Bangkok: Amarin Printing and Publishing Public Company Limited
[2] Paradee Panthupakorn. 2004. Study and Collection of Gingerbread Fretworks in Thailand, Chanthaburi Artisan Clan. Chon Buri: Department of Artisans
[3] Patravadee Siriwan. 2016. Study of Gingerbread Patterns in Thailand, Case Study: Bangkok and Its Vicinity and Phrae Province. Rajamangala University of Technology Suvarnabhumi Nonthaburi Bureau of the Royal Household. 2012. Vimanmek Mansion. Bangkok: Amarin Printing and Publishing Company Limited
[4] Worapol Panomai, Volunteering Official of Khum Chao Luang Mueang Phrae. (May 23, 2018).Interview.
[5] Sahayot Wongburi. Owner of Baan Wong Buri. (May 21, 2018). Interview.
[6] Phra Ratchawachiramoli. Abbot of Suan Plu Temple. (February 17, 2018). Interview.
[7] Worachaya Jinorot. Educationist, Office of Arts and Culture. Ban Somdet Chao Phraya Rajabhat University. (March 19, 2018). Interview.
[8] Pawinee Trichaiyut. Official of Sanam Chan Palace, Nakhon Pathom Province. (September 30, 2017). Interview.
[9] Ukrit Mongkolnavin. Chairperson of Prof. Dr. Ukrit-Thanpuying Monthinee Mongkolnavin Foundation (March 17, 2018). Interview.

CHARACTERISTICS ANALYSIS OF HOLLOW SHAFTED BLDC MOTOR USING FINITE ELEMENT METHOD

Hyun-Ji Lee[1)]*, Jung-Hoi Kim[1)], Chang-Eob Kim[1)]
[1)] *Dept. of Electrical Engineering, Hoseo University, Asan, Korea*

ABSTRACT: The permanent magnet brushless DC motor has been widely used because of its higher performances; energy efficiency, small volume and light weight, and high power density. The shaft in the conventional motor for fan blower is an obstacle for the fluid transfer. In this paper, a hollow shafted BLDC motor for fan blower is proposed in order to increase the efficiency of the fluid transfer. The characteristics of the motor are analyzed by finite element method in 2D and 3D, and the results are compared.

Keywords: *Hollow shafted, BLDC motor, finite element method, fluid efficiency*

1. INTRODUCTION

Unlike conventional DC motors, BLDC motors do not have brushes and commutators. Since there is no brush inside the electric motor, it can be used for a longer time than a general electric motor. In addition, it has the characteristics that excel in noise and performance compared with existing electric motors. Thus due to the excellent characteristics of the BLDC motor, it is used in various fields. [1-3]

In this paper, we propose a hollow shafted BLDC motor for fan blower application to increase the efficiency of fluid blowing. In the conventional motor for fan blower application, the shaft becomes an obstacle to fluid transfer. Fig 1 is a hollow shafted BLDC motor for fan blower application with a hollow shaft, and the specifications of the motor are shown in Table 1.

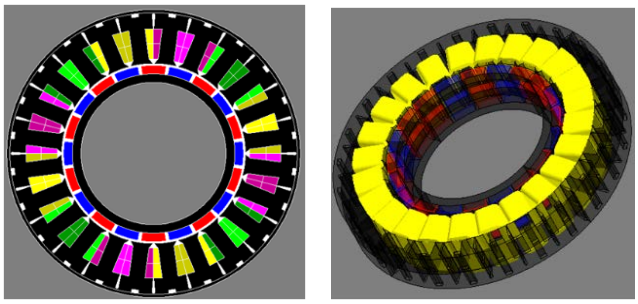

(a) 2D (b) 3D

Fig. 1 Modelling of hollow shafted BLDC motor

Table 1 Specification of a hollow shafted BLDC motor

Items	***Values***
No. of ploes	20
No. of slots	24
Rated RPM	3,500
Input voltage	DC 48[V]
Rated output	200[W]

The permanent magnet is ring-type with NdFeB material. Table 2 shows the characteristics of NdFeB, and it was magnetized with repulsive direction as shown in Fig. 2.

Table 2 Material characteristics of NdFeB magnet

Items	***Values***
Remanent flux density	1.24[T]
Relative permeability	1.05
Resistivity	1.5×10^{-6}[Ω·m]

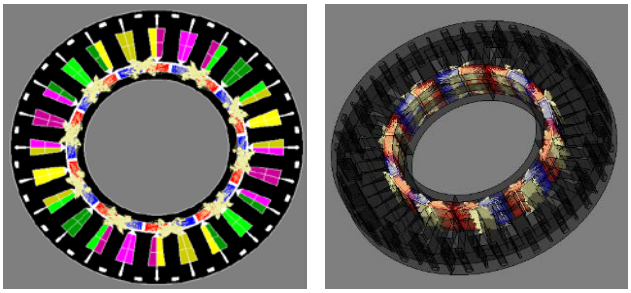

(a) 2D (b) 3D

Fig. 2 Magnetization direction

2. ELECTROMAGNETICANALYSIS OF HOLLOW SHAFTED BLDC MOTOR FOR FAN BLOWER

In this paper, the characteristics of the hollow shafted BLDC motor were analyzed using a finite element program in 2D and 3D and the results was compared. Fig. 3 indicates the mesh of the 2D and 3D models. Generally, 3D modeling is necessary because it is impossible to model the end parts. [4]

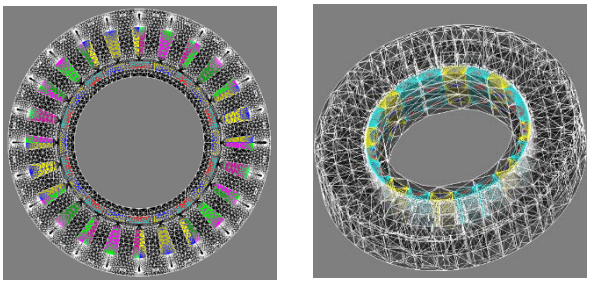

(a) 2D (b) 3D

Fig. 3 Mesh

2.1 Analysis of hollow shafted BLDC motor in 2D

Fig. 4 is the result of electromagnetic field analysis using the finite element method of hollow shafted BLDC motor for fan blower. Fig. 5 is the output and torque according to the rotation angle. The FLUX program was used in the analysis. The rated output is 201.24[W] at the rated speed of 3500 [rpm].

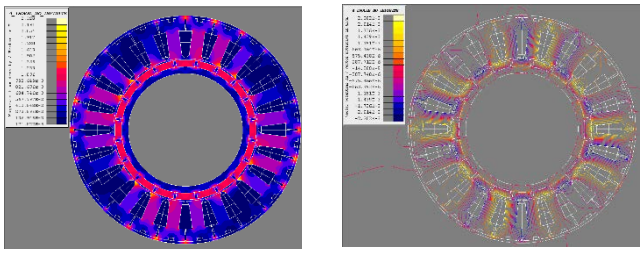

(a)flux density distribution (b) equipotential lines

Fig. 4 Flux density distribution and equipotential lines

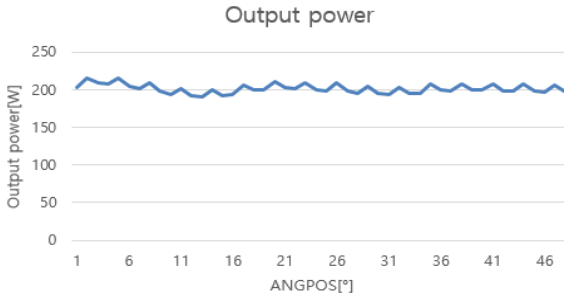

(a) output power

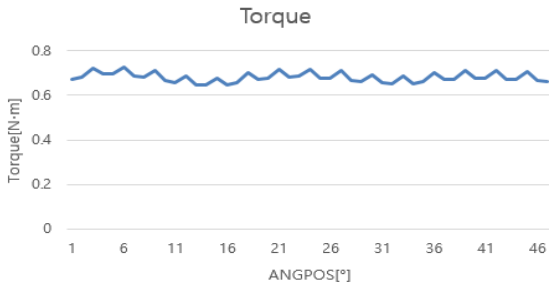

(b) torque

Fig. 5 Output power and torque

In 2D analysis, it is supposed that the characteristics of the analysis are same in the axial direction. So 3D modelling is needed in the case of motor with short axial direction.

2.2 Analysis of hollow shafted BLDC motor in 3D

3D modeling of the BLDC motor was performed similarly to the winding shape of the actual model. Fig. 6 is the result of electromagnetic field analysis of hollow shafted BLDC motor for fan blower using the finite element method in 3D. Fig. 7 is the output and torque according to the rotation angle. The rated output is 200.5[W] at the rated speed of 3500[rpm].

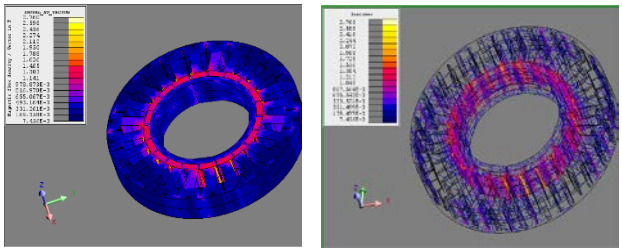

(a) flux density distribution (b) equipotential lines

Fig. 6 Flux density distribution and equipotential lines

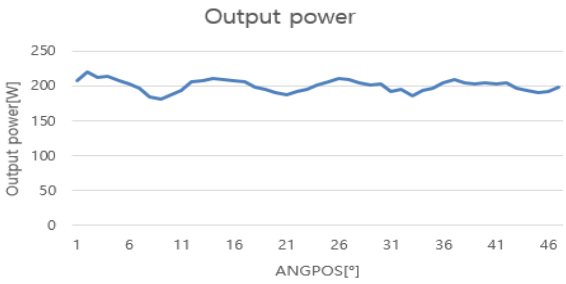

(a) output power

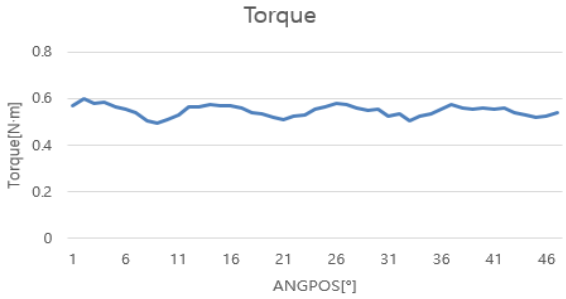

(b) torque

Fig. 7 Output power and torque

2.3 Comparison of 2D and 3D Analysis

Table 3 is the analysis result of the hollow shafted BLDC motor. Compared to 2D, the core loss in 3D decreases by 2.3 [W] and the efficiency improved by 1.5 [%].

Table 3 Analysis results of a hollow shafted BLDC motor

Items	***2D***	***3D***
Output power	201.2[W]	200.5[W]
Torque	0.55[Nm]	0.55[Nm]
Core loss	8.24[W]	5.92[W]
Copper loss	26[W]	24[W]
Input power	235.47[W]	230.32[W]
Efficiency	85.46[%]	87.05[%]

2.4 Characteristic analysis of conventional and hollow shafted BLDC motor

In this section, the comparison was made with the conventional and hollow shafted BLDC motor. Fig 8 is the conventional motor modelled in 3D. Table 4 is the results of the analysis of two motors. As shown in the Table 4, the characteristics of the two motors are almost same. But the weight of hollow shafted BLDC motor is reduced by 24.15[%] compared to the conventional one, so the cost can be reduced.

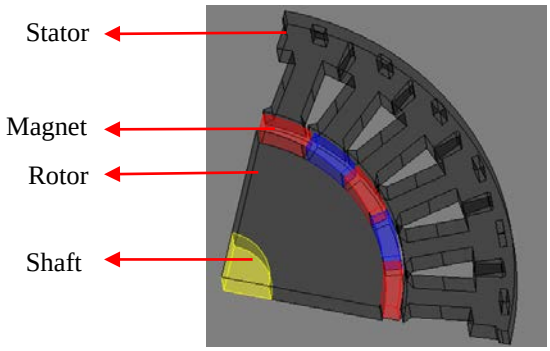

Fig. 8 Conventional BLDC motor

Table 4 Analysis results BLDC motor

Items	*Conventional BLDC motor*	*Hollow shafted BLDC motor*
Output power	200.1[W]	200.5[W]
Torque	0.55[Nm]	0.55[Nm]
Core loss	5.88[W]	5.92[W]
Copper loss	22[W]	24[W]
Input power	227.98[W]	230.32[W]
Efficiency	87.77[%]	87.05[%]

2.5 Manufacture of hollow shafted BLDC motor

Fig. 9 shows the photo of a hollow shafted BLDC motor manufactured for fan blower. .

Fig. 9 Hollowed shafted BLDC motor

3. FLUID ANALYSIS FOR FAN BLOWER

Fig. 10 shows the flow analysis result of the fan when a conventional motor and a hollow shafted motor are applied. Generally, the pressure decreases and increases on the upstream side and the downstream side respectively. When the pressure decreases, the speed of air intake is accelerated to the intake port. It is possible to confirm that the flow passes through the hole without stagnation at the center of the fan in the flow analysis. As a result of simulation using CFD, it was confirmed that the flow rate increased by 3.5[%] as compared with the fan with conventional BLDC motor. [5]

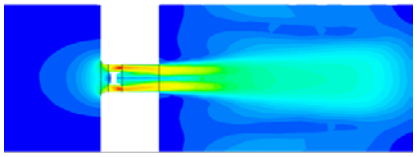

(a) fan with conventional motor

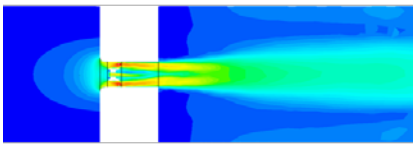

(b) fan with hollow shafted motor

Fig. 10 Comparison of velocity distributions

4. RESULTS AND CONCLUSION

As a result of analyzing the hollow shafted BLDC motor for fan blower application, the performance is similar to the conventional BLDC motor, and the weight is reduced by about 24[%]. Moreover, it was confirmed that the fluid flows smoothly, and the flow rate increases by 3.5[%] as compared with the fan with conventional motor. In this paper, we compared the characteristic analysis by 2D and 3D modeling of a hollow shafted BLDC motor and presented 2D and 3D characteristic analysis values.

5. REFERENCES

[1] Sang-Rog Han, Kang-Yeon Lee, Byeong-Ho Jeong, 2015, A Study On The Stator Slot Shape Design of BLDC Motor, *Journal of the Korean Institute of IIIuminating and Electrical Installation Engineers*, pp. 41~49

[2] Chang-Hwan Kim, Daesuk Joo, Duck-Shick Shin, Ju-Hee Cho, Sang-Taek Lee,Hee-Jun Kim, Kwang-Woon Lee, Dae-Kyong Kim, 2011, Development of a Low-cost Type Single Phase BLDCM and Driver, *Proceedings of the KIPS Power Electronics Society*, pp. 565-566

[3] Hoe-Cheon Kim, Tae-Uk Jung, Optimized Design of Rotor Considering Cost-Reduction of Small BLDC Motor, 2013, *The Transactions of the Korean Institute of Electrical Engineers*, Vol. 62, No. 4, pp. 495-501

[4] S.M Jang. S.S Jeong. H.S Yang, D.W Ryu, I.K Yoon. S.Y. Sung, 1999, Comparison of Magnetic Field Using Equivalent Reluctance 2D and 3D FEA for Linear Homopolar Synchronous Motor, *Proc. KIEE Conference, Summer A*, pp.19-21

[5] Hyun-Ji Lee, Jung-Hoi Kim, Ju-Hee Lee, Sung-Jun Joo, Chang-Eob Kim, 2018, Fluid Analysis of Hollow Shafted BLDC Motor for Fan Blower Application, *21st ICEMS*, pp.329-331

OPTIMAL PIDD^2 CONTROLLER DESIGN FOR BLDC MOTOR SPEED CONTROL BY CUCKOO SEARCH

Danupon Kumpanya[1)*]
[1)]*Department of Electrical Engineering, Faculty of Engineering and Architecture, Rajamangala University of Technology Suvarnabhumi, Suphanburi, Thailand*

ABSTRACT: This paper proposes an optimal PIDD^2 controller design for brushless DC (BLDC) motor speed control by the cuckoo search (CuS), one of the powerful metaheuristic optimization search techniques for solving the continuous optimization problems. The proposed control system is implemented on the TMS320F28335 DSP board interfacing to MATLAB/SIMULINK. With Back EMF detection, the proposed system is considered as a class of sensorless control. This scheme leads to the speed adjustment of the BLDC motor by PWM. In this work, the BLDC motor of 100 watt is conducted to investigate the control performance. As results, it was found that the speed response of BLDC motor can be regulated at the operating speed of 700 and 1400 rpm in both no load and full load conditions. Very satisfactory responses of the BLDC motor system can be successfully achieved by the proposed control structure and CuS-based design approach. In addition, the simulation results are confirmed by the experimental ones from the BLDC motor speed control system developed in the laboratory.

1. INTRODUCTION

The brushless dc (BLDC) motor has been increasingly used in different applications, for example, industrial automation, automotive, aerospace, instrumentation and appliances [1]. The BLDC motor uses permanent magnets for excitation. Rotor position sensors of such the motor are needed to perform electronics commutation. Usually, three Hall sensors are used as rotor position sensors for a BLDC motor. However, the rotor position sensors cause several disadvantages from the standpoint of total system such as cost, size and reliability. For these reasons, it is desired to eliminate these sensors from the motor. This leads the sensorless control.

In recent years, sensorless BLDC motor has been studied [2], [3]. The rotor position signal of the motor can be detected by motor voltage and current, etc. Among the methods of rotor position estimation, the Back EMF estimation is one of the major approaches [4]. However, the Back EMF is very small in the process of motor starting, and the commutation point is not easily achieved. For these reasons, the conventional sensorless drive needs a complicated starting procedure [2], [3], [4].

Design and implementation of the BLDC motor drive by proportional plus integral plus derivative and double-derivative (PIDD^2) controller [5] based on TMS320F28335 DSP board [6] interfacing to MATLAB/SIMULINK [7] is proposed in this paper. In order to obtain the optimal PIDD^2 controller, the cuckoo search (CuS), one of the powerful metaheuristic optimization search techniques for solving engineering optimization problems [8]. The CuS algorithm is based on the obligate brood parasitic behaviour of some cuckoo species in combination with the Lévy flight behaviour of some birds and fruit flies [9]. With both diversification and intensification properties, the CuS has been successfully applied to many engineering problems [9], [10]. The CuS is applied to achieve the optimal tracking and regulating responses. The trapezoidal Back EMF waveforms are modeled as a function of rotor position, while the switching function concept is adopted to model the voltage source inverter (VSI). With CuS-based, reponses of controlled system by the PID controller is compared to those by the PIDD^2 controller. As results, speed and current waveforms of the controlled system can be easily obtained.

2. BLDC MODEL AND DSP BOARD

2.1 Mathematical Model of BLDC motor

In practice, the commutation of the BLDC motor is done electronically. The position of rotor is very important for electronics commutation. Usually, the Hall sensors are placed in 120-degree intervals and the common operation of BLDC motor is achieved by Six-section. The Back EMF and Hall sensor signals are depicted in Fig. 1.

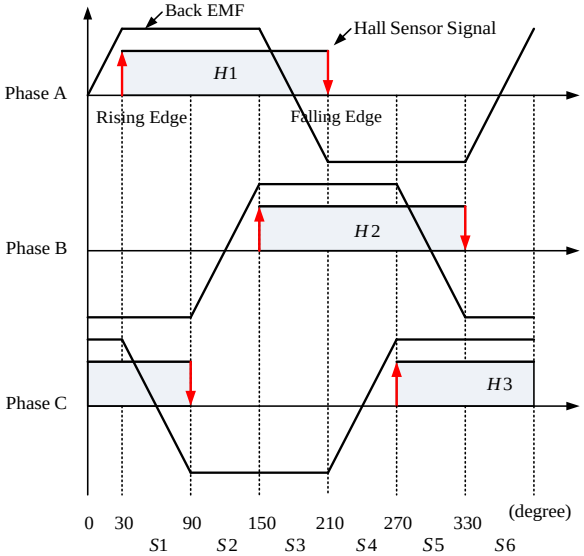

Fig. 1 Back EMF and Hall sensor signals

Once the magnetic poles of rotor come to Hall sensor, the sensory signals are generated. According to the Six-step as shown in Fig. 1, the commutation sequence is performed. The motor phases are supposed to conduct for 120 electrical degrees two times per cycle. The Two-phases are only conducted at one time. The Hall sensors signal has the rising and falling edges for each phase. This means that the Six-trigger signals are

generated per one cycle. Using these trigger signals, motor control is carried out. The switching sequence for commutation phase is given in Table 1. For forward and reverse directions of rotor, switching sequence is different.

Table 1 Switching Sequence

Directions	Switching Sectors					
	*S*1	*S*2	*S*3	*S*4	*S*5	*S*6
Forward	a^+b^-	a^+c^-	b^+c^-	b^+a^-	c^+a^-	c^+b^-
Reverse	b^+a^-	c^+a^-	c^+b^-	a^+b^-	a^+c^-	b^+c^-

Modeling of BLDC motor is similar to Three-phase synchronous machine. Since there is permanent magnet mounted on the rotor, some dynamic characteristics are different. Model of BLDC motor can be formulated through the electrical equivalent circuit represented in Fig. 2 [11]-[14].

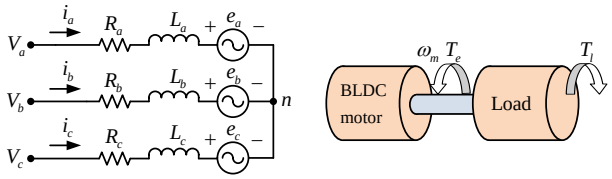

Fig. 2 Equivalent circuit of BLDC motor

The voltage equation in (1) consists of resistance, inductance and Back EMF voltages for *a*, *b* and *c* phases, where v_x is the input voltage, i_x is the current, R is the resistance, L is the inductance and e_x is the Back EMF, respectively. The subscript x stands for *a*, *b* and *c* phases. In upper voltage equation, L is the difference between Self-inductance L_s and Mutual-inductance L_m. That is, $L = L_s – L_m$.

$$v_x = Ri_x + L\frac{di_x}{dt} + e_x \tag{1}$$

$$e_x = K_w f\left(\theta_e - \frac{2n\pi}{3}\right)\omega_m \tag{2}$$

In the Three-phase BLDC motor, the Back EMF e_x in Eq. (2) is related to a function of rotor position, where K_w is Back EMF constant of one phase, θ_e is the electrical rotor angle and ω_m is the rotor angular velocity. The subscript x presents *a*, *b* and *c* phases. If x is *a*, *b* and *c* phase, n is 0, 1 and 2.

Unlike the induction motor or synchronous motor control, phase variables are used directly without any transformation equation in BLDC motor. The physical properties as current, flux and Back EMF perform rectangular forms. This implied that the coordinate transformation is not needed. The output power P_e and the torque T_e of the BLDC motor are expressed in Eq. (3) and Eq. (4), respectively.

$$P_e = e_a i_a + e_b i_b + e_c i_c \tag{3}$$

$$T_e = \frac{P_e}{\omega_m} = \frac{e_a i_a + e_b i_b + e_c i_c}{\omega_m} \tag{4}$$

If a motor is operated with Two-phase conduction type, the torque equation is modified. In *S*1 mode as shown in Table 1, the current ($i_a = I$, $i_b = –I$ and $i_c = 0$) and Back EMF ($e_a = E$ and $e_b = –E$). The torque T_e of the BLDC motor can be expressed in Eq. (5).

$$T_e = \frac{e_a i_a + e_b i_b + e_c i_c}{\omega_m} = \frac{2EI}{\omega_m} \tag{5}$$

The total output torque is a simple equation of Back EMF E and current I. Regarding to Eq. (5) for producing an electromagnetic torque, the sum of $e_a i_a$, $e_b i_b$ and $e_c i_c$ is constant as far as a certain speed is concerned. As shown in Fig. 2, this means that the rectangular phase currents with the corresponding Back EMF are required.

2.2 DSP Controller Board

The DSP controller board used in this work is the Texas Instrument model TMS320F28335 [6] consisting of a 32-bit CPU and a Single-precision 32-bit Floating-point. The 150 MHz system clock is provided by an on chip oscillator including the MATLAB/SIMULINK software platform [7]. The module board includes Three-phase PWM inverter 90V, 5A upto 25 kHz PWM frequency and measurement of motor currents in all 3 phases with DC voltage supply of 5Vdc.

The BLDC motor speed control system based on TMS320F28335 DSP board can be represented in Fig. 3. The MATLAB/SIMULINK platform is integrated to monitor communication program and DSP applications. Using the PC communication module, it can accessible to the TMS320F28335 DSP controller board and execute any application program in order to analyze and evaluate the overall system performance.

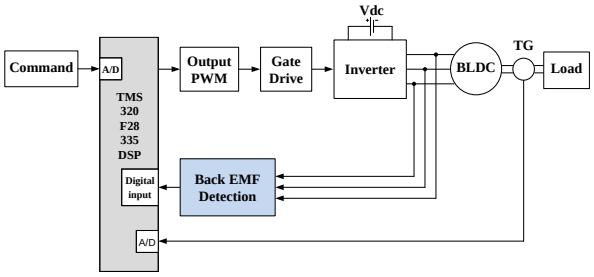

Fig. 3 Block diagram of BLDC motor

3. CUCKOO SEARCH

3.1 Cuckoo Breeding Behaviour and Lévy Flight

Yang and Deb [9] proposed the CuS in 2009 based on cuckoo bird's behaviour. This is because cuckoos are fascinating birds, not only due to the beautiful sounds they can make, but also due to their aggressive reproduction strategy [9], [10]. Cuckoos are brood parasitism. They can lays and abandons their eggs in the nest of another species. There are three basic types of brood parasitism: (i) intraspecific brood parasitism, (ii) cooperative breeding and (iii) nest takeover. From their study, some cuckoo species lay their eggs in communal nests, though they may remove others' eggs to increase the hatching probability of their own eggs [9].

Some host birds can engage direct conflict with the intruding cuckoos. If a host bird discovers the eggs that are not its owns, it will either throw these alien eggs away or simply abandons its nest and builds a new nest elsewhere. In nature, animals search for food in a random or Quasi-random manner [9], [10]. Not only animals and insects, but also birds and fruit flies have demonstrated the typical characteristics of Lévy flight for their foraging path. While flying, they follow the path of long trajectories with sudden perpendicular turning (90^o turn) combined with shortly random movements. Algorithms of the CuS developed by Yang and Deb are based on those cuckoo breeding behaviour and Lévy flight [9], [10].

3.2 Cuckoo Search Algorithm

As mentioned, the CuS algorithms are based on the general cuckoo bird's behaviour which can be described by three following idealized rules [9], [10].
a) Each cuckoo lays one egg at a time, and dumps it in a randomly chosen nest.
b) The best nests with high quality of eggs (Solutions) will carry over to the next.
c) The number of available host nests is fixed, and a host can discover an alien egg with a probability $p_a \in [0, 1]$. In this case, the host bird can either throw the egg away or abandon the nest, and build a completely new nest in a new location.

The last assumption can be approximated by a fraction p_a of the n nests being replaced by new nests (With New Random Solutions at New Locations). This means that each egg in a nest represents each solution, while a cuckoo egg represents a new solution. The worse solutions will be replaced by the new solution (Cuckoo Egg). Based on three rules, the CuS algorithms can be summarized by the pseudo code as shown in Fig 4.

Initialized:
- Objective function $f(\mathbf{x})$, $\mathbf{x} = (x_1,\ldots,x_d)^T$.
- Generate initial population of n host nests $\mathbf{x}_i$ (i = 1, 2,…,n).

while (t < *MaxGen*) or (termination criteria: TC)
- Get the j cuckoo randomly by Lévy flight.
- Evaluate its quality by the given objective function $\mathbf{F}_i$.
- Choose a nest j among n nests randomly.
- **if** ($\mathbf{F}_i$ < $\mathbf{F}_j$)
  - Replace j by the new solution.
- **end**
- A fraction (p_a) of worse nests are abandoned, and build new ones at new locations via Lévy flight.
- Keep best solution (or nests with quality solutions).
- Rank the solutions and find the current best.

end
- Report the best solution found.

Fig. 4 Pseudo code of CuS

New solutions $\mathbf{x}^{(t+1)}$ for cuckoo i can be generated by using a Lévy flight as stated in Eq. (6), where $\alpha > 0$ stands for the step size. In most cases, $\alpha = 0.1$ Eq. (6) can be used. Refereeing to Eq. (6), it can be considered as the stochastic equation for random walk which is a Markov chain whose next status/location only depends on the current location (The First Term in Eq. (6)) and the transition probability (The Second Term in Eq. (6)). A symbol $\oplus$ means Entry-wise multiplications, while a symbol Lévy(λ) represents a Lévy flight providing random walk with random step drawn from a Lévy distribution having an infinite variance with an infinite mean as expressed in Eq. (7).

$$x_i^{(t+1)} = x_i^{(t)} + \alpha \oplus \text{Lévy}(\lambda) \tag{6}$$

$$\text{Lévy} \approx u = t^{-\lambda}, \quad (1 < \lambda \le 3) \tag{7}$$

In the other hands, the step length s can be calculated by equation (8), where u and v are drawn from normal distribution as stated in Eq. (9). Standard deviations of u and v are expressed in Eq. (10). With fraction p_a, the CuS can effectively escape from any local entrapment. The global convergent property of the CuS algorithms has been proved and reported [9], respectively.

$$s = \frac{u}{|v|^{1/\beta}} \tag{8}$$

$$u \approx N(0, \sigma_u^2), \quad v \approx N(0, \sigma_v^2) \tag{9}$$

$$\sigma_u = \left\{ \frac{\Gamma(1+\beta)\sin(\pi\beta/2)}{\Gamma[(1+\beta)/2]\beta 2^{(\beta-1)/2}} \right\}^{1/\beta}, \quad \sigma_v = 1 \tag{10}$$

4. CONTROLLER DESIGN PROBLEM

The use of proportional plus integral plus derivative (PID) controller for industrial applications was first introduced in 1939 [15]. Due to ease of use and simple realization, PID controller has been increasingly employed in the control system over decades. The conventional control loop can be represented by the block diagram in Fig. 5. The controller receives the error signal, $E(s)$, and generates the control signal, $U(s)$, to regulate the output response, $C(s)$, referred to the input, $R(s)$ and to reject the disturbance signal, $D(s)$, where $G_p(s)$ and $G_c(s)$ are the plant and the controller transfer functions, respectively [16]. The theoretical function of the PID controller $G_c(s)$ is stated in Eq. (11) and, where K_P, K_I and K_D are the proportional, integral and derivative gains. While the theoretical function of the PIDD^2 controller $G_c(s)$ is stated in Eq. (12) and, where K_P, K_I, K_D, and K_{DD} are the proportional, integral, derivative, and double-derivative gains, respectively.

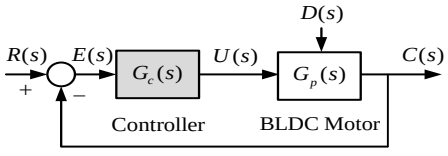

Fig. 5 Conventional control loop

$$G_c(s)\big|_{PID} = K_P + \frac{K_I}{s} + K_D s \tag{11}$$

$$G_c(s)\big|_{PIDD\wedge 2} = K_P + \frac{K_I}{s} + K_D s + K_{DD} s^2 \tag{12}$$

The CuS is applied to design an optimal PID and PIDD^2 controller in order to gain the optimal response of the BLDC system. The CuS-based PID or PIDD^2 controller design for BLDC system can be represented by the block diagram in Fig. 6, where $C(s)$ and $R(s)$ stand for actual and desired responses. The Sum-squared error (SSE) between $R(s)$ and $C(s)$ set as the objective function

F stated in Eq. (13) will be fed back to the CuS block to be minimized to obtain an appropriate parameters, i.e. K_P, K_I, K_D of PID controller and K_P, K_I, K_D, K_{DD} of PIDD^2 controller giving a satisfactory response.

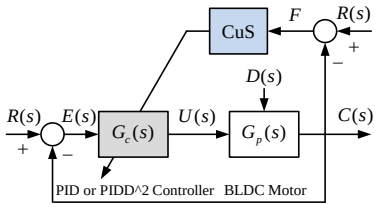

Fig. 6 CuS-based PID or PIDD^2 controller

$$\textbf{Minimize} \quad F = \sum_{i=1}^{N} \left[r(i) - c(i) \right]^2 \tag{13}$$

5. RESULTS AND DISCUSSIONS

5.1 BLDC Model Identification

The Open-loop responses of the BLDC system (Without Controller) at the speed of 1400 rpm can be obtained by experiment as depicted in Fig. 7. The plant $G_p(s)$ of the BLDC model can be identified via MATLAB/SIMULINK and CuS technique [17]. The Third-order transfer function model of BLDC motor obtained by this approach can be expressed in Eq. (14).

$$G_p(s) = \frac{0.04887}{5.72\times10^{-9}s^3 + 7.233\times10^{-6}s^2 + 0.002233s + 0.04147} \tag{14}$$

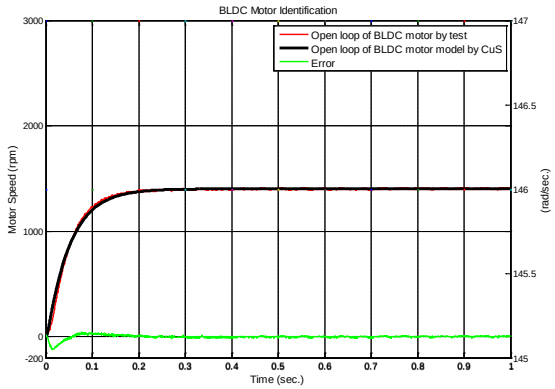

Fig. 7 Plots of BLDC model identification

5.2 Simulation Results

The CuS algorithms are coded by MATLAB run on Intel Core2 Duo 2.0 GHz 3 Gbytes DDR-RAM computer in order to design the optimal PID and PIDD^2 controllers of BLDC motor control system. The CuS search parameters are a priory set as follows: the numbers of nests n = 22 and the fraction p_a = 0.25. The maximum generation $MaxGen$ = 100 is then set as the termination criteria (TC). The boundaries of the PID and PIDD^2 parameters are set to perform the search space as stated in Eq. (15) and Eq. (16), respectively.

$$K_P \in [0, 20],\ K_I \in [0, 250],\ K_D \in [0, 0.1] \tag{15}$$

$$K_P \in [0, 120],\ K_I \in [0, 1000],\ K_D \in [0, 1],\ K_{DD} \in [0, 0.1] \tag{16}$$

The proposed design performs the search of 50 trials with different random initial solutions in order to obtain the best solution. After the search stopped, the optimal PID and PIDD^2 parameters are successfully achieved as declared in Table 2. Their corresponding speed responses are reported in Table 3, where t_r is rise time, t_s is settling time and M_p is maximum percentage of overshoot.

Table 2 Optimal controllers by CuS

parameter	PID controller	PIDD^2 controller
K_P	10.6899	108.4159
K_I	221.7578	800.8245
K_D	0.0097	0.3176
K_{DD}	–	0.0002

The system responses of BLDC motor speed control system with PID and PIDD^2 controller designed by CuS are depicted in Fig. 8. From Table 3 and Fig. 8, faster and smoother speed responses can be obtained by the controlled system designed by CuS.

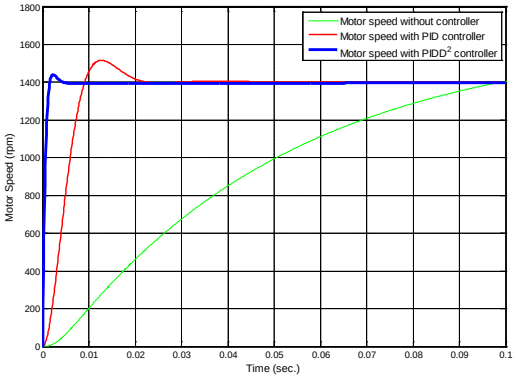

Fig. 8 System responses of BLDC motor

Table 3 Speed responses by CuS

Control Structures	Speed Responses			
	t_r(sec.)	M_p(%)	t_s(sec.)	e_{ss}(%)
PID	0.0090	8.33	0.0190	0.00
PIDD^2	0.0015	2.88	0.0029	0.00

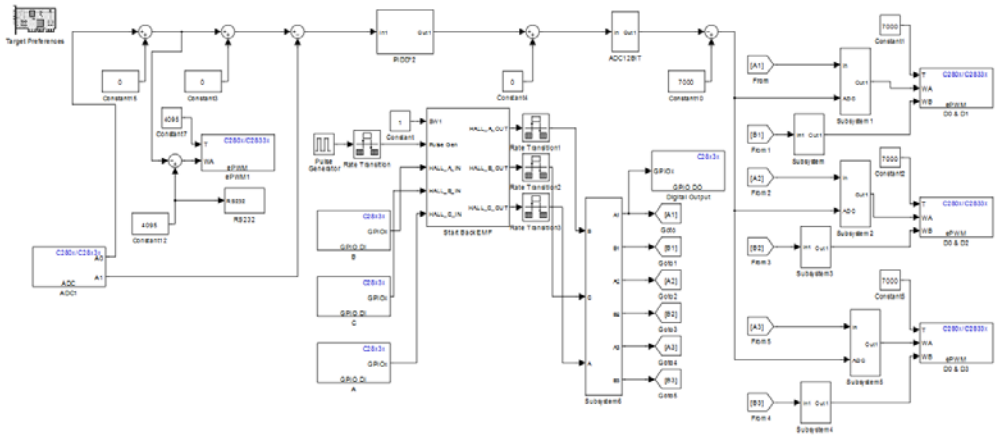

Fig. 10 Simulink block diagram of control system

Referring to Fig. 8, the system responses of the BLDC motor controlled system can be summarized in Table 3. From the Table 3, it was found that the CuS can provide the optimal PID and PIDD^2 parameters satisfying the constraints in Eq. (15) and Eq. (16). For the system responses in Fig. 8, the controlled system with PIDD^2 controller gives the better response than the parallel PID with shortest rise time and settling time as well as smallest overshoot, respectively.

5.3 Experimental Results

The BLDC motor speed control system is implemented by using the 100 watt, 1600 rpm BLDC motor as shown in Fig. 9. The speed of motor ranging from 0 to 1600 rpm can be measured by Tacho-generator of 0.825V/500 rpm. A speed transformed to be a voltage ranging from 0 to 3.3 V will be sent to A/D convertor. This scheme enables the user can adjust the speed of the motor by the power amplifier. The performance of implemented BLDC motor based on TMS320F28335 DSP [6] board with the MATLAB/SIMULINK [7] can be tested by sampling rate of 0.0001 sec.

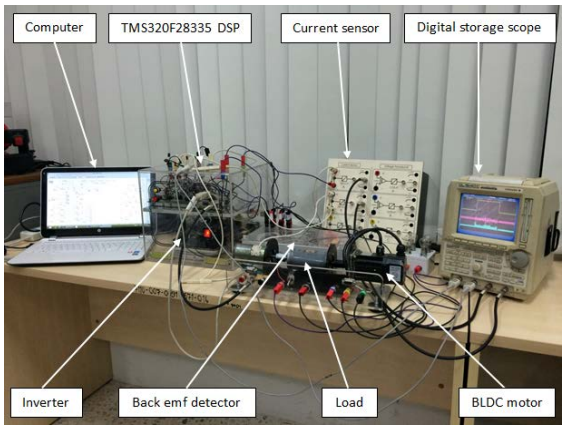

Fig. 9 Experimental setup

The measurements can be divided into two groups, the first is a step change of the speed reference at constant load torque and the second is a step change of the load torque at constant speed reference. Speed responses of the system via the step change from 700 to 1400 rpm of speed reference without and with rated load torque are investigated. The Simulink block diagram of control system is represented in Fig. 10. The Closed-loop responses of the system at 700 rpm and 1400 rpm can be simulated by such the simulation block diagram.

Supply phase voltage, phase current and DC current waveforms of BLDC motor at 700 rpm and 1400 rpm are measured by digital storage scope YOKOGAWA DL1540C in which the ratio of a current sensor is 2.424V/A.

For the PID control as the experimental results shown in Fig. 11 – Fig. 12, it was found that the speed responses of the BLDC motor controlled system from 700 to 1400 rpm both no load and full load conditions are very satisfactory. The phase current and DC current are distorted by noise which can be completely corrected by appropriated low-pass filters. Referring to Fig. 11 – Fig. 12, the entire performance of the BLDC motor system controlled by PID controller can be summarized in Table 4.

Table 4 Entire system performance by PID controller

Entry	System responses by PID			
	t_r (sec.)	M_p (%)	t_s (sec.)	e_{ss} (%)
No load	0.045	5.632	0.157	0.00
Full load	0.080	2.546	0.182	0.00

Referring to Table 4, it was found that at the speed from 700 rpm to 1400 rpm the system response reaches to desired steady state level. In case of no load, the step response declares values of t_r, M_p, t_s and e_{ss} almost as same as the those values obtained from simulation as can be observed in Fig. 8 and Table 3. However, t_r and t_s of the full load is a little bit slower than that of no load condition. Also, M_p of the full load is lower than that of no load condition. At both conditions, the BLDC motor system responses have no steady state error. Responses of load rejection by PID controller at 700 rpm and 1400 rpm can be observed in Fig. 13 – Fig. 14, respectively. It was found that the fast regulation responses once load torque is occurred can be successfully achieved by the proposed scheme.

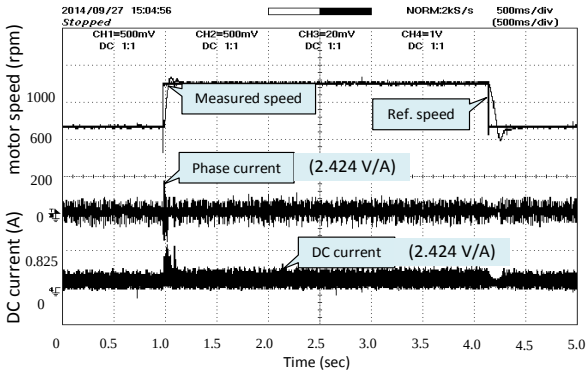

Fig. 11 Step change from 700 to 1400 rpm by PID controller (no load)

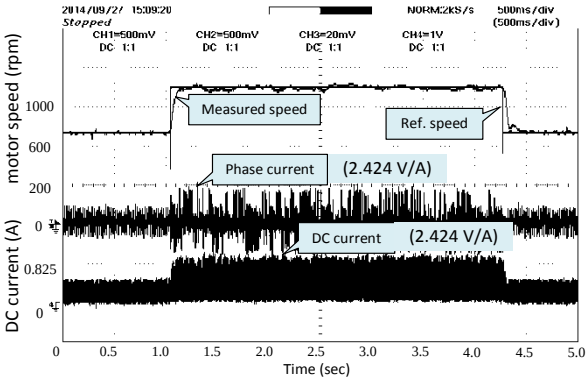

Fig. 12 Step change from 700 to 1400 rpm by PID controller (full load)

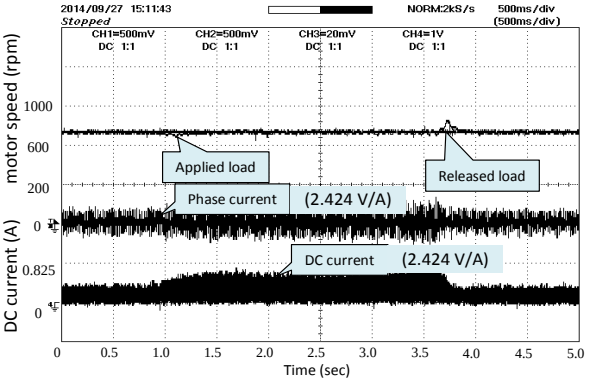

Fig. 13 Load regulation at constant speed of 700 rpm by PID controller

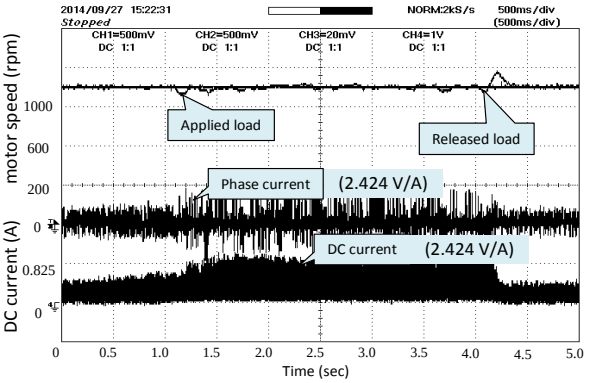

Fig. 14 Load regulation at constant speed of 1400 rpm by PID controller

For the PIDD^2 control as the experimental results shown in Fig. 15 – Fig. 16, it was found that the speed responses of the BLDC motor controlled system from 700 to 1400 rpm both no load and full load conditions are very satisfactory. The distortion due to unpredictable noise in phase current and DC current can be completely rejected by appropriated low-pass filters. Referring to Fig. 15 – Fig. 16, the entire performance of the BLDC motor system controlled by PIDD^2 controller can be summarized in Table 5.

Table 5 Entire system performance by PIDD^2 controller

Entry	System responses by PIDD^2			
	t_r (sec.)	M_p (%)	t_s (sec.)	e_{ss} (%)
No load	0.026	4.282	0.057	0.00
Full load	0.028	1.524	0.059	0.00

Like the PIDD^2 control when referring to Table 5, it was found that at the speed from 700 rpm to 1400 rpm the system response reaches to desired steady state level. In case of no load, the step response declares values of t_r, M_p, t_s and e_{ss} almost as same as the those values obtained from simulation as can be observed in Fig. 8 and Table 3. However, t_r and t_s of the full load is a little bit slower than that of no load condition. Also, M_p of the full load is lower than that of no load condition. At both conditions, the BLDC motor system responses have no steady state error.

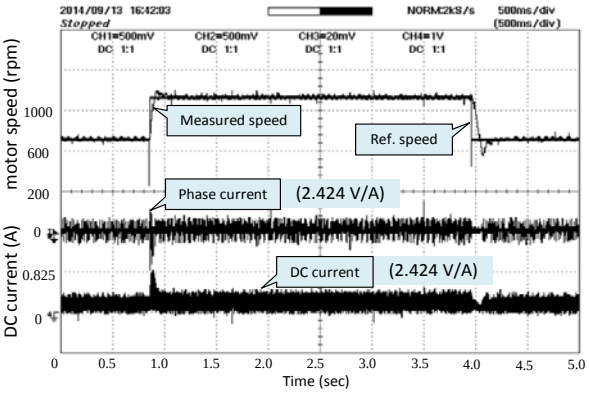

Fig. 15 Step change from 700 to 1400 rpm by PIDD^2 controller (no load)

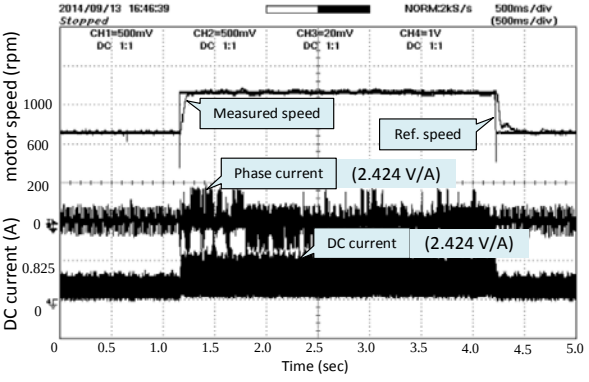

Fig. 16 Step change from 700 to 1400 rpm by PIDD^2 controller (full load)

Responses of load rejection by PIDD^2 controller at 700 rpm and 1400 rpm can be observed in Fig. 17 – Fig. 18, respectively. It was found that the fast regulation responses once load torque is occurred can be successfully achieved by the proposed approach. For overall system performance, it can be noticed that the BLDC motor speed control system by the PID and PIDD^2 controller designed by the CuS can provide very satisfactory responses in both no load and full load conditions as well as tracking and regulating responses in both speed levels, respectively.

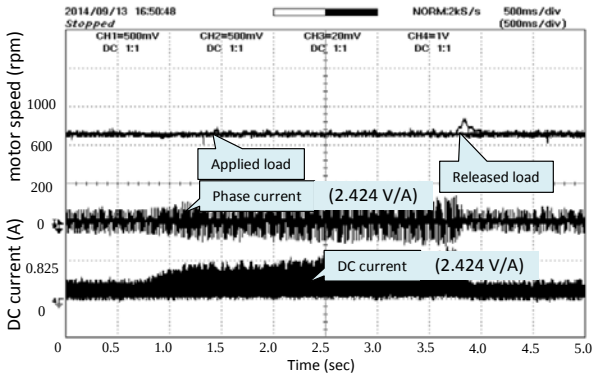

Fig. 17 Load regulation at constant speed of 700 rpm by PIDD^2 controller

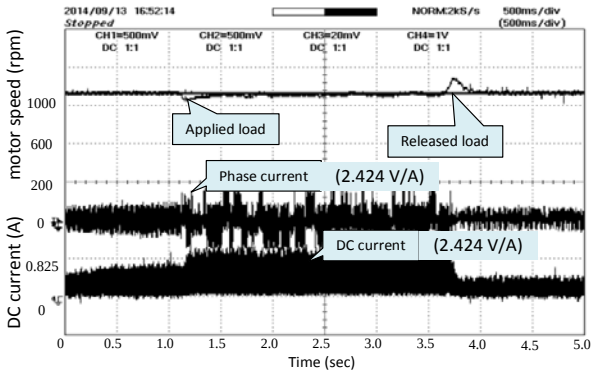

Fig. 18 Load regulation at constant speed of 1400 rpm by PIDD^2 controller

6. CONCLUSION

Designing an optimal PIDD^2 controller for the BLDC motor speed control based on the CuS has been proposed in this paper. By using Back EMF detection based on TMS320F28335 DSP board, the proposed control structure has been interfaced to MATLAB/SIMULINK. The CuS has been applied to design the PIDD^2 controllers to obtain the optimal tracking and regulating responses. Performance of the proposed system has been evaluated against the BLDC motor of 100 watt. As simulation results comparing with the PID and PIDD^2 controller, it was found that the controlled system with PIDD^2 controller provided better responses with shortest rise and settling times as well as smallest overshoot. As experimental results, it was found that the satisfactory tracking and regulating speed response of the BLDC motor can be achieved from 700 and 1400 rpm with no load and full load conditions. Experimental results strongly agree to simulation ones. This can be concluded that the proposed design approach and control structure are most efficient and alternative to control the BLDC motor effectively.

7. ACKNOWLEDGEMENT

The authors gratefully thank the laboratory support from Department of Instrumentation and Control Engineering, Faculty of Engineering, Pathumwan Institute of Technology (PIT), Bangkok, Thailand, 10330.

8. REFERENCES

[1] Yedamale, P., 2003, Brushless DC (BLDC) Motor Fundementals: AN885 Michrochip Technology Inc.
[2] Patel, V. K. S. and Pandey, A. K., Modeling and simulation of brushless DC motor using PWM control Technique, *IJERA*, Vol.3(3), pp.612–620.
[3] Alaeinovin, P. and Jatskevich, J., 2011, Hall-sensor signals filtering for improved operation of brushless DC motors, *IEEE Int. Conf. ISIE*, pp.613–618.
[4] Yun, S. Y., Lee, H. J., Han, J. H. and Lee, J., 2012, Position control of low cost brushless DC motor using hall sensor, The 6th *Int. Conf. ICEF*, pp.1–4.
[5] Lee, K. C., Jeong, Y. H., Koo, D. H. and Ahn, H. J., 2006, Development of a Radial Active Magnetic Bearing for High Speed Turbo-Machinery Motors, *SICE-ICASE*, pp.1543–1548.
[6] Texas Instruments, 2007, TMS320F28335, Digital Signal Controller.
[7] The MATLAB/SIMULINK, 1998, User's Guide, the Math Works Inc., Natick, MA.
[8] Glover, F. and Kochenberger, G.A., 2003, *Handbook of Metaheuristics*, Kluwer Academic Publishers, Dordrecht.
[9] Yang, X. S. and Deb, S., 2009, Cuckoo search via Lévy flights, *World Congress on NaBIC2009*, pp.210–214.
[10] Yang, X. S., 2010, Firefly Algorithm, Stochastic Test Functions and Design Optimization, Bio-Inspired Computation, Vol.2, pp.78–84.
[11] Sokira, T. J. and Jaffe, W., 1989, *Brushless DC motors: Electronic Commutation and Control*, Tab Books, USA.
[12] Krishnan, R., 2001, *Electric Motor Drives Modeling, Analysis, and Control*, Prentice-Hall International Inc., New Jersey.
[13] Krause, P. C., Wasynczuk, O., Sudhoff, S. D., 2002, *Analysis of Electric Machinery and Drive Systems*, IEEE Press, Piscataway, NJ.
[14] Acarnley, P. P., Watson, J. F., 2006, Review of position-sensor less operation of brushless permanent-magnet machines, *IEEE Trans. Industrial Electronics*, Vol. 53(2), pp.352–362.
[15] Minorsky, N., 1922, Directional Stability of Automatically Steered Bodies, *Journal of the ASNE*, Vol.34, pp.284.

[16] Katsuhiko Ogata, 1997, *Modern Control Engineering*, 3rd Prentice Hall International Edit.
[17] Kiree, C., Kumpanya, D., Tunyasrirut, S. and Puangdownreong, D., 2016, Parameter Identification of Brushless DC Motor by Intensified Current Search, *EMSES2016*, pp.111–115.

ARDUINO-BASED ROBOT AND MBLOCK: A HAND-ON STEM LEARNING EXPERIENCE FOR FRESHMAN'S PREPARATION PROGRAM

Preecha Sakarung[1)]
[1)]*Division of Electrical Engineering, Faculty of Engineering, Rajamangala University of Technology Suvarnabhumi, Suphanburi, Thailand Email: preecha.sakarung@gmail.com*

ABSTRACT: Nowadays, it is evident that robotic technology and STEM (Science, Technology, Engineering and Math) education are both becoming the mainstream teaching approach for modern engineering education. To get engineering freshmen interested in educational robotics as a part of an integrated STEM learning, a new freshman's preparation program was therefore developed exploiting Arduino board and mBlock programming, through which STEM subjects were able to be taught with fun while engaging the students throughout the process of learning. This developed Arduino-based robot is not only low-cost but easy to buy. In addition, an open-source graphic programming tool known as mBlock platform, which is rather comprehensible for those with limited background in programming was introduced. The teaching material has been developed in view of enhancing each electrical engineering student to gain an experience in designing process of an engineering task through Problem Based Learning (PBL). According to the latest 2018 survey conducted by twenty five freshmen, it revealed that class activity using robots with real-world applications helped improve freshmen's attitudes and interests towards robotic technology and STEM subjects. The survey result also emphasizes that a hand-on STEM learning with robotics is effective in various engineering's teaching settings.

1. INTRODUCTION

Educational robotics needs to become an integral part of many educational settings in engineering. It is simply because all engineers of the next generation are expected to be highly efficient in co-working with robots. In several engineering schools, robotics is now utilized as the key for courses requiring hands-on demonstrations such as computer programming, control system and so forth in accordance with the cognitive learning theory proposed by Jean Piaget, as revised by Seymour Papert [1].

Robotics, likewise, plays a crucial role in STEM education, in which science, technology, engineering and math are concurrently taught by illustrating connections between various disciplines, or through demonstration of the real-world application of various theoretical concepts. The STEM education philosophy is actually to promote the instruction of STEM concepts, principles, as well as techniques as an integrated teaching approach [2]. Hence, engineering design process is one of the popular teaching approaches used in engineering education which will be helpful for teachers who are designing STEM education programs. In addition, STEM education, claimed to be beneficial to students of all ages, greatly influences the instructional approach of the teachers who are interested in changing their students' learning style from passive to active learners.

For undergraduate engineering programs at RUS, the freshmen require a fundamental course to bridge their knowledge gained from high school to what is expected at the undergraduate level for the ease in their study. The session's length, still, is a major constraint since a single day scheduled for preparatory course was obviously not sufficient at all. Therefore, within such limited time, students' engagement is definitely the key success, and in order to engage them throughout the course as a part of an integrative learning approach, robotics can be used as an effective tool to do so.

To actively seek possible solutions to the set real-world problems, in this paper, both the problem based learning (PBL) instruction method and the engineering design process were exploited. With a simple assembly kit plus an open-source platform for robotic education, Arduino-based Robot along with mBlock programming, the students were able to construct real robots that could simulate behaviors of a three-wheel car. While STEM education has developed remarkably in its significance, there have been relatively few publications proposing or demonstrating practical lesson plans in sufficient details [3-4]. Another objective of this paper is hence to provide practical examples of STEM instructional materials.

2. METHODOLOGY

The major purpose of this paper is to promote the paradigm shift of both teachers' and students' classroom behaviors. In recent years, STEM education and robotic have been used as interesting tools to engage students through an exciting electrical engineering class activity [5]. In this study, therefore, STEM teaching approach and educational robotic materials designed particularly for RUS freshman's preparation program are shown.

2.1 Arduino-Based Robot

Each kit mainly includes an Arduino microcontroller board, which is probably the most popular open-source microcontroller board, sharing the code with wide range of applications on the world community development, a toy car's body, small dc electric motors, a motor's driver module, infrared distance sensors, as well as a Bluetooth wireless communication module.
The kit, shown in Figure 1, was developed basically from a three-wheel design, which primarily aims to provide simplicity and good balance while offering an easily accessible enclosure for the sensors and other electronic modules.

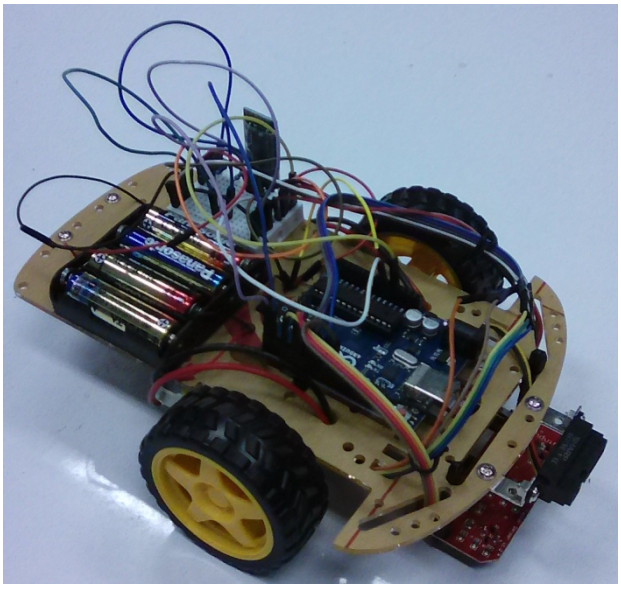

Fig. 1 Arduino-based robot

In addition, this open-source robotic education platform is to make the kit robust, reliable, and modular enough to accommodate a wide variety of applications with a low budget.

2.2 mBlock

Both mBlock and Scratch are handy open-source visual programming software. Scratch had been developed by MIT Media Lab Lifelong Kindergarten [6], and mBlock was then Makeblock's extension from Scratch software [7]. The additional difference of mBlock and Scratch is the ability in communication, both wire and wireless, with Arduino board. So, with this main feature, it allows us to control the education robotic in many different ways.
Below, the mBlock software version 3.4.11 is shown in Figure 2.

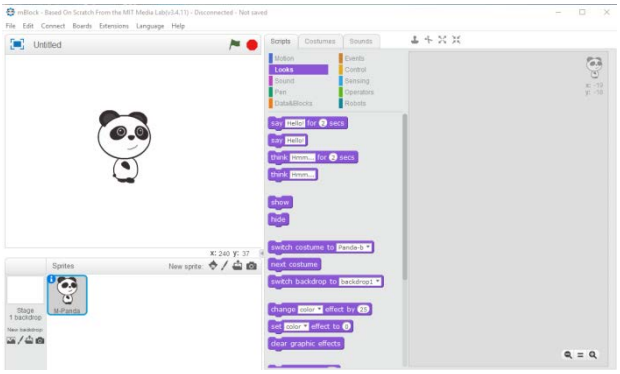

Fig. 2 The first page of the mBlock version 3.4.11

2.3 Freshman's Preparation Program

Problem Based Learning (PBL) was originally designed to replace the traditional lecture-based learning method in schools of medicine to actively engage students in self-directed and interdisciplinary learning through real-world applications [8]. In this study, starting with a real-world problem regarding the robot's movement, for instance, the students need to understand which skills, knowledge and processes are necessary in solving it.

Twenty-five first-year students are majoring in electrical engineering; physics, technology and mathematics were therefore selected to demonstrate the PBL approach with educational robotic. A one-day program was then tested because of the time constraint. The content and teaching schedule is presented below in Table 1. It also promotes student-centered learning approach, in which teachers act as facilitators of knowledge as they direct students to the information they need. This method is corresponding greatly with a learning theory known as constructivism, in which the students' active participation in problem solving leads them to construct their own knowledge by testing ideas which are based on their prior knowledge and experience and by applying them to a new situation [2]. In addition, student activity sheets are shown in Table 2 and Table 3 as examples.

Table 1 Freshman's preparation program schedules

Time	Contents
09.00 – 09.30	Introduction to mBlock software and obtain resources: tools, materials, supplies for the activity and group setting Objective: To learn how to use necessary tools and equipment
09.30 – 10.45	Demonstrate PBL: move the robot in square path Objective: To show how engineering design concepts are connected to real-world problem solving.
10.45 – 11.00	break
11.00 – 12.00	PBL 1: move the robot in circular path
12.00 – 13.00	lunch
13.00 – 14.00	PBL 2: move the robot in projectiles path
14.00 – 14.30	break
14.30 – 16.00	Communicating with others on stage

2.4 Engineering Design Process

Engineering design process can readily be integrated into PBL; meanwhile, STEM practices can be incorporated to enhance learning skills among the students in the field. The engineering design process can be described in brief as the seven iterative steps as follows; 1) identifying the problems and constraints, 2) examining the problems, 3) ideating or brainstorming solutions, 4) analyzing ideas and choosing the most appropriate solution, 5) building and creating a prototype, 6) testing and refining the created prototype, and finally 7) improving, redesigning, communicating and reflecting [9,10].

Step 1: Students will learn how to interpret information and write a concise but informative problem statement.
Step 2: Students will learn from related information in the literature. This step is a significant part in the process as it is to find as many possible solutions to the problems as one can. Students will be given applicable articles and challenged to read them and extract some pertinent data. They will also be given opportunities for discussions and

time to share insights. This will enhance their learning of the fundamental content.
Step 3: Students will learn how to make a plan, to think of different solutions to the problem, and to organize the ideas accordingly.
Step 4: Students will exercise their critical thinking skills and exploit the information gained during the activity in Step 2 to choose the best solution to the problem.
Step 5: Students, after they have chosen the solution, will begin to build the prototype of their design. This will not only put their construction skills to the test, but also help them realize how something designed on paper and in their minds can be built in the physical world.
Step 6: Students will test and evaluate their prototype. This is an essential step as students will see if what they built can perform accordingly to what they intended.
Step 7: Students will reflect on the design and determine appropriate ways that they can improve their design after testing and evaluating the prototype.

Table 2 Student activity sheet: movement of the robot

Task	Programming Description
Move Forward	Set speed of two motors at the same value and set logic signal for forward direction.
Stop	Set speed of two motors at zero value.
Move Backward	Set speed of two motors at the same value and set logic signal for backward direction.
Move Right 1	Set speed of left motors at positive value and set speed of right motors at zero.
Move Left 1	Set speed of right motors at positive value and set speed of left motors at zero.
Move Right 2	Set speed of two motors at positive value and forward direction. But speed on the left must be higher than the right.
Move Left 2	Set speed of two motors at positive value and forward direction. But speed on the right must be higher than the left.
Move Right 3	Set speed of left motors at positive value and forward direction. Set speed of right motors at positive value and backward direction.
Move Left 3	Set speed of right motors at positive value and forward direction. Set speed of left motors at positive value and backward direction.

Table 3 Student activity sheet: algorithm to move the robot in square path

Situation 1	Algorithms
The robot moves forward by about 10 cm.	Move forward ahead at the speed of 100 for 2 seconds. Then stop.
The robot moves right 90 degrees and moves forward by about 10 cm.	Move right at the speed of 100 for 2 seconds. Then stop. Move forward at the speed of 100 for 2 seconds. Then stop.
The robot moves right 90 degrees and moves forward by about 10 cm.	---------- ----------
The robot moves right 90 degrees and moves forward by about 10 cm.	---------- ---------- ----------

Remarks:
1) calculate the speed by using the distance between two points which is divided by duration time consume
2) left/right turning degree is the relationship between two variables which are speed (speed of motor depends on type of motor, remained battery power) and time of left/right turning

3. EXPERIMENT AND RESULTS

The preparation program for engineering students was scheduled as a one-day program (6 hours) in 2018. The ambiance of classroom activity was shown in Fig. 3, in which the student's collaboration was observed while each team tried to find the solution to the problem they were challenged. From the observation, additionally, the designed activity could help enhance student's creativity, self-direct learning, and other soft skills such as critical thinking, problem solving, communication, together with collaboration. Therefore, using PBL is one of the most effective ways not only to engage the students in STEM learning but to provide them with necessary basic skills to pursue their future career in electrical engineering.

Fig. 3 STEM classroom environment

In addition, the latest 2018 survey conducted with twenty-five freshmen revealed that most of them were impressed and satisfied with the preparation program, but the time for STEM subject was rather limited since it requires much longer time than the traditional lecture-based teaching does.

4. CONCLUSIONS

From both observation and interview, the results of this teaching experiment allowed us to make a number of important conclusions as follows:

Robotics in engineering schools can be considered a field of knowledge and technical creativity related to modern social trends where robots play a significant role.

Education robotic kits and instructional materials are both necessary to implement the technology in a regular classroom setting. The robotic kits and teaching materials can be exploited in teaching STEM subjects as it has been proven in this study. It was revealed that the motivation in learning increased when both theories and real-world problems were integrated as the tool and the challenge for the students.

Moreover, the budget is not the problem when the low-cost Arduino-based robot is used as the major part of the educational robotics. Furthermore, both mBlock and Scratch, which are open-source platforms functioning by visual style that eases the programming, are suitable for STEM education and PBL approach. However, in terms of software's qualifications, mBlock can be considered the best as it can communicate with Arduino board and it can run original Scratch files.

The result of this study showed that the power of educational robotics in engineering schools can lead to a successful and interesting classroom activity, but it does not limit to a particular field of science and technology.

12. REFERENCES

[1] Papert, S., 1980, *Mindstorms: Children, Computers, and Powerful Ideas*, McGraw-Hill, New York.

[2] Edward, M. R., 2013, Implementing Science, Technology, Mathematics, and Engineering (STEM) Education in Thailand and in ASEAN, IPST Report, May.

[3] Elena, O., Michael, E., and Ivan, I., 2015, Education robotics as an innovative educational technology, *Procedia, social and behavioral science 214*, pp. 18-26.

[4] Lukas, C. G., Agnes, C. K., Luke, H., and Ingmar, H. R., 2017, Liquid-handling lego robots and experiments for STEM education and research, *PLOS Biology*, pbio.2001413, pp. 1-9.

[5] Stephen, B., and Kevin, W., 2003, Robotics in the classroom, *IEEE. Robotics & Automation Magazine*, Sept., pp. 25-29.

[6] https://scratch.mit.edu/

[7] http://www.mblock.cc/

[8] Barrows, H.S., 1996, Problem-based in medicine and beyond: A brief overview. *New Dir. Teach. Learn.*, vol. 68, pp. 2-12.

[9] Corbett, K., and Coriell, J., 2013, STEM Explore, Discover, Apply - Elective courses that use the engineering design process to foster excitement for STEM in middle school students. *IEEE Frontiers in Education Conference.*, pp. 1108-1110.

[10] Nite, S., Margaret, M., Capraro, R., Morgan, J., and Peterson, C., 2014, Science, technology, engineering and mathematics (STEM) education: A longitudinal examination of secondary school intervention. *IEEE Frontiers in Education Conference*., pp. 1-7.

THERMOELECTRIC BASED POWER GENERATOR FROM SOLAR DRYING MACHINE

Sarayoot Thongkullaphat[1*)] and Worawit Inpan[1)]
[1)] *Department of Electrical Engineering, Faculty of Engineering and Architecture, Rajamangala University of Technology Suvarnabhumi, Nonthaburi 11000*
Email: sarayoot.t@rmutsb.ac.th

ABSTRACT: This paper proposed thermoelectric based power generator from solar drying machine, the thermoelectric is to generate an electrical power from the different temperature between inside and outside drying machine. The temperature ranges of the inside and outside machine are 85-90oC and 28-30oC, respectively. Thus, a study of energy conversion from different temperature to electric energy by the thermoelectric was considered. The experimental system was 5 series modules and 4 parallel set connections. It produced 21.89-23.15 watts of DC electrical power. This can prove that the heat of the inside machine from solar drying machine can be used for power generation for renewable energy household.

Keywords: Thermoelectric, Solar Drying Machine

1. INTRODUCTION

There are a lot of populations who increase members quickly, a lot of population nowadays. Electrical energy is used more and more for livelihood while they have limitedly. This result caused electrical energy shortage sharply in the industrial world sector to households. Many countries in the world create research and develop in renewable energy with geography style in each country to increase the amount of electrical energy that have enough and get the stability of energy.

Thailand is the part of all the countries which study and research in renewable energy for producing electrical energy such as wind energy, water energy, thermal energy, solar energy and then thermal energy which is from solar that researchers are interested in converting energy into electrical energy (Ning, Z. et al., 2014). Finding showed from industrial sector to households that use thermal energy in variety style to help processing and increasing the value of agricultural products. Thermal process uses energy more for moisture reduction of products that we can do it such as infrared drying, steamed, heater pump drying. The addition, drying with thermal energy from solar (Othman, M.H. et al., 2006) that is a part of technical popularly because they have low cost for producing than other and they are renewable energy. This article emphasize in using Solar Drying Machine (Fudholi, A. et al., 2010). It can receive radiation from solar which is shortwave radiation, it can penetrate through the glass and then when the short wave radiation touch with interior wall, it can absorb radiation and change to long wave which it can't penetrate through the glass and heat is collected in the dryer with high temperature and using other energy also. Researcher suggest that using heat in the dryer to change to electrical energy from thermoelectric equipment (Bimrew, T.A. et al., 2013) that is composed of semiconductor (n-type) which have seebeck coefficient with negative and semiconductor (p-type) which have seebeck coefficient with positive by using the difference of temperature at the seam of both. The results have electric potential difference at the seam and occur seebeck effect (Amir, Y.F. and Aliakbar, A. 2014). The heat side, it is collected heat with interior dryer that the temperature is about 85–90 oC and the another side, it is released heating with water (El-Adl, A.S. et al., 2018) that the temperature is about 28-30 oC. The both of them test with thermoelectric equipment for producing electrical energy to develop to be renewable energy.

2. RESEARCH METHODOLOGY

2.1. Solar Drying Machine

Solar drying Machine is the dryer which have glass to receive radiation from solar (Mustayen, A. et al., 2014) that is shortwave, it can penetrate through the glass and then when the short wave radiation touch with interior wall, it can absorb radiation and change to long wave which it can't penetrate through the glass and heat is collected in the dryer with high temperature and using other energy also. The result has less density and float on the top of the dryer and then through agriculture products that we desire dries. The drying is brought moisture to on the top of the glass and then it is released with ventilators.

Fig. 1 Solar Drying Machine

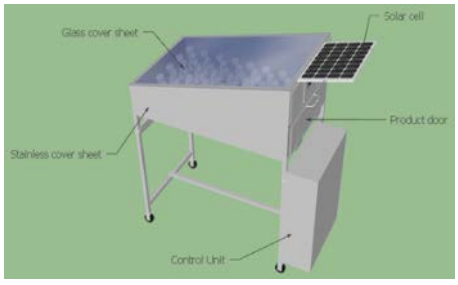

Fig. 2 Detail of Solar Drying Machine

This result affect less temperature and density of another temperature move to replace the heat transfer principle is shown in Figure 1 (Sharma, A. et al., 2009)

The feature of Solar Drying Machine is square shape and the side is high and the other side is low. The dryer size is 46 x 76 x 70 cm. (wide x length x high), the wall 2 layers which make from stainless. Inside the dryer has stainless steel grate 45 x 76 (wide x length) for put agriculture products. On the top, make from glass 5 mm. 15 degree and the below wall is punched for air circulation is shown in Figure 2.

2.2. Thermoelectric Modules

Thermoelectric Modules is material which change thermal energy to electrical energy 40 x 40 x 34 mm (wide x length x high), it can product the highest of electrical energy at 3.2 w, 4.8 v, 669 mA is Figure 3. It consists of semiconductor (n-type) which have seebeck coefficient with negative and semiconductor (p-type) which have seebeck coefficient with positive by using the difference of temperature at the seam of both. The results have electric potential difference at the seam and occur electricity in the circuit. Figure 4 and then electric potential difference at the seam and occur Seebeck effect (Seebeck, T.J. 1821).

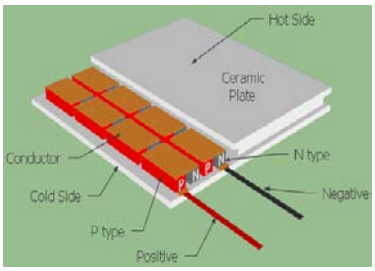

Fig. 3 Thermoelectric Modules

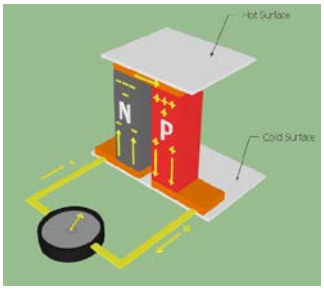

Fig. 4 Seebeck effect

When we write seebeck effect in the equation form of Relationship of difference between differential pressure and temperature as following.

$$\Delta V = S\Delta T \quad (1)$$

Where ΔV is the voltage difference (V), S is the seebeck coefficient (μV/K) and ΔT is the temperature difference (℃).

In the other hand, when we turn on the electric current through at the seam of conductor which occur heat that more or less dependent on flow of electricity. This phenomenon is called Peltier effect is shown in Figure 5.

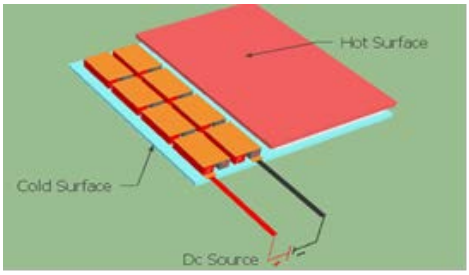

Fig. 5 Peltier effect

2.3. Cooling block

Cooling block is the material which make from aluminum that spread and cooling with the surface of Thermoelectric Modules 40 x 160 x 10 mm. (4 modules). The inside of cooling block consists of a lot of cooling fins by using pump, heat transfer and heat conduction for adjust the temperature to lower is shown Figure 6.

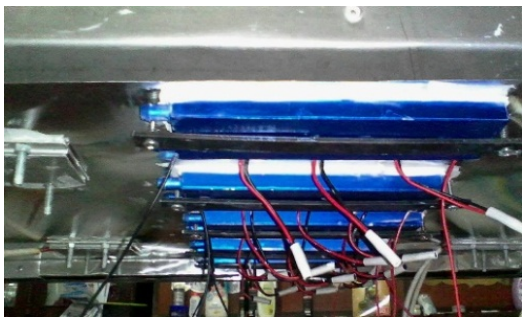

Fig. 6 Cooling block

2.4. Finding energy conversion efficiency

The capabilities of Thermoelectric have 3 attributes:

1. Able to conduct the high electricity and have heat from the low of electrical flow resistance.
2. Able to change thermal energy to electrical energy or change electrical energy to cooling energy.
3. Has low thermal conductivity for protecting thermal conductivity through material.

Finding the relation of principles of physics with thermoelectric material is calculated as (Hazama, H. et al., 2018):

$$ZT = (\sigma S^2 / K)T \quad (2)$$

Where ZT is dimensionless figure of merit of a thermoelectric material, S is seebeck coefficient of a thermoelectric material (μV/K), σ is electrical conductivity of a thermoelectric material (S/cm), K is thermal conductivity of a thermoelectric material (W/mK) and T is temperature of a thermoelectric material (°C).

$$\eta_{TEG} = \frac{T_h - T_c}{T_h} \; x \; \frac{(1+ZT_{ave})^{1/2} - 1}{(1+ZT_{ave})^{1/2} + (T_c / T_h)} \quad (3)$$

Where $\boldsymbol{T_h}$ is hot-side temperature of TEG (°C) and $\boldsymbol{T_c}$ is cold-side temperature of TEG (°C)

2.5. Experiment method

The data revealed that change of energy thermoelectric modules SP1848-27145 in electrical producing from Solar Drying Machine by using the differences of temperature at the conductors' seam and perform thermoelectric cycles 20 modules, each set connects series with 5 modules and then bring to be parallel 4 sets. After that constitute with thermal side of interior wall and cooling side from cooling with water through cooling set. And then bring Solar Drying Machine to test at the outdoor under condition: this experiment is tested at 8 a.m. – 5 p.m. for 9 hours per day for a week at the same state. We should record date during data logger trial every 1 minute by using Thermocouple Type K to connect with USB PC serial interface thermometer. We should record data from the changeable of electrical energy from UNI-T UT70C USB PC serial interface digital multimeter and then find the average of the difference of temperature for producing electrical energy, comparison voltage current and power output.

3. RESULTS

3. Experimental Results

This research showed that the transformation of thermal energy from Solar Drying Machine to electrical energy and set up measurement tool like Figure 7.

Fig. 7 Test and Record data

3.1. Temperature of the Solar Drying Machine and water cooling

The research showed that the temperature measurement from a part of Solar Drying Machine and water cooling which it transforms the thermal energy to electrical energy and trough data logger every 1 minute. The detail of the result revealed is shown table 1.

Table 1 Temperatures of Solar Drying Machine. Time (T), temperature at the hot-side of inner wall (T_h), temperatures the water inlet (T_c), Atmospheric temperature (T_a), temperature difference ($T_h - T_c$).

T (min)	T_h (°C)	T_c (°C)	T_a (°C)	$T_h - T_c$ (°C)
08:00	32.1	26.2	29.1	5.9
08:15	32.7	26.4	29.5	6.3
08:30	34	26.7	30	7.3
08:45	36.2	26.8	30.4	9.4
09:00	38.3	27	30.7	11.3
09:15	39.7	27.1	31.9	12.6
09:30	41	27.2	32.7	13.8
09:45	41.9	27.4	33	14.5
10:00	43.4	27.6	33.5	15.8
10:15	44.8	27.8	33.9	17
10:30	45	27.9	34.3	17.1
10:45	46.9	27.8	34.7	19.1
11:00	48.6	28	35.1	20.6
11:15	50.4	28.1	35.5	22.3
11:30	50.2	28.3	35.7	21.9
11:45	51	28.4	36	22.6
12:00	52.8	28.5	36.3	24.3
12:15	59.9	28.5	36.4	31.4
12:30	52.9	28.7	36.5	24.2
12:45	61.8	28.8	36.7	33
13:00	62.3	28.9	37	33.4
13:15	63.5	29	37.4	34.5
13:30	70.9	29.2	37.9	41.7
13:45	71.4	29.5	38	41.9
14:00	77.1	29.7	39.2	47.4
14:15	86.1	29.9	41	56.2
14:30	79.2	30.1	42.7	49.1
14:45	74.3	29.9	41.5	44.4
15:00	69	29.8	40.2	39.2
15:15	70.1	29.6	39.7	40.5
15:30	71.2	29.3	38.5	41.9
15:45	64.2	29	36.2	35.2
16:00	48.1	28.6	35.6	19.5
16:15	49.3	28.2	33.9	21.1
16:30	43.2	26.8	33.2	16.4
16:45	39	26.5	32.7	12.5
17:00	37.3	26.3	32.1	11

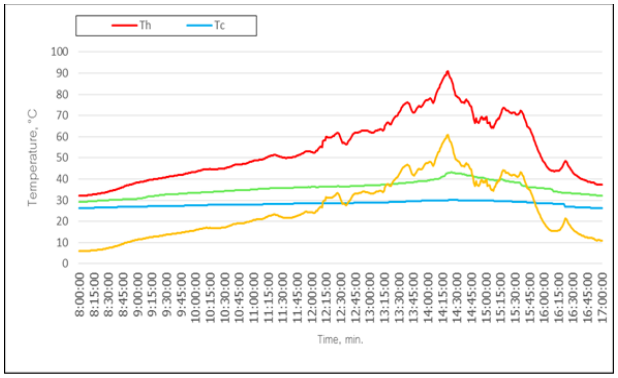

Fig. 8 Temperature dependence of hot-side of interior wall (T_h), temperatures the water inlet (T_c), Atmospheric temperature (T_a), temperature difference ($T_h - T_c$).

When we bring the result from data logger and then write it into the relation of temperature like Figure 8. The experiment showed that the difference of temperature (Th-Tc) change as follow as heat value which is collected inside the dryer and then. It has the maximum value is 2.00 – 2.45 p.m. and 45 - 60 °C. The heat side is absorbed from interior wall the dryer which has 85 – 90°C and the cool side is released the heat with water by heat extractor which has 28 – 30 °C respectively.

3.2. The comparison of voltage current and output power

The principles of the transformation of thermal energy from thermoelectric which is received solar radiation or short wave that can through the glass into interior and it is absorbed and changed to long wave or thermal energy which can't through the translucent material. Heat is collect in the dryer which is absorbed the heat and then transplant it to heat side of thermoelectric and the cool side from the heat release with water by using water pump for changing the less temperature.

This research is the measurement of electrical parameters from data logger every 1 minute and then brings the result to arrange like the result showed table 2.

Table 2 The output power of TEGs.

T (min)	V_{out} *(V)*	I_{out} *(A)*	P_{out} *(W)*
08:00	1.39	0.26	0.36
08:15	1.50	0.28	0.42
08:30	1.74	0.32	0.56
08:45	2.28	0.42	0.96
09:00	2.74	0.51	1.40
09:15	3.08	0.57	1.76
09:30	3.35	0.62	2.08
09:45	3.57	0.66	2.36
10:00	3.85	0.71	2.73
10:15	4.12	0.77	3.15
10:30	4.14	0.78	3.23
10:45	4.62	0.86	3.97
11:00	4.90	0.92	4.51
11:15	5.33	0.98	5.22
11:30	5.28	0.95	5.02
11:45	5.37	0.98	5.26
12:00	5.72	1.03	5.89
12:15	6.95	1.24	8.62
12:30	6.93	1.19	8.26
12:45	7.55	1.27	9.59
13:00	7.58	1.28	9.70
13:15	7.91	1.32	10.44
13:30	9.28	1.51	14.01
13:45	9.31	1.51	14.06
14:00	10.12	1.62	16.39
14:15	11.43	1.80	20.52
14:30	10.37	1.65	17.15
14:45	9.66	1.56	15.07
15:00	8.88	1.46	12.96
15:15	9.06	1.48	13.41
15:30	9.3	1.52	14.14
15:45	8.00	1.34	10.72
16:00	4.76	0.89	4.24
16:15	3.81	0.71	2.71
16:30	3.98	0.74	2.95
16:45	3.02	0.56	1.69
17:00	2.67	0.50	1.32

When we bring the result from data logger and then write it into the relation of electrical energy such as output voltage, current and power output as Figure 9 (a), (b) and (c) respectively.

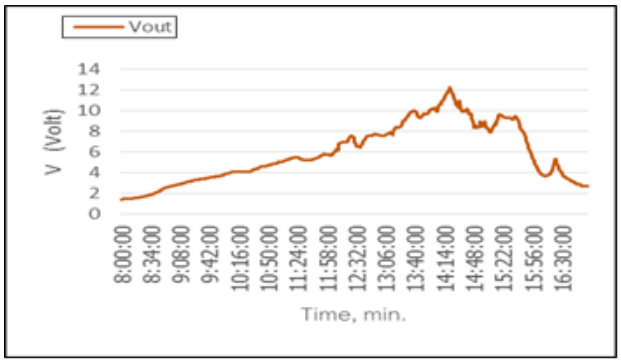

(a)

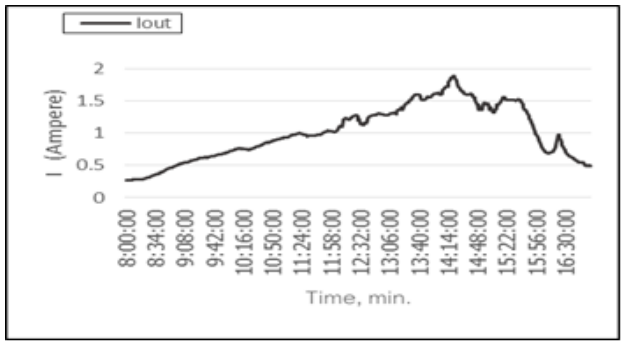

(b)

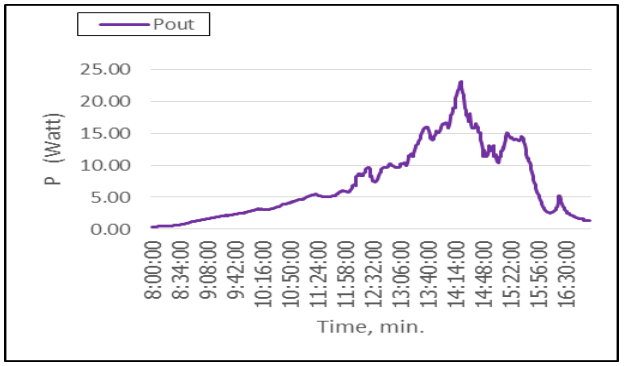

(c)

Fig. 9 (a) Variation of output voltage,
(b) variation of output current and
(c) variation of power output of TEGs.

The experiment showed that electrical power which thermoelectric products. They have different as temperature range that the electrical power of thermoelectric can product the highest electricity of heat temperature is 90.8°C, cool temperature is 30°C, power output 23.15 W, voltage 12.25 V, current 1.89 A are enough for using be renewable energy.

4. DISCUSSION

From the result of the comparison of the transformation of thermal energy to electrical energy of thermoelectric module with Solar Drying Machine, it found that electrical power output is product that has different as follow by heating which is collected into dryer each time and the performance of the transformation which the maximum duration is 2.21 p.m. power output 23.15 W.

5. CONCLUSION

The results indicated that the transformation of thermal energy of thermoelectric module SP1848-27145, cycles 20 modules with Solar Drying Machine. Each set connects series with 5 modules and then bring to be parallel 4 sets with the heat side of interior wall and the cool side from the heat releasing with water at 8 a.m. – 5 p.m. and has performance of the transformation of energy get power output 23.15 W voltage 12.25 V and current 1.89 A.

6. ACKNOWLEDGEMENT

This research was supported the power electronics laboratory in electrical engineering, by the Rajamangala University of Technology Suvarnabhumi (RMUTSB).

7. REFERENCES

[1] Amir, Y.F. and Aliakbar, A. 2014. Analysis of a symbiotic the rmoelectric system for power generation and liquid preheating. Applied Thermal Engineering, (71): 501-507.
[2] Bimrew, T.A. Xiaobing, L. and Jiawei, Y. 2013. Effects of temperature non-uniformity over the heat spreader on the outputs of thermoelectric power generation system. Energy Conversion and Management, (76): 533-540.

[3] El-Adl, A.S. Mousa, M.G. and Hegazi, A.A. 2018. Performance analysis of a passively cooled thermoelectric generator. Energy Conversion and Management, (173): 399 - 411.
[4] Fudholi, A. Sopian, K. Ruslan, H.M. Alghoul, M.A. and Sulaiman, M.Y. 2010. Review of solar dryers for agricultural and marine products. Renewable and Sustainable Energy Reviews, (14): 1–30.
[5] Hazama, H. Masuoka, Y. Suzumura, A. Matsubara, M. and Shin T. 2018. Cylindrical thermoelectric generator with water heating system for high solar energy conversion efficiency. Applied Energy. (226): 381 – 388.
[6] Mustayen, A. Mekhilef, and S. Saidur, R. 2014. Performance study of different solar dryers.Renewable and Sustainable Energy Reviews, (34): 463 – 470.
[7] Ning, Z. Takeru, M. Ryutaro, S. and Takashi, T. 2014. Development of a small solar power generation system based on thermoelectric generator. Energy Procedia, (52): 651-658.
[8] Othman, M.H. Sopian, K. and Yatim, B.D. 2006. Development of advanced solar assisted drying systems. Renewable Energy, (31): 703–709.
[9] Seebeck, T.J. 1821. Magnetische Polarisation der Matalleund Erze durch Temperature-Differenz. pp. 289-346 *In*: Abh. Akad. Wiss 1821, Berlin.
[10] Sharma, A. Chen, C. and Vulan, N. 2009. Solar – energy drying systems : a review. Renewable and Sustainable Energy Reviews, (13): 1185 – 1210.

A STUDY ON THE SHAFT SURFACE DAMAGE OF THE HATCH SHAFT USED BY TANK PILOTS

Dae Un Kim[1)], Kyung Seob Kuem[1)], In Taek Oh[1)], Sang Deuk Kim[1)], Byeong Jae Moon[1)]
[1)]Consolidated Maintenance Depot Republic of Korea Army, Changwon P.O.BOX92 57 Sangnam-dong Seongsan-gu Changwon-si Gyeongsangnam-do Republic of korea.
Email: akdong48@nate.com

ABSTRACT: This study in about the damage of the shaft surface of the hatch used when the pilot enters and exits the cockpit. We will investigate the cause of the surface damage of the hatch shaft and how to improve it. Due to frequent opening and closing of the hatch shaft, frictional force is generated by the contact of the two sleeve bearings installed inside. This damages the surface of the shaft and causes uneven wear of the shaft during long-term use. As a result of the study, structural problems were observed due to the concentrated load of the ball bearing on the contact surface of the shaft. A surface contact bearing is proposed as a countermeasure to disperse the concentrated load of the bearing. As a result, surface damage to the shaft is expected to be reduced.
Keywords: Shaft surface damage, Damage protection, Surface treatment, Contact bearing, Finite element method, Failure analysis.

1. INTRODUCTION

The tank`s pilot hatch serves as the gate of the pilot. The shaft of the opening and closing device is an important part which enables the opening and closing of the pilot hatch and the vertical movement and rotation of the hatch smoothly. The shaft is installed in the opening and closing device and consists of two sleeve bearings. Grease is used to reduce the frictional force of the bearings. The surface of the shaft is treated with S.F.L(Solid Film Lub) to prevent smearing and abrasion. However, due to the long use of the hatch, the coating of the shaft due to the bearing ball is damaged. In addition, due to the generation of rust due to the inflow of water during the field operation of the tank, the uneven wear of the shaft occurs, and the shaft is discarded and replaced with a new one.

Hardness of bearing is lower than HRC 60 because hardness of shaft of shaft is HRC 54~58. Therefore, during operation for a long period of time, the punching due to the static load of the bearing occurs, and the discarding rate of the shaft becomes higher. These problems shorten the exchange period of the opening and closing device axis and have the possibility of increasing the risk of accident of the pilot in the operation of the tank. Therefore, the purpose of this study is to find the solutions to the cause of damage of the shaft of the opening and closing device.

First, the function and properties of the surface treatment of the shaft were examined and it was confirmed whether the surface treatment affected the shaft damage. Then, the structural analysis was carried out to confirm the damage caused by the friction and static load of the ball bearing. Before the structural analysis, the stress distribution due to the bearing shape was compared and analyzed. In order to confirm the boundary condition, the surface analysis and the outer diameter of the shaft damaged part were measured. The purpose of this study is to identify the causes of shaft damage by confirming the surface treatment of the shaft, and to analyze the cause of direct damage to the shaft surface and to propose a solution.

First, it was confirmed that the surface of the shaft of the opening and closing device was the cause of the damage caused by the surface treatment. In addition, the cause anslysis of the damage caused by the friction and static load of the ball bearing was carried out by structural analysis and the difference of the stress distribution due to the bearing shape was compared and analyzed. In order to present the boundary conditions for F.E.A(Finite Element Analysis), the surface analysis and the outer diameter of the shaft damaged part were measured and the solution of the stress distribution and deformation of the shaft surface was suggested.

2. SHAFT OF OPENING AND CLOSING DEVICE

The shape of the opening and closing device of the pilot hatch is shown in Fig. 1 Vertical and rotary operation is performed during opening and closing operation to directly engage in opening and closing the door. In addition, when the trainer crosses the river by blocking the entrance of the tank, the inside of the cockpit is closed to prevent the inflow of water.

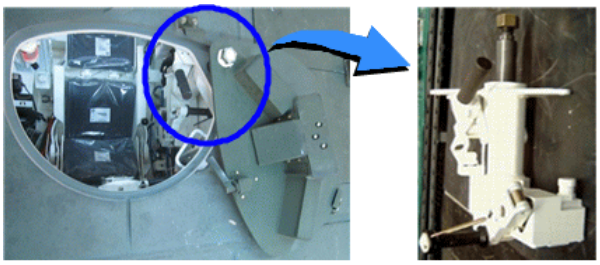

Fig. 1 Opening and closing device & Shaft

The material of the shaft is heat treated steel with surface hardness HRC 54~58 and it is treated with S.F.L. The basic properties are shown in Table 1.

3. S.F.L TREATING CHARACTERISTICS OF A SHAFT

S.F.L treating research has begun to address the problem of high temperature lubrication in the gas turbines of US navy aircraft in the 1950s. Since then, S.F.L treating has been actively researched and developed as applied to the space development plan since the 1960s. And it was put into practical use in advanced countries around this time. A representative example of this is as follows.

Table 1. Material properties of shaft

Standard	ASTM A332
Density	7.85g/cc
Modulus of elasticity	205Gpa
Hardness, Rockwell C	54 ~ 58

Unexpected damage occurred to 155mm flat springs of behind the battery at the time of the Vietnam War, and interest in application of the coating treatment was emerged. The reason for this was the rapid progress of corrosion and over abrasion in high-humidity tropical climates. The problem of corrosion and wear was a serious concern in the Navy. The shells on the shore are required to have new coating techniques due to the abrasion and corrosion caused by the salt contained in the air.

In order to solve all of these problems, we studied and analyzed the most effective surface treatment during water resistant surface treatment through corrosion test based on protective coating considering economy and compatibility. As a result, S.F.L treating has been proven to be the most effective coating treatment and has been used up to now.

To understand S.F.L treating, you first need to know the process. In order for this coating treatment to exhibit the best properties, the coating treatment process should be carried out after an appropriate pretreatment process. A suitable pretreatment film differs depending on the material and is a process for chemically and electrically forming a stable porous film on the surface of the material. S.F.L improves adhesion and adhesion life extension by increasing adhesion area. The process of S.F.L treating is shown in Table 2. As can be seen from the process of Table 2, the corrosion resistance is improved by the S.F.L treating after the phosphate coating treatment.

Table 2. Process of S.F.L treating

Basic Process (Steel Products)	Solvent Cleeaning → Masking → Sand air blow → P.C(Phosphate Coating) → Rinsing → Drying → S.F.L treating → Drying → Heat treatment

The characteristics of P.C and S.F.L treating are shown in Table 3.

4. INSPECTION OF SHAFT SURFACE DAMAGE

In order to precisely measure the surface state of the damaged shaft and the thickness of the surface film, a coating thickness test method(Eddy current test method) of KS D 0246: 2001 standard was applied; The reference surface is the portion without the coating. As shown in Table 4, the thickness of the coating in the operating range of the bearing was measured to be less than the reference value, and it was confirmed from the precision measurement that the friction damage occurred.

Table 3. Comparative analysis of characteristics

	P.C (Phosphate Coating)	S.F.L (Solid Film Lub)
Wear Resisting Quality	The first friction is peeled off	Abrasion resistance, Smooth friction
Use & Storage	Wearing during use and storage, repairing rust-oil remeval parts and application of antirust oil can be used for a long time.	It can be used for a longer time than P.C because it has its own waterproof and anti-rust effect.
Moisture content of surface	If water remains on the surface, water and rust preventive oil are separated and partial corrosion occurs.	Even if water remains on the surface, corrosion and waterproof effect are pervented and corrosion does not occur well.

Table 4. Measure the surface thickness of the damaged shaft

	Surface thickness measurement result		
Measuring section	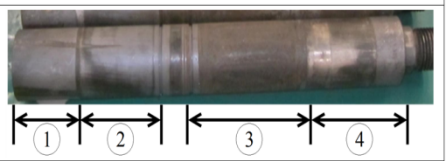		
Standard thickness (6 ~ 12㎛)	①,② 10.3 ~ 14.7㎛	③ 0 ㎛	④ 3.23 ~ 5.67㎛
Precision measurement of surface			

As a result of confirming the coating process of the shaft, it was confirmed that there was no problem in the S.F.L treating process. However, due to the long field operation, we could confirm the damage of the coating as shown in Fig. 2, and we could guess that the sleeve bearing was damaged due to ball damage. The cause of the surface damage of the shaft was supposed to be due to the ball stop load of the sleeve bearing.

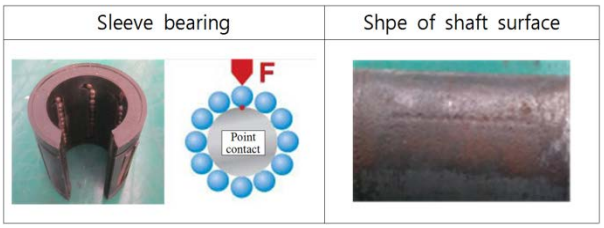

Fig. 2 Shape of shaft surface

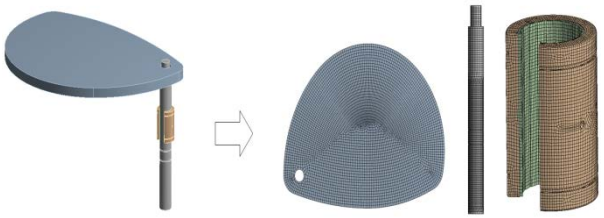

Fig. 3 3D Modeling of the opening and closing device

5. SHAFT MODELNG AND MECHANICAL PROPERTIES

Fig. 3 is a simplified representation of the actuator shaft of the pilot hatch, which is modeled in 3D with the shaft and bearing assembled. The position of the bearing is when the hatch is opened and the surface damage of the actual axis is serious. The material of the shaft is the SNCM 220 specified in the National Defense Code. This is nickel chromium molybdenum steel. The mechanical properties are shown in Table 5.

Table 5. The mechanical properties of shaft

Tensile Strength(Mpa)	1,226
Yield Strength(Mpa)	957
Quenching Temperature(℃)	843
Tempering(℃)	149
Carburizing(℃)	927

6. 3D MODELING FOR STRUCTURAL ANALYSIS

As shown in Fig. 4, the hexagonal and tetrahedral elements were used for grid generation to improve the convergence of the analysis. To increase the accuracy of the contact between the bearing and the shaft, the element was created with a size of 2mm.

7. STRUCTURAL ANALYSIS BOUNDARY CONDITION

The weight of the hatch is about 120kg, and an external force due to eccentricity exists. Because of this external force, we applied gravity and measured two axes diameters as shown in the Fig. 5 to simulate the shape of the surface impression of the shaft. For the minimum mean value of 0.02mm, forced displacement using a cylindrical coordinate system is applied and the model is simplified to shorten the analysis time.

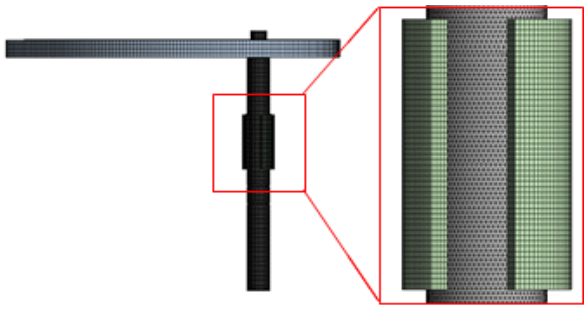

Fig. 4 3D modeling for structural analysis

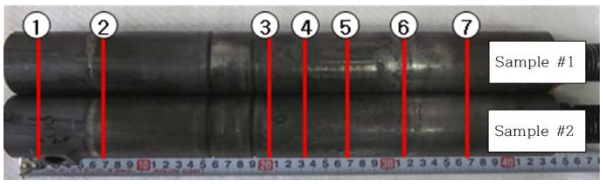

Fig. 5 Outer diameter measurement position

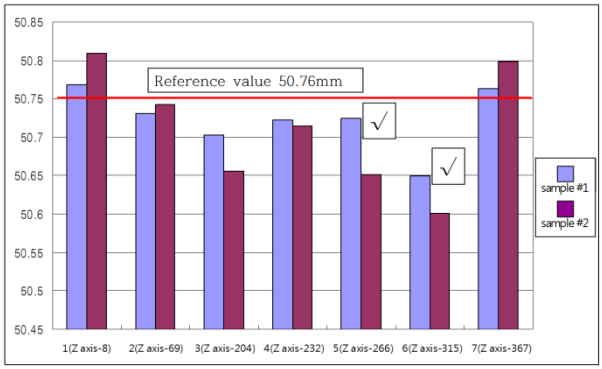

Fig. 6 Outer diameter measurement result value

A total of 7 external diameters were measured using CNC COORDIN ATE MEASURING. As a result, the measured value as shown in Fig. 6 was shown, and it was confirmed that the outer diameter was below the reference value in the measurement parts 5 and 6. It is confirmed that this is the contact area of the sleeve bearing due to the operation of the opening and closing device and that it is damaged by the concentrated load of the bearing ball. In the measurement part 3, damage by the ring and packing was confirmed.

However, this study does not cover ring and packing damage as a study of shaft surface damage by the opening and closing device operation. Fig. 7 shows the boundary conditions.

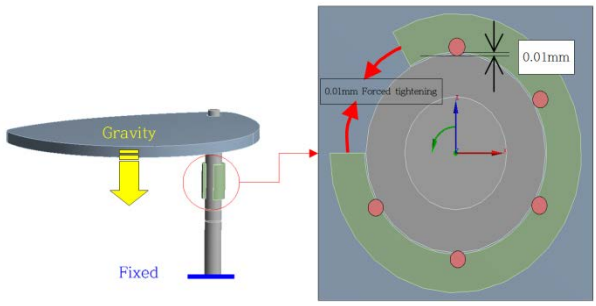

Fig. 7 Boundary conditions.

8. STRICTURAL ANALYSIS RESULT

Fig. 8 shows the contact pressure value through the stress analysis of the sleeve bearing. The contact pressure after applying the forced displacement of the sleeve bearing was calculated as 1764 MPa at maximum. As a result of comparing the analysis result with the damaged

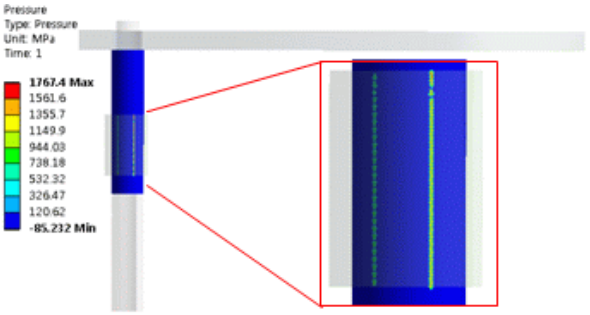

Fig. 8 Sleeve bearing contact pressure result

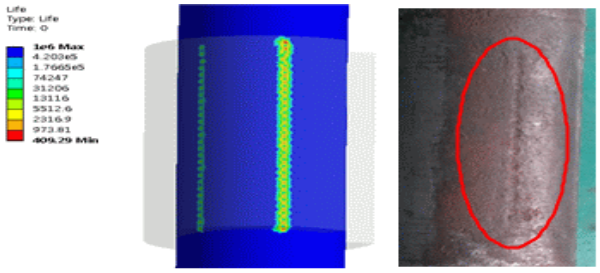

Fig. 9 Damage type simulation

$$\frac{\sigma_a}{S_e} + \frac{\sigma_m}{S_u} = 1$$

axis where the actual dent occurred, it is confirmed that the damage type is well simulated as shown in Fig. 9. The average stress was taken into account for the alternating loads and Goodman Equation was applied for the life calculation.

In the above equation, σ_a is the stress amplitude, S_e is the fatigue limit, σ_m is the mean stress, and S_u is the tensile strength. The fatigue life of the shaft was predicted by the forced displacement analysis using the cylindrical coordinate system. It is estimated to be about 41000 ~ 42000 Cycle, which is a good reference for life prediction when considering the operating time of 10 years.

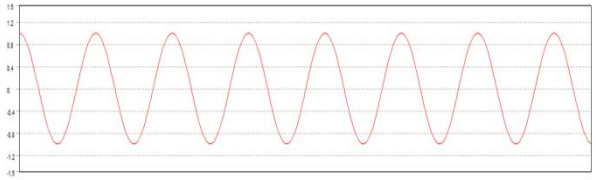

1. Constant amplitude load fully reversed

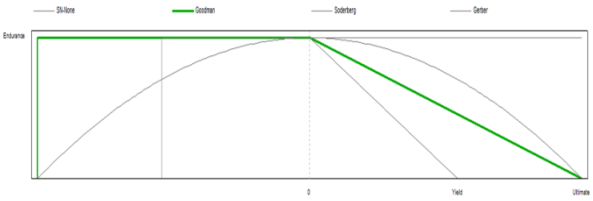

(b) Mean stress correction theory

Fig. 10 Fatigue evaluation condition

9. STREESS AND LIFE OF SLEEVE BEARING

Fig. 10 shows the curve for fatigue evaluation conditions, the alternating load was applied to the load. Actual experimental data tend to show between Goodman curve and Gerber curve, where Goodman is applied in fatigue life evaluation.

10. STUDY FOR PREVENT CONCENTRACTED LOAD

In order to reduce the stress, surface contact bearings were applied to the structural analysis under the same conditions. Fig. 11 shows the part where the surface contact bearing comes into contact with the shaft.

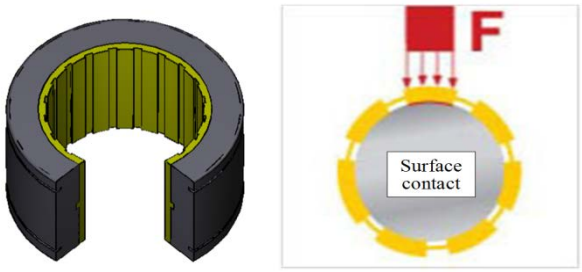

Fig. 11 Surface contact bearings

Fig. 12 shows the structural analysis results of the surface contact bearings, confirming that the stress is reduced. As a result of the structural analysis under the same condition as the sleeve bearing, it was found that the contact pressure of the region of interest was about 4MPa. It is confirmed that the stress reduction effect is about 400% higher than that of the conventional sleeve bearing. Through this structural analysis, the fatigue life and stress below the fatigue limit were predictive of the infinite life.

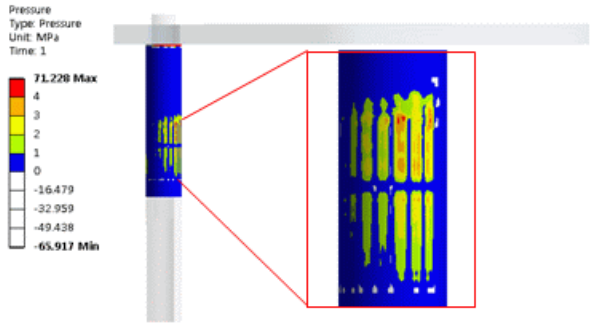

Fig. 12 Structural analysis results of surface contant bearings

11. CONCLUSION

We studied the causes of damages on the shafts of the opening and closing devices used by the trolleys and how to improve them. As a result of the study, it was found that there are many differences in the contact pressure due to the structural difference between the sleeve bearing and the surface contact bearings.

Surface damage of the hatch shaft is expected to be reduced by using surface contact bearings to prevent damage due to concentrated loads. In addition, chrome plating or spraying is applied to reuse of damaged shaft to improve the regeneration rate of surface treatment and to improve the problem of shaft damage in the case of water. This study will continue to carry out further research to prevent shaft damage.

12. REFERENCE

[[1] The report of surface treatment application for BIHO Gun ass'y in field condition, 2008.

[2]KS D 0246: "Method of Plating Thickness test(Eddy Current Type), 2001.

[3]Song,, S. H., Kim, S. D., Kim,, K. W., Stress Analysis at the Contact Boundary between the Work Roll and the Back-up Roll for a SmartCrown Roll Profile Shape, Transactions of Material Processing, Vol.24, No.3,2015.

[4] Bae,, M. W., Park, B. H., Jung,, H., A Study on Durability Characteristics for Plungers of Conventional Ceramic and Surface Modification by Power Coating Using High Velocity Oxygen Fuel Thermal Spary, Transactions of KSASE, Vol.24, No.3, pp.285-293, 2016.

[5] ANSYS, Theory Reference for ANSYS

An Experimental Study on the Heat Sink Temperature Distribution with Angle Change of 30 Watt LED Floodlight

Dae Un Kim[1)], Tae Hoon Kang[1)], Min Sik Choi[1)], Gwi Nam Kim[2)], Chung Seob Yi[3]
[1)]Consolidated Maintenance Depot Republic of Korea Army, Changwon P.O.BOX92 57 Sangnam-dong Seongsan-gu Changwon-si Gyeongsangnam-do Republic of korea.
Email: akdong48@nate.com
[2)]Suncheon Jeil College Gyeongnam National University of Science and Technology

ABSTRACT: This study was conducted to investigate the cooling characteristics of a heat sink such as a high efficiency LED floodlight in which cooling performance of the heat sink is one of the important factors in the lifetime of the LED. To study the effective cooling characteristics, we experimented with five installation angles. As a result, temperature distribution in 180˚ was high and 90˚ was low. 90˚ the reason why the temperature distribution is low is because the air passage is formed between the fins of the heat sink to facilitate the heat exchange with the atmosphere. The reason why the temperature distribution was high at installation angle 180˚, because the heat sink is facing the ground and the heat exchange with the atmosphere is slowed down.
Keywords: Heat sink, Cooling characteristics, LED Floodlight, Installation angles, Temperature distribution.

1. INTRODUCTION

LED is a light source for lighting, and it has a high efficiency of conversion of electric energy into light, so it can save energy and has a great effect on environment. Its life span is 25 times that of incandescent bulbs, which is a typical example of next generation light sources. LED has been attracting attention as a next generation high efficiency light source because it has high light conversion rate, long life, low power consumption and no harmful substance compared with existing light sources.

LEDs convert more than 80% of the supplied power to thermal energy. It is known that the temperature rise thus causes a shortening of the lifetime of the LED, and also causes a decrease in light output and a wavelength shift. Therefore, in the case of high-luminance and high-power lighting devices, such as security lamps and street lamps, which require tens to hundreds of watts of power, cooling technology for keeping the internal temperature at an appropriate temperature is becoming an important issue in order to secure luminous efficiency and reliability.

In order to maximize the energy saving effect, which is one of the major purposes of the LED industry, high efficiency, low cost and high reliability LED technology that can be supplied to consumers stably is indispensable. In addition to this, development of control system technology and heat dissipation technology that can maximize the advantages of LED are attracting attention as a new trend, and mechanism system technology that can compensate for the disadvantages of LED is newly emerging.

In this study, it was considered that the design, fabrication, installation position and angle of the heat sink are important for studying the high efficiency LED floodlight which has important heat dissipation performance. In addition, unlike normal LED front lamps that illuminate from top to bottom, the floodlight that illuminates high above the horizontal level is considered to be very important because the heat dissipation performance of the LED is directly related to the lifetime of the LED device.

Therefore, in order to study the effective heat dissipation performance of high-efficiency floodlighting, we investigate the heat dissipation characteristics to the atmosphere by heat conduction of the heat sink and experimentally study the heat transfer characteristics.

2. EXPERIMENTAL SYSTEM AND EXPERIMENTAL METHOD

In general, the heat transfer direction of the LED is shown in Fig. 1 As shown in Fig. 1, heat sink is conducted through the LED chip and the PCB, and heat is dissipated to the atmosphere. In this experiment, the heat dissipation characteristics according to the angle at which the LED floodlight is installed are examined. Also, the experiment was performed by applying the number of heat sink fin.

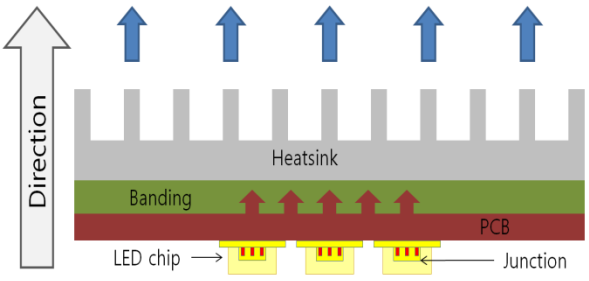

Fig. 1 LED thermal transfer structures

Fig. 2 shows a schematic diagram of an experimental apparatus for testing the heat dissipation characteristics of the heat sink. Fig. 3 shows the temperature measurement position of the thermocouple and a total of 4 measurement points are installed.

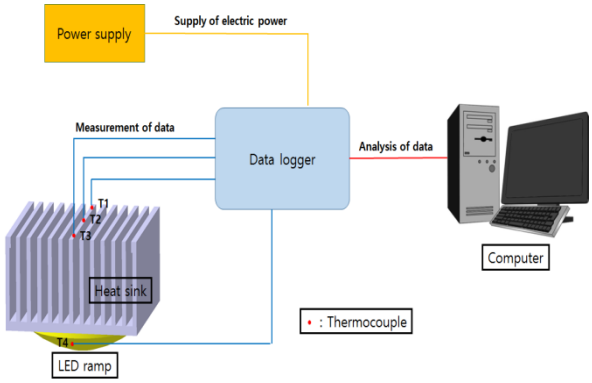

Fig. 2 Schematic of experimental setup

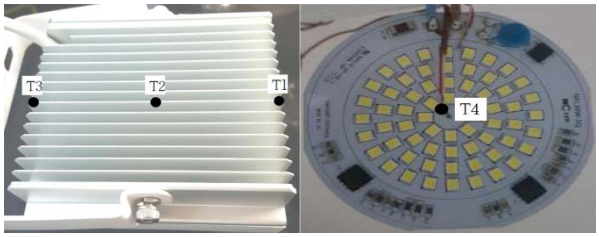

Fig. 3 Temperature measurement point.

The 30W LED floodlight used in this study has a PCB mounted on the heat sink and 64 of 0.5W LED devices on the PCB. The material of the heat sink is made of aluminum alloy, and in the case of cooling fins, it is made up of 15 pieces, and both sides are made of a support plate which can fix and install the light. Table 1 shows the specifications of the 30W LED floodlight.

Table 1. Specification of 30 watt LED

Item	Value	unit
Power dissipation	30	W
Forward Voltage	200 ~ 240	Vac
Forward Current	0.14	A
Power Facto	> 0.98	-
Luminous Flux	2,400	lm
Luminance Efficiency	80	lm/W
CCT(K), ±7%	3,000	K
CRI(Ra)	80	Ra
Number of LED	3528pkg.(0.6W) × 64	EA
Dimension	129 × 120 × 55(H)	mm
Weight	520	g
Operating Temp	-20 ~ 50	℃
Waterproof	IP65	-
Life Time	> 36,000	Hour
Heat Sink materials	Aluminum / anodizing	-

Fig. 4 shows a 3D model of the heat sink fin for the experiment. The number of fins except for the support plates at both ends was 15, 7, 3, and 0, and the distance between the fins was constant.

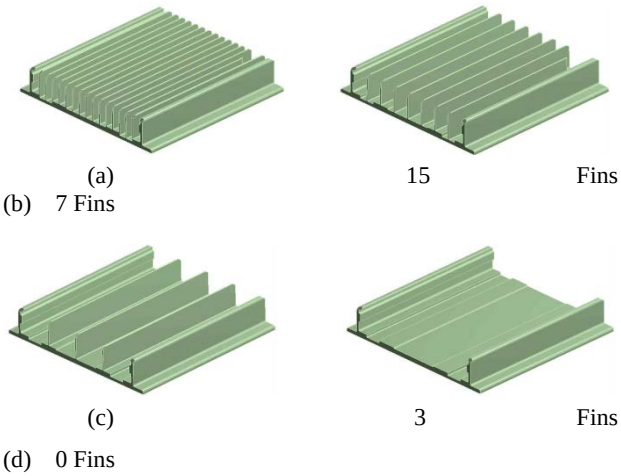

(a) 15 Fins
(b) 7 Fins
(c) 3 Fins
(d) 0 Fins

Fig. 4 Experimental parameter for the number of heat sink fins

Fig. 4 shows the experimental parameters for the number of heat sink fins. (a) shows the case of 15 fins before machining, and 7, 3, and 0 heat sinks were used as experimental variables. The spacing of the fins in each variable was the same. In addition, the fins on both ends are different from each other in thickness and shape because they are supported.

In order to study heat sink heat dissipation characteristics such as LED floodlight, heat radiation characteristics according to the angle of heat sink joint were experimented in parallel. The experiment angle was set to 0° when the LED light was perpendicular to the ground as shown in Fig. 5 and the heat sink joint angle was increased by 90°.

Fig. 5 Heat sink installation angle

3. EXPERIMENT RESULT AND DISCUSSION

When the heat sink angle is 0°, the LED light is directed downward, and the heat sink is tested for temperature distribution in the upward position. T1 and T3 are located at the edges of the heat sink. When the heat sink angle is 0°, the positions according to the angle changes are the same.

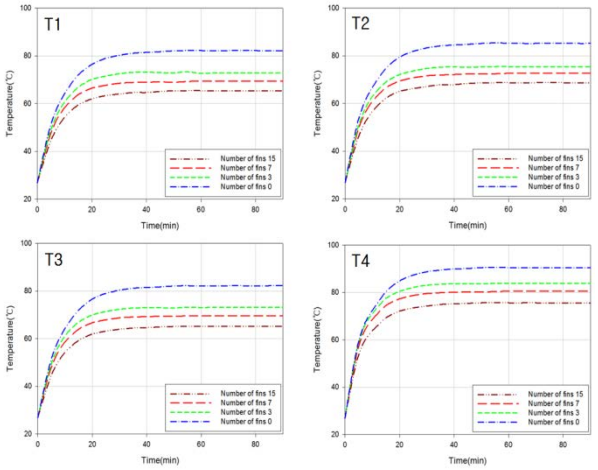

Fig. 6 Comparison of temperature distributions at heatsink angle 0°

Looking at the graph in Fig. 6, the temperature measurement positions of T1 and T2 are the edge of the heat sink, and in the case of T2, the center of the heat sink. The temperature measurement position of T4 was found to be higher than the temperature distribution of the other graphs at the center part of the PCB substrate where the LED chip is installed.

When we compare the temperature distribution graphs of T1 and T3, we can see that the temperature difference is almost similar to 1℃, because the height of the edge where the thermocouple is installed is almost same and the distance from the central part where heat is generated is almost same there was. Also, the temperature distribution of T2 graph shows that temperature is about 8~10℃ higher than that of T1 and T3.

In the temperature distribution graph of T4, it can be seen that the temperature of about 90.5℃ in the absence of fin is about 5.3℃higher than the temperature of the center of the heat sink of T2. Also, it was confirmed that the temperature is about 14.9℃ higher than that of 15 heat sink fins. It can be seen that the heat transfer area is larger when there is no fin, so the cooling performance is excellent and the temperature is low.

In the case of T1 and T3, the position of the temperature measurement part of the heat sink is the angle with the highest difference in the vertical direction up and down. Therefore, as shown in Fig. 7, it can be seen that the temperature difference is 3.5℃ in the case of the fins 15 and 4.3℃ in the case of the fin 0, that is, the temperature difference is larger than the case of the other angle. It can be seen that the fundamental law of thermodynamics is established as the characteristic that the heat moves from low to high.

In the case of T2, the temperature distribution due to the number of fins is large. When the temperature reached the steady state is compared with the case of 15 fins, when the temperature is 1.5℃, 5.7℃and 13.2℃, It was found that the cooling performance of the heat sink was very low. In the case of T4, the temperature distribution graph shows a pattern similar to the case of T2. This is because the heat generated by the LED chip reaches the T2 firstly through the PCB to the heat sink.

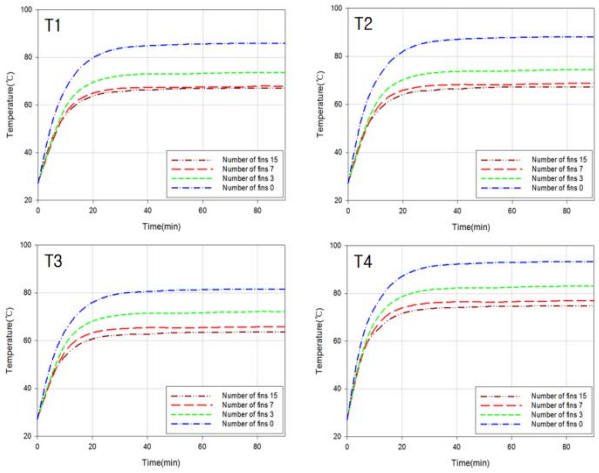

Fig. 7. Comparison of temperature distributions at heatsink angle 90°

In the case of T4 in which heat is generated, when the temperature reached the steady state of each fin is compared with the case of T2, it can be seen that the temperature difference is small at 2.2℃, 6.1℃, and 10.2℃. The cooling performance of the heat sink portion is better than that of the heat sink portion.

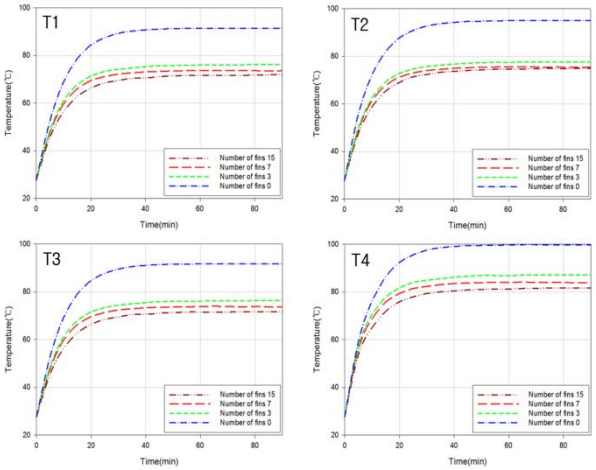

Fig. 8 : Comparison of temperature distributions at heatsink angle 180°

As shown in Fig. 8 above, the temperature distribution from T1 to T4 shows a higher temperature distribution than the previous experiment. This indicates that since the direction of the heat sink is directed toward the ground, the air after the heat exchange stays on the base of the heat sink, and the movement of the air is slowed to adversely affect the heat exchange.

In the absence of fins, it can be seen that the overall temperature distribution is high because heat generated from the LED chip is transferred to the base of the heat sink and heat exchange with the atmosphere is not performed properly. When the temperature reached the steady state when there was no fin, it was confirmed that the temperature was as high as 91.2℃ to 99.8℃.

In T1 and T3, we can see that the temperatures reached steady state are almost the same because the height of the temperature measurement part is the same as in the heat sink angle 0° experiment. In the case of T2, the heat generated from the LED chip is transferred to the center of the heat sink through the PCB substrate.

Therefore, in the case of T4, the cooling performance of the heat sink to the center of the PCB of the LED chip It is confirmed that the temperature distribution is high.

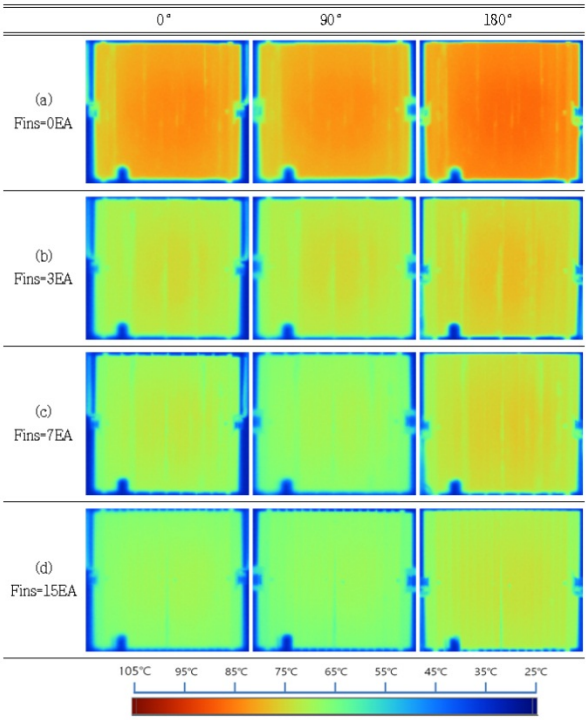

Fig. 9 : Comparison of thermal image on the heat sink after 60 minutes at angle

Fig. 9 shows the temperature distribution according to the number of heat sink fins after 60 minutes at each installation angle, using a thermal imaging camera. As shown in the Fig., when the number of heat sink fins is 15, the temperature distribution is the lowest, and as the number of heat sinks decreases, the temperature distribution tends to increase. Also, it was found that the highest temperature distribution is shown when the number of fins is zero.

Also, it can be seen that the temperature distribution is relatively low at the angle of 90, which shows that the heat exchange with the atmosphere is well done due to the formation of the air channel between the fin and the fin. The cooling performance is the best when the number of fins is 15, while the cooling performance is the worst when the number of fins is zero. Therefore, if it is 0, it is considered that it will affect the durability of the LED device due to generated heat.

4. CONCLUSION

The heat dissipation characteristics for the number of fins of 30W class LED floodlight were tested and the following results were obtained. At 180 ° where the position of the heat sink is directed toward the ground, the heat transfer is slowed and the temperature distribution is increased to adversely affect the heat dissipation characteristics. At 90° angle, Respectively.

Also, as the number of cooling fins of the heat sink decreases, the heat dissipation area decreases and the heat transfer is slowed, which results in a high temperature distribution in the heat sink.

5. REFERENCES

[1] Eo, I. S., "Analysis of the heat Radiation of LED Light Fixture using CF-design," Journal of the KAICS, Vol. 9, No. 6, pp. 1565-1568, 2008.

[2] Jang. H., Suh. J. S., Yi. C. S., " A Study on the radiant Heat Characteristic According to Type and Array of LED Lighting Heatsink, Journal of KSMPE, Vol. 12, No. 3, pp. 54-60, 2013.

[3] Cho. Y. T., "Heat Sink of LED Lights Using Engineering Plastics" Journal of KSMPE, Vol. 12, No. 4, pp. 61-68, 2013.

[4] Lee. S. H., Moon. H. J., Hue. S. B., Choi. S. D., "Development of LED Module Control-based PWM Current for Control of Heat-dissipation", Journal of KSMPE, Vol. 14, No. 6, pp. 129-135, 2015.

[5] Seo. J. K., Yu. Y. M., "A Study on the Thermal Characteristics Comparison of the LED Floodlight Luminaire using Vapor Chamber Manufacturing Technology", Journal of JIEIE, Vol. 29, No. 1, pp. 15-21, 2015.

[6] Han. M. S., Cho. J. U., "Durability Analysis through the Radiation of Heat of a Laptop",Journal of KSMPE, Vol. 15, No. 1, pp. 89-94, 2016.

[7] Lee. T. H., Choi. S. D., "Characterizations of Luminance for Varied LED Based Surface Lighting Designs", Journal of KSMPE, Vol. 15, No. 6, pp. 70-76, 2016.

DESIGN AND CONSTRUCTION OF ISOLATION TRANSFORMER FOR THE LED BACKLIGH TV

Prachum Utaprom[1)]
[1)] *Program in Electronics and Telecommunication Engineering field, Faculty of Industrial Education, Rajamagala University of Technology Suvarnabhumi, Suphanburi*

ABSTRACT: The study aimed at design and construction of isolation transformer can supply 5-35mA current for the LED backlight TV. In the design of 2 transformers. The connections parallel. The first input transformer voltage 180-220VAC and output transformer voltage 12VAC. The connection with the second transformer input voltage 12VAC and output transformer voltage 220VAC for protection of the leakage current while testing the LED can measure only one LED or more than one LED. And can wrong measurement electrode.
Keywords: Isolate transformer, LED backlight.

1. INTRODUCTION

Transformer is a device, the connection between different voltage systems. It will increase or decrease the voltage to suit the pay and power consumption Transformers are one of the most important devices in electronics. Failure or damage to the transformer will have a significant effect on the electricity consumption. Therefore, the transformer must have good performance in order for the power transmission system to be stable and reliable, the reliability of the transformer is shown, job loss.

In experimental radio and television engineering. Instruction is required to use an adjustable power supply with a power supply such as a coil or coil transformer. Used to test the worksheet. So if you are designing an alternator transformer. (Single phase transformer) with safe power supply is not harmful to the test of electrical equipment by the design and construction of the coil isolation transformer. 5-35mA power supply for LED Backlight Tester It is suitable for use because of the high power distribution. Easy to use, the cost is lower than the coil transformer with two separate coils and is lighter than the same coil. The LCD TV is a backlight display similar to a projector. The display of it really is black, but when the black light. It sends light through the display, allowing us to see people and colors. Adjusting the brightness of it is to adjust the brightness is very bright.

This research presents the design of single phase transformers by estimating the parameters of the coils and the coils. Influence of coil resistance and magnetic wire strength. This results in losses in conductor coils, an important variable of the transformer optimization. The scope of construction of the Insulation transformer the second input voltage is 180-220VAC input voltage output 12VAC per second transformer input voltage 12VAC output 220VAC output for the LED backlight LCD TV.

2. METHODLOGY

2.1 Single Phase Transformer

Transformers are electrical devices that change the voltage level. The transformer structure consists of

1) Core of the transformer is a square, hollow central. Mostly, it uses a thin sheet of thin steel. The coil of the steel core is responsible for combining the magnetic force from the primary coil. To induce current in the secondary coil.

2) The primary coil acts as a power supply from an alternating current source. In order to convert the voltage level.

3) Secondary Coil is a power supply unit that converts the level. Pay to load the structure of a single phase transformer (2 coils) is shown in Fig. 1.

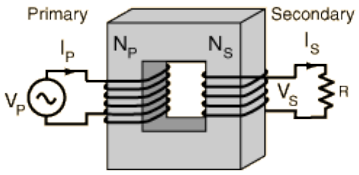

Fig. 1 Structure of single phase transformer

2.1.1 Principles

Primary coil when connected to AC supply source. There is a current flowing in the primary coil. This results in a magnetic field in the core. Faraday's Law and Lenz's Law have led to the induction of a primary coil, which causes the voltage opposite the source (e_p) and the induction Secondary coil lead The induction voltage (e_s) and current (i_s) flow to the connected load the transformer operating principle is shown in Fig. 2.

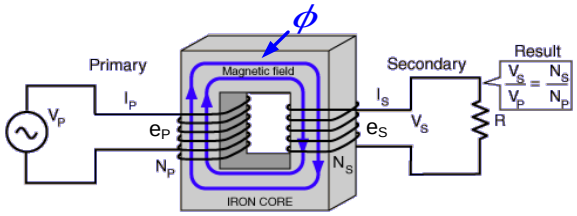

Fig. 2 Transformer operation principles

In case of transformer is ideal No magnetic resistance in the core, from the Faraday rules and the rules of the lens. The relationship is as follows.

$$V_p = e_p = N_P \frac{d\phi}{dt} \quad (1)$$

$$V_S = e_p = N_S \frac{d\phi}{dt} \quad (2)$$

Will get $$\frac{V_P}{V_S} = \frac{-N_P \frac{d\phi}{dt}}{-N_S \frac{d\phi}{dt}}$$

When V_p = Primary Voltage
V_s = Secondary Voltage
e_p = Primary Induced Voltage
e_s = Secondary Induction Voltage
I_p = Primary electricity
I_s = Secondary electrical current
N_p = Number of cycles of primary leads
N_s = Number of cycles of secondary leads
ϕ = Magnetic strings

From equation (1) and (2) The relationship of the equation is the ratio of the transformer. (Turn ratio : a) This is related to the voltage and current of the coil.

Will get $a = \frac{V_P}{V_S} = \frac{N_P}{N_S}$ by $\frac{d\phi}{dt} \neq 0$ (3)

Sum of electromagnetic force) mmf (in clockwise direction, the value is zero. ($mmf_p = I_pN_p$). Is the primary electromagnetic force and ($mmf_s = I_sN_s$) the secondary electromagnetic force of this relation is expressed as:) 4(

$$\sum mmf = 0 \quad (4)$$

$$mmf_p + mmf_s = 0 \quad (5)$$

When replacing the primary and secondary electromagnetic forces in equation (5), the ratio of the current to the number of coils of the coil is given by equation) 6) ,(7(

$$I_pN_p = I_sN_s$$

$$\frac{I_P}{I_S} = \frac{N_P}{N_S} \quad (6)$$

$$a = \frac{N_P}{N_S} = \frac{I_s}{I_p} \quad (7)$$

2.1.2 Power loss in transformer

The power losses occurring in the transformer are as follows.

- Core loss is the loss of power due to the flow in the core and the results of the Hysteria.
- Copper Loss is the power lost due to the resistance in the coil.

2.1.3 Equivalent Circuit

1) Equivalent Circuit in ideal way

Is the equivalent circuit is not worth the magnetic resistance. Do not consider the power loss in the transformer, can be shown in Fig. 3.

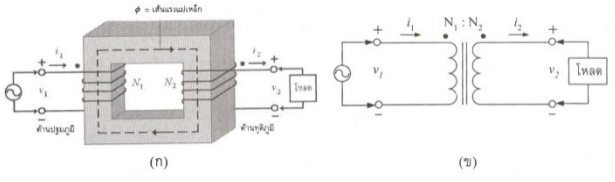

Fig. 3 Equivalent circuits in ideal way

(2Equivalent circuits in laboratory

Is the equivalent circuit considering the power lost in the transformer, magnetic induction inductor To make the magnetic core create a magnetic field and the effect of the loss of the magnetic force (Leakage Flux), because the magnetic force in the air instead of the magnetic axis.

The equivalent circuits in laboratory of the transformer are shown in Fig. 4.

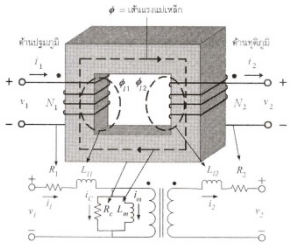

Fig. 4 Equivalent circuits in laboratory

When L_{l1}, L_{l2} Is Inductance is due to magnetic force loss lines.
L_m Is magnetic induction
R_1, R_2 Is the resistance in the coil
R_c Is the resistance in the iron core

In general, the design of the transformer is L_m very large so that the magnetizing current is less than the load current of the transformer.

2.1.4 Transformer Performance

The efficiency of the transformer can be obtained from

Performance = $\frac{\text{Secondary}}{\text{Primary Electrical coil}}$

$$\eta = \frac{P_{out}}{P_{in}} \quad (8)$$

$$= \frac{P_{out}}{P_{out} + P_{Loss}}$$

$$= \frac{P_{in} - P_{Loss}}{P_{in}}$$

3. DESIGN OF ISOLATION TRANSFORMER

3.1 Transformer calculation

Transformers are ideal when considering the ideal transformer (Ideal Transformer) with three conditions.

1(Do not consider the resistance of the coil.
2(Do not consider the magnetic force leaking line and the loss in the magnetic axis.

3(Determine the maximum permeability of the steel core.

3.2 Parameters for Transformer Design

This research is the single phase transformer, rated currents 5-35mA, 220 /12VAC power frequency 50 Hz (Hz). Fig. 5 shows the actual transformer and cross section of the prototype transformer and Table 1 shows the size and parameters of the main area. Cutting of conductor coils Number of coils of primary and secondary conductor the cross section of primary and secondary conductor wire.

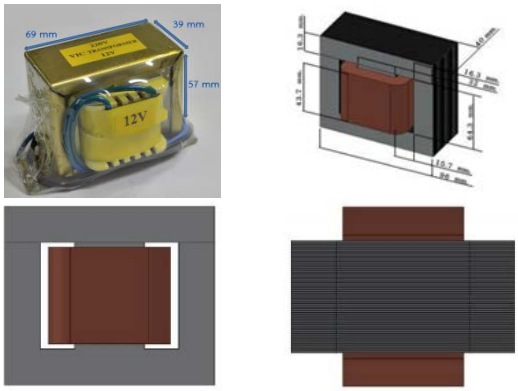

Fig. 5 Transformer and transformer prototype transformer

Table 1 Dimensions and Parameters of Transformer Master

parameter	Size
Steel core thickness (mm.)	39
Number of coils of primary coil (round)	950
Number of coils of secondary side (round)	80
Area of primary winding (square meter)	4.570×10^{-7}
Secondary winding area (square meter)	1.102×10^{-6}

3.3 Design of the isolation transformer

Design of isolation transformer It must be designed to suit the required voltage level, the input voltage varies between 180-220VAC, the output voltage is 12VAC and the discharge current must not be less than the primary coil current of the isolation transformer show in Fig. 6.

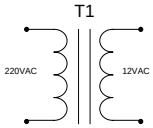

Fig. 6 The isolation transformer

3.4 The connect to 2 the isolation transformer.

The connect to the isolation transformer by using two transformers. Parallel by the first to input voltage is 180-220VAC output voltage 12VAC output to the second transformer. Input voltage 12VAC output 220VAC output to prevent leakage to the power supply, use while testing the LED. Measure the tube or measure the tube is not the tube does not break.

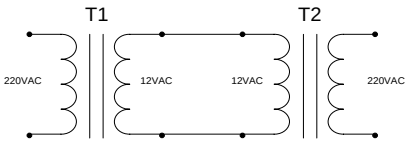

Fig. 7 The connect to 2 the isolation transformer

3.5 Voltage Supply Design

A constant DC voltage generator, to use for electricity supply for LED backlight testers, LCD TVs. The circuit will follow the picture.

Can calculate the resistor value, by setting the current to 20mA by using Ohm's law to calculate.

$$E = IR \quad (9)$$

Therefore $R = E/I$

The value of the formula E is derived from the direct current voltage measurement.

Let's say 290VDC.

$I = 20mA$

So that $R = 290/20mA$

$= 14.5K\Omega$ Use a resistor $15K\Omega$

Resistance value of resistor value we can calculate it. The 3W current rating is still valid, the resistor will be hot if we use one or less LEDs but if a lot of LEDs, the resistance of the resistor will be much lower.

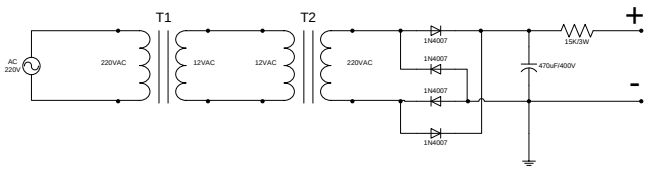

Fig. 8 LED backlight test circuit.

4. RESULTS

4.1 Test of impedance the isolation transformer

This is a test of the impedance of the isolation transformer to compare the input impedance versus the output impedance while not connected.

Table 2 Test results of transformer impedance the isolation transformer (Not circuit)

The isolation transformer	Resistance (measured)
Primary winding	75Ω
Secondary winding	600Ω

4.2 Test of voltage supply in unloaded condition (Not LED)

This is a test to see the output voltage level versus the input voltage in the unloaded state show in Fig. 10.

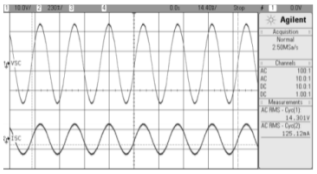

Fig. 9 Characteristics of voltage and current dimensions of the isolation transformer

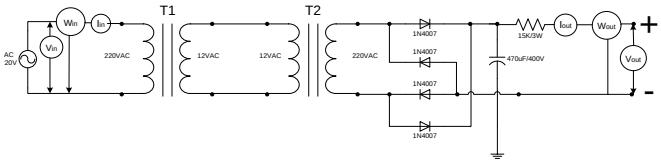

Fig. 10 Test the voltage supply in unloaded state. (Not LED)

Table 3 Test results of the unloaded voltage circuits. (No LED)

V_{in} (V)	I_{in} (A)	P_{in} (W)	PF_{in}	V_{out} (V)
180	0.10	10	0.75	180
190	0.11	10	0.75	192
200	0.12	10	0.75	208
210	0.18	10	0.75	215
220	0.30	14	0.75	290

4.3 Test of load voltages under load condition (Connect the LED chip)

This is a test to see the voltage level, the output voltage, and the input voltage and loss in load condition show in Fig. 11.

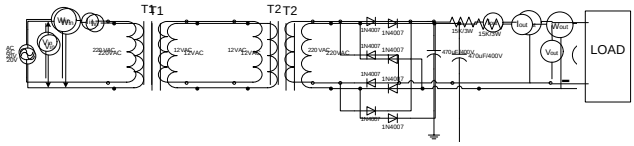

Fig. 11 Voltage Test in Loaded Condition LED Chip Connector SMD 3V

Table 4 Test results of the load-carrying voltage circuits. (Connect single LED SMD 3V)

V_{in} (V)	I_{in}(A)	P_{in}(W)	PF_{in}	V_{out}(V)	I_{out}(A)	P_{out}(W)	PF_{out}
180	0.09	16.20	0.75	180.20	0.12	21.62	0.99
190	0.09	17.10	0.75	192.50	0.12	23.10	0.99
200	0.10	20.00	0.75	208.56	0.12	25.02	0.99
210	0.10	21.00	0.75	215.28	0.12	25.83	0.99
220	0.12	26.40	0.75	290.00	0.12	34.80	0.99

Table 5 Test results of the load-carrying voltage circuits. (Connect 30 LED SMD 3V)

V_{in} (V)	I_{in}(A)	P_{in}(W)	PF_{in}	V_{out}(V)	I_{out}(A)	P_{out}(W)	PF_{out}
180	0.15	27.00	0.75	180.20	0.18	32.45	0.99
190	0.15	28.50	0.75	192.50	0.18	34.65	0.99
200	0.18	36.00	0.75	208.56	0.18	37.54	0.99
210	0.19	39.90	0.75	215.28	0.19	40.90	0.99
220	0.20	42.00	0.75	290.00	0.19	55.10	0.99

Table 6 Test results of the load-carrying voltage circuits. (Connect 60 LED SMD 3V)

V_{in} (V)	I_{in}(A)	P_{in}(W)	PF_{in}	V_{out}(V)	I_{out}(A)	P_{out}(W)	PF_{out}
180	0.15	27.00	0.75	180.20	0.18	32.43	0.99
190	0.15	34.20	0.75	192.50	0.18	34.65	0.99
200	0.18	38.00	0.75	208.56	0.19	39.62	0.99
210	0.19	42.00	0.75	215.28	0.20	43.05	0.99
220	0.20	55.00	0.75	290.00	0.25	72.50	0.99

Table 7 Test results of the load-carrying voltage circuits. (Connect 90 LED SMD 3V)

V_{in} (V)	I_{in}(A)	P_{in}(W)	PF_{in}	V_{out}(V)	I_{out}(A)	P_{out}(W)	PF_{out}
180	0.24	32.40	0.75	180.20	0.24	43.24	0.99
190	0.24	36.10	0.75	192.50	0.24	50.05	0.99
200	0.26	40.00	0.75	208.56	0.26	58.39	0.99
210	0.28	52.50	0.75	215.28	0.28	60.27	0.99
220	0.30	66.00	0.75	290.00	0.30	87.00	0.99

5. DISCUSSION

In the power supply, check the power of the LED backlight. LCD TV Can power up to 290VDC when the power supply to the point of a single LED to approximately 90 LEDs without damaging the power supply and the LED. Although the power supply is 290VDC, but when the ground will not be caught fire, the circuit is very simple, input voltage is 220VAC output voltage 220VAC output to the second transformer which is the primary coil and coil must be used to protect the suction power.

Transformer power does not require high current the size of the 30mA is enough after the coil transformer, to connect to the bridge diode. Equipped with a capacitor (C). (Filter) will use up to about 10uF / 400V up. Capacitor value is not critical. After the circuit is converted to DC. How to measure the DC voltage. Should use digital meter. We need direct pressure to calculate the resistance or use the value in the circuit. The key of the power supply is Resistors (R) to act to reduce the pressure. And the flow to pay as needed.

LED Backlight The display through a small light bulb three colors are red, green and blue, resulting in different colors. But the brightness is adding pressure to a small light bulb. More bright But the LEDs will have a certain voltage, such as 3-5VDC, the pressure will be adjusted. If more than this, the tube is broken. So, the brightness may be set to just 3-4VDC, because if it reaches 5VDC, it will work more efficiently too.

Direct-LED LED backlighting is horizontal, mounted on the back of the panel and provides direct illumination, by providing this kind of light. Although it does not make the display more vibrant, it's like the RGB-LED backlight, but it can control the brightness of each LED independently. The details of the dark and bright parts of the image is clearer. Or make the monitor have a higher dynamic contrast. Nowadays it can be found on most LCD TV.

6. CONCLUSION

Appropriate parameter estimation the purpose is to make the coil transformer can solve the coil transformer. By using 220VAC transformer and 12VAC output power, the coil of the two transformers is connected in parallel. When we enter the 220VAC input it converts the power down. At the same time, another transformer will convert the power back to 220VAC volts. This way, we will get a 220VAC coil transformer. The design was able to estimate the parameters properly, can prevent leakage. When using this unit, test the LED backlight of the LCD TV. I do not know the volt that makes the tube light up. The cable to the negative plus the leg of the LED. The

need to test the bias forward until the tube is lit. Use an anode polarizer and remove the output. Readable values Voltage at the LED light that.

7. ACKNOWLEDGEMENT

Researcher would like to thank Electronics and Telecommunication Engineering Faculty of Industrial Education Rajamangala University of Technology Suvarnabhumi SuphanBuri Center for Research and Development Tools and equipment. The research was successful.

8. REFERENCES

[1] Chaichan Hingoed. 2559.“ AC Motor”. Bangkok: Technology Promotion Association of Thailand - Japan).

[2] M. Arjona, C. Hernandez and M. C. Gonzalez, “Hybrid optimum design of a distribution transformer based on 2-D FE and a manufacturer design methodology”, IEEE Transactions on Magnetics, vol. 46, No. 8, pp. 2864-2867, 2010.

[3] N. Tutkun and A. Moses, “Design optimization of typical strip wound toroidal core using genetic algorithms”, J. Magn. Magn. Mater. , vol. 277, No. 1-2, pp. 216-220, 2004.

[4] S. Elia, G. Fabbri, E. Nistico and E. Santini, “Design of cast-resin distribution transformers by means of genetic algorithms”, in Proceedings of International. Symposium of Power Electronics, Electrical drives, Automation and Motion, pp. 1473-1477, 2006.

[5] Supachai Surinwong. 2543. “1-phase and 3-phase Power Transformers”. 1st time, Bangkok: Technology Promotion Association of Thailand - Japan).

STUDY ON THE SOLAR-HYBRID OTEC SYSTEM USING R134A

Myung-Bo Gang , Nam-Jin Kim†
Department of Nuclear & Energy Engineering, Jeju National University, Republic of Korea

ABSTRACT: Ocean thermal energy conversion (OTEC) is an electric power generation method that utilizes temperature difference between the warm surface seawater and cold deep seawater of ocean, and the OTEC system has problems of low efficiency and high investment cost because the temperature difference between the surface and the deep sea is small, long pipe line and pumping cost for using cold deep water. Therefore, in this present study, the OTEC system combines with solar system. It evaluated the thermodynamic performance of solar-OTEC convergence system for the simultaneous production with electric power and desalinated water. The results showed that the performance of solar-hybrid OTEC system is the highest at the inflow fluid temperature of evaporator of 80 °*C* , and the highest production of desalinated water is 59.01 L/min. Also, the optimal solar collector area is 6,887 ㎡. The system efficiency, electric power and desalination production enhancement ratios were approximately 3.5, 3.5, 14.5 times higher than that of the base hybrid OTEC system.

1. INTRODUCTION

Since D'Arsenoval conceived the Ocean Thermal Energy Conversion(OTEC) concept in 1881[1], there has been considerable research effort aimed at improving the performance of an OTEC plant due to their low efficiency. Uehara et al. [23,4] examined the performance of an OTEC plant using R-22 and ammonia as the working fluid. Also, Kazim [12] suggested hydrogen production using ocean thermal energy, and Ikegamia et al.[13, 14] reported desalination using an integrated hybrid cycle and an open OTEC cycle. Kim et al. and Park et al. [16, 17] examined the thermodynamic performance of an OTEC plant using the condenser effluent from a nuclear power plant. Jebaraj [19] reported that the renewable energy technologies such as OTEC optimize the level of power generation through existing commercial energy technologies and new energy technologies based on objective function and constraints. Rodrigo [20] reported that the efficiency of 740MW coal-fired power plants can be improved around 1.3% by fusing OTEC. As a by-product, 5.8 million tons per year of desalinated water will also be produced. Straatman et al. [21] reported the efficiency of the OTEC-OSP was 4 times higher than that of the simple OTEC system. Also, Yamada N. et al. [22] showed the efficiency of the solar-boosted OTEC system was 1.5 times that higher than that of the simple OTEC system.

In order to improving the performance of an OTEC plant, in this present study, we evaluated the thermodynamic performance of solar – hybrid OTEC convergence system for the simultaneous production with electric power and desalinated water.

2. HYBRID OTEC SYSTEM

Fig. 1 illustrates the hybrid OTEC system, which combines aspects of the open OTEC system and the simple OTEC system, and, similarly to the open OTEC system, is capable of producing desalinated water. Its performance is similar to that of the simple OTEC system. There are actually two different types of hybrid OTEC system: the joint hybrid OTEC system and the integrated hybrid OTEC system, the difference being the latter's inclusion of a flash evaporator. Uehara et al. reported that the integrated hybrid OTEC system out-performs the joint hybrid OTEC system [13].In the integrated hybrid OTEC system, the working fluid, upon completing the heat exchange with the surface seawater in the evaporator, enters the flash evaporator. The resulting steam is condensed in the condenser after exchanging heat with the deep seawater therein. Finally, the liquid flows into a tank of desalinated water. This hybrid OTEC system, like the open OTEC system, consumes power to eliminate non-condensable gases, though at a cost only of around 2.8% of the total power [24].

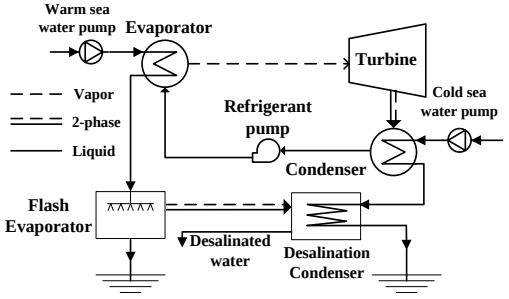

Fig. 1 Hybrid OTEM system

3. SOLAR - HYBRID OTEC SYSTEM

Fig. 2 is a schematic diagram of the solar-hybrid OTEC system that is suggested in this research. The system consists of a solar collector, heat storage tank, circulating pump, flash evaporator, evaporator, refrigeration pump, turbine, generator, and condenser. The working fluid is heated by the solar collector, moves to the heat storage tank, and continues to move into the flash evaporator after losing its heat by refrigeration in the evaporator. The working fluid moved into the flash

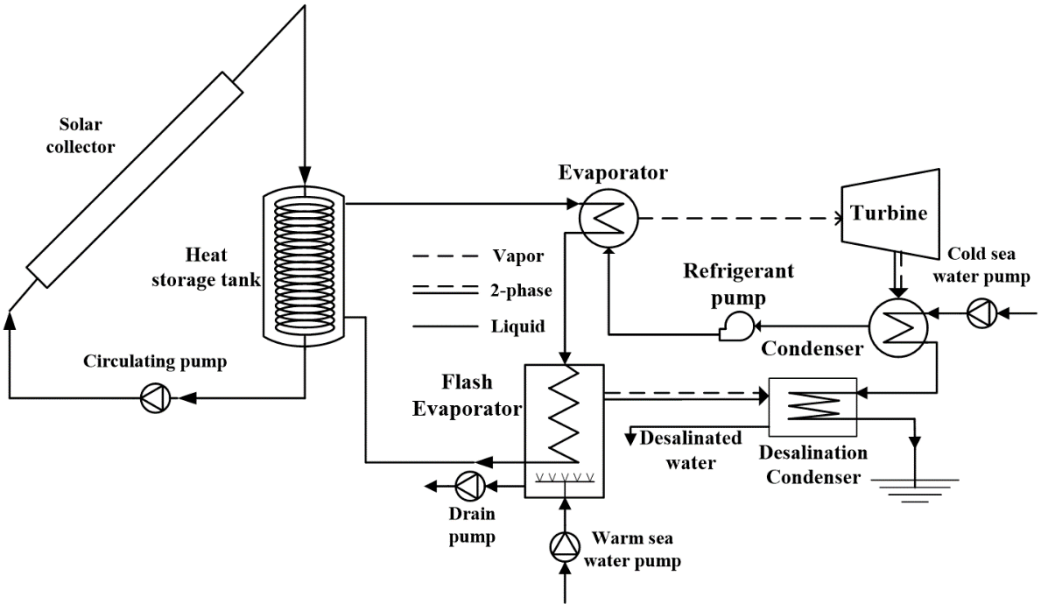

Fig. 2 Solar – Hybrid OTEM system

evaporator after losing its heat by refrigeration in the evaporator. The working fluid moved into the flash evaporator exchanges its heat with sea water and continues to be moved again to the solar collector by the circulating pump. Refrigeration in the evaporator generates electricity by turning the turbine and generator, is condensed in the condenser, and is then moved to the evaporator by the refrigeration pump. The cold seawater is flown into the condenser in order to condensate the refrigeration, and then moves to the desalination condenser. Consequently the evaporated steam from the flash evaporator becomes desalinated water by exchanging its heat with the cold seawater in the desalination condenser.

4. ANALYTICAL METHODS

The evaporator was divided into three separate areas for the purposes of a heat-transfer analysis: a subcooled area, a two-phase area, and a superheated area. The condenser was divided into two separate areas: a subcooled area and a two-phase area. The heat exchanges among the working fluid, cooling water and deep seawater were estimated as [25]

Where, the f ratios denote the heat ratios in the subcooled area, the two-phase area and the superheated area of the heat exchanger. The system efficiencies of each cycle were compared under the conditions listed in Table 1.

$$UA_e = UA_{sube_s} + UA_{tpe} + UA_{supe} \quad (1)$$

$$\frac{1}{LMTD_e} = \frac{f_{sube}}{LMTD_{sube}} + \frac{(1 - f_{sube} - f_{supe})}{LMTD_{tpe}} + \frac{f_{supe}}{LMTD_{supe}} \quad (2)$$

$$UA_c = UA_{subc} + UA_{tpc} \quad (3)$$

$$\frac{1}{LMTD_c} = \frac{f_{subc}}{LMTD_{subc}} + \frac{(1 - f_{tpc})}{LMTD_{tpc}} \quad (4)$$

Table 1. Cycle operating conditions

Basic conditions	Warmsurface-sea-water inlet temperature (℃)	28
	Warm-surface-sea-water outlet temperature (℃)	25
	Colddeep-sea-water inlet temperature (℃)	4
	LMTD in evaporator (℃)	2.5
	LMTD in condenser (℃)	2.5
	Isentropic turbine efficiency (%)	90
	Isentropic pump efficiency (%)	85
	Heat-transfer rate in evaporator (kW)	150
	Mass flow rate of warm seawater (kg/s)	11.96
	Mass flow rate of cold seawater (kg/s)	11.72
	Superheating (℃)	2.0
	Subcooling (℃)	2.0
Open OTEC system	Mass flow rate of warm seawater	11.96

	(kg/s)	
	Mass flow rate of cold seawater (kg/s)	11.72
Solar-open OTEC system	Working fluid temperature in the flash evaporator (℃)	60,65,70,75,80
	Flash evaporator pressure (kPa)	2.5,5,10,15, 2.5,30,35,40
Solar-hybrid OTEC system	Working fluid temperature in the evaporator (℃)	60,65,70,75,80

5. PERFORMANCES OF THE SOLAR-HYBRID OTEC SYSTEM

Fig. 3 shows the system efficiencies of working fluids which is adoptable to the solar-hybrid OTEC system. According to the chart, when R134a refrigeration is used, the highest system efficiency can be obtained, which is about 3.65% efficiency. The chart also concludes that en R410a refrigeration is used, the system efficiency of the base Hybrid OTEC system is at its lowest. Fig. 4 is a line graph of the hybrid OTEC system usingR134a. 28°C seawater exchanges its heat with refrigeration R134a and evaporates the refrigeration. The evaporated refrigeration becomes condensed in condensation by moving the turbine and generator, and then is moved to the evaporator again via the refrigeration circulating pump. Fig.s 5 and 6 depict the production of desalinated water and each working fluid output of the hybrid OTEC system using the conditions of Table1. As shown in the Fig.s, the output becomes the highest when utilizing R134a refrigeration, while productions of desalinated water are equally at 4.08 L/min no matter which working fluid is used. This is because 28°C seawater flows in the evaporator at the same temperature after exchanging its heat equally with the refrigeration in the evaporator. The reason that the production of desalinated water is higher than in the base open OTEC system is because the mass flow of the surface water of the hybrid OTEC system is 11.96 kg/s, which is higher than the 6.16 kg/s mass flow of the base open OTEC system. Therefore according to this research, R134a refrigeration as a working fluid would be the most optimal for the solar-hybrid OTEC system. Fig. 7 is a comparison of relative turbine size versus each of the working fluids using R22 as the relative average. Turbine size is determined by the quotient of the enthalpy difference between the inlet and outlet of the turbine over the specific volume of working fluid flown into the turbine. Supposing the turban size of R22 to be 1.0, turbine sizes that are below this average increases in size in the order of R32, R410a, R125, and R143a. If these fluids were used as refrigeration the turbine sizes would be smaller than if R22 and R717 were being used, two fluids suggested by many researchers. Fig. 8 shows the comparison between the efficiencies of the hybrid OTEC system and base hybrid OTEC system under the conditions of using R134a as the working fluid and changing the temperature of the working fluid flown into the evaporator from 60 to 65, 70, and 80°C. As seen from the chart, as the temperature

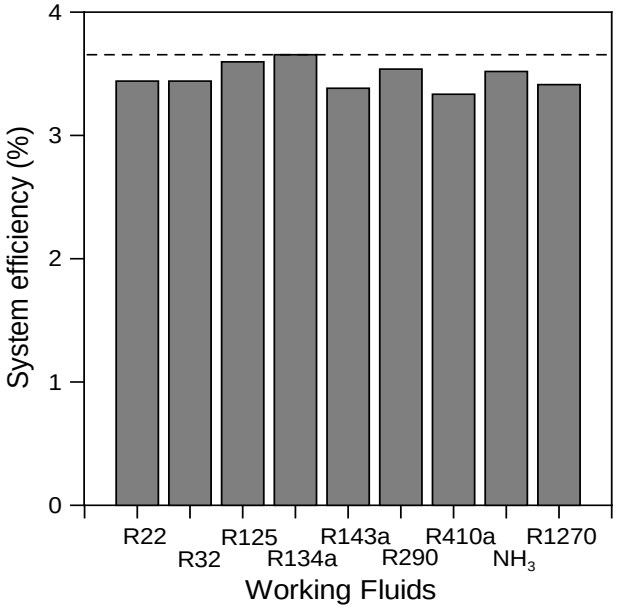

Fig. 3 System efficiency of the various working fluids

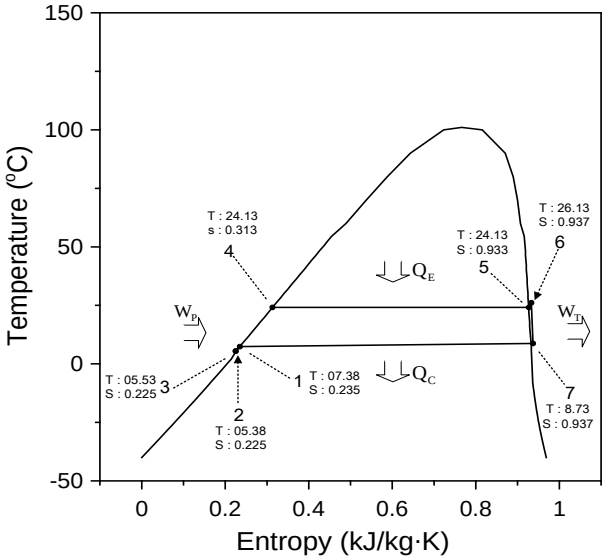

Fig. 4 T-s diagram of the hybrid OTEC system using R134a.

of the working fluid increases, the system efficiency increases proportionately; moreover, the efficiency at 80°C is around 12.65%, 3.5 times higher than the base hybrid OTEC system. Fig. 9 is a graph that illustrates the differences between the outputs of each system when the working fluid of the solar-hybrid OTEC system is R134a and the temperature of the working fluid flown into evaporator is 60, 65, 70, 75, and 80°C. As explained above, the higher the temperature of the working fluid, the higher the output of the system. To note in particular, the output when the fluid is 80°C is 3.5 times higher than the base hybrid OTEC system. Fig. 10 is a graph that compares the production of desalinated water in the solar-hybrid OTEC system with the base hybrid OTEC system according to the temperature of the working fluid flown into the evaporator. As seen from the chart, the higher the

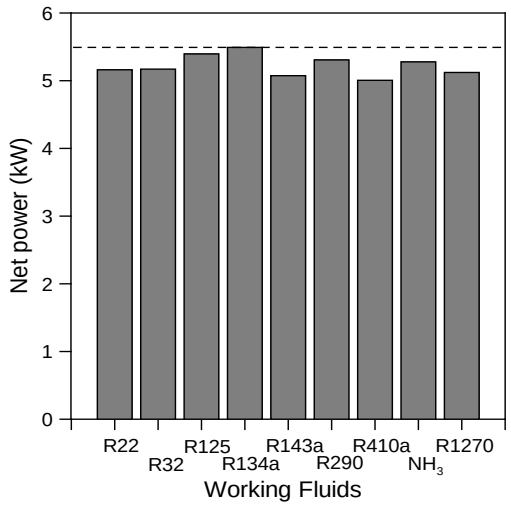

Fig. 5 System output according to the various working fluids.

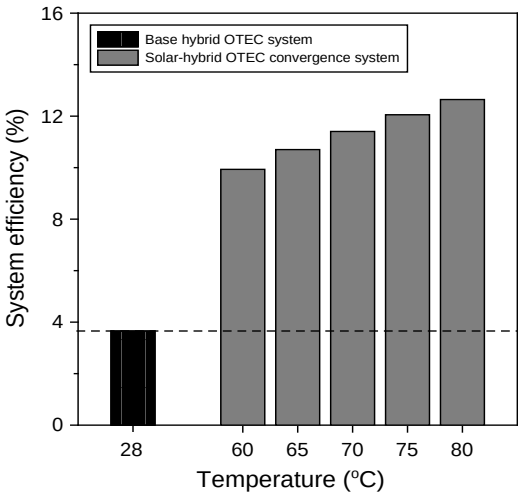

Fig. 6 System efficiency according to the various working fluid temperature in the evaporator.

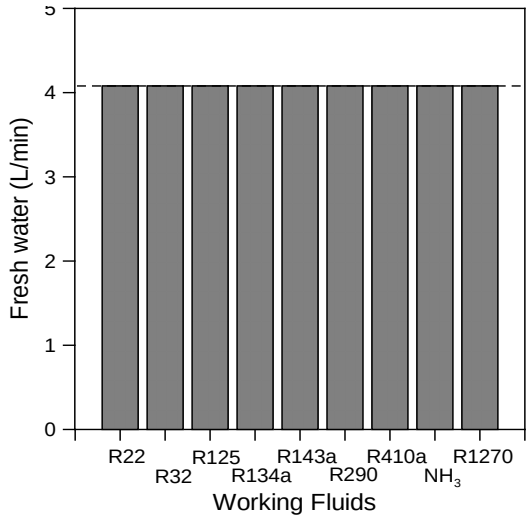

Fig. 7 Production of desalinated water according to the various working fluids.

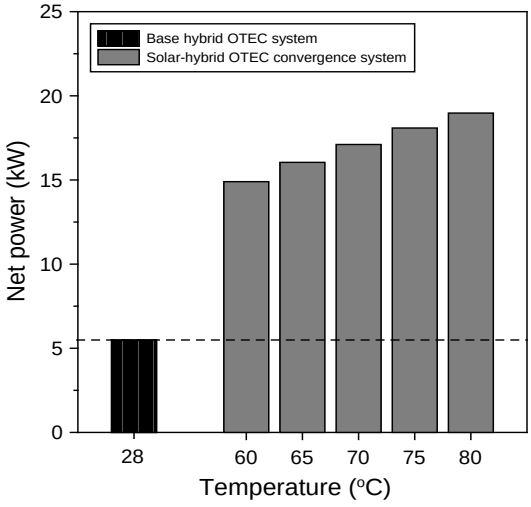

Fig. 8 System output according to the various working fluid temperature in the evaporator.

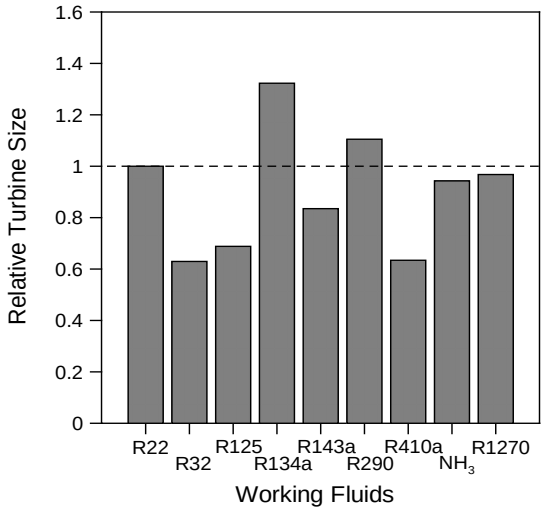

Fig. 9 Relative turbine size according to the various working fluids.

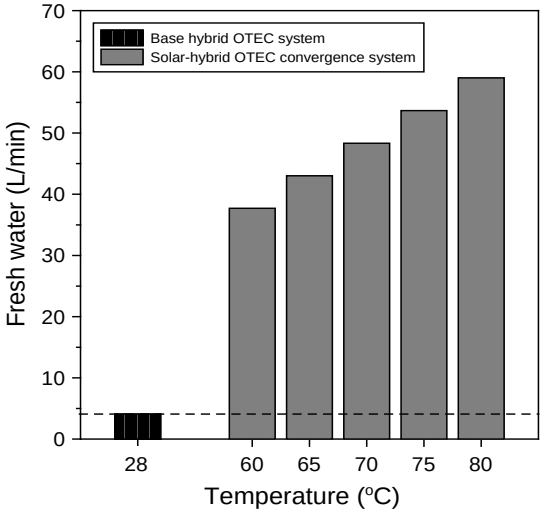

Fig. 10 Production of desalinated water according to the various working fluid temperature in the evaporator.

temperature of the working fluid, the higher the production of desalinated water. The highest production of desalinated water, which is 59.01 L/min, can be displayed when the temperature is 80°C. Converted into the unit of tones, this translates into 3.54 ton/day, meaning a maximum of 3.5 tones can be produced in a day. This is 14.5 times higher than the base hybrid OTEC system.

6. CONCLUSIONS

Ocean thermal energy conversion(OTEC) is a power generation method that utilizes temperature difference between the warm surface seawater and cold deep seawater of ocean. As potential sources of clean-energy supply, OTEC power plants' viability has been investigated. Therefore, in this study, the performance analysis of solar-OTEC convergence system was carried out as the fluid temperature, saturated temperature difference and pressure of flash evaporator under equivalent conditions in order to overcome the low efficiency of the OTEC systems. The results showed that the performance of solar-hybrid OTEC system is the highest at the inflow fluid temperature of evaporator of 80℃. The system efficiency, electric power and desalination production enhancement ratios were approximately 3.5, 3.5, 14.5 times higher than that of the base hybrid OTEC system.

7. REFERENCES

[1] d'Arsonval A. Utilisation de forces naturelles, Revue Scientifique 1881; 17:370-372.
[2] Uehara H, Kusuda H, Monde M, Nakaoka T. Ocean thermal energy conversion plant with Freon 22, Proceeding, Sixth OTEC Conference 1979; 6.
[3] Nakaoka T, Uehara H. Performance test of a shell-and-tube plate type evaporator for OTEC, Exp. Therm. Fluid Sci. 1988a; 1:283-291.
[4] Nakaoka T, Uehara H. 1988b. Performance test of a shell-and-tube plate type condenser for OTEC, Exp. Therm. Fluid Sci. 1988b; 1:275-281.
[5] Owens WL, Optimization of closed-cycle OTEC plants, ASME–JSME Thermal Engineering Joint Conference 1980; 2:227-239.
[6] Uehara H, Ikegami Y, Optimization of a closed-cycle OTEC system, J. Solar Energy Eng. 1990; 112(4):247-256.
[7] Uehara H, Ikegami Y, Parameiric performance analysis of OTEC using Kalina cycle, ASME joint solar engineering conference 1993; 203-207.
[8] Uehara U, Ikegami Y and Nishida T. Performance Analysis of OTEC System Using a Cycle with Absorption and Extraction Processes, J. of The JSME 1998; 64(624):384-389.
[9] Rabas TJ, Panchal CB, Stevens HC. Integration and optimization of the gas removal system for hybrid-cycle OTEC power plants, J. Solar Energy Eng. 1990; 112:19-28.
[10] Tseng CH, Kao KY, Yang JC.,Optimal design of a pilot OTEC power plant in Taiwan, J. Energy Resour. Tech. 1991; 113:294-299.
[11] Abraham R, Jayashankar V, Ikegami Y, Mitsumori M, Uehara H, Analysis of power cycle for 1 MW floating OTEC plant, Proceedings of International OTEC/DOWA, Imari, Japan 1999; 123-131.
[12] Kazim, A. Hydrogen production through an ocean thermal energy conversion system operating at an optimum temperature drop, Applied Thermal Engineering 2005; 25:2236-2246.
[13] Uehara H, Miyara A, Ikegami Y, Nakaoka T. Performance analysis of an OTEC plant and a desalination plant using an integrated hybrid cycle, Journal of Solar Energy Eng. 1996; 118:115-122.
[14] Ikegamia Y, Sasakib H, Goudab T, Uehara H. Experimental study on a spray flash desalination, Desalination 2006; 194:81-89.
[15] Faizal M and Ahmed R. On the ocean heat budget and ocean thermal energy conversion, International Journal of Energy Research 2011; 35: 1119-1144.
[16] Park S.S., Kim W.J., Kim Y.H., Hwang J., and Kim N.J., Regenerative OTEC systems using condenser effluents discharged from three nuclear power plants in South Korea, International Journal of Energy Research 2015; 39;397-405.
[17] Kim N.J., Ng K.C., and Chun W.G, Using the condenser effluent from a nuclear power plant for Ocean Thermal Energy Conversion(OTEC). International Communications in Heat and Mass Transfer 2009; 36:1008-1013.
[18] Vadus J. A Strategy for OTEC Commercialization, Processing of the 1997 International OTEC/DOWA Association 1997; 235-247.
[19] Jebaraj S, Iniyan S, Goic R. An optimal electricity allocation model for sustainable resource use in India. International Journal of Energy Research 2013; 37:923–935.
[20] Soto R, Vergara J. Thermal power plant efficiency enhancement with ocean thermal energy conversion. Applied Thermal Engineering 2014; 62:105–112.
[21]Straatman. P. J. T, Sark. W. G. J. H. M. V., A new hybrid ocean thermal energy conversion-offshore solar pond(OTEC-OSP) design: A cost optimization approach, Solar Energy 2008; 82: 520-527.
[22]Yamada.N.,HoshiA.,Ikegami.Y.,Performance simulation of solar-boosted ocean thermal energy conversion plant, Renewable Energy 2009; 34:1752-1758.
[23] Penny T, Bharathan D, Althof J, Parsons B. Open-Cycle Ocean Thermal Energy Conversion (OTEC) Research: Progress Summary and a Design Study, ASME Paper 1984; 84-WA/Sol-26.
[24] Panchal CB, Bell KJ. Simultaneous Production of Desalinated Water and Power using a Hybrid - Cycle OTEC Plant, Transaction of the ASME 1987; 109:156-160
[25] Shin SH, Jung DS, Kim CB, Seo TB. Analysis of a simple Rankine Cycle and Regenerative Rankine Cycle for OTEC Application, Proceedings of the International OTEC/DOWA Conference 1999; 142-151.

STOCHASTIC PHENOMENON OF METHANE HYDRATE FORMATION

Min-Soo Jeon, Nam-Jin Kim*
[1)] *Department Nuclear & Energy Engineering, Jeju National University, Republic of Korea*

ABSTRACT: Methane hydrate is a mixture of methane and water that is frozen into an ice. The crystalline structure of the frozen water molecules forms a cage-like lattice inside of which is trapped high concentration of methane molecules. When methane hydrate is artificially formed, the amount of consumed gas becomes low. In addition, there is no reproducibility at the repetition experiments of the same conditions. Therefore, for the practical purpose in the application, the present investigation focuses on the rapid production and reproducibility. The results show that subcooling condition of methane hydrate must be above 7K in order to form hydrate rapidly. And the amount of consumed gas is a stochastic phenomenon. When the subcooling temperature increases, the stochastic phenomenon is decreased.

1. INTRODUCTION

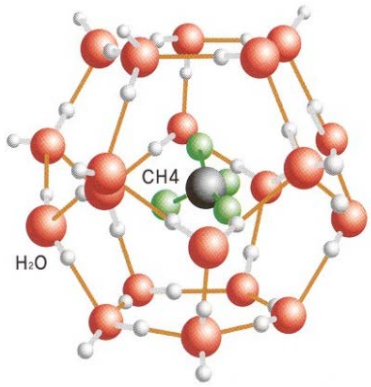

Fig. 1 Methane hydrate.

Methane hydrate is a mixture of methane and water that is frozen into an ice. The crystalline structure of the frozen water molecules forms a cage-like lattice inside of which are trapped high concentrations of methane molecules. Methane hydrates form in generally two types of geologic environments, in permafrost regions (where cold temperatures dominate) and beneath the sea in sediments of the outer continental margins.

The principles for producing methane hydrate nuclei are as follows. As shown in Fig. 2, methane gas is not dissolved in water but is injected in [A] phase where hydrolyte can be generated, and water and methane gas are injected, resulting in immediate instability [B] clusters. These unstable clusters then evolve to [C] phase by forming a semi-stable nucleus-lie assembly through the decimation or increase process. However, the collection of [C] steps is also below the hydrate nuclear threshold, so it reaches the critical size through a repetitive and probabilistic process that increases or decreases, resultion in the [D] phase where the initial hydrate nucleus is generated and grows.

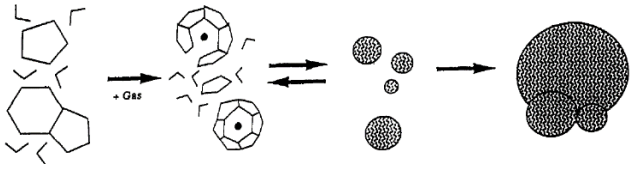

[A] Initial condition [B] Labile cluster [C] Agglomeration [D] Primary nucleation and growth

Fig. 2 Schematic model of labile cluster growth

1 m^3 of methane hydrate can be decomposed into a maximum of 216 m^3 of methane gas under standard conditions [4]. If this characteristic of hydrates is utilized in the opposite sense, natural gas can be fixed into water in the form of a hydrate solid. Therefore, hydrates are considered to be a great way to transport and store natural gas in large quantities. As shown in Fig. 3, the methane hydrate supply chain consists of three main partsviz the production, marine transportation and regasification processes. The procuction part can be located on land using loading facilities for large hydrate carriers. Transportation is performed by bulk carriers specially designed for dry hydrates, hydrate slurries, and pellet type hydrates. The regasification part of the frozen hydrate takes place at a receiving terminal located close to the market of natural gas [7]. In particular, the transportation cost of methane hydrate is expected to be 18-24% lower than that of liquefied natural gas [5][6]. Therefore, many researchers have studied the methane hydrate formation methods for Natural Gas transport and Storate.
However, the formation of methane hydrate is a stochastic phenomenon [8, 10]. Therefore, the present study focuses on the stochastic phenomenon of hydrate formation time and the amount of consumed gas.

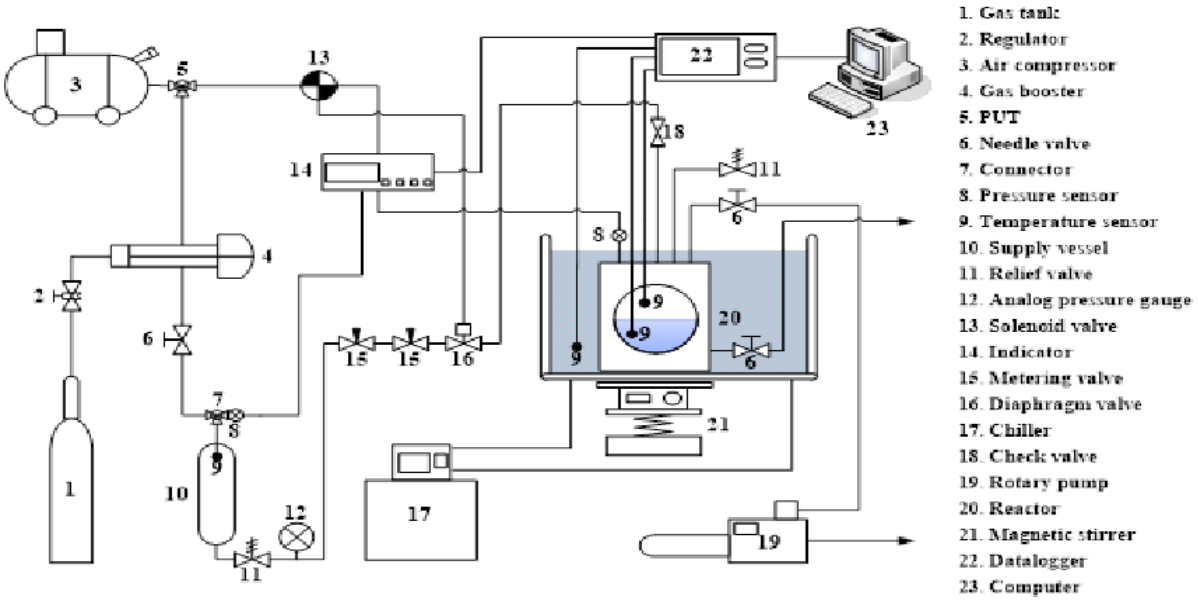

Fig. 3 Schematic diagram of experimental apparatus

2 . EXPERIMENTAL APPARATUS

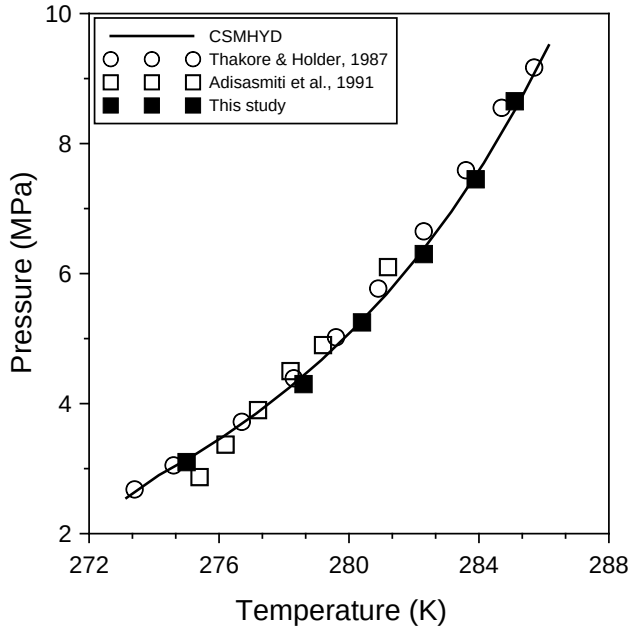

Fig. 4 Hydrate equilibrium points

Fig. 4 shown schematic diagram of the experimental apparatus used in this study. A 350mL reactor (20) and 100mL supply vessel (10) were manufactured with SUS316 to endure a pressure of overw 10 MPa and salt erosion. The reactor was immersed in a constant temperature bath (water + ethylene glycol). Two copper-constantan thermocouples (9) were used to measure the temperatures of the gas and liquid in the reactor, and on pressure gauge (8) was installed to check the inside pressure of the reactor. One thermocouple (9) and one pressure sensor (8) were inserted in the supply vessel to calculate the number of moles of gas consumed in the hydrate phase. Considering the high pressure operations in the reactor, in order to prevent the back-flow of gas. Quartz glasses with a diameter of 30mm were installed at the front and rear sides of the reactor (20) to allow for the observation of the reaction. A diaphragm valve (16) was installed to supply the gases while maintaining constant

pressure in the reactor. Especially, for experimental precision, two metering valves were installed between the supply vessel (10) and the diaphragm valve (16) to control the flow rate. As the gas in the reactor is consumed to form the hydrate, additional gas is automatically supplied from the supply vessel and the pressure in the reactor is kept constant with the help of the diaphragm valve. During the experiment, a data logger(22) acquisition system was used to scan the pressure and temperature every second and record the average values every 10 seconds. The reactants used were secondary distilled water and 99.95% methane gas (Rigas Co.) Table 1 shews the properties of the MWCNTs used in this experiment and SEM micrographs of the MWCNTs are shown in Figs 6(a) and (b)

3. EXPERIMENTAL RESULTS AND DISCUSSION

3.1 Equilibrium measurement

Hydrate is generally stable under high pressure and low temperature. It is easily decomposed to water and gas out of the stable region. Since the formation and decomposition of hydrate can be visually confirmed, phase equilibrium is performed considering the specialty of experimental apprtus. Model cases are shown in Fig. 6.

One is that hydrate is formed at arbitrary temperature, B(T_{equ}) and pressure, A(P_{exp}), which is higher than

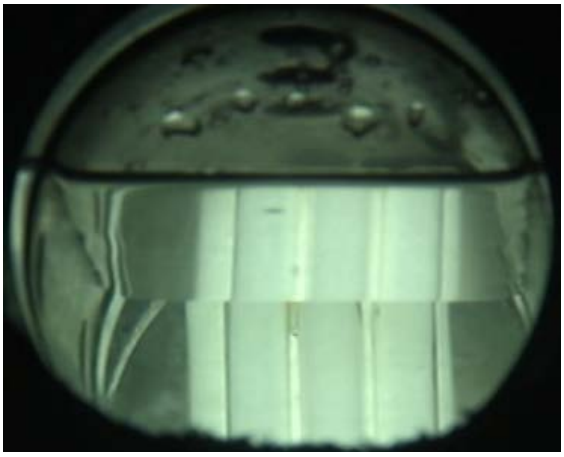

Fig. 5 Photograph of Methane hydrate formation

pressure, D(P_{equ}), and pressure is gradually decreased at constant temperature in the course, A→B. The other is that temperature is gradually increased in the course, A→C. After performing two experiments in the present study, the second method is found to be more convenient than the first. Since the decomposition of hydrate can be visually observed, the experiments have been performed in the following ways

Fig. 5 shows good agreements between the prior results [8] and equilibrium points from this study. Therefore, the experimental apparatus and method of the present investigation is proven to be adequate.

3.2 Hydrate formation time

The subcooling temperature, (ΔT_{subc}) is defined as the difference between the experimental and equilibrium temperature [9]. Like the previous researcher [10], Distilled water was poured into the reactor. The reactor was cooled to the experimental temperature and the gas was then sprayed. After reaching the experimental pressure, the hydrate crystal was observed for 24 hours in the circle as shown in Fig. 6. The results are plotted in Fig. 7. As shown in the Fig., the time increased as the system approached equilibrium. At the same time, it was found that the time decreases with increasing the subcooling temperature. And methane hydrate formed rapidly when the subcooling temperature was 8K or above, but the time increased linearly as the subcooling temperature decreased 8K or under. Also, the Fig. shows the hydrate formation time is a stochastic phenomenon. The empirical equation to predict the time can be expressed as

$$t(\min) = -157.226 \times \Delta T_{subc} + 1241.511$$

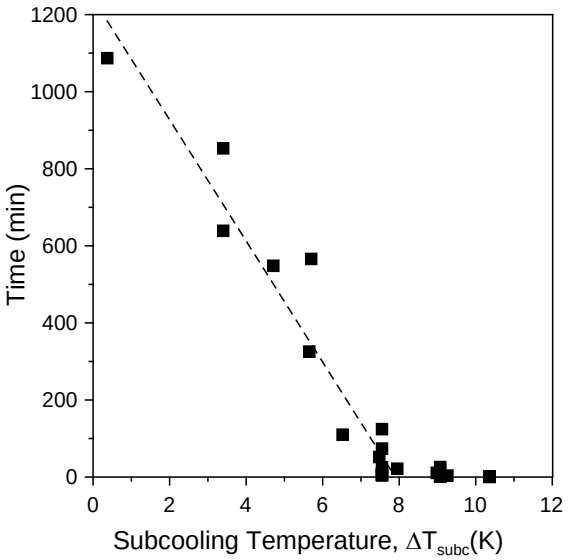

Fig. 6 Methane hydrate formation time

3.3 Measurements of gas consumption on subcooling

150 mL of distilled water was poured into the reactor and colled to 274.15K and the experimental gas ingected at the experimental pressure. The experiments were carried out for 12 hours and the temperature was kept constant until the termination of the experiments. As the experimental gas reacts with distilled water to form the hydrate, the gas is replenished by the diaphragm valv and metering valves and the pressure is kept constant. At any point in time, the number of moles of the gas that have been consumed so far is equal to the difference between the number of moles of the gas at time t=0 and the number of moles of the gas at time t present in the supply vessel. The following equation is used to calculate the number of moles of gas consumed, where V_{sv} is the volume of the supply vessel and z is the compressibility factor, which is calculated by Pitzer's correlations [13]

$$\Delta n = V_{sv}\left(\frac{P}{zRT}\right)_0 - V_{sv}\left(\frac{P}{zRT}\right)_t$$

As shown in Figs 9-11, the amount of consumed gas is a stochastic phenomenon. When the subcooling temperature increases, the stochastic phenomenon is increased too. Also, The mean, maximum, and minimum values are indicated in Fig. 12. (Maximum-average)/ The mean deviation from which the mean was calculated is shown in Fig. 8. As shown in the Fig., the mean deviation was up to ±40% at the same over-temperature, but as the over-coldness increased, the mean deviation decreased linearly. This means that the lower the over-coldness, the less repeatability of the methane amount collected in the hydrate, but as the over-cooling increases, the more likely and irregularly the mean variation between the [B] and [C] phases of the clusters.

Fig. 13 shows the increase of the amount of consumed gas can be observed because the level of subcooling increases with increasing pressure at a constant temperature

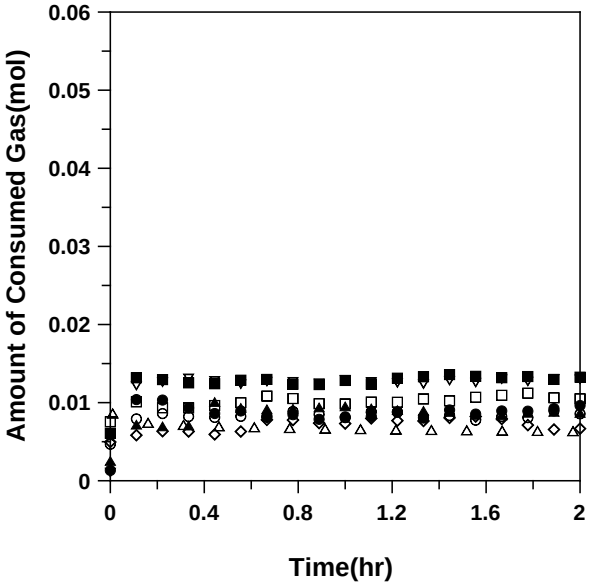

Fig. 7 Amount of consumed gas at ΔT_{sub}=0.5K

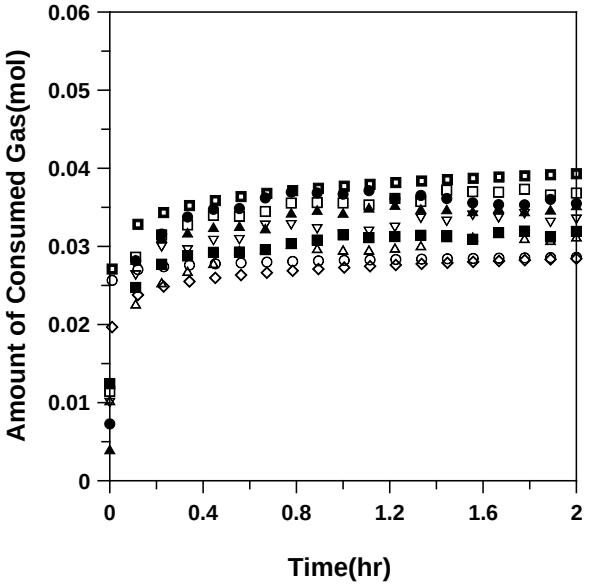

Fig. 9 Amount of consumed gas at ΔT_{sub}=9.7K

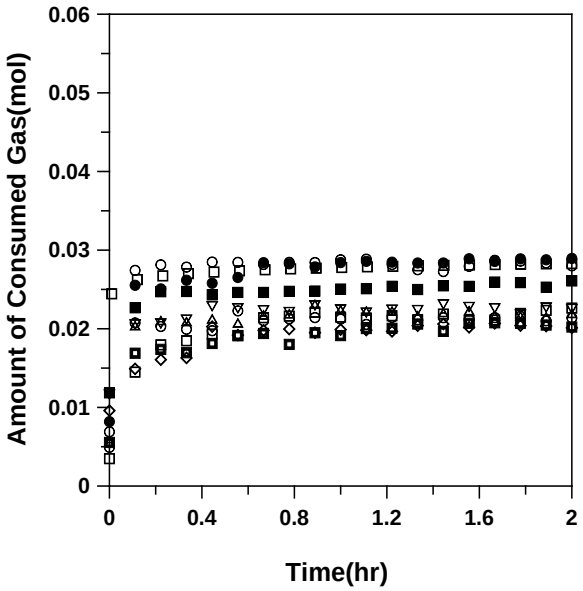

Fig. 8 Amount of consumed gas at ΔT_{sub}=5.7K

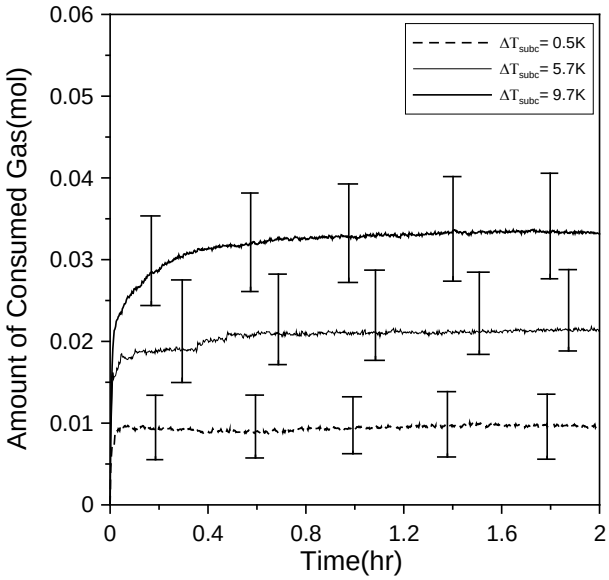

Fig. 10 Average amount of consumed gas with the change of subcooling

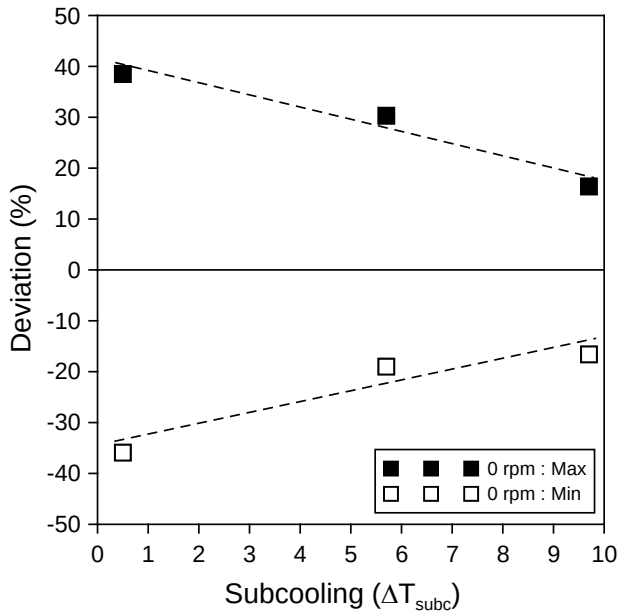

Fig. 11 Mean deviation with the change of subcooling

4. CONCLUSIONS

The formation of methane hydrate is a stochastic phenomenon. Therefore, the present study focuses on the stochastic phenomenon of hydrate formation time and the amount of consumed gas. The results show that subcooling condition of methane hydrate must be above 8K in order to form hydrate rapidly, and the hydrate formation is a stochastic phenomenon. However, the stochastic phenomenon is depressed, if the water is agitated by magnetic stirrer. Also, the increase of the amount of consumed gas can be observed because the level of subcooling increases with increasing pressure at a constant temperature

5. ACKNOWLEDGEMENT

"This research(or This presentation or This work) was financially supported by The Project Management Center

Cultivating Smart Grid & Clean Energy Manpowers(CK-Ⅰ), JNU"

6. REFERENCES

[1]Sloan, E. D., Clathrate hydrates of natural gases(2nd ed.), Marcel Dekker, inc., New York, (1998), pp. 1-64.
[2] Kvenvolden, K, A., Methane hydrate a major reservoir of carbon in the shallow geosphere, *Chem. Geol.*, 71(1988), pp. 41-51
[3] Chang, D. G., Kim, N. J., Lee, J. Y., and Kim, C. B., Simulation of two phase flow in porous media after dissociation of methane hydrate, *Proceeding of the KSME 2000 Fall Annual Meeting*, Seoul, KOREA (1980), pp. 241-246.
[4] Okuda, Y., Exploration research on gas hydrates in Japan, *Proceeding of the 5th Petroleum exploration and development symposium*, (1996), pp. 62-98.
[5] Gudmundsson, J. S., Mork, M., and Graff, O. F., Hydrate Non-Pipeline Technology, *Proceedings of the 4th International Conference on Gas Hydrate*, Yokohama, Japan (2002), pp. 997-1002.
[6] Kanda, H., Economics study on natural gas transportation with natural gas hydrate pellets, *Proceeding of the 23rd world gas conference*, Amsterdam, the Netherlands (2006).
[7] Gudmundsson, J. S. and Boslashrrehaug, A, Frozen hydrate for transport of natural gas, *Proceeding of the 2nd International Conference on Natural Gas hydrate*, Toulouse, France (1996).
[8] Seo, Y. W. , Lee, S. M., Seo, Y. T., Lee, J. D., and Lee, H., Phase equilibria and thermodynamic modeling of ethane hydrate in porous silica gel, Proceedings of the 6th international Conference on Gas Hydrates (http://www.icgh.org), Vancouver, Canada(2008)
[9] Ryu, Y. B., Lee, J. D., Kim, Y. S., Yoon, S. Y., and Lee, M. S., Influence of nanosized materials on the formation of CH_4 hydrate, *Proceedings of the 6th International Conference on Gas Hydrates (http://www.icgh.org)*, Vancouver, Canada (2008)
[10] Yulong, W., Fei, W., Guohua, L., Guoqing, N., and Mingde, Y., Methane storage in multi-walled carbon nanotubes at the quantity of 80 g, *Materials Research Bulletin*, 43(2008), pp. 1431-1439.
[11] Smith, J. M., Van Ness, H. C., and Abbott, M. M., *Introduction to Chemical Engineering Thermodynamics (7th ed.)*, McGraw-Hill (2001), pp. 64-124
[12] Lin, W., Chen, G. J., Sun, C. Y., Guo, X. Q., Wu, Z.K., Liang, M.Y., Chen, L.T., and Yang, L.Y., Effect of surfactant on the formation and dissociation kinetic behavior of methane hydrate, *Chemical Engineering Science*, 59(2004), pp. 4449-4455.
[13] Cho, B. H. and Lee, Y. C., Observation of natural gas hydrate crystal in initial stage and structure analysis by spectroscopy with water added ionic surfactant, *Proceedings of Korea Conference on Innovative Science Technology*, Anmyenondo, KOREA (2006), pp. 307-311
[14] Englezos P, Kalogerakis N, Dholabhai P. D., and Bishnoi P. R., Kinetics of formation of methane and ethane gas hydrate, *Chemical Engineering Science*,;42(11) (1987), pp. 2647-2658.
[15] Lingelem M, Majeed A., Challenges in areas of multiphase transport and hydrate control for a subsea gas condensate production system, *Proceedings of the 68th GPA Annual Convention*, Texas, USA (1989), pp. 19-29.
[16] Lingelem, M., Majeed, A., Challenges in areas of multiphase transport and hydrate control for a subsea gas condensate production system, Proc. Of the 68th Ann. Gas Proc. Assoc. Conventions, San Antonio, Texas, March 13-14 (1989)
[17] Smith, J. *Introduction to Chemical Engineering Thermodynamics*, New York McGraw-Hill, Inc.2001

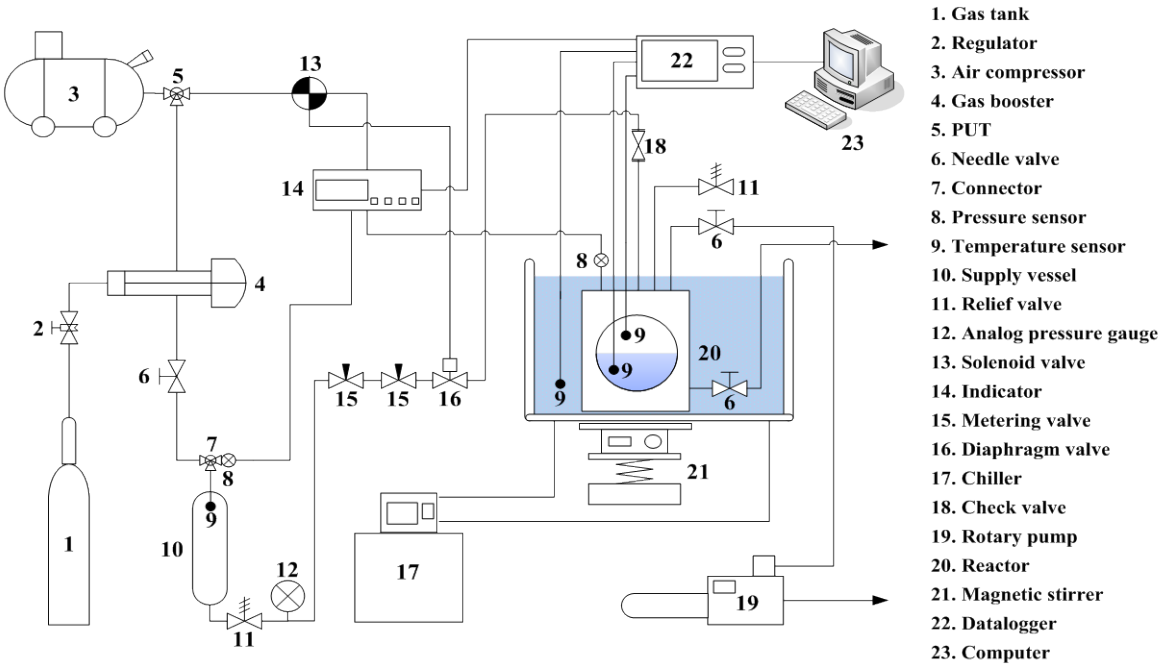
1. Gas tank
2. Regulator
3. Air compressor
4. Gas booster
5. PUT
6. Needle valve
7. Connector
8. Pressure sensor
9. Temperature sensor
10. Supply vessel
11. Relief valve
12. Analog pressure gauge
13. Solenoid valve
14. Indicator
15. Metering valve
16. Diaphragm valve
17. Chiller
18. Check valve
19. Rotary pump
20. Reactor
21. Magnetic stirrer
22. Datalogger
23. Computer

A DESIGN AND DEVELOPMENT OF AUTOMATIC PAPER CUP PACKAGING SYSTEMs

Natt Siriwattananon[1], Chaiyapon Thongchaisuratkrul [2]
[1] *Department of Teacher Training in Mechanical Engineering, Faculty of Industrial Education, Rajamangala University of Technology Suvarnabhumi, Thailand. nuttiq@gmail.com*
[2] *Department of Teacher Training in Electrical Engineering, Faculty of Technical Education, King Mongkut's University of Technology North Bangkok, Thailand. srptc@hotmail.com*

ABSTRACT: This paper presents a design and development of an automated paper cup packaging system by designing and developing a new packaging model, which can improve the packaging processes. One machine per unit can control three filling machines per person. The result shown that the operating cost can reduced from 412,401 Baht/year to 137,467 Baht/year, or about 67.7% of the total cost. The energy cost reduced from 258,785 Baht/year to 126,969 Baht/year, or about 48.7% of the total cost. Based on the techniques and design methods developed, the researcher hopes that this research will be a guideline for other packaging systems development. It can reduce the cost of production and help to save energy.

Keywords: design and development, automatic systems, paper cup packaging

1. INTRODUCTION

According to a study on the economy of the packaging industry the situation and trend of packaging industry in Thailand was grown. Considering the volume of production in 2016, it was found that the paper packaging, the highest production volume was 2,130,130 tons, followed by plastic packaging 1,714,430 tons, glass packaging 822,429 tons and metal packaging 418,213 tons, respectively. [1]

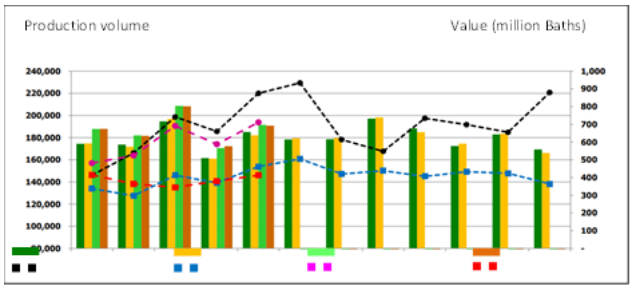

Fig. 1: Production volume of paper packaging 174,147 tons (July 2561) [2]

Kasikorn Research Center, It is expected that the packaging and printing business in 2018 will be recovery since the year 2017, resulting in the demand for packaging. In response to both domestic and international economic activity has increased, approximately 4.63 million tons of packaging used in 2018 with 3.9% of total packaging. The highest proportion of packaging was in the following four categories: 1) Paper packaging 48% 2) Plastic packaging 23.5% 3) Glass packaging 20% and 4) Metal Packaging 8.5%. [3]

By analyzing the competitiveness of SMES's strengthened manufacturing sector for its entry into the ASEAN Economic Community in 2011, the printing and packaging industry saw a shortage of Thai and foreign workers. [4]-[5]. According to the report on employment in micro and small enterprises in Thailand (EMSET), there is a shortage of workers in Bangkok and its suburbs, Inadequate labor in the country [6]. Foreign workers are more likely to find migrant workers due to relocation.

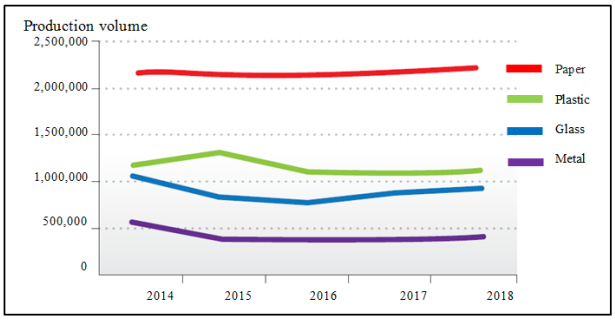

Fig. 2: Packaging consumption in 2018 is about 4.63 million tons.

Paper packaging industry, there is a growing demand for labor in production.
Survey on the problems of the paper packaging industry, the researchers conducted the survey only paper packaging single-use paper cups, such as cups of drinking water, coffee cups, etc. The researcher was conducted in industrial plants. One of the largest paper packaging factories in the country. Both domestic and export to overseas production of more than 2,000 million leaves a year. The machine used to produce paper cups automatically and must be counted as a pack in a bag and then sealed in a bag, clean, not dirty, and then shipped to the customer.
There is a shortage of labor to seal a paper cup bag since the production line is necessary to work 24 hours a day. The workers work repeatedly every day. It requires skill and speed to keep up with the production of automatic paper cup forming machines. Now, the production has enabled the machine to support the production of forming paper cups 30 machines per day with 2 rounds a day. The average capacity is about 4,000,000 pieces / day. Now, packing and sealing bags needs 1 worker for 1 machine (25 paper cups/1 pack or depending on the order). The automatic packing and sealing machines are expensive. The prices range from 0.7 million to more than a million. This is a very high cost for many companies. Therefore, the development of an automatic

packaging machine to improve the productivity will be important. Researchers are interested in doing research by designing and developing the automated paper cup packaging systems. This will solve the problem of production.

2. THEORY [7-9]

The following work processes are involved the automatic production system.

2.1 Paper cup production

The paper cup production process is as follows.

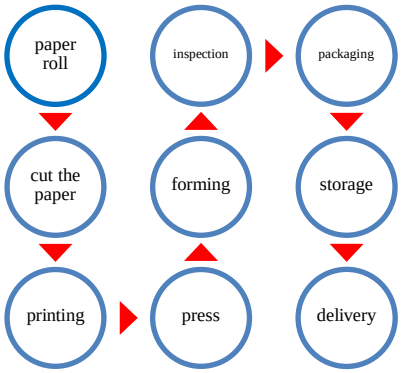

Fig. 3 Paper cup production process

2.2 Automatic paper cup manufacturing

2.2.1 Automatic production process

1. Sort the printed paper to make a cup shape,
2. roll the paper into a cup shape,
3. automatic sealing paper cup as a cone with internal heat,
4. close the bottom of the cup automatically with the heat inside,
5. roll the mouth of the cup and bending the top of cup as a shape
6. finished a paper cup.

Fig. 4 automatic paper cup processes

2.2.2 Packing process

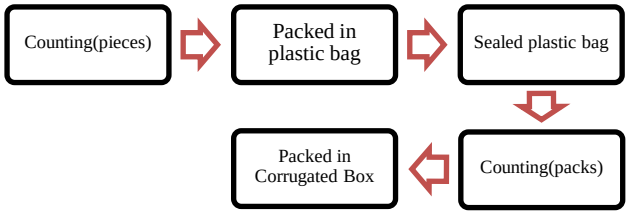

Fig. 5 Paper cup packing process

3. AUTOMATIC PAPER CUP PACKING MACHINE DESIGN [7]

Automatic packaging system is helping R&D team to solve the manufacturing problems. The results can be easily modified to reduce labor time, labor costs, production costs, and energy consumption.

Researchers have collected data from the factory. The result is used to design the automatic machine. This machine can replace 2-3 workers and reduce the working area as well. In addition, this reduces the waiting time during packing cup to the bag. The machine is shown in Fig. 6.

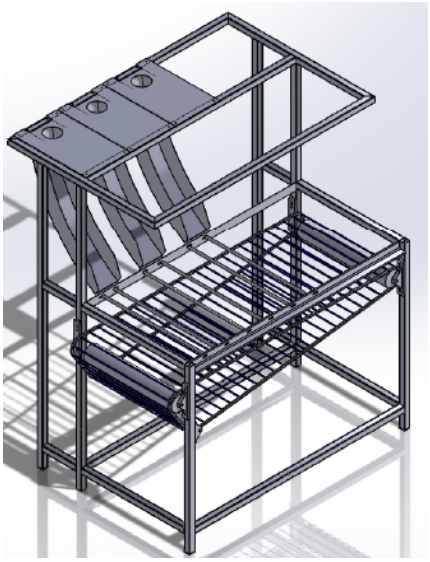

Fig. 6 Automatic packing machine

4. AUTOMATIC PACKING MACHINE TESTING

The test of automatic filling machine sequence is as follows.

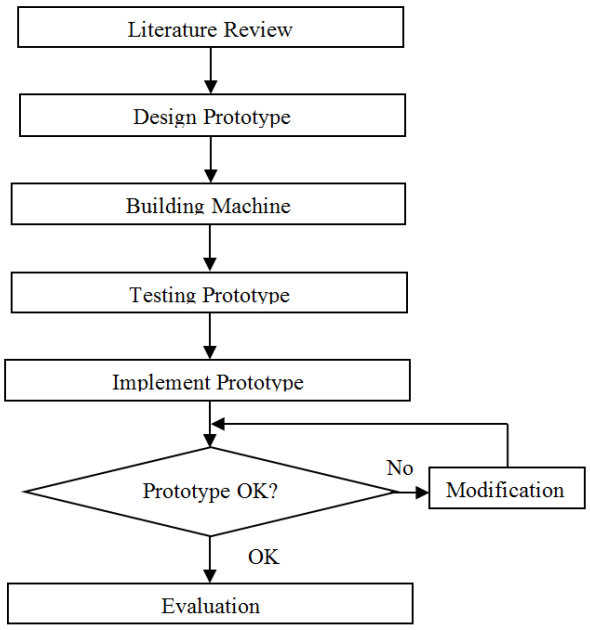

Fig. 7 The test of automatic filling machine sequence

5. CASE STUDY

Three machines M33 M34 M63 are studied as the case study. The production speed of each machine is 120-180 cups per minute. The results are shown as follow:

Table 1 Production of paper cups of machine

Production volume 2017			
Month	M33	M34	M63
Jan	649,340	2,005,723	416,612
Feb	548,580	2,975,827	314,368
Mar	1,402,442	2,209,221	383,680
Apr	87,674	2,481,317	704,684
May	197,680	2,984,445	771,740
Jun	1,474,390	2,110,372	447,498
Jul	1,319,708	1,403,394	521,917
Total	5,679,814	16,170,299	3,560,499
Total 3 units			25,410,612

5.1 Automatic filling machine

To improve the performance of automatic packaging machine, the performance before and after must be tested. The electric power meter (Kyoritsu KEW 6310) was used to measure the power consumption.

5.2 Performance before improvement

The performance of automatic filling machine before improvement was testing. The measurements and data are as follows.

The wages cost before development

The labor costs information for packing seals of machines M33, M34, M63 (3 units), are 3 employees, one employee per one machine.

3 workers = (wages+(OT2.5 hrs.))x (days/month)x(man)
= (300+(140.6))x (26x1) x (3)

Costs/month = 34,366.80 Baht/month
Labor cost = 412,401.60 Baht/year

The energy costs before development

The energy costs information for packing seals of machines M33, M34, M63 (3 units), are 3 units, one units per one machine. (1 machine. = 3.2 kw)

3 units = (energy x hrs.)x 3.6 Bath) x (days/month)x(machine.)
= (3.2kw x24 hrs. x 3.6)x (26x1) x (3)
Costs/month = 21,565.44 Baht/month
Energy cost = 258,785.28Baht/year

5.3 Performance after improvement

The wages cost after development

The labor cost information for packing seals of machines M33, M34, M63 (3 units) is as follows since one employee per three machines.

3 workers = (wages+(OT2.5 hrs.))x (days/month)x(man)
= (300+(140.6))x (26x1) x (1)
Costs/month = 11,455.60 Baht/month
Labor cost = 137,467.20 Baht/year

The energy costs after development

The energy costs information for packing seals of machines M33, M34, M63, are 3 units, 3 units per one machine. (new machine. = 4.7 kw)

3 units = (energy x hrs.)x 3.6 Bath) x (days/month)x(machine.)
= (4.7kw x24 hrs.x3.6)x (26x1) x (1)
Costs/month = 10,558.08 Baht/month
Energy cost = 126,696.96 Baht/year

5.4 Results

In this study the result is used to design the automatic machine. This machine can replace 2-3 workers and reduce the working area as well. The Comparison performance between before and after improvement

The labor cost can reduced = 22,911.2 Baht/ month
= 274,934.4 Baht/year
or about
= 67.7% of the total cost.

The energy cost can reduced = 11,007.36 Baht/month
= 132,088.32 Baht/year
or about
= 48.7% of the total cost.

6. CONCLUSIONS

Performance before improvement
Labor cost = 412,401.60 Baht/year
Energy cost = 258,785.28 Baht/year
Total = 671,186.88 Baht/year
Performance after improvement

Labor cost = 137,467.20 Baht/year
Energy cost = 126,696.96 Baht/year
Total = 264,164.16 Baht/year
The operating cost reduced = 671,186.88
-264,164. 16 Bath/year
= 407,021.28 Bath/year

The operating cost can reduced 60.64 %

The result shown that the operating cost can reduced from 412,401 Baht/year to 137,467 Baht/year, or about 67.7% of the total cost. The energy cost reduced from 258,785 Baht/year to 126,969 Baht/year, or about 48.7% of the total cost. Based on the techniques and design methods developed, the researcher hopes that this research will be a guideline for other packaging systems development. It can reduce the cost of production and help to save energy.

7. REFERENCES

[1] Praweera Photisuwan. “According to a study on the economy of the packaging industry in Thailand.” The Office of Industrial Economics, Ministry of Industry, 2016.
[2] Monthly Report. According to a study on the economy of the packaging industry. The Office of Industrial Economics, Ministry of Industry, July 2018.
[3] Kasikorn Research Center. “The packaging and printing business in 2018” Research data, March 2018.
[4] The ASEAN Economic Community in 2011, the printing and packaging industry saw a shortage of Thai and foreign workers. The Office of Industrial Economics, Ministry of Industry, Sep 2011.
[5] According to the report on employment Samutsakhon Provincial employment Office Samutsakhon, 2017.
[6] Sarawut Pitoonpong. “The Depth study on employment in micro and small enterprises in Thailand” Office of the Permanent Secretary, Ministry of Labour.
[7] Chaiyapon Thongchaisuratkrul. “ Energy Management in Buildings” King Mongkut's University of Technology North Bangkok, ISBN: 974-620-737-7, Bangkok, May 2011.
[8] Pisanurat kejorn. “ PLC and Sequence control MELSEC FX Series” Fostmex Company Limited, 2016.
[9] Patara Pongkittikoon. “Pneumatics and Hydrualics” SE-EDUCATION Public Company Limited, 2012.

WASTE REDUCTION IN LEATHER GLOVES PRODUCTION PROCESS

P. Trinrachatametee[1)*], N. Sukachat[2)] , N. Udomsri[3)]
[1)*] *Rajamangala University of Technology Suvarnabhumi, Nonthaburi.*
[2)] *Rajamangala University of Technology Suvarnabhumi, Nonthaburi.*
[3)] *Rajamangala University of Technology Suvarnabhumi, Nonthaburi.*
Email: prawit19738@gmail.com

ABSTRACT: This project aims to reduce waste in leather gloves production process, and to improve production process to increase the efficiency of leather gloves production. Data were collected from the plant and the resultsshowed that the works did not meet the standards. As this result, the goal was set for reducing waste from the production process under a condition of waste that would not exceed 5 percent. Then, the studies were conducted to explore procedural and waste information in order to reduce the waste occurred in the production process, from the preparation procedure to the blade monitoring, which are standard operations.The theory of quality tools was used in this study. Problem analysis and technical questions 4M, 5W 1H and PDCA principle were used to improve the performance of producing leather gloves. This study also applied industrial engineering and explored side effects by collecting experimental data and comparing the production performance of leather gloves before and after updating. The results showed that the amount of waste due to rash problem was reduced from 10% to 3.75%, or the waste reduction at 6.25%, adding value to the plant at 16,200 baht per month.

1. INTRODUCTION

Leather export and production company in the country and the foreign countries was informed about the high demand of long leather gloves based on the information regarding demand in 3 months. It resulted in 2,848 pairs of waste on average out of the total 28,888 pairs. The ratio of long leather gloves in high demand from customer to other products was 80 out of all products.

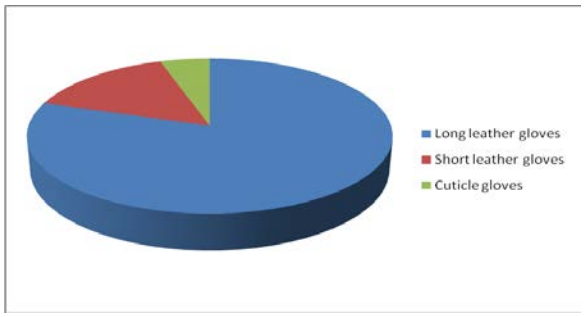

Fig. 1 The proportion of leather gloves export

Creating system robustness should be made during the design phase and not during operation [1], When most system parameters already are set. Each production system is the result of a unique and context dependent development process, and its comprising design and evaluation activities are most vital for system performance.

A Study of Process Improvement Best Practices, [2] Software project success depends on various reasons including project control, software standards and procedures. Formal process improvement frameworks have emerged widely to promote the use of systematic processes for software engineering. These approaches identify best practices for managing software engineering quality.

Research that linked experience, [3] Practice builds skills with existing products and process, in part by bounding novelty and the introduction of complexity in order to maintain stability within learning cycles. Process improvement, by contrast, often requires increasing the number and range of experimental factors to search for the best product and process changes.

2. PROBLEM ANALYSIS TOOLS

According to the data collection about customer-returned defects of long leather gloves, there were 3 types of wastes: undesirably deformed gloves, tore gloves, and undersized gloves, 2,278 pairs, in total. They were returned for further analysis revealing that undesirably deformed gloves outnumbered the rest.

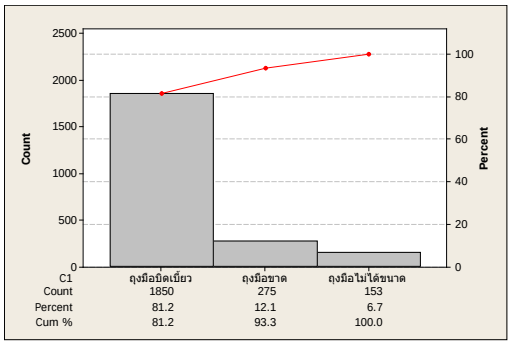

Fig. 2 The Pareto diagram showing the proportion of long leather gloves defects

Based on the Pareto diagram [4], "Trivial Many" was used to analyze and found that defect occurred in long leather gloves caused by deformed gloves based on 80-20 principle.

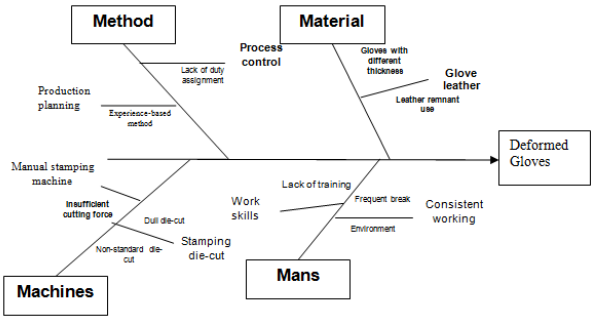

Fig. 3 Fishbone diagram showing causes

Table 1 Cause Analysis Table

Main Reason	Subtraction	Solutions
Machine	Undersized die-cut as stipulated by the company	Reform new die-cut according to the company's stipulation.
Methods	Lack of details in production procedures Unconventional production No quality assurance	Create working instruction (WI) Provide quality assurance certificate
Mans	Poor working standard	Organize training to improve skills

3. RESULTS AND DISCUSSION

The causes of the defects were analysed to solve the problem regarding new die-cut leather gloves to be appropriately sized and result in different sizes that avoid defects from employees' hand-sewing.

Fig. 4 Die-cut leather gloves

Therefore, employees must be trained to sharpen skills by inspecting quality of leather gloves to comply with the production standard.

Table 2 Comparison between before and after the update

Before	After
  Mark is set to sew.	 Add a bookmark to facilitate leather gloves sewing for more easy and convenient to work.
 Finger does not fit with the rest	 Increase 5 mm. in the length of the cutting edge and sew it to fit the other parts.
 The middle finger and the finger have the same size.	 Increase length of middle finger

4. CONCLUSIONS

Based on the experimental results and analysis of 4-week period as shown in table 3, it could be concluded as follows.

Table 3 The manufacturing and jobs lost after the update

Week	Number of production (Piece)	Check Number) (100%)	Number Couple		The value (Baht)
			Good	Bad	
1	7200	7200	6840	360	5400
2	7200	7200	6912	288	4320
3	7200	7200	7008	192	2880
4	7200	7200	6960	240	3600
Total	28800	28800	27720	1080	16200

Based on weekly data, data were divided into four weeks. From the table, after the update, of total production of 28,800 pieces, there were 27,720 good work pieces and 1,080 deformed work pieces.

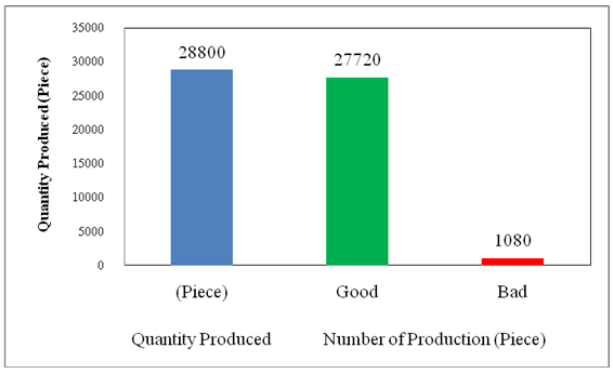

Fig. 5 Information on production and waste after the update

The findings of this study could lead to the suggestions. Template options should be prepared in stamping leather gloves, according to size, as determined by the company. Marks should be added to conveniently and easily sew according to company documents, operational method, and work instruction. For example, clearly detailed procedure and clear documents of the audit logs should be displayed to meet the quality standards. Standard documents should be prepared by the company to reduce waste as follows: 1 chart from the trial operation from the comparison chart after the update. It can be seen that the waste could be reduced to 6.25 percent from the original 10 percent, accounting for 3.75 percent waste reduction and added value would be 16,200 baht according to the set goal.

5. REFERENCES

[1] Monica, B., and Kristina, S. F., 2004, Production System Design and Evaluation for Increased System Robustiness, *Second World Conference on POM and 15th Annual POM Conference, Cancum, Mexico*, April 30 May 3, Abstract 002-0536.

[2] Kuala,. L., and Johor, M., 2011, A Study of Process Improvement Best Practices, *Proc. 5th Int. IT&Multimedia at UNITE (ICIMU 2011)*, Malaysia., 14-16 November.

[3] Steven, J. Spear., 2003, Building process improvement capacity: Structuring problem solving as skill-building exercises, Working paper: 02-006, February.

[4] Juran Institute Inc., 1990, *The Tools of Quality : Part IV Histograms, Quality Progress*, 23(9), September.

PREDICTION OF OPTIMUM WELDING PARAMETERS FOR FRICTION STIR WELDING USING GA AND ANN: A REVIEW

Amit Kumar[1)*], Abhishek Kumar[2)] and Amit Tiwari[3)]
**CASRAE, Delhi Technological University, Delhi-110042,India*
[1)] CASRAE, Delhi Technological University, Delhi-110042,India
[2)] MWC, Bharat Electronics Limited, U.P-201001,India
[1]amitmech159@gmail.com, [2]abhishekkumar8708362@gmail.com, [3]amittiwari@bel.co.in

ABSTRACT: Friction Stir Welding (FSW) is an innovative solid-state joining technique in which atoms are bonded together without any melting. Dissimilar alloys can also be joint by the same process and have been put in service in industries for joining Aluminium, magnesium, zinc and copper alloys. We present a comprehensive review of multi-response optimization of Friction Stir Welding (FSW). We utilize Artificial Neural Networks (ANN) and Genetic Algorithms (GA) to derive optimal parametric combination to yield favourable tensile strength and impact strength. Weld quality is predominantly affected by welding input parameters such as the tool rotational speed, welding speed, axial force, which plays a major role in deciding weld quality. Tool rotation speed and welding speed shows notable influence on mechanical properties of welded joints as compared to tool tilt angle and tool geometry. Friction Stir Welding tools are also reviewed in which square pin profile is identified to be suitable for the dissimilar welding of different alloys, which produces sound joints. However, in other published studies threaded cylinder or threaded taper provide better joints. FSW has been also proven to be too able to join metal matrix composites (MMCs). The current review aims to establish a global state-of-art of friction stir welding and different points of interest will be discussed. This study also illustrates the correlation between the input and output responses. It is concluded that ANN model with genetic algorithm may provide a good ability to predict the friction welding process parameters to weld different alloys.

1. INTRODUCTION

Friction stir welding (FSW) is a novel solid state joining process which can join two similar or dissimilar materials without melting them. Friction stir welding technique was invented and patented by W.M. Thomas et al. of The Welding Institute(TWI), the UK in December 1991[1]. In FSW two materials are joined by the friction heat generated in the interface of the materials due to rotation of one-part relative to other and the material flow due to intense stirring action[2]. Friction stir welding can be employed to join materials which are difficult-to-join or unweldable by traditional fusion welding methods such as high strength aluminium alloys especially AA2xxx and AA 7xxx[3-5]. Since there is no need of melting of parent metal for welding in FSW.

Friction stir welding become the prominent option to weld Al, Mg and other materials, etc. There is a problem of liquefaction of these metal during welding by other methods like MIG, TIG, ARC, and GAS welding[9]. Friction stir welding gives improvement in mechanical properties of material to be joined such as tensile strength, fatigue strength, corrosion resistance, residual strength, etc. as compared to other conventional fusion welding process such as TIG, Meal inert gas welding(MIG) and Laser beam welding[3]. The typical uses of FSW in the manufacturing of Aerospace fuel tank, high-speed train body[6] and it also has good ecological aspects also such as for diminishing of the material weld and avoid emissions of harmful radiations and gases which usually associated with fusion welding process.

FSW process consists of inserting of rotating pin into the abutting edges of plates to be joined as well as the traversed movement of the tool with stirring action. This process can be easily understood in three different stages

I. Plunging - This is the first stage of the FSW process. In which the rotating tool pin is shove into the neighboring edges of the plates to be joined.
II. Dwelling - After the plunging, the tooling pin is rotated in contact with the sides of the plates to be entered for a certain time duration. This rotation of tool results in the generation of initial frictional heat needed for softened the material before the traversed motion of the tool.
III. Welding - As the material starts softened the tool is given a traverse motion along the joint line. This causes to flow of material due to intense stirring action. And the required heat input is provided by the compressive force across the joint[2,8].

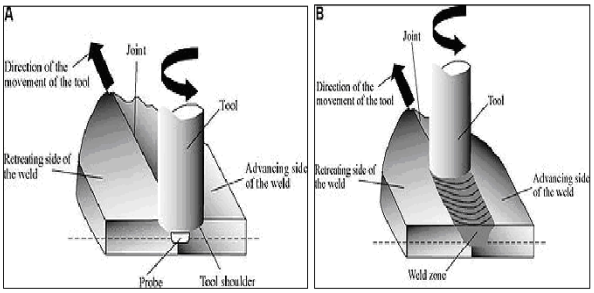

Fig 1: Schematic diagram of the FSW process [10]
(A)Two different work-material joining together.
(B) Showing the weld zone during the Process

The aim of this paper is to give the basic understanding about the relationship of these FSW parameters on the weld quality to the reader using a mathematical model. For the augmentation of the welding parameters ANN and GA was employed.

2. EFFECT OF FSW PARAMETERS ON YIELDING, TENSILE STRENGTH & IMPACT STRENGTH

2.1 Tool Rotational speed

W.Y.Li [11] uncover that while keeping constant rotational speed, UTS slightly increases with the increasing welding speed. And also found that the slightly increment in grain size with the increase in the ratio of rotational speed to welding seed.

Ravi [12] presented work on Aluminium alloy, i.e., AA5052-H38, consequences of rotational tool speed was analyzed and experimentally determined the value of MTSLFL (maximum tensile shear lap shear fracture load) was comes to be 4215 N.

Shiva [13] observed that at middling tool rotational speed, better mechanical properties were attained. And at the conical taper of tool profile, equiaxed grains are found.

Y.Ni [14] investigated for the optimum travel speed which comes to be 2 cm/sec, which further concluded that in Friction stir welding high travel speed with HRS (high rotational speed) is more appreciative for getting sound joint performance. And less heat produces during the high travel speed.

Ravi et al. [15] investigated the joint manufactured at 5 different rotational speed, and the rpm which executed the best tensile properties is at 1000 rpm. This study also recommends that to get defect free welds; moderate tool speed is the best option.

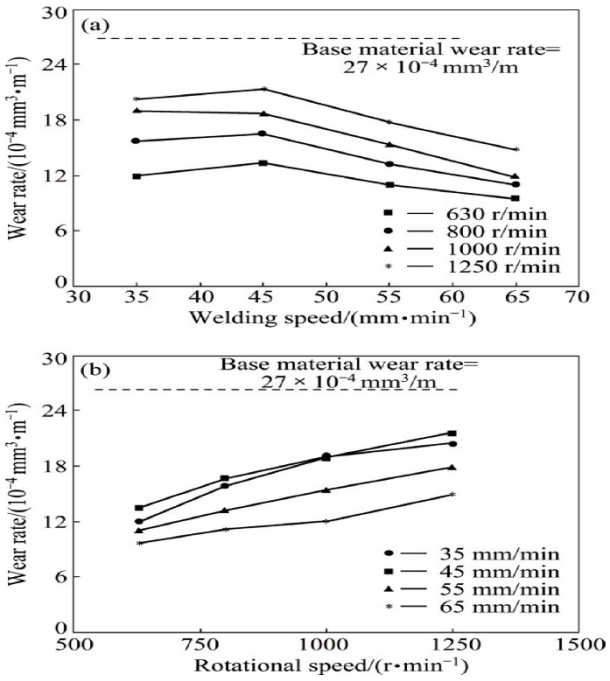

Fig 2: Wear rate vs welding speed at various Rotational speed (a) wrt to rotational speed at different welding speeds (b) for FSW AMCs welded joints [16].

Marathe [17] experimentally proven that the ultimate tensile strength of an FSW joint increases with the increase in tool feed up to a certain level after that ultimate tensile strength start decreases with the further increment. Also concluded that as the heat generated because of friction is more at high tool rotation speed will lead to an increment in ultimate tensile strength if FSW joints.

Satish [18] investigated by welded AA5083 at different rotation speeds and different tool profile and concluded that at the rotation speed of 11.83 mm/sec, 0.667 mm/sec using the threaded profile with tapering resulting into a good mechanical property.

2.2 Welding speed

Dehghani et al. [19] investigated the effect of WS (welding speed) on FSW of Al, i.e., 7075-T6 Al. It was observed that decrement in the intermetallic compound layer on increasing the welding speed, which tends to reduce the weld heat input.

3. EFFECT OF TOOL TILT ANGLE AND GEOMETRY

3.1 Tool tilt angle

Past experiments conducted and have shown that the tool tilt angle is linked with the weld integrity[20]. Dehghani [19] proven that the tensile strength of different Al-mid steel FSW welds decreases with the increase in tool tilt angle, this was because as the tool tilt angle increases, a notable increment in IMC (intermetallic compound) was found.

Kimapong and Watanabe [21] investigated the affection of strength of the weld by considering tool tilt angle and found that with the increment in tool tilt angle, the IMC thickness tends to increase which leads to decrement in shear strength of welds.

Chen et al. [23] in their experiment it is found that heat generation is affected by tool tilt angle and if it properly managed defect-free welds can be obtained. And Z. barlas [24] experimentally observed that 20^0 tilt could give the defect-free weld.

Abhijit et al.[22] investigated that the volume displacement of a material increases with the increment in tool tilt angle.

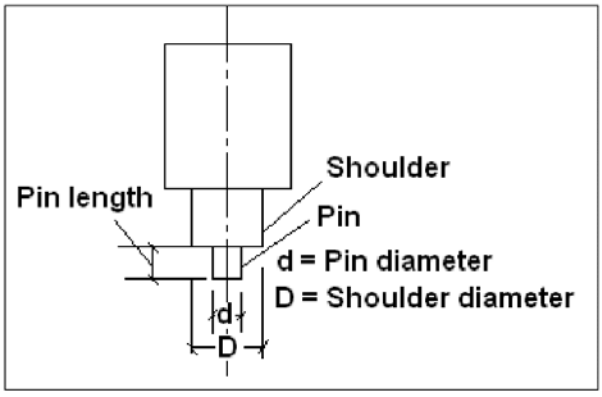

Fig 3: Tool Profile[8].

4. TOOL GEOMETRY

Different tool geometry like shoulder and pin material, shoulder diameter, pin diameter, pin length, thread pitch can determine the outcomes of the welding process.

And with the concern with heating aspects, the considerable parameters are, the relative size of tool pin and shoulder. It is also shown that diameter of that tool's shoulder is proportional to torque at persistent rotational speed[25].

Prakash et al.[26] concluded from his study that

the most commendatory result is found by using a concave shoulder tapered pin tool.

P. Mastanaiah et al.[27] observed that the curve slopes during cooling phase and heating phase are near to equal due to the residence time of the tool increases due to low welding speed, of the conical threaded tools.

Conical profile tool in friction stir welding possess maximum stress distribution and max. Vector sum displacement and the least with threaded cylindrical profile [28].

Some studies have been done on tool geometry used in FSW process, and it comes to be that Pentagon shaped tool gives better material mixing effect and maximum UTS, while the square-shaped tool is not able to produce a required amount of heat. And it is also found that the hexahedron shaped tool generates less temperature due to the flat faces near the pin[26].

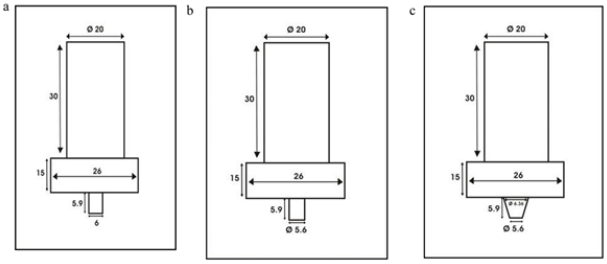

Fig 4: Different shapes of tool and standard dimension of tools
(a) Square pin profile (b) Cylindrical Pin profile
(c) Tapered pin profile [29].

5. METAL MATRIX COMPOSITES

Periyasamy et al. [30] investigated that to join MMC (Metal Matrix Composites), i.e., Al/SiCp, with the tool rotational speed at 22.83 rev/sec, axial force 9600 N and welding speed 8.89 cm/min yields the maximum ultimate tensile strength of 265,000 Pa.

Hemath et al. [31] experimentally proven that at the nearest to the tool, a temperature is being maximum and with increasing the distance temperature falls considerably.

Hosseinzadeh [32] Aluminium alloy 2024 has been investigated in this study at high temperatures and ambient conditions. Following conclusions have been drawn some of them are: Implanting Silicon Carbide particles to enhance the microhardness of material; the yield strength is found to be 2.5 times.

Devanathan [33] they have experimentally proven that there was no such tool wear, only Al particles were settles at tool pin. It was also concluded from the study that axial force has more noticeable effects on tensile strength by a rotational tool speed or by transverse speed.

6. ANN AND GA TO PREDICT THE WELDING PARAMETERS

Okuyucu et al.[34] used ANN to attain correlation between FSW parameters and mechanical residences of Al plates. From last decades, many researchers have investigated the effects of different welding parameters on the strength properties of FSW joints using various materials [34-41]. Many researchers use various optimization models and solution techniques, but ANN is coming to be the prominent solution.
And using the Genetic algorithm can also lead to the optimized parameters in the FSW process. Some studies have been done in last few years, some of them are presented in this paper.

DUTTA et al. [42] uses artificial neural networks and regression analysis to model the gas tungsten arc welding and founds that the ANN has a better performance as contrast with regression analysis.

ATES et al.[43] presented his work by using the ANN for finding the optimized parameters of a gas arc welding. OKUYUCU et al. [34] confirmed the opportunity of using the ANN for the mechanical residence calculation of FSW Al plates assimilate of process parameters considering of rotational speed and welding velocity.

Lakshminarayanan et al. [44] evaluated that artificial neural networks perform better than any methods. Also, this technique works better with the greater no. of experiments. It also concluded that from his study that tensile strength is greatly affected by Rotational speed [44].

7. SUMMARY AND FUTURE SCOPE

Many experiments and theoretical studies were conducted to analyze and improve its affecting parameters.
Some important conclusion can be drawn from this review:

- Volume of material displaced increase with the increase in tilt angle
- Larger shoulder diameter could results into increase in axial pressure, but affects the weld quality as the weld shape changes.
- Friction stir welding can be considered as the prominent option for MMCs as it done below to Melting point of the material which prevents the formation of theta phase which results into stronger joints.
- The predictive GA and ANN models are found to be capable of better predictors of tensile strength within the range that they trained. The result of ANN model has indicated that, it is the more robust accurate in estimating the values of tensile strength when compared with other models.

8. REFERENCES

[1] Thomas, W. M. W. et al. Friction stir welding—process developments and variant techniques. SME Summit (1991).
[2] Muthu Krishnan, M., Maniraj, J., Deepak, R. & Anganan, K. Prediction of optimum welding parameters for FSW of aluminium alloys AA6063 and A319 using RSM and ANN. in Materials Today: Proceedings (2018). doi:10.1016/j.matpr.2017.11.138
[3] Wakchaure, K. N., Thakur, A. G., Gadakh, V. & Kumar, A. Multi-Objective Optimization of Friction

Stir Welding of Aluminium Alloy 6082-T6 Using hybrid Taguchi-Grey Relation Analysis- ANN Method. in Materials Today: Proceedings (2018). doi:10.1016/j.matpr.2017.11.380

[4] Buffa, G., Patrinostro, G. & Fratini, L. Using a neural network for qualitative and quantitative predictions of weld integrity in solid bonding dominated processes. Comput. Struct. (2014). doi:10.1016/j.compstruc.2014.01.019

[5] LAKSHMINARAYANAN, A. K. & BALASUBRAMANIAN, V. Comparison of RSM with ANN in predicting tensile strength of friction stir welded AA7039 aluminium alloy joints. Trans. Nonferrous Met. Soc. China (English Ed. (2009). doi:10.1016/S1003-6326(08)60221-6

[6] Long, L., Chen, G., Zhang, S., Liu, T. & Shi, Q. Finite-element analysis of the tool tilt angle effect on the formation of friction stir welds. J. Manuf. Process. (2017). doi:10.1016/j.jmapro.2017.10.023

[7] Meshram, M. P., Kodli, B. K. & Dey, S. R. Friction Stir Welding of Austenitic Stainless Steel by PCBN Tool and its Joint Analyses. Procedia Mater. Sci. (2014). doi:10.1016/j.mspro.2014.07.016

[8] Ullegaddi, K., Murthy, V., Harsha, R. N. & Manjunatha. Friction Stir Welding Tool Design and Their Effect on Welding of AA-6082 T6. in Materials Today: Proceedings (2017). doi:10.1016/j.matpr.2017.07.133

[9] Singh, S. & Dhuria, G. Investigation of post weld cryogenic treatment on weld strength in friction stir welded dissimilar aluminium alloys AA2014-T651 and AA7075-T651. in Materials Today: Proceedings (2017). doi:10.1016/j.matpr.2017.07.237

[10] Yang, B., Yan, J., Sutton, M. A. & Reynolds, A. P. Banded microstructure in AA2024-T351 and AA2524-T351 aluminum friction stir welds. Part I. Metallurgical studies. Mater. Sci. Eng. A (2004). doi:10.1016/S0921-5093(03)00532-X

[11] Li, W. Y. et al. Effects of tool rotational and welding speed on microstructure and mechanical properties of bobbin-tool friction-stir welded Mg AZ31. 64, 714–720 (2014).

[12] Sekhar, S. R., Chittaranjandas, V., Govardhan, D. & Karthikeyan, R. Effect of tool rotational speed on friction stir spot welded AA5052-H38 aluminum alloy. Mater. Today Proc. 5, 5536–5543 (2018).

[13] Shiva, M., Kumar, P. S. & Devaraju, A. ScienceDirect Influence of Tool Rotational speed and Pin Profile on Mechanical and Microstructural Characterization of Friction Stir Welded 5083 Aluminium Alloy. Mater. Today Proc. 5, 3518–3523 (2018).

[14] Ni, Y., Fu, L. & Chen, H. Y. E ff ects of travel speed on mechanical properties of AA7075-T6 ultra-thin sheet joints fabricated by high rotational speed micro pinless friction stir welding. 265, 63–70 (2019).

[15] Ravi, B., Naik, B. B. & Kumar, G. R. ScienceDirect Influence of Tool Rotational Speed on the Mechanical and Microstructure Properties of Friction Stir Welded Al-B 4 C MMCs ſ. Mater. Today Proc. 5, 1411–1417 (2018).

[16] Hassan, A. M., Almomani, M., Qasim, T. & Ghaithan, A. Effect of processing parameters on friction stir welded aluminum matrix composites wear behavior. Mater. Manuf. Process. (2012). doi:10.1080/10426914.2012.700156

[17] Shalin, M. & Hiten, M. Experimental Analysis on Effect of Tool Transverse Feed, Tool Rotational Speed and Tool Pin Profile Type on Weld Tensile Strength of Friction Stir Welded Joint of AA 6061. Mater. Today Proc. 5, 487–493 (2018).

[18] Kumar, P. S., Shastry, C. S. R. & Devaraju, A. Influence of Tool Revolving on Mechanical Properties of Friction Stir Welded 5083Aluminum alloy. Mater. Today Proc. 4, 330–335 (2017).

[19] Dehghani, M., Amadeh, A. & Akbari Mousavi, S. A. A. Investigations on the effects of friction stir welding parameters on intermetallic and defect formation in joining aluminum alloy to mild steel. Mater. Des. (2013). doi:10.1016/j.matdes.2013.01.013

[20] Chen, H. Bin et al. The investigation of typical welding defects for 5456 aluminum alloy friction stir welds. Mater. Sci. Eng. A (2006). doi:10.1016/j.msea.2006.06.056

[21] Kimapong, K. & Watanabe, T. Effect of welding process parameters on mechanical property of FSW lap joint between aluminum alloy and steel. Mater. Trans. (2005). doi:10.2320/matertrans.46.2211

[22] Banik, A., Saha Roy, B., Deb Barma, J. & Saha, S. C. An experimental investigation of torque and force generation for varying tool tilt angles and their effects on microstructure and mechanical properties: Friction stir welding of AA 6061-T6. J. Manuf. Process. 31, 395–404 (2018).

[23] Chen, Z. W. & Cui, S. On the forming mechanism of banded structures in aluminium alloy friction stir welds. Scr. Mater. (2008). doi:10.1016/j.scriptamat.2007.10.026

[24] Barlas, Z; Ozsarac, U. Effects of FSW Parameters on Joint Properties of AlMg3 Alloy. Weld. J. (2012).

[25] Ullegaddi, K., Murthy, V., Harsha, R. N. & Manjunatha. Friction Stir Welding Tool Design and Their Effect on Welding of AA-6082 T6. Mater. Today Proc. 4, 7962–7970 (2017).

[26] Dabeer, P. & Shinde, G. Perspective of Friction Stir Welding Tools. Mater. Today Proc. 5, 13166–13176 (2018).

[27] Mastanaiah, P., Sharma, A. & Reddy, G. M. Role of hybrid tool pin profile on enhancing welding speed and mechanical properties of AA2219-T6 friction stir welds. J. Mater. Process. Technol. 257, 257–269 (2018).

[28] Sucharitha V, V.Thirumal Reddy, Bhargavi Pokala,“Comparison of Threaded and Unthreaded Tool Pin Profiles in Friction Stir Welding using Ansys” International Journal of Current Engineering and Technology (2016)Vol.6, No.1 2347– 5161.

[29] Shalin, M. & Hiten, M. Experimental Analysis on Effect of Tool Transverse Feed, Tool Rotational Speed and Tool Pin Profile Type on Weld Tensile Strength of Friction Stir Welded Joint of AA 6061. Mater. Today Proc. 5, 487–493 (2018).

[30] Periyasamy, P., Mohan, B., Balasubramanian, V., Rajakumar, S. & Venugopal, S. Multi-objective optimization of friction stir welding parameters using desirability approach to join Al/SiCpmetal matrix composites. Trans. Nonferrous Met. Soc. China (English Ed. 23, 942–955 (2013).

[31] Kumar, G. H., Vishwanath, B., Purohit, R. & Rana, R. S. ScienceDirect Mechanical Behaviour Of Friction Stir Welding On Aluminium Based Composite Material. 4, 5336–5343 (2017).

[32] Hosseinzadeh, A. & Yapici, G. G. High temperature characteristics of Al2024/SiC metal matrix composite fabricated by friction stir processing. Mater. Sci. Eng. A 731, 487–494 (2018).
[33] Devanathan, C. & Babu, A. S. Friction Stir Welding of Metal Matrix Composite Using Coated Tool. Procedia Mater. Sci. 6, 1470–1475 (2014).
[34] Okuyucu, H., Kurt, A. & Arcaklioglu, E. Artificial neural network application to the friction stir welding of aluminum plates. Mater. Des. (2007). doi:10.1016/j.matdes.2005.06.003
[35] Lee, W.-B., Yeon, Y.-M. & Jung, S.-B. Mechanical Properties Related to Microstructural Variation of 6061 Al Alloy Joints by Friction Stir Welding. Mater. Trans. (2004). doi:10.2320/matertrans.45.1700
[36] Rajakumar, S., Muralidharan, C. & Balasubramanian, V. Predicting tensile strength, hardness and corrosion rate of friction stir welded AA6061-T6 aluminium alloy joints. Mater. Des. (2011). doi:10.1016/j.matdes.2010.12.025
[37] Cavaliere, P., De Santis, A., Panella, F. & Squillace, A. Effect of welding parameters on mechanical and microstructural properties of dissimilar AA6082-AA2024 joints produced by friction stir welding. Mater. Des. (2009). doi:10.1016/j.matdes.2008.05.044
[38] Peel, M., Steuwer, A., Preuss, M. & Withers, P. J. Microstructure, mechanical properties and residual stresses as a function of welding speed in aluminium AA5083 friction stir welds. Acta Mater. (2003). doi:10.1016/S1359-6454(03)00319-7
[39] Elangovan, K., Balasubramanian, V. & Babu, S. Predicting tensile strength of friction stir welded AA6061 aluminium alloy joints by a mathematical model. Mater. Des. (2009). doi:10.1016/j.matdes.2008.04.037
[40] Shanmuga Sundaram, N. & Murugan, N. Tensile behavior of dissimilar friction stir welded joints of aluminium alloys. Mater. Des. (2010). doi:10.1016/j.matdes.2010.04.035
[41] Rajeesh, J., Balamurugan, R. & Balachandar, K. Process parameter optimization for friction stir welding of aluminium 2014-t651 alloy using taguchi technique. J. Eng. Sci. Technol. (2018). doi:10.1016/S1003-6326(08)60096-5
[42] Dutta, P. & Pratihar, D. K. Modeling of TIG welding process using conventional regression analysis and neural network-based approaches. J. Mater. Process. Technol. (2007). doi:10.1016/j.jmatprotec.2006.11.004
[43] Ates, H. Prediction of gas metal arc welding parameters based on artificial neural networks. Mater. Des. (2007). doi:10.1016/j.matdes.2006.06.013
[44] LAKSHMINARAYANAN, A. K. & BALASUBRAMANIAN, V. Comparison of RSM with ANN in predicting tensile strength of friction stir welded AA7039 aluminium alloy joints. Trans. Nonferrous Met. Soc. China (English Ed. 19, 9–18 (2009).

REDUCE TIMES FROM THE MANUFACTURE CAR SEAT: THE COMPANY CASE STUDY

N. Udomsri [1]* S. Piriyayon [2]P.Trinrachatametree[3] B. Wattananaphakasem [4]
1, 2,3,4 Department of Industrial Engineering, Faculty of Engineering and Architecture,
Rajamangala University of Technology Suvarnabhumi, Nonthaburi
*E-mail: Nonthachoti@hotmail.com**

ABSTRACT: This research aims to reduce the time of car seat production process : A Case Study of Car Seat Production Company by reducing staff time in the bottleneck, there are two main reasons: 1) Inadequate production processes lead to inadequate production, and 2) Overworked employees. Improvements were made to the study of each production line to improve production lines, improvements by work study, seven wastes, ECRS and Production Line Balancing. The production line in the original production line A had 5 rows of car seats, used 57 machines and 56 employees to reduce the cycle time. For technique, the balance has been the production line. The results of the research show that the production line can be controlled and reduced at the same time. In the production line, there are 5 rows and 4 production lines. The production time is 346.91 minutes. The production time were 225.60 minutes, the productivity were 146 car set per day, 58 employees were employed, and 47 machines were reduced. The operation time was 121.31 minutes, equivalent to 53.77 %

Keywords: Work study, 7 waste and ECRS, Production Line Balancing

1. INTRODUCTION

The major produced car seat manufacturers in Rayong provice Thailand, Thai-American joint venture. The car seat manufacturers model Leather and High included 1) Seat Assembly 2) Door Assembly The company has the technology and ability to manufacture the car seat in modern style in the seat system. The finished product is sat comfortable. At present, the company produces Leather and High in line A to produce the order quantity from customers increased. The company must extend its workforce (Overtime), but the company has to spend more capital to produce upholstery. Producing car seat meet the amount of customers. In Line A car production, Leather and High models are divided to several stages, including cutting, stitching, assembly and inspection. The production department is required to reduce work time. Employee demand quantity and quality are in line with the customer. In line A, the production line balancing and work studies timed to reduce the working time of the production line. And find out to reduce costs, increase productivity to meet the needs of customers in terms of price quality and on-time delivery.

1.2 Research Objectives

1.2.1 To reduce the time of car seat production in line A the model Leather and High
1.2.2 To balance the production line of car seat in line A the model Leather and High

2. THEORY AND LITERATURE REVIEW

2.1 The seventh waste is a system to eliminate the satisfaction and improve quality in 7 Waste. It is time consuming, Low quality products. And high cost consist of 1) Overproduction 2) Inventory 3) Transportation 4) Motion 5) Processing 6) Delay 7) Defect [1, 3]

2.2 The 7 quality tools are important for today's industry. In addition, to the competition price product quality is another important factor in reducing production costs of include 1) Check Sheet 2) Pareto Diagram 3) Graph 4) Cause & Effect Diagram 5) Scatter Diagram 6) Control Chart 7) Histogram [2]

2.3 The Reduction of waste by ECRS Effective waste management will result in lower production costs and the result is a chance to make more profits consist of E = Eliminate C = Combine R = Rearrange S = Simplify [3,8]

2.4 Line balancing is a technique used to solve problems in the production line. It leads to the reduction of the imbalance between workers and the minimum workload. The achievement desired production rate. Thus, balance the amount of work in each station, and the number of workers in the station to a minimum. It will be divided into sub-tasks to maintain or maintain the same production rate. [3,4]

2.4.1 Cycle Time is the amount of time employees spend on each production cycle. An employee may be responsible for only one or several jobs, starting from the beginning of the work until the beginning of the work to commence production in the next round. [5,6]

2.4.2 Takt Time is the speed of production, which we use Takt Time to set the pace of production per piece according to the pace that customers want. All employees must control the rhythm of production in one production station not exceeding the time specified. The equation 1 [3,7]

$$\text{Takt time} = \frac{normal\ working\ hours\ in\ day}{Number\ of\ workpieces\ required} \quad (1)$$

The unit of T / T is the unit of time per piece of work (second /piece, minute / piece or hour / piece).

3. RESEARCH METHODOLOGY

3.1 Study of production problems before production line A Before the renovation, there are 5 rows of car seats as follows: Row 1 Front Back (FB) Row 2 Front Cushion (FC) Row 3 Rear Back 40 %, 60% (RB) Rear Cushion 40%, 60% (RB) Rear Back (3Row) and Rear Cushion (3 Row). In production, 56 employees and 57 machines were used as shown in Fig 1.

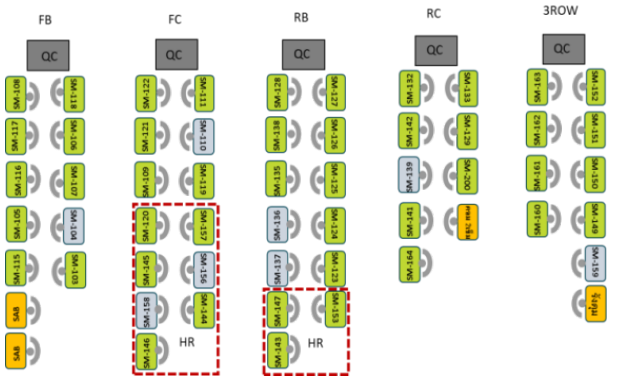

Fig. 1 Production Line A

3.2 The Improvement of production line A due to increasing demand for car seats as shown in Table 1.

Table 1. The customer Car Seat demand

Option	Jul.	Aug.	Sep.	Oct.	Nov.	Dec.
Leather	1,994	2,521	1,018	1,224	2,751	1,614
Fabric	714	778	620	824	1,015	669
Total	2,708	3,298	1,638	2,048	**3,765**	2,283

3.3 The common problem analysis team of engineers and supervisors in the production line with Cause & Effect Diagram The problem is that, 1) the person (Man) must develop the skill to work by the training of the staff, 2) the method must be to related the production line by doing line balance and adding Overtime.

3.4 Improvements in Line A production from the original production of 5 rows as shown in Fig 1. The new production line is 4 rows as follows: row 1 Front Back (FB) and row 2 Front Cushion (FC) in row 1 row Rear Back 40%, 60% (RB) Row 4 Rear Cushion 40%, 60% (RC) Total Row 2 Production Line 5 New 3rd Row Production Rear Back 50% (3RB) with 50% (3RC) Rear Cushion Improve Work by Moving Employees from Row 1 and Line 2 to Headrest (HR). The production was divided into 2 groups. The total number of staff employed was 58, divided to 2 shifts of which 29 person and 47 machines were used for production, as shown in Fig 2.

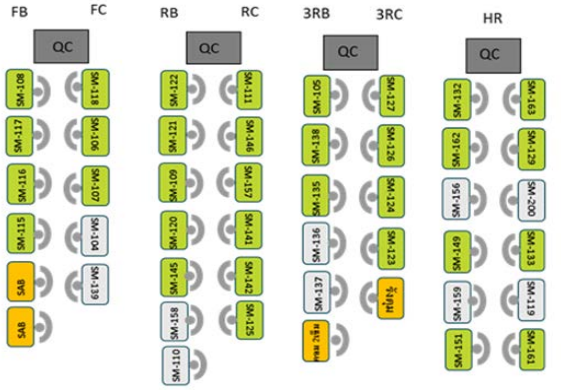

Fig. 2 New line Balance Line A

3.5 Improvement of Row in Line A by New Balance

Row 1 Front Row (Front 1) and Row 2 Front Row (Row 2 FC) Machine 18 Machine Single Needle 13 Sewing Machine 3 Sewing Machine and 2 Airbag machines Used by 16 employees. After, improvement Row 1 FB and FC produce Front Back (FB) and Front Cushion (FC) using 11 machines, 7 needles, 2 seam machines and 2 Airbag machine 14 employees are produced as shown in Fig 2.

Row 2 Before, production Row 3 Rear Back40%, 60% (RB) and Row 4 Production Rear Cushion 40%, 60% (RC) Machine 19 Single Sewing Machine 14 Sewing Machine 4 Sewing Machine 2 Needle 1 Machine used by 18 of employees. After, production Row 2 RB and RC. Both Rear Back 40%, 60% (RB) and Rear Cushion 40%, 60% (RC) using 14 machines, 11 single needle machines, 2 seam machines, and 2 needles machines. Employee 21, are produced as shown in Fig 2.

Row 3 Before, production row 5 Rear Back50% + Rear Cushion50% using 10 machines sewing machine single needle 8 sewing machine 1 stitch machine and knitting needles 1 machine used 12 employees. After, renovation to row 3 the same machine used 11 machines as a single needle machine, 8 machines, 2 stitch machines, Machine 2 and machine needle 1 machine used all 13 employees as shown in Fig 2.

Row 4 Before the production line. Headrest (HR) is moving machines and employees from row1 and row 2 and row 2 After the row 4 using 12 machines as a sewing machine, 8 sewing machine stitch seam, 2 machines added to the seam machine 2 machines used by 10 person according to the original process as shown in Fig 2.

4. RESULT AND DISCUSSION

Before the improvement of production line A all 5 rows have been analyzed work process. All of work, rows do not flow in one direction. Backflow takes zero to walk, pick up, or move in the process. The results of new production line balances reduce production time and productivity. as shown in Table 1 and Fig 3, Fig 4. This research related [8] S.Muankaw, S.Puajindanetre and S.Sirikulvadhana, Brainstorming all implementer to improve new working method under ECRS technique are elimination, combination, rearrange and simplification,

and This research related S.PartPake, R.Chompu-inwai.[9] this causes the bottleneck process to happen in some production procedures as a result of poor manufacturing performance and unnecessary procedures which cause time waste. Therefore, the researcher improves the process by using ECRS theory to enable the production of packed Thai garlic cloves to be more convenient, fast, straightforward, and more effective, and This research related T. Sunarak.[10] Improve performance and increase efficiency in production line of Stator D Frame from a case study manufacturer by applying the motion and time study, production line balancing and reducing waste by using ECRS method.

Table 2. Comparison of work time before and after improvement.

Title (L=Leather, H= High)	Before (Minute)		After (Minute)	
	Job/ Hrs.	CT(min./ CS)	Job/ Hrs.	CT(min./ CS)
1.Front back (L)	5	36.67	7	20.45
2.Front back (H)	5	25.45	7	18.39
3.Front cushion (L)	5	31.59	7	17.25
4.Front cushion (H)	5	18.32	7	8.76
5.Rear back 40% (L)	5	21.68	7	14.87
6.Rear back 40% (H)	5	17.62	7	12.56
7.Rear back ,60% (L)	5	31.13	7	20.36
8.Rear back ,60% (H)	5	26.65	7	19.61
9.Rear cushion 40% (L)	5	18.77	7	11.21
10.Rear cushion 40% (H)	5	15.68	7	11.54
11.Rear cushion ,60% (L)	5	25.85	7	14.34
12.Rear cushion ,60% (H)	5	18.55	7	13.65
13.Rear back 50% (L)	5	18.59	7	12.87
14.Rear back 50% (H)	5	15.56	7	10.82
15.Rear cushion 50% (L)	5	13.09	7	9.37
16.Rear cushion 50% (H)	5	11.71	7	9.55
Total	80	346.91	119	225.60

$$\text{Reduce time to work} = \frac{225.60 - 346.91}{225.60} \times 100$$

Reduce production time = 53.77 %

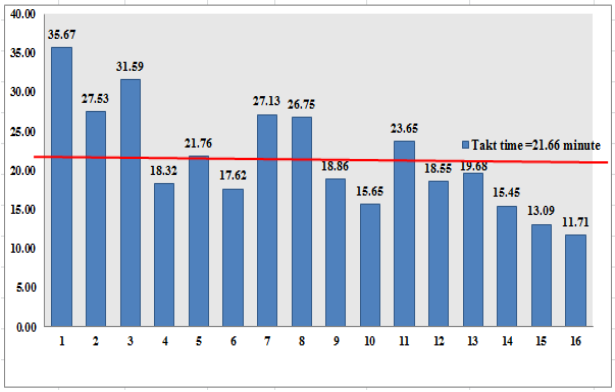

.

Fig. 3 Graph of work time before improvement.

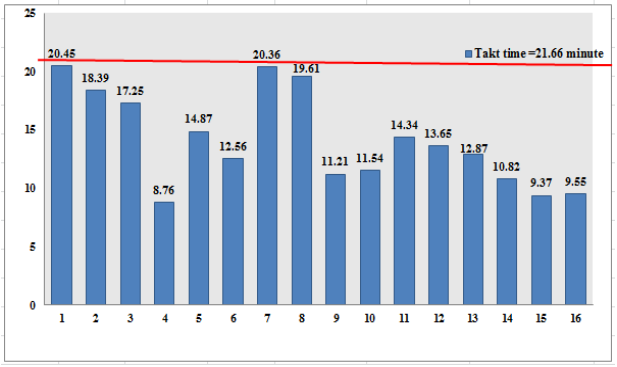

Fig. 4 Graph of work time after improvement.

5. CONCLUSION

The result of improved performance with new line balancing used in the production of Line A, Leather and High. Before the update In September, 2,560, 10.5 hours / shift produced 100 cars / day, equal to 5 cars per hour to employed 56 of employees and 57 of machines. After improving the balance of the line to work faster, it is estimated that 10.5 hours / shift produced 146 cars / day is 7 cars per hour. Employ 58 employees and use 47 machines to reduce the time to work 117.30 minutes. Production increased from 100 to 146 units per day, 46 units per day, or 46%, reducing the use of machinery by 10 units. This research will be beneficial to the company in the implementation of the production line of Leather and the High (Fabric) in order to order the car in November 2,560 customers 3765 cars / month. The company operates Monday - Friday 22 days / month, employs 87 employees. Takt time = 3,765 cars / month. Working 10.5 hours / shift = (22 × 21 × 60) / 3,765 = 7.36 min1 CS = 7.36 * 60 = 441 sec. 1 Hrs. = 60 * 60 = 3,600 sec. It is equal to 87 cars per hour, employing 87 employees. The new line balancing works 10.5 hours / shift, producing 146 units / day, calculated from = (146 / 10.5x2 = 695). 7 cars / 22 hours of work will have 146 × 22 = 3,212 cars to employed 58 of employees. Therefore, 22 working days cannot meet the needs of customers. We cannot add people to support a single month's production. To get the desired result, customers will be able to produce 146×26 = 3,796 cars per month. Customers at 3,765

6. ACKNOWLEDGMENTS

This work was done in the Research and Development department of Industrial Engineering. Thank you, Production Manager, All employees, Car Seat Manufacturing Company Facilitates the research to be completed. And, the research to use to reduce time and increase productivity in Rayong Thailand company effectively.

7. REFERENCES

[1] D. ShevaphayaRoj, and S. Ponganan "7 Wastes". National Productivity Institute, 2001.

[2] P. Buranajarukorn 7 quality tools, information from http://www.nubi.nu.ac.th/webie/7qctool.htm (Date searched 19 August 2017)

[3] Jeffrey, K. Linker and D. Meier. 2006. The Toyota Way Field book. McGraw-Hill, United State of America

[4] P. Buranajarukorn "The balance of assembly lines. By the way, ".Defintional Evolution ", case study sample garment factory" Department of Industrial Engineering Faculty of Engineering Ubon Ratchathani University, 2014)

[5] R. Kanjanapanyakom. Education work Industry, Bangkok: Imprint, 2009.

[6] W. Wongnil. Adding to the production process of the girl skirt, Dhurakij Pundit University, 2015.

[7] Y. Jong Chan, N. Ket Muang, N.Burapha. Balancing production lines to reduce wastage. Dump Mounting Process, Conference Industrial Engineering 2012, 17-19 October 2012, Cha Am Phetchaburi.

[8] S.Muankaw, S.Puajindanetre and S.Sirikulvadhana. Reduction of Operational Process Time in Paper Manufacturing Business, Conference Industrial Engineering 2012, 17-19 October 2012, Cha Am Phetchaburi.

[9] S.ParPake, R.Chompu-inwai. Reduce time waste During the production process of packed Thai garlic cloves production, Seminar in Industrial Engineering and Industrial Management 1 st year, 2017

[10] T. Sunarak. Production Line Efficiency Improvement: A Case of Stator D Frame Model Production Line, Conference Industrial Engineering 2012, 17-19 October 2012, Cha Am Phetchaburi.

PERFORMANCE MEASUREMENT OF PALM OIL INDUSTRIAL COMPANY IN THE STOCK EXCHANGE OF THAILAND

Pittayut Kongpoung[1]
[1] *Faculty of Business Administration and Information Technology, Rajamangala University of Technology Suvarnabhumi, Suphan buri, Thailand.*
E-mail: mrpittayut@gmail.com

ABSTRACT: The objective of this research is to evaluate and rank the potentiality of 6 palm oil industrial companies that are in the Stock Exchange of Thailand, from 2015 to 2017 by using Data Envelopment Analysis technique (DEA: RCCR model) for calculate efficiency scores (DEA Score) of each companies. The method to evaluate and rank potentiality uses 3 inputs (property, plant and equipment, total expense, depreciation and amortization) and 2 outputs (total revenue, net profit). The result showed that efficiency scores of Lam Soon (Thailand) Public Company Limited rank 1st from 2015 to 2017.

Keyword: data envelopment analysis, dea, performance measurement

1. INTRODUCTION

Crude palm oil and crude palm kernel oil is one of the major agricultural output of Thailand. Palm oil is an important raw material for many kinds of industries such as the petroleum industry, cosmetics industry and food industry. Many products that are used in everyday life. The world's major oil palm producing region is ASEAN, Indonesia and Malaysia being the 1st and 2nd largest producers with total output of 52.5 million tonnes, or 85% of world production and more than 90% of all exports. Thailand 3rd place with 2 million tonnes/p.a., 1.2% of global output. During the 2008-2012, the plantations of palm oil expansion in the North and Northeast of Thailand, due to the support of the Government for development of alternative energy supply. By 2016, oil palm producing an annual total of 11.2 million tons. However, there are problems with the sector of palm oil. The production was reached by devoting a greater area of land to cultivation of oil palm, rather than increasing yields on production. This paper use Data Envelopment Analysis technique (RCCR Model) for measurement and ranking effective score of each palm oil for cooking company. The results will provide important information for each company, the 1st effective company can be used as a model for development an operations of other companies for optimize the company's operations.

2. LITERATURE Review

2.1 Performance Measurement

Performance measurement is a concept that was first proposed by Michael J. Farrell, which is the concept of production performance measurement under the statistical output function with constant return to scale and replacement ability of production inputs (1992, Battest) unit of production or decision-making units mean manufacturers that want to measure operating performance. What kind of performance can be divided into 3 categories as follows:

1. Technical efficiency: TE is the ability of a manufacturer to produce the most output when fixed inputs or the ability of a manufacturer to use minimal inputs to generate the output in any quantity (Rhaman, 2013)
2. Allocate efficiency: AE is the ability of the manufacturer to determine the proportion of each type of production factors for productivity under the restrictions, the prices of factors of production and productivity to be produced (Tzouvelekas et al., 2002).
3. Economic Efficiency: EE is the ability of producers to use inputs are minimal and manufacturing costs are low compared to the productivity of a given quantity (Coelli et al., 2005).

2.2 Data Envelopment Analysis

Data Envelopment Analysis is presented in the (Charnes et al., 1978) is a technique used manufacture border line is standard for measuring productivity. This method used linear programming technique for calculate the weighted value of each Input and output to make all the production units which are considered effective. The most output of each organization that contribute to weight efficient production will be used as the performance of the organization (DEA Score), which is used to compare the efficiency of organizations operations. It is under the assumption of constant returns to scale. The Organization with a DEA Score of 1.0 is a powerful organization with efficiency. The models of this Data Envelopment Analysis type are called "CCR Model", which is calculated as follows: Performance Score (Prasopchai Pasunon, 2007).

$$Max\, T_i = \sum_{r=1}^{s} V_r Y_{ir} \quad (1)$$

$$\sum_{r=1}^{s} V_r Y_{ir} \le \sum_{j=1}^{m} U_i X_{ij} \quad (2)$$

$$\sum_{j=1}^{m} U_i X_{ij} = 1 \quad (3)$$

$$U_j, V_r \ge \in \ (j = 1, 2, ..., m; r = 1, 2, ..., s) \quad (4)$$

Later (Banker et al., 1984) have proposed a new model, BCC Model, the model used to calculate the minimum value of the inputs or the maximum value of the output

as model (CCR), but it is under the assumption returns the size variable (VRS), which performs the following equation to calculate the score.

$$Max\, T_i = W_i + \sum_{r=1}^{s} V_r Y_{ir} \quad (5)$$

$$W_i + \sum_{r=1}^{s} V_r Y_{ir} \le \sum_{j=1}^{m} U_i X_{ij} \quad (6)$$

$$\sum_{j=1}^{m} U_i X_{ij} = 1 \quad (7)$$

$$U_j, V_r \ge \in \ (j = 1, 2, ..., m;\ r = 1, 2, ..., s) \quad (8)$$

2.3 Data Envelopment Analysis (RCCR Model)

Most popular Data Envelopment Analysis models is BCC and CCR, DEA scores of both will be between 0-1 if the operation effectively (DEA Score) is equal to 1.0 . The organization is efficient in operation, if the score is equal to 1.0, if the score is lower than 1.0, an organization does not have an operational performance. The issue of BCC and CCR Model is cannot sort on the performance of individual organizations because several companies can have a score equal to 1.0, these problems are solved by (Andersen and Petersen, 1993) which has the presentation of new technique, which the DEA named RCCR Model, DEA score of each organization will have the specific value. Makes it possible to rank operation effectively score. The subject, which has covered the performance equation RCCR. which is calculated as follows:

$$Max\, T_i = \sum_{r=1}^{s} V_r Y_{ir} \quad (9)$$

$$\sum_{r=1}^{s} V_r Y_{qr} \le \sum_{j=1}^{m} U_i X_{qj} \ (q = 1, 2, 3, ..., n; q \ne i) \quad (10)$$

$$\sum_{j=1}^{m} U_i X_{ij} = 1 \quad (11)$$

$$U_j, V_r \ge \in \ (j = 1, 2, ..., m;\ r = 1, 2, ..., s) \quad (12)$$

When

X_{ij} = *Input type j of* Production *Unit i*

Y_{ir} = *Output type r of* Production *Unit i*

U_j = *Weight of Input j*

V_r = *Weight of Output* (r = 1, 2, 3,…, *s*)

M_r = *Amount of Input* (j = 1, 2, 3,…, *m*)

S_{ir} = *Amount of Output* (r = 1, 2, 3,…, *s*)

3. METHOD

Operation procedure for annual performance measure of 6 palm oil industrial Public Company Limited, 1. United Palm Oil Industry (UPOIC), 2. Univanich Palm oil (UVAN) 3. Chumporn Palm Oil Industry (CPI) 4. Vichitbhan Palm Oil (VPO) 5. AI Energy (AIE), 6. Lam Soon Thailand (LST), analyzing the half-year data from 6 month financial statement there are 4 steps . as follows:

1. Literature Review to find the best Input and output factors for RCCR model
2. Collect Input and Output Data from 6 Month Financial Statement of each Companies, 3 year historical data used. 2560 , 2559 , 2558
3. Create RCCR Model for Calculate Efficiency Score of each year.
4. Calculate Efficiency Score of each year (DEA Score)
5. Summary and Result Analysis.

4. RESULT

The results of performance measurement using Data Envelopment Analysis (RCCR Model) as shown in Table 1.

Table 1: Data Envelopment Analysis Score of each company (2015-2017)

Company	Data Envelopment Analysis Score		
	2015	2016	2017
UPOIC	0.63	0.61	0.47
UVAN	0.91	0.78	1.17
CPI	2.46	3.74	3.14
VPO	2.10	1.87	2.07
AIE	0.56	0.46	0.51
LST	6.07	8.94	10.18

5. CONCLUSION

The research result clearly shows that Lam Soon Thailand is the best on operation performance in the years 2558-2560, with DEA score 6.07, 8.94 and 10.18.The results can be applied to improve operation performance of other 5 companies by using implementation of Lam Soon Thailand Public Company Limited as a model, total revenue of each year is greater than the total expense cost. Three factors that can make difference in operation is Technical efficiency, Allocate efficiency and Economic efficiency and

6. REFERENCES

[1] Battest, G.E. 1992. Frontier production functions and technical efficiency: a survey of empirical applications in agricultural economies. *Agricultural Economics*,7, 185-208.

[2] Rahman, S.A. 2013. *Farm production efficiency: The scale of success in agriculture*. The 4th Inaugural Lecture. Nassarawa State University, Keffi, Nigeria.

[3] Tzouvelekas, V., C. J. Pantzios, and C. Fotopoulos. 2002. Measuring multiple and single factor technical efficiency in organic farming: The case of Greek wheat farms. *British Food Journal*, 104(8), 591-609.

[4] Charnes, A., W.W. Cooper, and E. Rhodes. 1978. Measuring the efficiency of decision-making units. *European Journal of Operational Research*, 2(6), 429-444.

[5] Prasopchai Pasunon. 2007. Organization performance measurement using DEA technique and excel calculate. *Business Administration Journal*, 30(114), 25-38.
[6] Banker R.D., A. Charnes and W.W. Cooper. 1984. Some models for estimating technical and scale inefficiencies in data envelopment analysis. *Management Science Journal*, 30(9), 1078-1092.
[7] Andersen, P. and N.C. Petersen. 1993. A procedure for ranking efficient units in data envelopment analysis. *Management Science Journal*, 39, 1261-1264.

EXTRACTION METHOD OF LEUKOCYTE MOTIONS USING SPATIOTEMPORAL IMAGE ANALYSIS IN A MICROVESSEL

Eung Kyeu Kim[1)]*, Jae Won Lim[2)], and Byunghyun Jang[3)]
[1)-2)]*Department of Information and Communication Engineering, Hanbat National University, Daejeon 34158, Korea*
[3)]*Department of Computer and Information Science, The University of Mississippi, University, MS 38677, USA*

ABSTRACT: We propose an extraction method of leukocyte motions using spatiotemporal image analysis in a microvessel and also show an estimated result of the leukocyte velocities from an image sequence. We use the constraint that leukocytes move along the blood vessel wall contours and extract the leukocyte motions using spatiotemporal image analysis method. The generated spatiotemporal image is processed by a special orientation-selective filter and then subsequent grouping processes which are newly developed for this application. The subsequent grouping processes select and group the leukocyte trace segments among all the segments obtained by simple thresholding and skeletonizing operations. Leukocyte velocities are estimated from the obtained trace segments by grouping when threshold at three hundred.

1. INTRODUCTION

Dynamic analysis of blood cells in blood vessel wall plays a crucial role in the field of physiology research. Leukocytes in blood vessels usually protect the human body from bacterial infection through phagocytosis, which preys upon foreign substances or bacteria that infiltrate from outside the body. It is known that 4,000 to 10,000 leukocytes typically reside in one $\mu\ell$ of blood[1-2]. Leukocyte velocity offers an important information [3] in the analysis of interactions between blood vessel walls and leukocytes. In the conventional works, the measuring methods of leukocyte velocity are not accurate, and their accuracy depends on the amount of collected data, which involves manual human intervention. Our final aim is to develop a leukocyte extraction system that adheres to microvessel walls and to measure their velocities from an image sequence.

Several image processing systems have been developed for the measurement of erythrocyte velocity and arteriolar vasomotion [4-5]. These systems use only simple image processing techniques such as frame subtraction and edge tracking.

However, in order to extract and measure the leukocyte motions that adhere to a blood vessel wall, it is necessary to introduce excellent leukocyte extraction techniques because the identification of moving objects from a image sequence is one of the most difficult problems in a leukocyte extraction system. In biomedical applications, it is a main point to combine domain dependent constraints with contemporary leukocyte extraction techniques in order to develop a practical method. We use the constraint that the leukocytes move along a blood vessel wall contours to generate a spatiotemporal image, and the leukocyte motions are extracted using the spatiotemporal image analysis method [6]. An orientation-selective filter and perceptual grouping processes are newly developed in order to lead to a full system for motion analysis of leukocyte that adhere to a microvessel wall.

2. PROBLEM DEFINITION AND EXTRACTION OF BLOOD VESSEL REGION

2.1 Problem Definition

Fig. 1 (omitted) shows two frames from the microscopic image sequence that include moving leukocytes in rat mesentery microvessel. The image sequences consist of one hundred frames. Each frame is 300x200 pixels in solution, and the frame interval is 1/30 second. The problem is to identify and localize individual leukocytes that adhere to blood vessel walls and to measure their velocities from the image sequence. The overall task flow of this research is shown in Fig. 2 (omitted).

First, all frames of the image sequence are registered. In the image sequence, global translational motions occur at each frame because of some internal movement. There is a translation between two different frames as shown in Fig. 1. These translations can be easily estimated using simple template matching.

Second, a blood vessel region is extracted. The motions of leukocytes that adhere to blood vessel walls can be visualized as the motions along the contours of a blood vessel region in an image. Therefore, the contours of a blood vessel region provide a strong constraint for the identification and localization of leukocytes.

Next, moving leukocyte traces are extracted by spatiotemporal image analysis. It is hard to find leukocytes from only a single frame because a blood vessel also includes many erythrocytes. However, moving leukocytes can be extracted because their velocities are relatively slow. Leukocytes also generate spatiotemporal images by the selection of a curve parallel to the contour line of a blood vessel as a spatial axis because they move along the contour line. Leukocyte trace extraction is performed by combining an orientation-selective filter and a perceptual grouping method which are newly developed for this application.

2.2 Extraction of Blood Vessel Region

The constraint that we use for the extraction of a blood vessel region is that blood cells are flowing continuously in a blood vessel region while other regions remain stationary. This means that a gray level of each pixel in a blood vessel region will vary frame by frame while a gray level in other regions will be almost the same in all frames.

The temporal variance image $S(x, y)$ is defined with Equ. (1).

$$S(x,y) = \frac{1}{n-1}\sum_{i=1}^{n}(I_i(x,y) - \bar{I}(x,y))^2 \qquad (1)$$

Where, $I_i(x,y)$ is the i^{th} frame of an image sequence, and n is the number of images. $\bar{I}(x,y) = \frac{1}{n}\sum_{i=1}^{n} I_i(x,y)$. A blood vessel region is extracted by simply thresholding the temporal variance image $S(x,y)$. The extraction result of a blood vessel region is shown in Fig. 3 (omitted). A blood vessel region can be extracted by removing regions with small area from binary image shown in Fig. 3(b).

3. EXTRACTION AND MEASUREMENT OF LEUKOCYTE MOTION

Although the shape of blood vessel is tube, microscopic images are two dimensional projections of this tube. The leukocytes that adhere to a blood vessel wall flow through outside region of a blood vessel wall, while erythrocytes flow through the central region of a blood vessel wall. Fig. 4(a) (omitted) shows the cross-section of a blood vessel and the region that erythrocytes pass through. Figs. 4(b) (omitted) and (c) (omitted) illustrate two different leukocyte locations; in Fig. 4(b) leukocytes can easily be found, whereas in Fig. 4(c) the leukocytes are difficult to find because erythrocytes overlap it from this viewing direction.

3.1 Formulation for Spatiotemporal Image Problem

The leukocytes as shown in Fig. 4(b) move along a blood vessel contours in the image. Therefore, spatiotemporal images are generated by selection of a curve parallel to the contour line of a blood vessel as a spatial axis, as shown in Fig. 5 (omitted). Fig. 6 (omitted) shows generated spatiotemporal images. The horizontal axis is a spatial axis.

In Fig. 6(a), there are three leukocyte traces. Two of them cross each other. The identification and localization of moving leukocytes have been formulated as the isolation and detection problem of an individual leukocyte trace from spatiotemporal images.

3.2 Orientation-Selective Filter for Leukocyte Traces Enhancement

The feature extraction such as curves and edges is a fundamental problem in development of this extraction system. One of the most well-known filters for this purpose is the Laplacian of Gaussian filter [7]. More recently, as a paradigm of general feature detection, the Gaber filter and wavelet theory has been applied [8-9]. These theories provide design methods for multiresolution frequency filters. Our filter is motivated from Gaber filters and designed on the basis of the constraint of leukocyte motions and nature of our spatiotemporal images.

In order to design a line enhancement filter in our application, the following properties should be considered

First, the orientation of leukocyte trace is always north-east to south-west in spatiotemporal images because leukocytes move to only one direction.

Second, the range of the width of leukocyte traces is known to some extent.

Third, the gray-level patterns which do not move in a blood vessel region appear as lines parallel to the vertical axis in spatiotemporal image, and the gray-level patterns which only happen at few frames appear as lines parallel to the horizontal axis. These patterns are dominant noise components in spatiotemporal image. Thus, these patterns should be removed.

These properties are represented as the constraints in the frequency domain as follows:

First, the response of the filter should be tuned for north-east to south-west directional components and zero for any components of north-west to south-east directions so as to enhance only leukocyte traces.

Second, the response of the filter should be tuned for the known range of the width of leukocyte traces. That is the filter should be a kind of bandpass filter.

Third, the response of the filter should be zero on the two axes in the frequency domain so as to remove horizontal and vertical directional components.

From the above considerations, we define a filter H(u,v;σ) having a width parameter σ as

$$\mathrm{H(u,v;\sigma)}\begin{cases} e^{\left(-2\pi^2\sigma^2(u^2+v^2)\right)uv}, & for\ uv > 0 \\ 0, & for\ uv \le 0 \end{cases} \qquad (2)$$

The bandpasscharacteristic is realized by combination with a Gaussian filter. Let $\mathrm{t(s,t)}$ be a spatiotemporal image, and $\mathrm{T(u,v)}$ be its Fourier transform. Let $F^{-1}\{\cdot\}$ represent the Fourier inverse transform. The filtered image $\mathrm{k(s,t)}$ is then given by

$$k(s,t) = F^{-1}\{T(u,v) \times H(u,v)\} \qquad (3)$$

For comparison with other filters, Fig. 7 (omitted) shows perspective plots of Laplacian of Gaussian (LOG) filter and diagonally directional second derivative of Gaussian filter. Unfortunately, these conventional filters do not completely remove vertical and horizontal components, whose affection to the filtered image is considerable. Our filter has no parameter to be adjusted except for a width parameter, and it is one of the simplest ones which satisfy the above constraints.

3.3 Global Optimizing for Grouping and Selecting Leukocyte Trace Segments

After enhancing leukocyte traces by the orientation-selective filter, we can identify an individual leukocyte motion and measure its velocity. After thresholding the filtered spatiotemporal image, we perform skeletonizing operations [10-11] to extract the candidates of leukocyte trace segments. However, it is unavoidable to extract false segments or fails to extract complete segments by using only those simple image processing techniques. Therefore, we use a subsequent optimization process for grouping and selecting leukocyte trace segments. This process is different from conventional boundary following processes [12], in which it is assumed that only one boundary exists in an image. In Fig. 6(a) (omitted), there are three traces, and two of them cross each other. At an intersection point, leukocyte traces tend to be split as shown in Fig. 8 (omitted).

We formulate the problem as a combinational optimization problem which can be solved by a Hopfield-style network [13]. Let $p_1, p_2, \cdots, p_n$; represent the probabilities that possible connections are

true. We select the best connections by finding P minimizing.

$$E(p) = -\frac{1}{2}\sum_{ij} r_{ij}\, p_i p_j - \sum_i c_i p_i \qquad (4)$$

After selecting the optimum connections, the gaps of the selected connections are filled. We extract sufficiently long connected segments, and regard them as true leukocyte traces. The velocity of each leukocyte trace is easily computed from a tangent direction at each point of a leukocyte trace.

We believe that the grouping method proposed here is applicable to general curve grouping problems as well as the particular problem addressed in this research. Recently, a couple of grouping methods have been proposed [14-15]. While their method finds a curve one by one, our method can extract multiple curves simultaneously by optimizing global consistency.

4. EXPERIMENTAL RESULTS

In this section, we show the experimental results of the orientation-selective filter and the grouping method using spatiotemporal images shown in Fig. 6(a).

Fig. 10 shows the output image of the the orientation-selective filter. We also show the output images of conventional filters in Fig. 11. The width of filter was σ=8 pixels. As shown in Fig. 11(a), the output of the LOG filter was largely affected by vertical and horizontal components. Even in the output of the directional derivative of Gaussian filter shown in Fig. 11(b), leukocyte trace components were disturbed by vertical and horizontal components. As compared with the conventional filters, the output of the orientation-selective filter effectively enhanced the leukocyte traces.

Fig. 10. Spatiotemporal image after orientation selective filtering

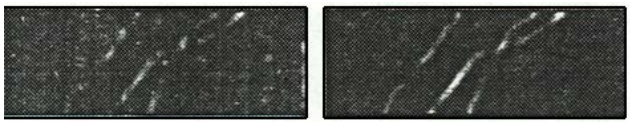

(a) Lapaacian of Gaussian (b) Directional second derivative of Gaussian

Fig. 11. Results of Laplacian of Gaussian filter and directional second derivative of Gaussian filter

The output of the orientation-selective filter was thresholded and skeletonized. We tested it using three different threshold values. Possible connections were extracted from the obtained segment descriptions. Fig. 12 shows the results of the grouping processes. When we thresholded at three hundred, we could extract the true leukocyte traces by using the detected possible connections without disambiguation in the grouping processes. Fig. 12(b) shows three extracted traces. When we thresholded at one hundred and five hundred, several conflicted traces were extracted as shown in Figs. 12(a) and (c), respectively. However, we could obtain only three traces which are almost the same as the traces in Fig. 12(b) after the grouping processes. In the grouping processed, we selected connections satisfying $p_i \geq 0.8$ as true connections. We could perform the stable extraction of leukocyte traces independent of thresholds by using the subsequent grouping processes.

Fig. 13 (omitted) shows the results of the velocities of three leukocytes estimated from the traces obtained when we thresholded at three hundred.

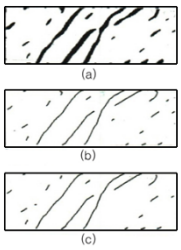

Fig.12 Candidate segments extraction of leukocyte traces when thresholded at three hundred

5. CONCLUSIONS

This paper presents an extraction method of leukocyte motions in a microvessel and shows a measurement result of the leukocyte velocities. We formulated the problem of extracting leukocyte motions as finding curved lines in a spatiotemporal image. In order to enhance the curved lines which was caused by leukocyte motions, the orientation-selective filter was designed based on the properties of the noise components of spatiotemporal image and constraints on the orientation and thickness of the curved lines. We demonstrated that the proposed filter is very effective as compared with the conventional filters. We extracted candidate segments for leukocyte traces after thresholding and skeletonizing the filtered image. Leukocyte velocities are estimated from the obtained trace segments by grouping when threshold at three hundred.

6. REFERENCES

[1] m.blog.daum.net/lkpet/9440105.
[2] www.happycampus.com/doc/111176789/
[3] G. W. Schmid-schonbein, S. Usami, R. Skalak, and S. Chein, The interaction of Leukocytes and erythrocytes in capillary and postcapillary vessels, *Journal of Microvascular Research*, Vol. 19, pp. 45-70, 1980.
[4] B. P. Fleming, B. Klitzman, and W.O. Johnson, Measurement of erythrocyte velocity by use of a periodic differential detector, *American Journal of Physiology*, Vol. 249, (Heart Cird Siology 18), H.899-H.905, 1985.
[5] C.Y.J. Yip, S. Y., Aggarwal, K. R. Diller, and S. C. Bovik, Simultaneous multiple site arteriolar vasomotion measurement using digital image analysis, *Journal of Microvaslular Research*, Vol. 41, pp. 73-83, 1985.
[6] Eung Kyeu Kim, Generation Method of spatiotemporal Images for Detecting Leukocyte Motions in a Microvessel, *Journal of the Institute of Electronics and Information Engineers*, Vol. 53, No. 9, pp. 1397-1406, 2016.

[7] Eung Kyeu Kim and Jae Won Lim, Performance Evaluation of multiresolution Extraction Filter for Pulmonary Nodules Shadow in Chest X-ray Images, *Proceeding of the Summer Conference of the Korean Institute of Signal Processing and Systems*, Vol. 12, No. 1, pp. 42-45, 2011.
[8] Sang Wan Lee, Dae Jin Kim, Yong Soo Kim, and Zeungnam Bien, An Adaptive Gaber Wavelet Neural Networking-based Facial Expression Recognition System, *Journal of the Korea Fuzzy Logic and Intelligence Systems*, Vol. 16, No. 1, pp. 1-7, 2006.
[9] Jin-Woo Kim, Measurement of Leukocyte Motions in a Microvessel Using Spatiotemporal Image Analysis, *International Journal of the Korea Institute of Maritime Information and Communication Sciences*, Vol. 6, No. 3, pp. 315-319, 2008.
[10] C. J. Hilditch, Linear skeleton from sequare cupboards, in Machine Intelligence 6, Edinburgh University Press, pp. 403-420, 1969.
[11] A. Darabi, F. Chandelier, G. Baroud, Thickness analysis and reconstruction of trabecular bone and bone substitute microstructure based on fuzzy distance map using both ridge and thinning skeletonization, *Canadian Journal of the Electrical and Computer Engineering (SCIE*), Vol. 34, No. 1/2, pp. 57-62, 2009.
[12] Norio Baba, Norihiko Ichse, and Toshiyuki Tanaka, Image Area Extraction of Biological Objects from a Thin Section Image by Statistical Texture Analysis, *Journal of the Electron Microse*, Vol. 45, pp. 298-306, 1996.
[13] Jae Hoo Joo, Hoon Kang, 3D Information and Stereo Matching using Hopfield Neural Network and Wavelet Decomposition, *Journal of the Institute of Information Communication in Chung-Ang University*, Vol. 2, No. 2, pp. 1-10, 2000.
[14] R, Mohan and R. Nevatia, Segmentation and description based on perceptual organization, *Proceeding of Computer Vision and Pattern Recognition*, pp. 333-341, 1989.
[15] Lindeberg Tony, Detecting salient blob-like image structures and their scales with a scale-space primal, Proceeding of Computer Vision, Vol. 11, No. 3, pp. 283-318, 1993.

COMPARATIVE STUDY ON MAGNETICALLY MODIFIED PEANUT HULLS OF RED - AND WHITE - SEEDED VARIETIES FOR THE COLOR REMOVAL OF METHYLENE BLUE

***OhnOhn Soe[1], Lat Lat Aung[2]**
[1]*Education, LoikawUniversity, Loikaw, Myanmar, drohnohnsoe@gmail.com*
[2]*Education, Yangon Technological University, Yangon, Myanmar, lattlatta@gmial.com*

ABSTRACT: Magnetically responsive nanocomposite materials, prepared by medication of diamagnetic materials by magnetic fluids (ferrofluids) have already found many important applications in various areas of biosciences, medicine, biotechnology, environmental technology etc. In this study the colour removal efficiencies of magnetically modified peanuts hulls of red- and white - seeded varieties were investigated using methylene blue as model dye pollutant. From EDXRF analysis, the calcium and iron were observed as main components in magnetic peanuts hulls (white-seeded variety) MPH(W) whereas manganese and iron were observed in magnetic peanuts hulls (red- seeded variety) MPH(R). FT IR spectral data showed the presence of ionisable groups such as carboxyl, carbonyl, and hydroxyl which can involve in biosorption process of both magnetic peanuts hulls. SEM micrographs of these biosorbents indicated the porous nature of the surface. The optimum conditions for removal of methylene blue (a cationic dye) by prepared MPH (R) and MPH (W) were studied in terms of contact time, concentration of methylene blue, dosage of sorbents, pH, stirring speed and temperature. Higher colour removal of methylene blue was obtained by MPH(R) (97.55%) compared to that of MPH(W) (96.86%) after contact time of 120 min at pH 7 and 30°C. The results clearly demonstrate that waste peanut hull after magnetic modification, can be considered as a very promising low-cost material for removal of cationic dyes..

Keywords: ferrofluids, magnetic peanut hulls, methylene blue, biosorbents, colour removal efficiency

1. INTRODUCTION

Dyes are widely used in the textile, food, cosmetics, pharmaceutical, tanneries, electroplating factories and host other industries (Sayan, 2006). The methods of colour removal from industrial effluents include biological treatment, chemical coagulation followed by sedimentation, flotation, adsorption, oxidation and photocatalytic discoloration (Ozkan and Gokcay, 2010). Among these methods, sorption processes appear to be preferable techniques. Materials whose physical properties can be varied by application of external magnetic fields belong to a specific class of smart materials. In many cases magnetically responsive composite materials can be formed by modification of originally diamagnetic materials by magnetic nanoparticles, present in different types of magnetic fluids (ferrofluids). Such composite materials have already found many important applications in various areas of biosciences, biotechnology, medicine and environmental technology (Safarik and Safarikova, 2002). Nanoparticles exhibit good adsorption efficiency especially due to higher surface area and greater active sites for interaction with metallic species and can easily be synthesized and several researches have used it as an adsorbent (Hritcu*et al.*, 2009).World annual production of shelled peanuts was 42 million tons in 2014. Since peanuts are grown as a plant, they are a renewable resource (Brown *et al.*, 2000). As a by-product, the hulls are easy and inexpensive to obtain because industries are in need of only the peanut as the main ingredient in their products.

Magnetically responsive peanut hulls materials can be prepared by modification of diamagnetic materials by magnetic fluids (ferrofluids). Ferrofluid modified biological waste (peanut hulls) has been successfully used for the separation and removal of water soluble organic dyes and thus this low cost adsorbent could be potentially used for wastewater treatment. Modification of agricultural by-product could enhance their natural adsorption capacity or add another additional value to the by-product (Taha and Magraby, 2014).The present work is concerned with the synthesis of magnetic peanut hull as a biosorbent for removal of dye.

2. MATERIALS AND METHODS

2.1 Materials

In this research, Peanut hulls (white & red) were collected from broker house at Ba Yint Naung, Yangon Region, Myanmar. All chemicals used were of analytical reagent grade.

2.2 Preparation of Magnetic Peanut Hulls

The collected raw peanut grains samples (red- and white - seeded varieties) were roasted on the sand bath to obtain roasted peanut hulls. The roasted peanut hulls were washed with tap water to remove dirt and other impurities and then sprayed with distilled water. After that, the peanut hulls were dried in an oven at 80 ºC and then crushed in milling machine to obtain powdered form. The powder was sieved with 600 µm sieve and stored in the dried plastic bottle.

A 2.1 g of iron (II) sulphate and 3.1 g of iron (III) chloride were placed into a 250 mL beaker containing 80 mL of distilled water. Then the solution was heated to 80 ºC, after stirring for 30 min and 25 mL of 25 % (v/v) ammonium hydroxide solution was slowly added into the

beaker containing solution mixture. The black precipitates were obtained.10 g each of peanut hulls powders (red- and white- seeded varieties) were suspended in the ferrofluid solution at 80 ºC. The suspension was mixed on a stirrer for 30 min. The magnetically modified peanut hulls particles (red-seeded variety),MPH(R) and (white- seeded variety), MPH(R) were obtained. The particles were then left to cool to room temperature and washed with distilled water and then dried until complete dryness and stored in the dried plastic bottle.

2.3 Characterization of Peanut Hulls and Prepared Magnetically Modified Peanut Hulls (Red- and White- Seeded Varieties) by EDXRF, FT IR and SEM

Peanut Hulls and Prepared Magnetically Modified Peanut Hulls (MPW and MPR) were characterized by EDXRF, FT IR and SEM.

2.4 Colour Removal Efficiency of Methylene Blue Model Dye Solution by Prepared Magnetic Peanut Hulls (Red- and White- Seeded Varieties)

In this research, prepared magnetic peanut hulls used for investigation of colour removal efficiency. The stock solutions of MB (1000 mg/L) were prepared in distilled water. All working solutions were prepared by dilution of the stock solution with distilled water to get the required concentrations. Adsorption experiments were carried out in a rotary shaker at different speeds and ambient temperature, using 250mL shaking flasks containing 100 mL different concentrations of dye solutions 5-25 mg/L. The initial pH values of the solutions were previous adjusted with 0.1 M HCl or NaOH using a pH meter. Different doses of sorbent were added to each flask. After shaking the flasks for predetermined time intervals, the samples were withdrawn from the flasks and the dye solutions were separated from the sorbent by filtration and then centrifugation. Dye concentrations in the supernatant solutions were estimated by measuring absorbance at wavelength of maximum absorption of dye with a UV-visible (1240) spectrophotometer (Shimadzu, Japan) (Taha and Maghraby, 2015). The removal percent was calculated by the following equation

$$R\ \% = A_0 - A_e / A_0 x \quad 100$$

wfhere A_0 and A_e (ppm) are the liquid-phase concentrations of dye at initial and at any time t, respectively.

3. RESULTS AND DISCUSSION

3.1 Relative Abundance of Elements in Peanut Hulls

The elemental compositions of the peanut hulls were determined by X-Ray Fluorescence Spectrometer. Iron and calcium were the main components in the peanut hulls whereas iron was observed as main component in magnetic peanuts hulls (Table 1 and Fig. 1).

3.2 FT IR Analysis

The FTIR spectra of native and magnetic peanut hulls biomass were studied in the range of 400–4000 cm^{-1} using (FTIR-8400 Shimadzu, Japan) (Figs.2-5).The peanut hull is a complex material consisted of polyphenol such as catechol, pyrogallic acid and m-trihydroxybenzene, mineral, lipid, and cellulose, etc (Kargi and Cikla,2006).FT IR spectral data showed the presence of ionizable groups (carbonyl, hydroxyl) able to interact with protons, metal or positive dye ions and these functional groups may be the major biosorption sites for dye removal(Table 2).

3.3 SEM Analysis

The scanning electron photomicrograph of peanut hulls illustrated the fibrous nature of the surface morphology and changed after coating with ferrofluid(Fig. 6). Coated materials were seen on the surface and more pores were observed on the surface of magnetic peanut hull with red –seeded variety.

3.4 Batch Adsorption Study

The batch experiments were done by studying different parameters.

3.5 Effect of contact time

To study the effect of contact time, the contact time between the adsorbent and adsorbate was varied as 20,40,60,80,100,120 and 180 min on rotary shaker. After 60 min contact time the colour removal percent by MPHR was found to be 90.36 %. Whereas MPHW removed only 77.05% (Table 3 and Fig. 7). As the contact time increased the colour removal percent also gradually increased. However, after 120 min the colour removal percent did not change appreciably due to the saturation of the active sites of adsorbent. Thus the optimum contact time was found to be 120 min.

3.6 Effect of concentration

In this study, the initial concentration of methylene blue solution was varied such as 5, 10, 15, 20 and 25 ppm while other factors kept constant. As the concentration increased the colour removal percent also increased. However, the colour removal efficiency of MPHR was higher than that of MPHW. After 20 min the colour removal percent decreased due to the saturation of the active sites of adsorbent(Table 4 and Fig. 8). The maximum colour removal efficiency was obtained at initial concentration of 20 ppm after 120 min.

3.7 Effect of dosage of adsorbent

The dosage of adsorbent was varied in the range of 0.025g to 0.3 g while keeping contact time and concentration of methylene blue at their optimum values of 120 min and 20 ppm respectively. Lower amount of dosage of adsorbent removed lower percentage of colour. As the dosage of adsorbent increased the colour removal by both MPHR and MPHW increased, however, the increase was higher by treatment with MPHR. The maximum colour removal percent was observed at the dosage of 0.2 g for both MPHR (97.55%) and MPHW(96.86 %).When the amount of dosage increased to 0.3 g the colour removal percent slightly decreased

due to the desorption of adsorbate (Table 5 and Fig. 9). The optimum dosage was found to be 0.2 g.

3.8 Effect of pH

The colour removal of methylene blue solution having initial concentration of 20 ppm by 0.2 g of adsorbent dosage was tested for different pH values of 4, 6, 7, 8 and 10. The stirring speed was set at 200 rpm for 120 min on rotary shaker. The colour removal efficiency was found to be not more than 77 % in acidic pH. At neutral pH of 7 the colour removal percentages were found to be the highest (97.55 % for MPHR and 96.86 % for MPHW). Beyond pH 7 (basic condition) the colour removal percent decreased by treatment with both MPHR and MPHW(Table 6 and Fig. 10).

3.9 Effect of Stirring Speed (RPM)

To study the effect of stirring speed, the stirring speed was varied as 50, 100, 150, 200 and 250 rpm. The other parameters such as contact time, concentration, adsorbent dosage and pH were set to their optimum value *i.e.*, 120 min, 20 ppm, 0.2g andpH 7, respectively. The optimum stirring speed was found to be 200 rpm(Table 7 and Fig. 11).

3.10 Effect of temperature

To study the effect of temperature, the temperature was varied as 20, 25, 30, 35 and 40 °Cwhile keeping the other parameters constant to their optimum values. The contact time, concentration, adsorbent dosage, pH and stirring speeds was taken as 120 ppm, 0.2g, 7 pH and 200 rpm respectively.The optimum temperature for colour removal efficiency was found to be 30 °C for both MPHR and MPHW (Table 8 and Fig. 12).

Table1. Relative Abundance of Elemental Compositions of Peanut Hulls and Magnetic Peanut Hulls (MPW and MPR)

Sample	% Composition								
	Ca	Fe	S	Ti	Mn	Cu	Zn	Sr	Rb
Peanut hulls (Red)	30.556	15.958	4.449	1.223	1.019	0.762	0.41	0.397	0.212
Peanut hulls (White)	42.317	12.334	-	-	0.777	0.684	0.451	0.790	-
Magnetic Peanut hulls (red)	0.390	99.125	-	-	0.485	-	-	-	-
Magnetic Peanut hulls (white)	1.009	99.47	-	-	0.465	-	-	0.056	-

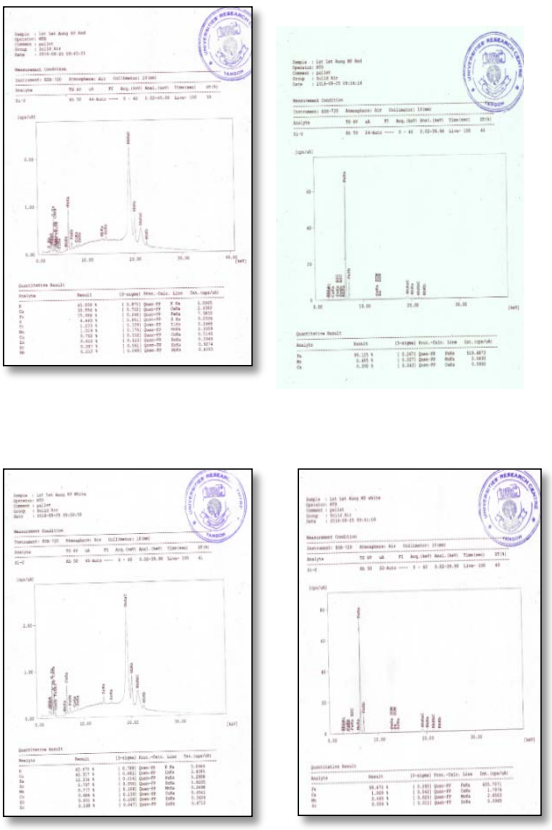

Fig. 1. EDXRF spectrum of peanut hulls and prepared magnetic hulls (MPW and MPR)

Figure 2. FT IR spectrum of peanut hulls (MPR)

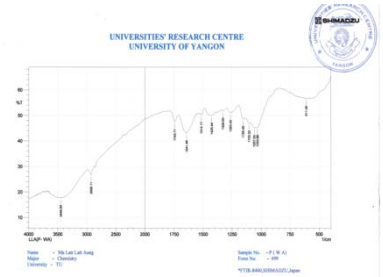

Fig. 3. FT IR spectrum of peanut hulls (MPW)

Table 2. Assignment of FT IR Spectral Data of Peanut Hulls and Magnetic Peanut Hulls, (MPWand MPR)

No.	Observed Values (cm^{-1})				Literature value (cm^{-1})	Interpretation
	P(Red)	P (White)	MP (R)	MP (W)		
1	3441	3449	3362	3426	3600-3200	υ_{OH} O-H stretching
2	2945	2926	2899	2924	3000-2850	υ_{CH} C-H stretching
3	1735	1743	1735	1743	1820-1670	$\upsilon_{C=O}$ C= O stretching
4	1641	1641	1639	1629	1680-1620	$\upsilon_{C=C}$ C=C stretching
5	1512	1514	1510	-	1600-1400	Aromatic CH_2 stretching
6	1419	1425	1404	1408	1410-1310	δ_{CH} CH bending
7	1263	1263	1259	1265	1350-1260	δ_{OH} O-H in plane bending
8	1143	1155	-	1107	1260-1000	υ_{C-C-O} C-C-O asymmetric stretching
9	895	-	-	-	1000-675	δ_{CH} C-H bending
10	607	611	-	-	720-590	υ_{Fe-O} Fe-O group (asymmetric)

Nakanishhi(1962)

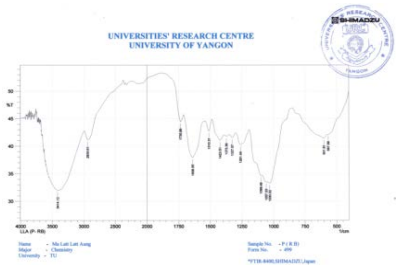

Fig. 4. FT IR spectrum of prepared magnetic peanut hulls (MPR)

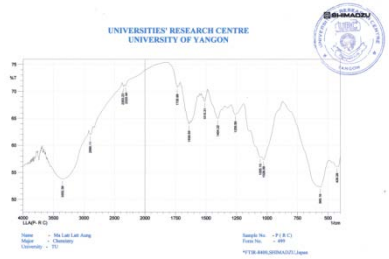

Fig. 5. FT IR spectrum of prepared magnetic peanut hulls (MPW)

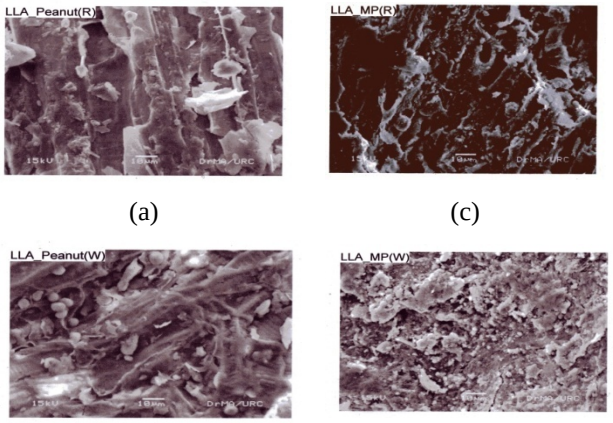

Fig. 6. SEM images of (a) peanut hulls (red)
(b) peanut hulls (white)
(c) prepared magnetic peanut hulls red (MPR)
(d) prepared magnetic peanut hulls white (MPW)

Table 3. Removal Percent of Methylene blue by Magnetic Peanut Hulls (Red and White) as a Function of Contact Times

No.	Contact Time (min)	Magnetic Peanut Hulls (Red) Removal % ± STD	Magnetic Peanut Hulls (White) Removal % ± STD
1	20	60.35 ± 0.03	55.54 ± 0.11
2	40	77.66 ± 0.09	75.88 ± 0.11
3	60	90.36 ± 0.06	77.05 ± 0.03
4	80	90.73 ± 0.03	78.59 ± 0.03
5	100	96.99 ± 0.01	90.86 ± 0.03
6	120	97.55 ± 0.06	96.86 ± 0.07
7	140	97.49 ± 0.01	96.82 ± 0.01
8	160	96.94 ± 0.07	96.82 ± 0.01
9	180	96.88 ± 0.03	96.77 ± 0.02

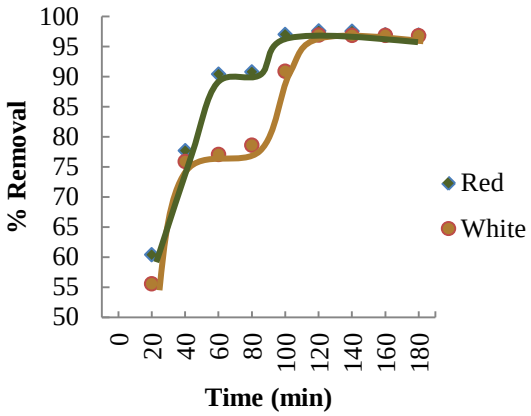

Fig. 7. Removal percent of methylene blue model solution by magnetic peanut hulls (red and white) as a function of contact times

Table 4. Removal Percent of Methylene blue by Magnetic Peanut Hulls (Red and White) as a Function of Concentrations

No.	Concentration (ppm)	Magnetic Peanut Hulls (Red) Removal % ± STD	Magnetic Peanut Hulls (White) Removal % ± STD
1	5	81.58 ± 0.22	79.05 ± 0.11
2	10	86.12 ± 0.10	82.17 ± 0.08
3	15	89.89 ± 0.11	83.28 ± 0.05
4	20	97.55 ± 0.06	96.86 ± 0.06
5	25	75.50 ± 0.07	71.50 ± 0.07

Experimental condition

Weight of Peanut Hulls = 0.1 g
Temperature = 30 °C
Stirring rate = 200 rpm
Contact time = 120 min
pH = 7

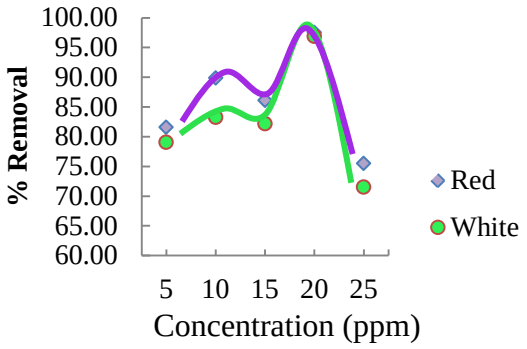

Fig. 8. Removal percent of methylene blue model solution by magnetic peanut hulls (red and white) as a function of concentration

Table 5. Removal Percent of Methylene blue by Magnetic Peanut Hulls (Red and White) as a Function of Dosages

No.	Weight of Dosage (g)	Magnetic Peanut Hulls (Red) Removal % ± STD	Magnetic Peanut Hulls (White) Removal % ± STD
1	0.025	60.35 ± 0.03	55.54 ± 0.10
2	0.05	77.66 ± 0.09	75.88 ± 0.09
3	0.1	91.44 ± 0.06	80.80 ± 0.09
4	0.2	97.55 ± 0.06	96.86 ± 0.06
5	0.3	97.29 ± 0.06	96.77 ± 0.06

Experimental condition

Contact time = 120 min
Temperature = 30 °C
Concentration of dye = 20 ppm
pH = 7
Stirring rate = 200 rpm

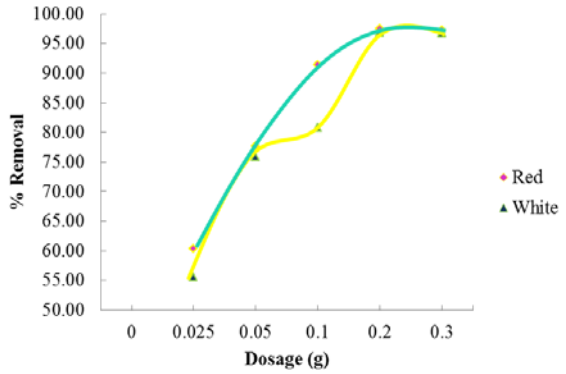

Fig. 9. Removal percent of methylene blue model solution by magnetic peanut hulls (red and white) as a function of dosages

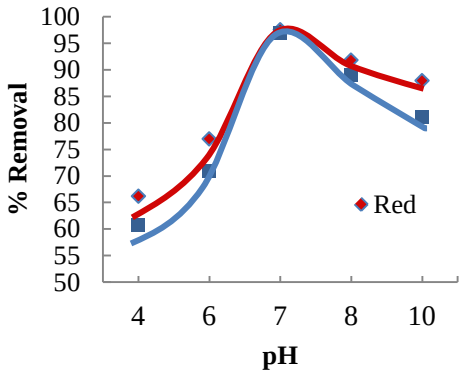

Fig. 10. Removal percent of methylene blue model solution by magnetic peanut hulls (red and white) as a function of pH

Table 6. Removal Percent of Methylene blue by Magnetic Peanut Hulls (Red and White) as a Function of pH

No.	pH	Magnetic Peanut Hulls (Red)	Magnetic Peanut Hulls (White)
		Removal % ± STD	Removal % ± STD
1	4	66.23 ± 0.75	60.86 ± 0.02
2	6	77.00 ± 0.02	70.92 ± 0.05
3	7	97.55 ± 0.01	96.86 ± 0.03
4	8	91.81 ± 0.02	88.94 ± 0.05
5	10	87.98 ± 0.02	81.08 ± 0.06

Experimental condition

Concentration of dye = 20 ppm
Temperature = 30 °C
Stirring rate = 200 rpm
Contact time = 120 min
Weight of dosage = 0.2 g

Table 7. Removal Percent of Methylene blue by Magnetic Peanut Hulls (Red and White) as a Function of Stirring Speeds

No.	Stirring Speed (rpm)	Magnetic Peanut Hulls (Red)	Magnetic Peanut Hulls (White)
		Removal % ± STD	Removal % ± STD
1	50	87.52 ± 0.15	85.20 ± 0.12
2	100	93.18 ± 0.05	92.66 ± 0.05
3	150	93.37 ± 0.06	93.30 ± 0.71
4	200	97.55 ± 0.03	96.86 ± 0.10
5	250	95.21 ± 0.06	94.06 ± 0.06

Experimental condition

Concentration of dye = 20 ppm
Temperature = 30 °C
pH = 7
Contact time = 120 min
Weight of dosage = 0.2 g

4. CONCLUSION

In this research, synthetic magnetic peanut hulls (MPHW and MPHR) were used as materials to remove the dyes from wastewaters. Removals of methylene blue by the prepared magnetic peanut hulls (MPHW and MPHR) were studied using model solutions of methylene blue.

In this work, synthetic magnetic peanut hulls biomaterial was prepared by treatment with peanut hull powders and ferrofluid. Characterization of the prepared magnetic peanut hulls was carried out by EDXRF, FT IR and SEM techniques.

EDXRF anlaysis showed that calcium and iron were the main component in the peanut hulls. FT IR spectra showed the presence of ionizable groups such as carboxyl, carbonyl and hydroxyl in both samples of magnetic peanut hulls (MPHW and MPHR).SEM micrographs indicated the porous nature of the surface so thatdye could enter the pores of the samples. The adsorption efficiencies of methylene blue solution on the magnetic peanut hulls (red- and white-Seeded Varieties were investigated as a function of the contact times, concentrations of methylene dye solution, amount of samples, pH, stirring speeds and temperatures.

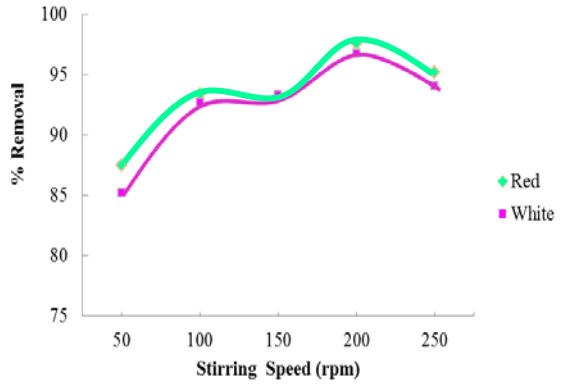

Fig 11. Removal percent of methylene blue model solution by magneticpeanut hulls (red and white) as a function of starring rate

Table 8. Removal Percent of Methylene blue by Magnetic Peanut Hulls (Red and White) as a Function of Temperatures

No.	Temperature (℃)	Magnetic Peanut Hulls (Red) Removal % ± STD	Magnetic Peanut Hulls (White) Removal % ± STD
1	20	93.07 ± 0.23	94.91 ± 0.03
2	25	93.17 ± 0.05	95.39 ± 0.03
3	30	97.55 ± 0.15	96.86 ± 0.28
4	35	97.38 ± 0.03	96.27 ± 0.25
5	40	97.25 ± 0.14	96.16 ± 0.03

Experimental condition

Concentration of dye = 20 ppm
Stirring speed = 200 rpm
pH = 7
Contact time = 120 min
Weight of dosage = 0.2 g

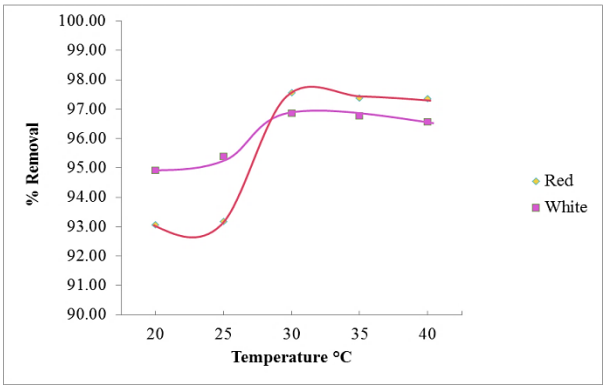

Fig 12. Removal percent of methylene blue model solution by magnetic peanut hulls (MPW and MPR) as a function of temperatures

The highest removal efficiency of MB by magnetic peanut hulls red (97.55%) and white (96.86%) were found at 120 min of contact times. The optimum concentration of MB was 20 ppm for the colour removal by both sample red –seeded variety (97.55%) and white-seeded variety (96.86%).The optimum dosages of both samples were observed to be 0.2 g. The optimum pH value for colour removal efficiencies of both samples were observed as pH 7. The optimum stirring speed and temperature were observed to be 200 rpm and 30 ℃ for bothmagnetic peanut hulls samplesof red- and white-seeded varieties. Red-seeded variety of magnetic peanut hulls (MPHR) showed higher colour removal efficiencies than white -seeded variety (MPHW).

Peanut hulls are readily available and relatively cheaper than synthetic resins. Therefore magnetically modified peanut hulls can be used to reduce the impacts of industrial wastewater pollution in the environment.

5. REFERENCES

[1] Nakanishi, K. (1962). *Infrared Absorption Spectroscopy, Pratical*.Sanfrancisco: Holden Day ,Inc, 728

[2] Brown, P., Jefcoat,I. A. Parrish,D., Gill,S. and Graham,E., (2000), Evaluation of the adsorptive capacity of peanut hull for heavy metals in solution, *Adv. Environ. Res., Vol.*4, pp.19-29.

[3] Hritcu, D., Popa,M.I,Popa, N., Badescu, V.andBalan, V., (2009), Preparation and characterization of Mmgnetic chitosan nanospheres, *Turk.J.Chem.*, Vol.33, pp.785–796.

[4] Kargi F., and Ciklak,S., (2006), Biosorption of Zinc (II) ions onto powered waste sludge (PWS): kinetic and isotherms .*Enzyme Microb, Technol.*, Vol.38,pp.705–710.

[5] Ozkan-Yucel, U.G., and Gokcayk, C.F., (2010), Effect of initial azo dye concentration and biomass acclamation on sludge digestion and dye co-treatment, *Clean-Soil Air Water*, Vol. 38,pp.387–393.

[6] Safarik, I., and Safarikova, M., (2002), Magnetic nanoparticles and biosciences, MonChem, Vol.133,pp.737-759.

[7] Sayan, E., (2006), Optimization and modeling of decolorization and COD reduction of reactive dye solutions by ultrasound-assisted adsorption, *Chem. Eng. J.*, Vol.119, pp.175–181.

[8] Taha, N.A., and Maghraby, A.E. (2014), Characterization of peanut hulls and adsorption study on basic dye: isotherm and kinetic analysis,*International journal of innovative research in technology & science*, **2**(2), pp.9-18.

[9] Taha N.A., and Maghraby, A.E., (2016),Magnetic peanut hulls for methylene blue dye removal isotherm and kinetic study,*Global NEST journal*,Vol.18,No.1, pp.24-36

GAUSSIAN NOISE REMOVAL IN DIGITAL IMAGES ANALYSIS FOR AUTOMATED COLONY AND CELL COUNTING

Klatnatee Vepulanont [1)]*, Pornpen Phuasakun[1)], Sakon Chankhachon[2)], and Atikom In-on[1)]
[1)] *Department of Chemistry, Faculty of Science, Prince of Songkla University, Hat Yai, Songkhla,Thailand.*
[2)] *Department of Computer Science, Faculty of Science, Prince of Songkla University, Hat Yai, Songkhla,Thailand*
Email: klatnatee.v@psu.ac.th

ABSTRACT: Counting cells and colonies is an integral part of screens, cellular assays and quality control tests in various subjects from medical treatment to food industry. The manual method is time-intensive in nature, which hinders the process. The objective of this research was to develop an automated method for fast, low cost and reliable cell and colony counting from digital im-ages. Gaussian noise is one of the significant initial factors which can be developed to achieve the better counting results.

Gaussian noise on RGB digital image can have a high impact on cell and colony evaluation. Therefore, the restoration process is crucial step toward the suitable image by creating a signal estimator to restore the signal as close to the original image as possible for colony counting software. The proposed filter was developed from the Rank Order Distance (ROD) statistic, which is a powerful statistical tool for detecting maximum values and Fuzzy set for resembling individual pixels on an image. The output of these filters is determined by comparing a lower- and an upper-order statistic to the middle sample in the filter window. Also it is determined by the appropriate weighting for estimation pixels. These filters can be designed for smoothing and sharpening, or outlier rejection. Based on the results, the pro-posed filter can eliminate the impulse noise in the colonial images. The restored image is suit-able for image processing to count the number of colonies.

Keywords: Colony counting, Digital image processing, Gaussian noise

1. INTRODUCTION

Counting cells and colonies is an integral part of screens, cellular assays and quality control tests in various subjects from medical treatment to food industry. By measuring microorganisms in a Petri dish present using the standard plate count method, which has the advantage of being low cost as it uses only an expert opinion. However, there are several disadvantages. This method is time consuming, inaccurate and requires an expert. This research aims to develop a tool to count colonies of Escherichia coli, Staphylococcus aureus and Pseudomonas aeruginosa. Before entering into the image processing process, the highest quality digital photos must be studied and improved. The digital images are subject to specific interference or noise. Gaussian noise is one of the significant initial factors which can be developed to achieve the better counting results. This research proposes a filter to reduce the Gaussian noise, which affects every pixel on a digital image. Each individual pixel will have been altered by having an increase in intensity or a decrease intensity comparing with the original image. The increasing or decreasing value of pixels has the probability of Gaussian equation distribution.

2. METHODOLOGY

2.1 Image restoration

The restoration of the image is an estimate of the image signal from the reduced image quality. Newly restored images will be updated to the same resolution and be as sharp as the original image before being corrupted.

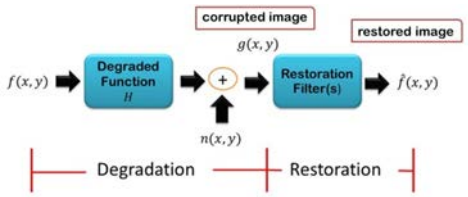

Fig. 1 The model of Image Restoration Process (Gonzalez, 1977)[1]

Fig. 1 shows the model of image restoration process. When $f(x,y)$ is the original image and it was degraded by the Degradation function (H) and the added noise. $n(x,y)$ The image $f(x,y)$ is damaged or reduced the image quality into $g(x,y)$. If a restoration filter has been used with image $g(x,y)$, it could have been improved to its original.

This study investigates only the restoration of interfering images by Gaussian's noise. It is assumed that the images used in the research are not reduced quality and no other interference other than Gaussian noise. Therefore, researchers have created a specific filter for Gaussian noise. (Chankhachon, 2016)

2.2 Gaussian noise

Noise interference is an unwanted signal that further inserts into the normal signal. This noise interference causes the image to be damaged. The colour is distorted to lack of sharpness. Gaussian noise is the noise that affects every pixel. Images that are disturbed by Gaussian noise have a distorted intensity. As a result, the image is distorted and the features are different.

2.3 Noise Model

Noise simulations were made to mimic natural

interference. The purpose is to study and learn how to eliminate the interference.

- Gaussian noise model with Gaussian distribution.

It is a form of interference that has a deviation of the original light intensity by the difference I light intensity, both increased and decreased

$$p(z) = \frac{1}{\sqrt{2\pi\sigma}} e^{-(z-\bar{z})^2/2\sigma^2}$$

This increase or decrease will be probable in the Gaussian distribution as in Equation 1. [3] The random variable z represents the intensity of light $\bar{z}$ representing the mean of the random variable z and σ represents the standard deviation of the noise.

2.4 Noise interference filter

Filter is a new signal estimator using the knowledge of noise model and statistics on the estimated value of the signal. This will make the images that are closest to the original image. In this research, the following basic filters are used:

- Mean Filter

This filter is an average estimator that is less complex. This filter will consider the centre of the window to be noise. The filter changes the pixel by finding the average of the surrounding pixels. But this method the new image will lose clarity. Set Sxy to represent the set of coordinates in the window of the noise image, $g(x,y)$, by the size of the window is $M \times N$. The coordinates of the centre pixel of the window are (x,y). The mean filter of the image pixels in the window defined by $f(x,y)$is based on the fundamental equation 2.

$$\hat{f}(x,y) = \frac{1}{MN} \sum_{(s,t)\in S_{xy}} g(s,t)$$

- Median Filter

It is a statistical filter. This uses statistical estimation to determine the value of the signal. Sort the intensity of the image pixels in the window, and then estimate the value from the median or median filter. The median value for the middle of the window is represented by the median or median $f(x,y)$. The median of all pixels in the window is as shown in Equation 3

$$\hat{f}(x,y) = median_{(s,t)\in S_{xy}}\{g(s,t)\}$$

This method requires sequencing, which is a highly time-consuming process. The advantage is that the image does not lose clarity.

Example:

1	2	1	3		2	3	4	3		3	2	1	4		2	2	1	3
4	2	2	1		5	3	4	1		2	1	4	0		4	2	4	1
0	1	1	3	,	3	2	4	2	,	1	4	2	0	=	1	2	2	2
2	2	1	1		1	3	1	2		2	4	0	2		2	3	1	2

Image 1 Image 2 Image3 Outcome

Fig. 2 The noise reduction by the median filter.

- Modal Filter

This method is similar to the median method. But does not use data sorting. The most frequently used light intensity is selected. This is a virtual vote. The highest vote is the winner. This method is suitable for less frequent and minimising interruptions.

Example:

1	2	1	3		2	3	4	3		3	2	1	4		2	2	1	3
4	2	2	1		5	3	4	1		2	1	4	0		4	2	4	1
0	1	1	3	,	3	2	4	2	,	1	4	2	0	=	1	2	2	2
2	2	1	1		1	3	1	2		2	4	0	2		2	3	1	2

Image 1 Image 2 Image3 Outcome

Fig. 3 The noise reduction by the model filter.

- Weight averaging Filter

It is an estimated filter with the sum of the intensity of each light is multiplied by the weight. Then divide by the sum of the weighted values. The weight filters can be adjusted to the above filters by weighting and configuration in the form of Equations 4. Let w be the weighted value and g be the pixel in the window.

$$\hat{f}(x,y) = \frac{\sum_{(s,t)\in S_{xy}} w(s,t)g(s,t)}{\sum_{(s,t)\in S_{xy}} w(s,t)}$$

2.5 Filtering using windows

Image Filtering In this way, a window is used to determine the extent of the consideration to determine the intensity of light in the beginning. The light intensity of the pixel around the centre of the window is brought to an average. The average is the light intensity of the pixel in the image. The window is shifted to the positions in the image until all pixels.

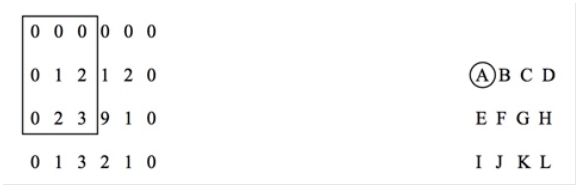

Original image Outcome image

Fig. 4 Filtering using windows

From Fig. 4, there is a 3x3 window in the upper left corner of the initial image. The light intensity at the centre of the window is equal to 1. The intensity of the pixels in the resulting image at the centre of the window

at the top of the image (pixel A) can be calculated from the average light intensity of every pixel in the window. There are three methods to find the mean: mathematical mean, median, and average mean. Mathematical mean is obtained by finding the sum of the light intensity of every pixel in the window and dividing it by the total number of pixels in the window. From the example in Fig. 4, the light intensity at pixel A is equal to (0 + 0 + 0 + 0 + 1 + 2 + 0 + 2 + 3) / 9 = 8/9. Light intensity at other pixels can be calculated by scrolling the window to the centre pixel corresponding to the desired pixel. Finding the median is done by bring all values to the table in ascending order or vice versa. Then the value in the middle of the sequence is selected as the light intensity of the pixel in the outcome image. If the number of pixels in the window is even number, the result is calculated by the average value between the two mid-pixels. From the example in Fig. 4, the sorting of intensity is as follows (0 0 0 0 0 1 2 2 3). The value in the middle is 0, so the light intensity at pixel A is 0. Finding the average value of a mode by choosing the most commonly used light intensity in the window as the answer. The problem with using this method is that it has several frequently used light intensity levels (Many answers). The solution is to average or shift to a median. From the example in Fig. 4, the most commonly used light intensity is 0, so the light intensity at pixel A is 0.

In addition to the results obtained by means of the mean of 3 as mentioned above. Another way to find the result is to find an average of k pixels where the intensity is closer to the light intensity of the centre of the window. This is called k-closest averaging. Calculate the result from the light intensity of every pixel in the window in ascending order. Then the number of value around the value of the middle of the window k values will be selected for the average. This average is the light intensity of the pixel in the resulting image. In the calculation of the average, the colour intensity at the centre can be calculated. From the example in Fig. 4, the order of intensity is as follows (0 0 0 0 0 1 2 2 3). If k = 4 and the value at the centre (1) is not calculated, the light intensity at pixel A is equal to (0 + 0 + 2 + 2) / 4 = 1. If the centre value is taken into the account, the light intensity at pixel A is equal to (0 + 0 + 1 + 2 + 2) / 5 = 1.

1 2 2 1	0 1 1 0	0 0 0 0	1 2 1 3
1 2 2 2	1 2 2 1	0 2 2 1	2 2 3 1
1 2 2 1	0 2 1 0	0 0 0 0	1 4 2 1
(A)	(B)	(C)	(D)

Fig. 5 Display the results of the various methods.

Fig. 5 Image filtering using window (A) use the mathematical average (show results after rounding); (B) use the median (C) use the mode (use the median instead for the pixel in question) (D) Use k-closest averaging (show results after rounding)

2.6 Rank order distance statistic (ROD)

This method uses a window to determine the extent of the consideration to determine the degree of light intensity of the pixels in the initial image. The light intensity of the pixel around the centre of the window is taken for the difference and the sum of the four least significant differences results in an ROD value, and then the ROD is replaced.

Fig. 6 Valuation of ROD (Aurélio, 2006)

From Fig. 6, there are 3x3 windows in the top left corner of the initial image. The light intensity at the centre of the window is equal to 1, and the light intensity of the pixels around the four pixels highlighted is the pixel with the difference with the most central pixel. The ROD of the centre pixel is equal to (3-2) + (2-1) + (1-0) + (2-1) = 4. ROD = 4 is stored at pixel A in the ROD result image at the position that corresponds to the centre of the window on the initial image.

2.7 Similarity function

This function brings ROD values to a weighted value for image restoration. The ROD can be calculated for similarity as equation below

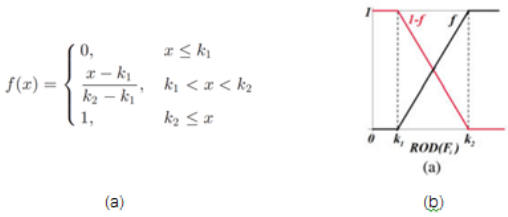

Fig. 7 Equations and graphs of similarity function (Aurélio, 2006)

From Fig. 7 (a) $f(x)$ is the similarity value from 0 to 1. k1 is the standard deviation of ROD and x is the mean of ROD. The similarity function of the plot is given in Fig. 7 (b). (Konstantinos, 2006)

3. Experimental procedure

In this part, the researchers will design the filter to eliminate Gaussian noise from the generated device. The Matlab program is used to write commands by the

workflow, as shown in Fig. 8

Fig. 8 Flowchart of the developed program.

In the first step, the system receives a noise image and then creates a filter window for the ROD statistic. By knowing the statistic ROD, the next step is to find the similarity by the similarity function to be a weighted window. The weighted window is used to multiply the pixel of images with Gaussian noise. The code is written as Fig. 9.

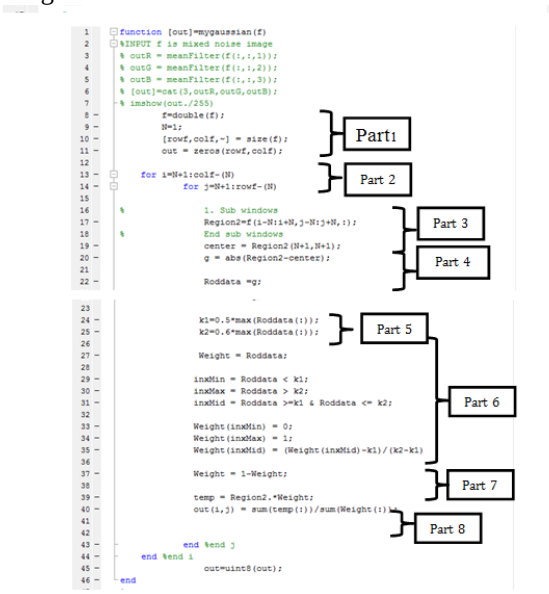

Fig. 9 The code of the developed filter.

- Step of coding

1) Part 1

- Set the image to double (8).
- The N = 1 N is used as a window filter runner, 3 x 3, and is used to determine the filter pixel of each filter window. (9)
- Stores the size of the input image in the rowf and colf. (10)
- Create a matrix 0 that is the same size as the input image. Use this matrix to store the intensity in the next step.(11)

2) Part 2

- Set the centre pixel of each filter window. The middle pixel of each filter window is used to run the filter window when processing orders completed. (13-14)

3) Part 3

- Determines the size of the filter window. (17)
- Set the centre pixel of the filter window. (19)

4) Part 4

- Find the statistic ROD by taking each pixel in the filter window and delete it with the centre point. (20)
- Collect statistician ROD in the form of variable Roddata (21)

5) Part 5

- Define conditions of similarity function.

6) Part 6

- Check ROD value against similarity function conditions.
- Convert conditions to values from 0 to 1.
- Find the weighted of the pixel to be restored.

7) Part 7

- Apply a weighted window to the image window and store the result in a variable. temp
- Find the weight averaging of the temp and store it in the array. out (i,j)

8) Part 8

- When the loop is complete, the result is reached. out (i,j) Each in a variable. Out (Gonzalez, 1977)

3. Results

The effect of noise filtering using the developed filter.

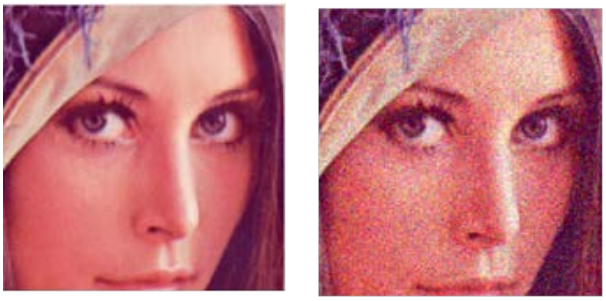

Fig. 10 The original image and image with the simulated Gaussian noise

The above Fig. shows the simulated Gaussian noise to imitate the actual Gaussian noise in the images of the research. Then, Using the developed filter for this research which is specific to the Gaussian noise to eliminate the noise.

Fig. 11 Gaussian noise images using a developed filter in the research

Fig. 11 is a representation of Gaussian noise with a developed filter for this research. Experiment tests to see the effectiveness of the developed filter, designed to be able to apply to the actual image of the research.

4.2 Comparison of PSNR

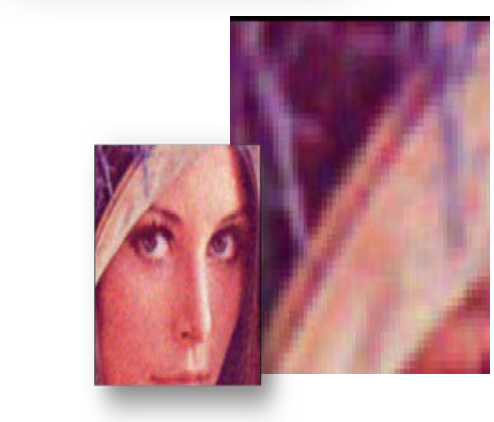

Fig. 12 Display Gaussian noise filter output using Mean filter

Fig. 12 is a Gaussian image which Gaussian noise is filtered out using the typical means (Mean filter).The PSNR from Mean filter was then compared to the PSNR from developed filter (Fig. 13).

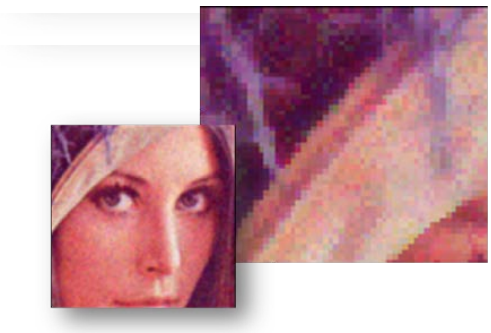

Fig. 13 Display Gaussian noise filtered images using developed filter

Table 1 shows the results of the measurement and evaluation of PSNR performance.

	Impulse noise	Impulse noise filter	
		Developed filter	Mean filter
PSNR	22.1153	27.3552	28.1224

As a result, the PSNR value of the designed filter is close to the PSNR of the Mean filter, but the clarity and detail of the image is clearly better.

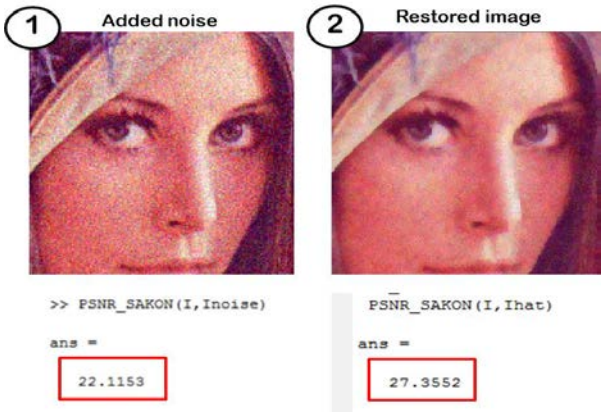

Fig. 14 Compare the PSRN value of the interfering image (1) with the image using the developed filter (2).

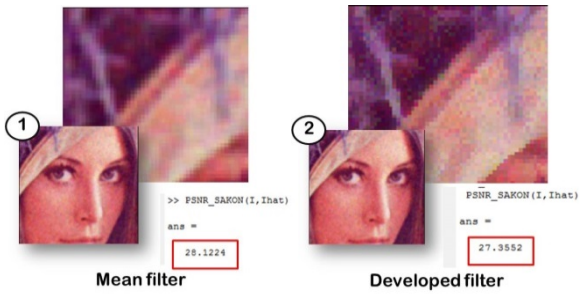

Fig. 15 Compare the contrast of the image through the Mean filter (1) filter with the developed filter (2).

Images from the Mean filter lose the sharpness of the image. So it makes the image blurry. The lines and edges are not clear. Unlike the image obtained from the developed filter, which have a better resolution and clarity.

4. CONCLUSION

By using the colony imaging device, it appears that the image has a clear Gaussian noise. The problem seems to come from insufficient light inside the device. The image has several white pixels due to the light inside the tool is not enough, the colony imaging device needs to compensate for light, resulting in a slightly distorted color and Gaussian noise.

Therefore, this research has designed a filter to reduce the Gaussian noise by using MATLAB program in the design. The developed program can eliminate Gaussian noise. Considering the increased PSRN (PSRN is the similarity of the image compared to the ideal image), the higher the value, the better the image quality. Higher PSRN indicates that the image quality is improved. By comparing, the image obtained from the developed filter is better than the image from mean filter because it is much clearer. Although Gaussian noise can

be filtered out by using mean filter also but this method has a negative effect on the image (blurring). Therefore mean filter is not suitable to eliminate the Gaussian noise before automated colony counting. So the developed filter is effective and can be used as part of the further research. In the future research, the ability of imaging tools will be developed to be able to shoot more effectively. In the field of computer programming, coding will be designed to improve noise elimination capability for more than one type. Removing these interferences prepares the image before entering the colony counting process, which results in fewer errors.

5. ACKNOWLEDGEMENT

This research was supported by Ministry of Science and Technology and Prince of Songkla University. We appreciate our colleagues from Chemistry department, Faculty of Science, Prince of Songkla University, Hat Yai Campus. We would like to show our gratitude to the Centre for Innovation in Chemistry (PERCH-CIC) for their support during the course of this research.

6.REFERENCES

[1] Aurélio,C., 'Image Analysis and Recognition', Portugal,Póvoa de Varzim,2006, (accessed 25 October 2016).
[2] Chankhachon,S., 'Localised rank-ordered differences vector filter for suppression of high-density impulse noise in colour images', 2016
[3] Gonzalez,R. and Woods,R., 'Digital image processing'New jersey, pretrice hall',1977, (accessed 16 October 2016).
[4] Konstantinos Plataniotis, Taxonomy of Colour Image Filtering and Enhancement Solutions, 2006.

THE EFFECTS OF LAYERS OF CORN HUSKS AND FIBER EXTRACTION METHODS ON YIELDS AND PHYSICAL PROPERTIES OF CORN HUSK FIBERS

Walapa Tamthong[1)]*, Suteeluk Kraisuwan[1)], and Kajijarus Piromthamsiri[1)]
[1)]* *Department of Home Economics, Faculty of Agriculture, Kasetsart University, Bangkok, Thailand*

ABSTRACT: The objective of this research was to study the effects of layers of corn husks and fiber extraction methods on yields and physical properties of sweet corn, ATS 12, husk fibers. Two layers of corn husks: outer and inner corn husks and six fiber extraction methods: 2.5 g/l NaOH, 5.0 g/l NaOH, 2.5 g/l NaOH and 0.5% cellulase enzyme, 2.5 g/l NaOH and 1.0% cellulase enzyme, 5.0 g/l NaOH and 0.5% cellulase enzyme, and 5.0 g/l NaOH and 1.0% cellulase enzyme were utilized. The long thick stands of corn husks used in these experiments were extracted from dried corn husks by water retting process. The experimental design used was 2 × 6 factorial experiments in randomized complete block design. The yields and physical properties: lengths, fineness, and crimps of corn husk fibers were analyzed by mean, standard deviation, two-way analysis of variance and least significant difference. The results showed that the fiber yields obtained were between 15.82 to 25.74 percent of the corn husks. The inner corn husks had higher fiber yield than outer corn husks ($p \leq .01$). The fiber extraction methods and interaction between the layers of corn husks and the fiber extraction methods significantly affected fiber yield ($p \leq .01$ and $p \leq .05$). The fiber lengths were between 155.38 to 181.75 mm. The fibers extracted from the outer corn husks had higher length than those extracted from the inner corn husks ($p \leq .01$). The fiber extraction methods significantly affected fiber length ($p \leq .01$). The fiber fineness were between 15.01 to 24.00 tex. The fibers extracted from the outer corn husks had higher fineness value than those extracted from the inner corn husks ($p \leq .01$). The fiber extraction methods significantly affected fiber fineness ($p \leq .01$). The fiber crimps were between 21.01 to 37.43%. The fiber extraction methods and interaction between the layers of corn husks and the fiber extraction methods affected fiber crimp ($p \leq .01$ and $p \leq .05$). However interaction between the layers of corn husks and the fiber extraction methods did not affected fiber length and fiber fineness. Moreover the layers of corn husks did not affected fiber crimp.

NOMENCLATURE

g/l = gram per liter
min. = minute
mm. = millimeter
NaOH = sodium hydroxide
sd = standard deviation
$\bar{X}$ = arithmetical mean
% = percentage

1. INTRODUCTION

Sweet corn (*Zea mays* L. var. saccharata) is a plant in the family Poaceae. It is agricultural commodity that Thailand has potential to distribute in country and export. This is because Thailand has suitable areas and environment for growing sweet corn in all regions and all year round. Moreover sweet corn has a very short period of optimum harvest maturity (approximately 69-90 days) [1]. In 2016, Thailand had total area of 202,942 rai in which to grow sweet corn, total production of 263,548 tons. The first five provinces where sweet corns grown were Chiang Mai, Chiang Rai, Kanchanaburi, Nakhon Sawan and Sukhothai, respectively [2].

Sweet corns are sold as fresh corn and processed corn products. Due to a lot of consuming sweet corns in these ways, there are a large amount of sweet corn husk waste. It is because sweet corn husk waste is renewable, sustainable and environmentally friendly that it is used in many ways such as fuel briquette, corn paper, corn husk crafts, and roof tile composite materials.

Sweet corn husks have large size and long leave with oval shape. Corn husks consist of weak fibrous parts and long thick stands which held together by natural gum. The long thick stands can be used to produce corn husk fibers. Various methods have been reported to extract fiber from agricultural plants. Each of these methods had different advantages and disadvantages. Moreover, different methods affected fiber characteristics and properties differently. Water retting process [3, 4], alkalization process [5, 6], and enzymatic treatment [7, 8, 9] may be given as examples of extraction methods. So the study of yield and properties of corn husk fibers extracted from different layers of corn husk and fiber extraction methods were proceeded to obtain good quality fibers and suitable for textile uses.

The objective of this research was to study the effects of layers of corn husks and fiber extraction methods on yields and physical properties of corn husk fibers.

2. MATERIALS AND METHODS

2.1 Materials

Corn husks which had been separated manually from ears of sweet corn, ATS 12, were used in this study.

Chemicals used in this experiment were NaOH (pellets, Ajax Finechem, Australia), cellulase enzyme (approximately activity 31,000 unit/g, Tokyo chemical industry, Ltd., Japan) and acetic acid (100%, Merck KGaA, Germany).

2.2 Methods

2.2.1 Sample Preparation

A layer of corn husk was separated manually from ears of sweet corn. The first and second layer from inside to outside and from outside to inside of corn ears were discarded, and remaining corn husks were divided equally into two groups: outer corn husk and inner corn husk. Corn husks were left to dry under ambient condition until they were fully dry. Dried corn husks were dried in hot air oven at a temperature of 105°C for 90 min. follow by cooling in desiccator. Repeat the process of heating and cooling until the mass was constant. Both ends of the corn husk were 1 inch cut off.

The factors of this experiment were two layers of corn husk; outer and inner and six fiber extraction methods; 2.5 g/l NaOH, 5.0 g/l NaOH, 2.5 g/l NaOH and 0.5% cellulase enzyme, 2.5 g/l NaOH and 1.0% cellulase enzyme, 5.0 g/l NaOH and 0.5% cellulase enzyme, and 5.0 g/l NaOH and 1.0% cellulase enzyme. The experimental design used was 2×6 factorial experiments in randomized complete block design with four replications.

2.2.2 Long Thick Stand Extraction

The long thick stands of corn husk used in these experiments were extracted from dried corn husks by water retting process. Dried corn husks were immersed in water with open lid but without contacting the air using the liquor ratio of 1:50 for 30 days. They were taken out of water and separated by hand. The long thick stands were left to dry under ambient condition for 24-48 hours until they were fully dry. The dried long thick stands were dried in hot air oven at a temperature of 105°C for 90 min. follow by cooling in desiccator. Repeat the process of heating and cooling until the mass was constant.

2.2.3 Fibers Extraction by Alkali Solution

The dried long thick stands were subjected to alkali solution: 2.5 g/l NaOH and 5.0 g/l NaOH with liquor ratio 1:50 at a temperature of 100°C for 60 min. Alkalization was follow by rinsing with water until the pH is 6-7. The corn husk fibers were left to dry under ambient condition for 24-48 hours until they were fully dry. Dried corn husk fibers were dried in hot air oven at a temperature of 105°C for 90 min. follow by cooling in desiccator then weigh. Repeat the process of heating and cooling until the mass was constant.

2.2.4 Fiber Extraction by Alkali and Enzyme Solution

The dried long thick stands were subjected to alkali solution: 2.5 g/l NaOH and 5.0 g/l NaOH with liquor ratio 1:50 at a temperature of 100°C for 60 min. Alkalization was follow by rinsing with water until the pH is 6-7. The corn husk fibers were left to dry under ambient condition for 24-48 hours. Dried corn husk fibers were dried again in hot air oven at a temperature of 105°C for 90 min. follow by cooling in desiccator then weigh. Repeat the process of heating and cooling until the mass was constant. The corn husk fibers were then subjected to enzyme solution: 0.5% cellulase enzyme and 1.0% cellulase enzyme with liquor ration of 1: 30 at 55°C for 60 min. which was suitable for activation cellulase enzyme. Enzymatic treatment was follow by rinsing with water until pH was 6-7. The corn husk fibers were left to dry under ambient condition for 24-48 hours. The dried corn husks were dried again in hot air oven at a temperature of 105°C for 90 min. follow by cooling in desiccator then weigh. Repeat the process of heating and cooling until the mass was constant.

2.2.5 Characterization

Yields, lengths, fineness and crimps of the corn husk fibers were investigated. The corn husk fibers were subjected to conditioning at 27 ± 2°C and 65 ± 2% relative humidity for at least 24 h prior to characterization processes.

Fiber yields were determined by weighting the extracted fibers then calculate the percentage of fiber yield using this formula:

$$\text{Fiber yields, \%} = \frac{\text{weight of fibers, g}}{\text{weight of dried corn husk, g}} \times 100$$

Fiber length was determined according to ASTM D 5103-01 standard test method for length and length distribution of manufactured staple fibers (single-fiber test). Each fiber to be tested was gripped at the tips with forceps, fully extended without stretching, and measured using a ruler (mm. scale).

Fiber fineness was determined according to ASTM D 1577-01 standard test methods for linear density of textile fibers. The fiber lengths were measured using a ruler (mm. scale) and the weight was measured to the 0.1 mg accuracy. Then fiber fineness is calculated in tex unit (grams per 1000 meter)

Fiber crimps were measured by measuring a 10 cm long fiber in its relaxed form to mm. scale and then in its extended form when all waviness of the fiber disappears. The crimps were calculated according to the following formula [10]:

$$C = \frac{EL - RL}{EL} \times 100$$

where C denotes fiber crimp, EL stands for extended length of the sample, and RL represents the relaxed length of the sample

The findings of aforementioned characterization were analyzed by mean and standard deviation. Means are compared by two-way analysis of variance and least significant difference.

3. RESULTS AND DISCUSSION

The effects of layers of corn husks and fiber extraction methods on yields, lengths, fineness, and crimps of corn husk fibers have been investigated and the finding are shown in Table 1

3.1 Fiber Yields

The fiber yield values obtained ranged between 15.84 to 25.80% of dried corn husks. Different results were obtained by Yilmaz et al. [4] who reported that the average yield was 5.63%. It is because those fibers extracted from fresh undried corn husks, therefore lower yield was obtained.

The layers of corn husks significantly affected fiber yields ($p \leq .01$). The average fiber yield from outer corn husks (21.45%) was higher than that from inner corn husks (19.05%).

The fiber extraction methods significantly affected fiber yields ($p \leq .01$). The average fiber yield ranged from 17.05 to 24.48%. The fiber extraction method using 2.5 g/l NaOH had higher yield than other methods ($p \leq .01$). The fiber extraction methods using 5.0 g/l NaOH, 2.5 g/l NaOH and 0.5% cellulase enzyme, and 2.5 g/l NaOH and 1.0% cellulase enzyme had higher yield than the methods using 5.0 g/l NaOH and 0.5% cellulase

enzyme and 5.0 g/l NaOH and 1.0% cellulase enzyme ($p \leq .01$). Moreover, the fiber extraction method using 5.0 g/l NaOH and 0.5%

Table 1 Yields and physical properties of corn husk fibers extracted from outer and inner corn husks using different methods

Layers of corn husks	Fiber extraction methods	Fiber yield, %		Fiber lengths, mm.		Fiber fineness, tex		Fiber crimps, %	
		$\bar{X}$	sd	$\bar{X}$	sd	$\bar{X}$	sd	$\bar{X}$	sd
outer	2.5 g/l NaOH	23.16	0.18	181.78	3.75	24.00	1.76	37.43	5.78
	5.0 g/l NaOH	19.48	1.44	179.70	6.41	22.36	3.35	23.16	0.88
	2.5 g/l NaOH and 0.5% cellulase enzyme	17.66	1.09	179.45	2.00	23.27	2.98	27.94	3.20
	2.5 g/l NaOH and 1.0% cellulase enzyme	20.40	0.59	176.28	5.29	21.19	1.27	23.17	4.31
	5.0 g/l NaOH and 0.5% cellulase enzyme	17.77	1.13	169.65	10.53	20.31	2.27	25.08	3.89
	5.0 g/l NaOH and 1.0% cellulase enzyme	15.84	1.49	170.83	4.25	18.05	2.63	21.01	4.34
inner	2.5 g/l NaOH	25.80	1.86	178.55	10.77	21.17	1.04	24.87	6.59
	5.0 g/l NaOH	21.27	1.23	172.20	1.61	21.04	1.50	22.35	3.62
	2.5 g/l NaOH and 0.5% cellulase enzyme	22.49	0.40	170.65	7.58	17.69	1.97	30.35	5.32
	2.5 g/l NaOH and 1.0% cellulase enzyme	22.03	1.02	170.58	5.43	17.01	1.15	26.24	4.70
	5.0 g/l NaOH and 0.5% cellulase enzyme	18.83	0.76	163.63	3.13	20.34	2.85	27.06	5.29
	5.0 g/l NaOH and 1.0% cellulase enzyme	18.27	1.13	155.38	4.76	15.01	1.10	24.46	6.31

cellulase enzyme had higher yield than the method using 5.0 g/l NaOH and 1.0% cellulase enzyme ($p \leq .05$). The results indicated that using the milder concentration of NaOH and cellulase enzyme can increased fiber yield.

The interaction between layers of corn husks and fiber extraction methods significantly affected fiber yields ($p \leq .05$). In the case of the fibers extracted from outer corn husks, it was found that using only NaOH had higher yield than using NaOH and cellulase enzyme. The extraction method using 2.5 g/l NaOH had higher yield than other methods ($p \leq .01$). The extraction method using 5.0 g/l NaOH had higher yield than using 5.0 g/l NaOH and 1.0% cellulase enzyme ($p \leq .01$), 2.5 g/l NaOH and 0.5% cellulase enzyme, and 5.0 g/l NaOH and 0.5% cellulase enzyme ($p \leq .05$). The extraction method using 2.5 g/l NaOH and 0.5% cellulase enzyme had higher yield than using 5.0 g/l NaOH and 1.0% cellulase enzyme ($p \leq .05$). The extraction method using 2.5 g/l NaOH and 1.0% cellulase enzyme had higher yield than using 2.5 g/l NaOH and 0.5% cellulase enzyme, 5.0 g/l NaOH and 0.5% cellulase enzyme, and 5.0 g/l NaOH and 1.0% cellulase enzyme ($p \leq .01$). The extraction method using 5.0 g/l NaOH and 0.5% cellulase enzyme had higher yield than using 5.0 g/l NaOH and 1.0% cellulase enzyme ($p \leq .05$). In the case of the fibers extracted from inner corn husks, it was found that the extraction method using 2.5 g/l NaOH had higher yield than other methods ($p \leq .01$). The extraction method using 5.0 g/l NaOH, 2.5 g/l NaOH and 0.5% cellulase enzyme, and 2.5 g/l NaOH and 1.0% cellulase enzyme had higher yield than using 5.0 g/l NaOH and 0.5% cellulase enzyme and 5.0 g/l NaOH and 1.0% cellulase enzyme ($p \leq .01$).

3.2 Fiber Lengths

The fiber length obtained values ranged from 155.38 to 181.78 mm. Goswami et al. [11] stated that the staple fibers longer than about 50 mm. (2 inches) are described as long staple. Therefore, the corn husk fibers are long staple fibers and suitable for textile purposes. Cook [12] reported that the actual length can be infinitely long, but should not be shorter than 6-12 mm. (1/4-1/2 inch), or it may not hold together after spinning.

The layers of corn husks significantly affected fiber lengths ($p \leq .01$). The average length of the fibers from the outer corn husks (176.28 mm.) was higher than that from the inner corn husks (168.50 mm.). This may be due to the fact that the average length of outer corn husks are higher than that of inner ones. So, the fibers obtained from outer corn husks tend to be longer than those obtained from inner ones.

The fiber extraction methods significantly affected fiber lengths ($p \leq .01$). The average fiber length ranged from 163.10 to 180.16 mm. The fibers extracted by using 2.5 g/l NaOH had higher length than those extracted by using 5.0 g/l NaOH and 0.5% cellulase enzyme, 5.0 g/l NaOH and 1.0% cellulase enzyme ($p \leq .01$), and 2.5 g/l NaOH and 1.0% cellulase enzyme ($p \leq .05$). In addition the fibers extracted by using 5.0 g/l NaOH, 2.5 g/l NaOH and 0.5% cellulase enzyme, and 2.5 g/l NaOH and 1.0% cellulase enzyme had higher length than those extracted by using 5.0 g/l NaOH and 0.5% cellulase enzyme and 5.0 g/l NaOH and 1.0% cellulase enzyme ($p \leq .01$). In general, the increased concentration of alkalization treatment affected the fiber length negatively, as expected. This is because the higher NaOH concentration can remove larger amount of the hemicellulose, lignin, wax, and oil from the fiber surface, thereby decreasing its length. However interaction between the layers of corn husks and fiber extraction methods did not affected fiber length.

3.3 Fiber Fineness

The fiber fineness values obtained ranged from 15.01 to 24.00 tex (the higher fineness value are coarser fiber). Cook [12] reported that the staple fibers of 12.15-23.49 tex are described as coarse fiber. Therefore the corn husk fibers are coarse and very coarse staple fibers.

The layers of corn husks significantly affected fiber fineness ($p \leq .01$). The average fineness value of the fibers from the outer corn husks (21.53 tex) was higher (coarser) than that of those fibers from the inner corn husks (18.71 tex). This is in agreement with the fact that the outer corn husks were more mature and coarser than the inner corn husks. Similar results were obtained by Yilmaz et al. [4] who reported that fibers extracted from the outer corn husks showed greater fiber fineness values (coarser) compare to the inner ones.

The fiber extraction methods significantly affected fiber fineness ($p \leq .01$). The average fiber fineness

ranged from 16.53 to 22.58 tex. The fibers extracted by using 2.5 g/l NaOH had higher fineness value than those extracted by using 2.5 g/l NaOH and 1.0% cellulase enzyme, 5.0 g/l NaOH and 1.0% cellulase enzyme ($p \leq .01$), and 5.0 g/l NaOH and 0.5% cellulase enzyme ($p \leq .05$). The fibers extracted by using 5.0 g/l NaOH had higher fineness value than those extracted by using 5.0 g/l NaOH and 1.0% cellulase enzyme ($p \leq .01$) and 2.5 g/l NaOH and 1.0% cellulase enzyme ($p \leq .05$). In addition the fibers extracted by using 2.5 g/l NaOH and 0.5% cellulase enzyme, 2.5 g/l NaOH and 1.0% cellulase enzyme, and 5.0 g/l NaOH and 0.5% cellulase enzyme had higher fineness value than those extracted by using 5.0 g/l NaOH and 1.0% cellulase enzyme ($p \leq .01$, .05, and .01 respectively). This point out that stronger concentration of NaOH and cellulase enzyme resulted in a decrease of fiber fineness value (finer). However interaction between layers of corn husks and fiber extraction methods did not affected fiber fineness.

3.4 Fiber Crimps

The fiber crimp values obtained ranged from 21.01 to 37.43%. In this sense, corn husk fibers, which may be regarded as leaf fibers, differ from bast fibers which have virtually no crimp at all [9]. The layers of corn husks did not affected fiber crimps.

The fiber extraction methods significantly affected fiber crimps ($p \leq .01$). The average fiber crimp ranged from 22.74 to 31.15%. The fibers extracted by using 2.5 g/l NaOH had higher crimp than those extracted by using 5.0 g/l and 1.0% cellulase enzyme ($p \leq .01$), 2.5 g/l NaOH and 1.0% cellulase enzyme, and 5.0 g/l NaOH and 0.5% cellulase enzyme ($p \leq .05$). The fibers extracted by 2.5 g/l NaOH and 0.5% cellulase enzyme had higher crimp than those extracted by using 5.0 g/l NaOH and 5.0 g/l NaOH and 1.0% cellulase enzyme ($p \leq .05$). Different results were obtained by Yilmaz et al. [13] who reported the crimp of dried corn husk fibers varies between 5.4-7.0%. This may be due to the fact that xylanase enzymes break the covalent bond between lignin and cellulose and depolymerize hemicellulose in the fiber. So, the obtained fibers tend to be lower crimp than the fiber obtained from this study.

The interaction between layers of corn husks and fiber extraction methods significantly affected fiber crimps ($p \leq .05$). The fibers extracted from outer corn husks by using 2.5 g/l NaOH had higher crimp than those extracted by using other methods ($p \leq .01$) and the fibers extracted by using 2.5 g/l NaOH and 1.0% cellulase enzyme had higher crimp than those extracted by using 5.0 g/l NaOH and 1.0% cellulase enzyme ($p \leq .05$). Furthermore, the fibers extracted from inner corn husks by using 2.5 g/l and 0.5% cellulase enzyme had higher crimp than those extracted by using 5.0 g/l NaOH ($p \leq .05$).

4. CONCLUSION

Corn husk fibers were extracted from different layers of corn husks by different extraction methods. The effects of layers of corn husks and fiber extraction methods on fiber yields, fiber lengths, fiber fineness, and fiber crimps were investigated. The results showed that the layers of corn husks significantly affected fiber yields, fiber lengths, and fiber fineness, but did not affected fiber crimps. The fibers extracted from outer corn husks had lower yield, but higher length and fineness value than those from inner corn husks. The fiber extraction methods significantly affected fiber yields, fiber lengths, fiber fineness, and fiber crimps. The highest fiber yield, the highest fiber length, the highest fiber fineness value, and the highest fiber crimps were achieved by using 2.5 g/l NaOH. The interaction between layers of corn husks and fiber extraction methods significantly affected fiber yields and fiber crimps. It was observed that the fiber yields, fiber lengths, fiber fineness value, and fiber crimps tend to decrease as either concentration of NaOH or that of cellulase enzyme increase. The results concerning yields and physical properties of corn husk fibers provide guidance for further studies related to obtaining corn husk fiber suitable for textile uses.

5. REFERENCES

[1] Boonrueang, S., and Chankroot, A, 2008, Handbook of agricultural extensionist: corn (animal feed corn and sweet corn), Bureau of Agricultural Commodities Promotion and Management, Department of Agricultural Extension, Bangkok.

[2] Information Technology and Communication center, Department of Agricultural Extension, Ministry of Agriculture and Cooperatives, 2559, Vegetable: sweet corn in 2016, Available source: http://www.agriinfo. doae. go.th/year60/plant/rortor/veget/16.pdf, October 8, 2017.

[3] Kant, D. R., and Alagh, P., 2013, Extraction of Fiber from Sansevieria Trifasciata plant and its properties, *International Journal of Science and Research* Vol.4, No.7, pp.2547-2549

[4] Yilmaz, N. D., Sulak, M., Yilmaz, K., and Kalin, F., 2016, Physical and chemical properties of water-retted fibers extracted from different locations in corn husks, *Journal of Natural Fibers*, Vol. 13, No. 4, pp. 397-409.

[5] Sricharassin, W., 2009, Story of pineapple fabric (not pineapple), *Colourway*, Vol. 15, No. 85 pp.21-25.

[6] Kambli, N., Basak, S., Samanta, K. K., and Deshmukh, R. R., 2016, Extraction of natural cellulosic fibers from cornhusk and its physico-chemical properties, *Fibers and Polymers*, Vol. 17, No. 5, pp. 687-694.

[7] Reddy, N., and Yang, Y., 2005, Properties and potential applications of natural cellulose fibers from cornhusks, *Green Chemistry*, Vol. 7, pp. 190-195.

[8] Huda, S. and Yang, Y., 2008, Chemically extracted cornhusk fibers as reinforcement in light-weight poly (propylene) composites, *Macromolecular materials and Engineering*, Vol. 293, pp. 235-243.

[9] Yilmaz, N. D., Çalıskan, E., and Yilmaz, K., 2014, Effect of xylanase enzyme on mechanical properties of fibres extracted from undried and dried corn husks, *Indian Journal of Fibre & Textile Research*, Vol. 39, pp. 60-64.

[10] Udomkijdecha, V., 1999, Fiber Science, Chulalongkorn University Printing House, Bangkok.

[11] Goswami, B. C., Anandjiwala, R. D., and Hall, D. M., 2004. Textile sizing, Marcel Dekker, Inc., New York.

[12] Cook, J. G., 2001, Handbook of textile fibers vol.1 natural fibres, 6th ed., Replika Press Pvt Ltd., Delhi.

[13] Yilmaz, N. D., 2013, Effect of chemical extraction parameters on corn husk fibres characteristics, Indian Journal of fibres & Textile Research, Vol. 38, pp. 29-34.

COMPARATIVE STUDY OF CONNECTING ROD WITH DIFFERENT MATERIALS AT TRANSITION ZONE

Mukesh Yadav[1)*], and Aahan malhotra[1)]
[1)] *CASRAE, Delhi Technological University, New Delhi, India*
Email: mukeshyadav_bt2k16@dtu.ac.in

ABSTRACT: Connecting rod is amongst the most important components of an IC engine. It is connected between piston and the crankshaft whose function is to convert the reciprocating motion of the piston into the rotary motion of the crank. It is very important for the connecting rod to be strong or it will lead to its fracture thus causing the failure of the engine. In modern automotive, the connecting rod is usually made up of carbon steel as steel has ability to absorb high impact although its durability is not that high. In this paper, the use of three different materials having three different properties have been used at the parts of the connected rod which experiences high stress such as at the transition region between the big end and connecting shank which is at maximum compression condition and the chances of failure is high. Carbon Nano tubes have very good mechanical properties which has very high energy absorbing capacity and can also be used in very high temperatures whereas aluminum alloy has high factor of safety, low weight and is easily available. The connecting rod was designed and modeled using Solidworks 16.0 software and the static structural analysis of the model was carried out in Ansys 16.0 software. The tests conducted in the software were the equivalent stress (von misses stress) and strain, directional and total deformation, fatigue test. Three tests were conducted using carbon steel, aluminum alloy and carbon Nano tubes and the results were compared.

Keywords: Carbon Nano tubes, Transition zone, Structural analysis.

1. INTRODUCTION

Connecting rod, a component of an IC engine which acts as the link between the piston and the crankshaft. It is connected between the piston and the crankshaft whose main function is to pull or push the piston inside the cylinder. There are two ends in the connecting rod; a small end and a large end. The small end also called the eye end of the connecting rod is connected to the piston and the large end is connected to the crankshaft of the engine.

2. LITERATURE REVIEW

Mohammed Mohsin Ali H et al [1], in his study, analyzed fatigue stresses on connecting rod which is modelled on CATIA, which is subjected to concentrated loads and analysis is performed using ANSYS, to check the fatigue life and alternating stress development due to service and assembly loads with variation in load distribution. [ISFT 1]T.R Sydanna et al. [2], in his study, modelled a connecting rod using solid works software and then the model is imported into ANSYS workbench and some boundary conditions were applied and structural analysis is performed on aluminium based composite and aluminium alloy, it's some physical properties were evaluated using ANSYS.Magesh Kumar et al. [3], in his paper reviewed various studies on structural analysis of connecting rod with different materials like titanium, etc. Weight optimization is possible using composite materials without varying the allowable stresses and boundary conditions. Prof. N.P. Doshiet al. [4], in his study, performs analysis using analytical and Finite element method on connecting rod, analytical result compared with numerical result among all load conditions and the maximum value of equivalent stress was found to be 197.41 MPa when crank end of connecting rod is in tension. This stress is less than yield strength of material. It gives a factor of safety of 3.2, the minimum stresses among all loading conditions, were found at crank end cap as well as at piston end. So, the material can be reduced from those portions, thereby reducing material cost. Ramadhan S. Shenoy [5], in his paper, performed optimization and dynamic load analysis, the optimized geometry is 10% lighter and cost analysis indicated it would be 25% less expensive than the current connecting rod, in spite of lower strength of C-70 steel compared to the existing forged steel. PM connecting rods can be replaced by fracture split able steel forged connecting rods with an expected cost reduction of about 15% or higher, with similar or better fatigue behavior. At locations like the cap-rod outer edge, the extreme end of the cap, and the surface of the piston pin end bore; the stresses were observed to be significantly lower under conditions of assembly. Bin Zheng et al. [6], in his paper performed fatigue analysis of connecting rod, found following results, the maximum stress and deformation values are 190.23 MPa and 0.0507mm respectively. The critical location is at the transition region between the big end and connecting shank at maximum compression condition. The maximum stress and deformation values are 459.21 MPa and 0.0702283 mm respectively. Safety factor is 1.584. In order to increase the reliability of CR, some improvement is carried out. Safety factor of CR increases by 59%.Vahid jamadar et al. [7], in his study, performed finite element analysis of connecting rod, CAD model is made on PRO-E software, and static analysis is performed on ANSYS, The input conditions like time and money. Material Properties, static load, boundary conditions etc. are given. The loads on the connecting rod were obtained as a function of crank angle. Working Factor of Safety 5.6.Mohamed Abdulsalam Hussein et al. [8], in his study, modelled connecting rod on solid works software, and static analysis using ANSYS, the material used is ALUMINIUM ALLOY 7068 T6, T6511, and found that minimum stresses among all loading conditions, were at crank end cap as well as at piston end. So, the material can be reduced from those portions, thereby reducing material cost. Leela Krishna Vegi et al. [9], in his study analysed connecting rod using forged steel, forged steel has more factor of safety, reduce the weight, increase the stiffness and reduce the stress and stiffer than other material like carbon steel. With Fatigue analysis we can determine the lifetime of the connecting rod.

3. RESULTS

The structural finite element analysis of the connecting was performed using ANSYS 16.0 software. The materials selected were CNT along with structural steel at the high stress zones, aluminium alloy and steel alloy . The high stress zones are the regions in the blade in which the chances of failure are high. The design model of the connecting rod was imported in the Ansys 16.0 software and its finite element analysis was done.

Finite Element Analysis:

The stress analysis of a connecting rod is a very complicated process. Finite Element Method is an analytical method or numerical simulation method to calculate the solutions. In Finite element analysis the body or solid is modeled and is hypothetically subdivided into an assembly of small parts called elements finite elements. Here, the finite elements mean that the geometry is divided into a finite set of small elements. The elements are connected to one another and meet at a point called joint. Thus FEA has become a very powerful tool for the analysis of complex geometries in engineering.

Equivalent elastic stress:

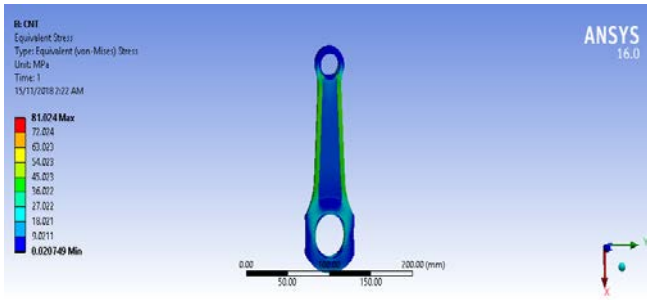

Fig 1.1 CNT

Maximum value= 81.024MPa

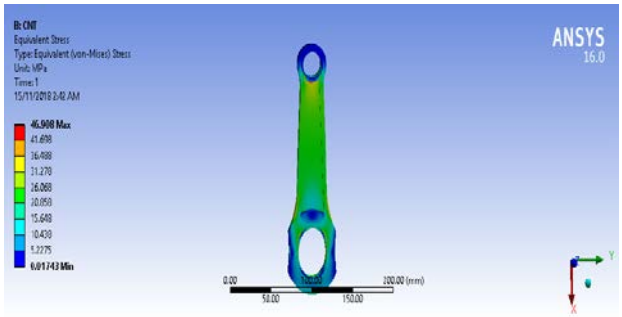

Fig 1.2 Aluminium alloy

Maximum value= 45.508MPa

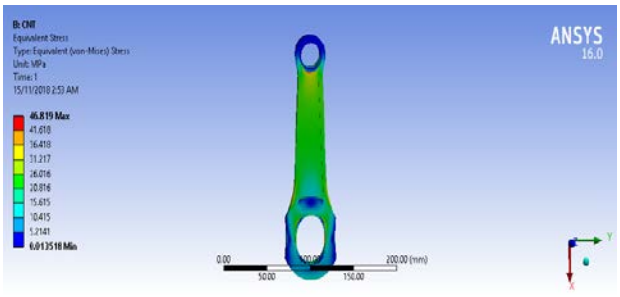

Fig 1.3 Steel Alloy

Maximum value= 46.85MPa

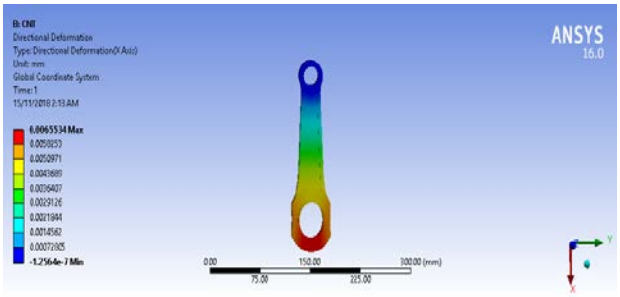

Fig 2.1 CNT

Maximum value= .0065mm

Total deformation:

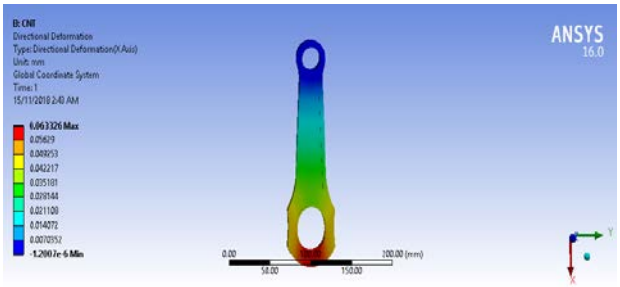

Fig 2.2 Aluminium alloy

Maximum value= .063mm

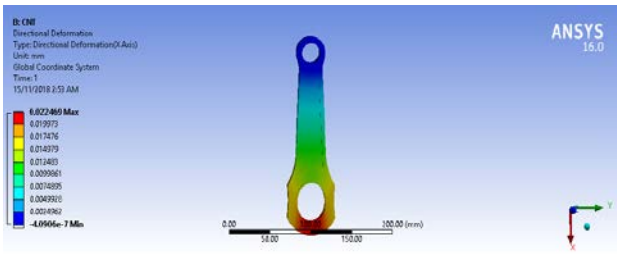

Fig 2.3 Steel Alloy

Maximum value= .022mm

Equivalent Strain:

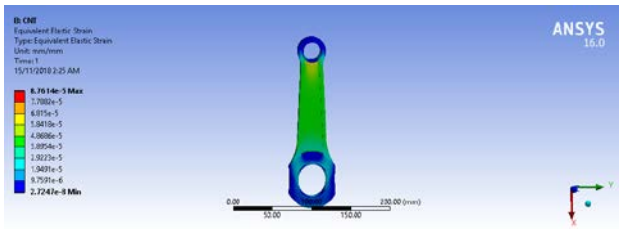

Fig 3.1 CNT

Maximum value= 8.75e-5

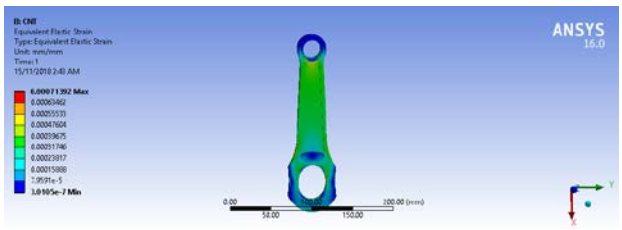

Fig 3.2 Aluminium Alloy

Maximum value= .0007135

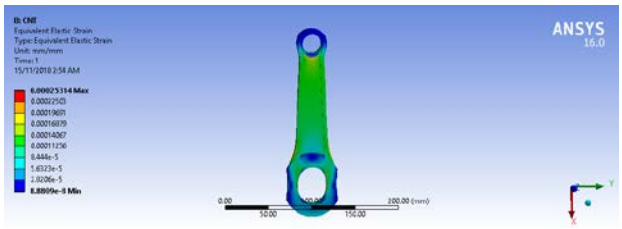

Fig 3.2 Steel Alloy

Maximum value= .00025

4. CONCLUSION

The finite element structural analysis of the connecting rod with three different material compositions i.e. Steel with CNT at the transition zone, aluminium alloy and steel alloy was done. Three solutions which are equivalent stress, equivalent strain and the total deformation were calculated. From the analysis is was observed that :

• The equivalent stress of the aluminium alloy was found to be the minimum whereas the steel alloy was found to be the maximum

• The equivalent strain was minimum for Steel with CNT where as it was maximum for steel alloy.

• The total deformation was minimum for Steel with CNT and maximum for steel alloy.

Thus, from the observed result the use of Steel with CNT at the transition zones is the most suitable among the three compositions. From this study, it can be concluded that the mechanical failure of the connecting rod is very common in the engine. To avoid the failures, the selection of the material of the blade is a very important step. The material chosen should be such that, it should withstand both the mechanical stresses as well as thermal stresses which are produced during the operation of the engine.

5. REFERENCES

[1] Mohammed Mohsin Ali Ha, Mohamed Haneef , “Analysis of Fatigue Stresses on Connecting Rod Subjected to Concentrated Loads At The Big End’ Materials Today: Proceedings 2 (2015) 2094 – 2103

[2] T.R Sydanna , B Sunil Kumar , ‘Design And Analysis Of Composite Connecting Rod’ International Journal Of Professional Engineering Studies Volume VIII /Issue 3 / APR 2017

[3] Magesh Kumar, ‘A Review Paper on Design Analysis of Connecting Rod’ International Journal on Recent and Innovation Trends in Computing and Communication ISSN: 2321-8169 Volume: 5 Issue: 6

[4] P S Shenoy, A Fatemi, ‘Dynamic analysis of loads and stresses in connecting rods’ DOI: 10.1243/09544062JMES105

[5] Bin Zheng, Yongqi Liu and Ruixiang Liu , ‘Stress and Fatigue of Connecting Rod in Light Vehicle Engine’ The Open Mechanical Engineering Journal, 2013, 7, 14-17

[6] Prof. Gurunath V Shinde1, Prof.Vinayak D Yadav, Prof.V.M.Jamadar, Prof.G S Jadhav, Karad Dr S M Sawant , “Stress Analysis of Connecting Rod using FEA”

[7] Mohamed Abdusalam Hussin1, Er. Prabhat Kumar Sinha2, Dr. Arvind Saran Darbari, “DESIGN AND Analysis of Connecting Rod Using Aluminium Alloy 7068 T6, T6511” International Journal Of Mechanical Engineering And Technology (Ijmet)

[8] Leela Krishna Vegi1, Venu Gopal Vegi , “Design And Analysis of Connecting Rod Using Forged steel” Internationl Journal of Scientific & Engineering Research, Volume 4, Issue 6, June-2013 2081 ISSN 2229-5518

THERMAL ANALYSIS OF A CAST IRON PISTON USING FINITE ELEMENT METHOD

Abhiroop Dey[1)]*, Lalit Kumar Choudhary[2)]
[1)]*CASRAE, Delhi Technological University, New Delhi, India*
[2)] *CASRAE, Delhi Technological University, New Delhi, India*

ABSTRACT: Internal Combustion Engines play a key role in the ever flourishing automotive industry. The I.C. Engine involves the combustion of fuel in a combustion chamber; this energy from it is transmitted to a rotating crankshaft through a reciprocating piston. The piston is manufactured from a variety of materials like Cast Iron, Cast Steel, Aluminum and other alloys. It relays the impact of the explosion of air-fuel mixture inside the combustion chamber, to the crankshaft through a connecting rod. During this process, the piston has to undergo immense stresses of the continuous explosions at extreme temperatures of around 700°C. A piston must, thus, be able to handle these thermal and mechanical stresses that it undergoes inside the combustion chamber without developing fractures or failures. This paper focuses on the thermal analysis of a piston manufactured from Cast Iron using Finite Element Method (FEM) and compares the results of the analysis with another piston having the same dimensions made out of hypereutectic Aluminum Silicon alloy. The piston is modeled on SolidWorks v17 and for the study of the piston, ANSYS is used. The results obtained are compared and a conclusion is drawn.

Keywords: Finite Element Method, ANSYS hypereutectic

1. INTRODUCTION

The automotive industry has been on the rise with more and more people being able to buy vehicles of their own as a result of the improvement in the standard of living of people and the reduction in the cost of production of automobiles. Furthermore, the improvement in technology has also seen an improvement in the performance of the vehicles. A Piston is a barrel-shaped reciprocating motor component inside the cylinder of an I.C. Engine that transfers the impact from the expanding gas in the cylinder to the crankshaft via the connecting rod. The stresses caused due to the combustion takes place over the piston crown, as a result of which, the piston stands risk of undergoing fatigue damage and cracks and also piston side wear.

As a result, pistons must be able to withstand these thermal and inertial stresses that are caused due to the explosions in the combustion chamber. A typical piston is shown in Figure 1.

Fig. 1 A Piston

Pistons are generally made out of Cast Iron because of its good mechanical and thermal properties. Grey CI is preferred over White CI as it has a higher melting point, greater strength and lower brittleness than White CI.

Global efforts to reduce harmful exhaust emissions, reduce costs and improve the already existing features of the engines in the newer automobiles has paved the way for alternative alloys which are used for making pistons of IC Engines, namely Hypoeutectic (A383) and Hypereutectic (A390) Al-Si Alloy pistons.[2]

Hypereutectic alloys are metallic alloys which have a composition beyond the eutectic point (lies to the right of the Eutectic Point in a phase diagram), thus, Al-Si Alloys that contain more than 11.7 wt% Si are called hypereutectic alloys that normally consist the Si phase in the eutectic matrix.[3]

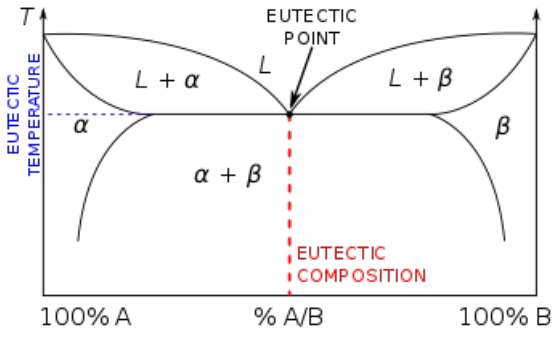

Fig. 2 Phase diagram showing the Eutectic point of any mixture with components A and B.

2. SELECTED ALLOYS FOR THE PISTON

Two different alloys, CI alloy and Hypereutectic Al-Si alloy, are selected for making the piston in this paper, which will further be analyzed by using Finite Element Method (FEM) through ANSYS.

2.1 Cast Iron Alloy

The CI alloy selected for the analysis is Grey CI. Its properties are highlighted in Table 1.

Property	Value
Density	7200 kg/m^3
Coefficient of Thermal Expansion	1.1 x 10^{-5} °C^{-1}
Young's Modulus	110GPa
Poisson's Ratio	0.28
Bulk Modulus	83.33GPa
Ultimate Tensile Strength	240MPa

Table I Properties of Grey CI

2.2 Hypereutectic Al-Si Alloy

The Hypereutectic Al-Si alloy selected for the analysis is A390. A390 alloy has a composition of at least 75.3 wt% Aluminum and at least 16 wt% Silicon and 4.0 – 5.0 wt% Copper. It also consists of Magnesium, Iron, Titanium and Manganese in extremely small quantities.[4]

Hypereutectic aluminum – silicon alloys are preferred over simple aluminum alloys for making pistons as they are more durable and have better thermal and mechanical properties than simple aluminum alloys. The properties of A390 have been tabulated in Table 2.

Property	Value
Density	2710 kg/m^3
Coefficient of Thermal Expansion	2.0 x 10^{-5} °C^{-1}
Young's Modulus	80GPa
Poisson's Ratio	0.33
Bulk Modulus	78.43GPa
Ultimate Tensile Strength	317MPa

Table II Properties of A390 (Hypereutectic Al-Si Alloy)

3. DESIGN OF THE PISTON

Pistons need to be constructed keeping their uses in mind, as a consequence of which, there's a depression on the surface of the piston crown which allows all the fuel to be accumulated right before the combustion.

Also, the piston pin region is subjected to a lot of forces because of frequent directional changes it has to undergo. It is likewise exposed to thermal expansion caused by the exchange of heat from the head to the body of the cylinder.

The piston used for this analysis is designed on SolidWorks v17, and has he following design dimensions:

Piston Crown Diameter	2.75 in
Piston Height	2.35 in
Pin Diameter	0.562 in

Table III Dimension of the Piston

Fig. 3 Side view of the piston modeled

Fig. 4 Front view of the piston modeled

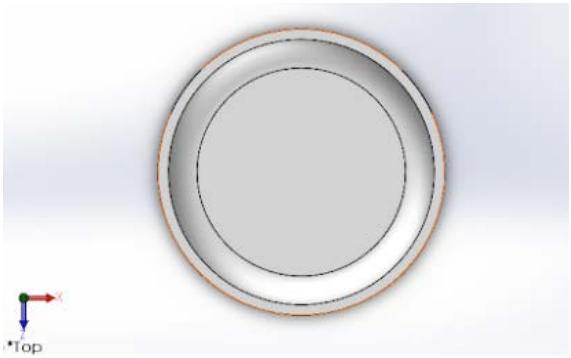

Fig. 5 Top view of the piston modeled

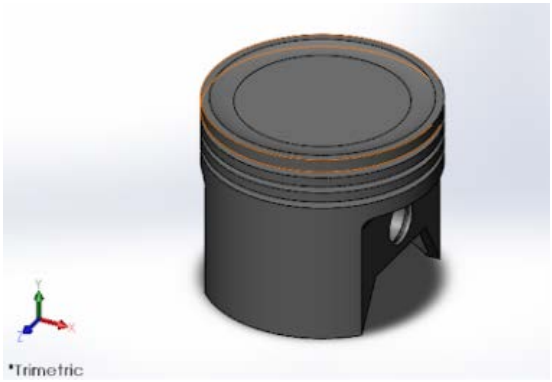

Fig. 6 Isometric view of the piston modeled

4. ANALYSIS OF THE PISTON

The piston generated thus far, will undergo Transient Thermal analysis on ANSYS v17. ANSYS is a finite element analysis software that simulates CAD models of structures, machine parts and segments to recreate quality, toughness, flexibility, temperature distribution, electromagnetism, and different properties.[5]

Transient Thermal analysis on any component predicts the temperatures and other thermal quantities that vary over time. The loads that are applied during the analysis are a function of time. In this project, the Total Heat Flux and Temperature distribution are studied. Heat flux is the amount of heat energy transferred per unit area per unit time.[6] Temperature distribution shows which part of the piston goes through what amount of thermal stresses.[7]

To study these effects and for the piston to undergo analysis, it needs to be Meshed.

Meshing is the process of dividing the whole part into finite elements, namely nodes and elements, so that the load applied is distributed uniformly across the entire component. The number of nodes and elements in this analysis are 594925 and 409059 respectively.

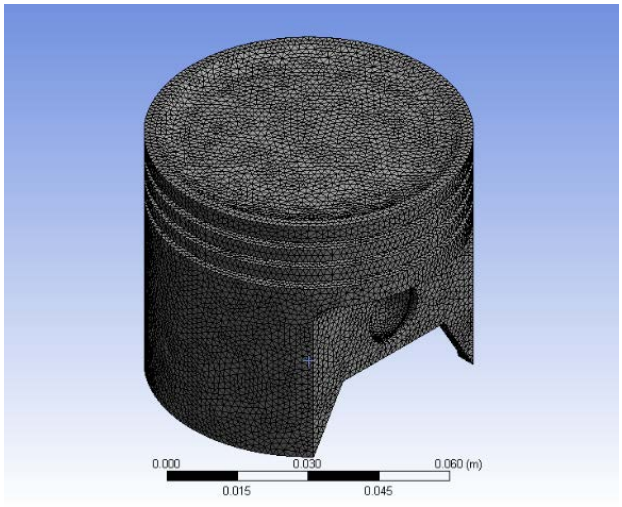

Fig. 7 Meshed piston

The Meshed figure shown here is common to both the Grey CI and Hypereutectic Al-Si alloy piston. In the next step, the loads are applied and the analysis is carried out.

The following figures show the solutions obtained during the analysis:

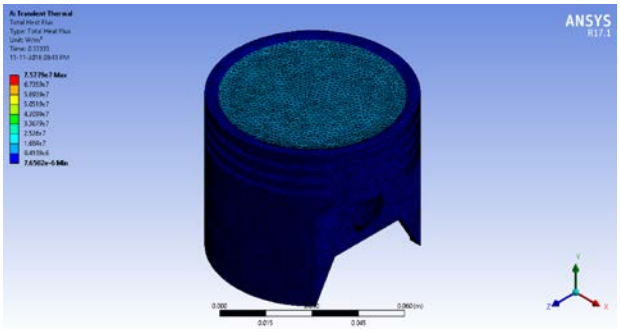

Fig. 8 Heat Flux for Grey CI at t=0.33 s

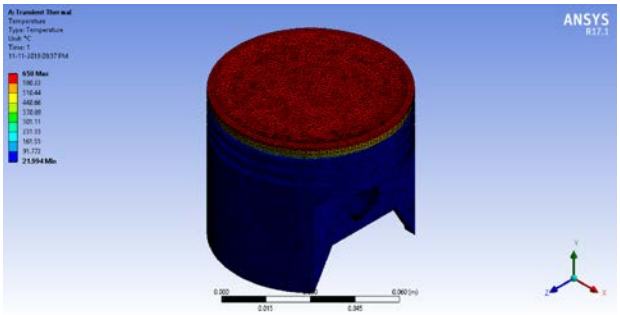

Fig. 9 Temperature distribution for Grey CI Piston

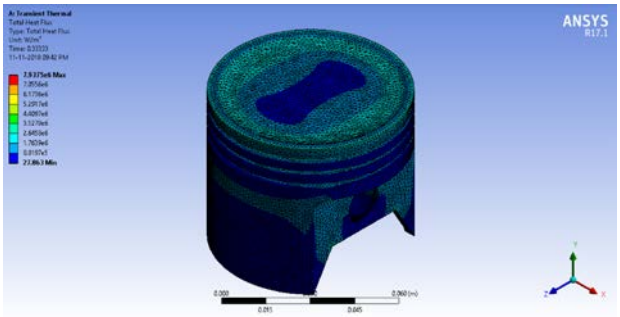

Fig. 10 Total Heat Flux for A390 Piston at t=0.33s

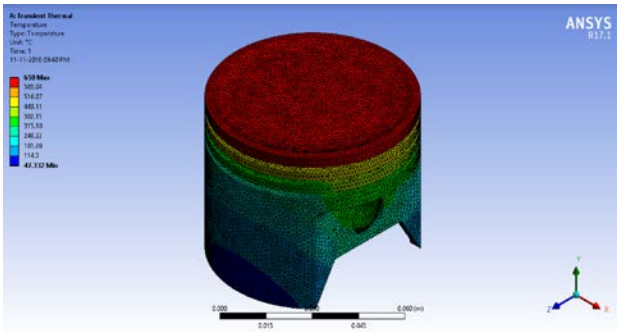

Fig. 11 Temperature distribution for A390 Piston

5. RESULTS

The results of the entire Transient Thermal Analysis are tabulated in the table:

MATERIAL	Heat Flux (W/m^2)		Temperature (℃)	
	Min.	***Max.***	***Min.***	***Max.***
Grey Cast Iron	7.6502e-6	7.5779e7	21.994	650
Hypereutectic Al-Si Alloy A390	27.863	7.9375e6	47.32	650

Table IV Results of the analysis

The analysis procedure witnessed a variation of total heat flux observed with time during the analysis. The curves obtained for the variation are shown in fig

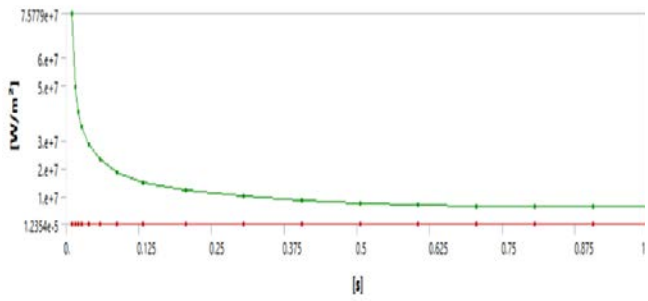

Fig Variation of Heat Flux over time for Grey Cast Iron

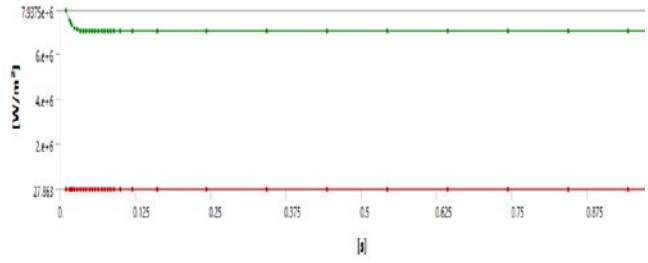

Fig. Variation of Heat Flux over time for A390

Thermal analysis is performed for both Grey Cast Iron and A390, the inference being that the Heat transfer rate of Cast Iron is more than that of A390.

6. CONCLUSIONS

The Cast Iron piston has a heat flux more than that of the hypereutectic Al-Si alloy. This clearly justifies that hypereutectic Al-Si A390 alloy is much more suitable for the manufacture of the piston as A390 can better absorb the thermal shock.

The hypereutectic piston will also reduce the mount un-burnt fuel trapped between the piston rings during a cold start up.

7. REFERENCES

[1] Mathur, M.L., and Sharma, R.P. 2015. *Engine Components and Basic Engine Nomenclature*, “Internal Combustion Engine”

[2] Buyukkaya,Ekrem, "*Thermal analysis of functionally graded coating AlSi alloy and steel pistons*.", Surface and Coatings Technology,Volume 202, Issue 16,2008

[3] Callister, W.D., R.P 206. *Materials Science and Engineering*. In Phase Diagrams.

[4] https://www.makeitfrom.com/material-properties/A390.0-A13900-Cast-Aluminum

[5] https://www.ansys.com/about-ansys

[6] https://nptel.ac.in/courses/112106139/pdf/3_1.pdf

[7] https://www.ansys.stuba.sk/html/guide_55/g-the/GTHE3.htm

[8] Riyadh A., A, Al- Samarai, Haftirman, Ahmad,K.R., Al-Douri, Y.,2012. “*Effect of Roughness of Hypo- and Hyper-Eutectic Al-Si Piston Alloy on Wear Characteristics under Lubriction*.”, Mechanical And Manufacturing Engineering, MUCET 2012, Pages 616-623

A STUDY OF ELDERLY COLOR VISION ON MONITOR DISPLAY AT DIFFERENT BRIGHTNESS LEVELS

Komwat Chotpipatwong[1)], Runyaporn Supharatraveekul[1)], Siwaporn Saneha[1)], Siam Yamsaengsung[1)] and Sumet Angkasirikul[1)]
[1)] *School of Information Technology, King Mongkut's University of Technology Thonburi, Bangkok, Thailand*

ABSTRACT: This study examined the elderly's preferred brightness level on a display screen for different pairs of texts and background colors and to compare this preference with early adults under the same experimental environment. The participants consisted of 20 early adults (aged 20-40 years) and 20 elderly (aged 60-81 years). Research tools used in the experiment are the Thai text "ทดสอบ" in 20-point TH SarabunPSK font displayed on 6 computer display screens with differing screen brightness levels at 20, 40, 60, 75, 95, and 120 lux. The 7 pairs of texts and background colors are cyan on black, yellow on black, white on black, black on white, black on yellow, white on navy, and white on green. The participants were instructed to read the text at a distance of around 40 centimeters and indicate the best brightness level for each color pair. The location of testing has a brightness in the range of 300-500 lux. The collected data is analyzed using descriptive statistics. The results showed that more than half of the elderly (57.86%) preferred display brightness level at 95 and 120 lux for in all pairs of texts and background colors but the early adults preferred display brightness level at 40 and 60 lux for reading text. Hence the brightness level that the elderly and the early adults chose was different. The elderly also chose black text on yellow background to be the most easily read color pair but the early adults chose white text on navy background. The information obtained from this pilot study can be used as a basis for the development of automatic brightness adjustment on various display screens to suit different user groups.

Keywords: Elderly, Early adults, Color vision, Display brightness, Computer display screen

1. INTRODUCTION

Thailand has entered the Aging Society since 2005, and the Ministry of Health expects Thailand will enter the Complete Aged Society by 2025 [1]. Based on the United Nations statistics [2], in 2017 Thailand had a population about 69,038,000 people and 11,736,460 of those is the elderly which accounted for 17% of the total population as such, there is a large and growing elderly population country is Thailand.

Information and Communication Technology (ICT) has developed rapidly and has played a role in all aspects of daily life. The number of people using information and communication technology increased even in the elderly. According to the information from National Statistical Office on ICT [3] from 2013 to 2017 reported that the elderly who used computers, internet and mobile phones tends to be increase every year. In 2013, elderly who used computers, internet and mobile phones accounted for 46.67% of the elderly population but in 2017 increased to 71.82%.

Chantana [4] reported that the elderly is more limited by age and have more degenerative physical changes i.e. deterioration of the optic nerve which becomes less sensitive to light as well as reduced sensitive to contrast. The deterioration will further increase at the age of 80, especially the decrease in color perception in the blue-green group. At present, most software applications have user interface design for normal sighted people which have a beautiful colors and patterns, But the application system is not well-suited for the elderly, resulting in the elderly misinterpreting the information that designer intended [5].

Nareerat et al. [6] Conducted a study on the ability of the elderly to recognize colors and symbols at different illuminance levels of warning signs. And it was concluded that the warning signs inside the building should be white symbol on the red background and outside the building should be white symbol on a blue background. From the research, it is clear that different illuminance levels in different environments impact the ability of the elderly to recognize colors and symbols on the warning signs differently.

Nowadays, the elderly use information technology with more computers and mobile phones. Both devices are electronic devices that use display screens. They can produce light and colors on the screen themselves and the light on the screen affect color and symbol recognition of the elderly. As such, this work is interested in learning which brightness level is preferred by the elderly and which pairs of text and background colors are the most easily read, and How these preferences compare to other age group. We could not find research works which answered these questions for computer displays, thus, we set up a pilot study for this issue.

The purpose of this research is to study the preferred brightness level on display screen that the elderly could see each pair of text and background colors most clearly and to compare this preference with other age group. The research also studies the pairs of text and background colors with the best readability on a computer display screen for the elderly.

It is expected that the results of the research can be used as a basis for the development of age customized automatic brightness adjustment on the display screens such as mobile phones, computers. And to offer text-background color combination to be more appropriate and in accordance with the needs of the elderly.

2. RELATED RESEARCH

Anja et al. [7] studied on the readability and easily

read in printing and digital media to test the readability and understanding of the text. As a result of the experiment, the authors reported that black text on a white background and black text on a yellow background can be easily read and green text on an orange background and red text on a green background was not recommended for use.

Nareerat et al. [6] studied on the ability of the elderly to see the color of warning signs under different brightness levels. The study examined brightness levels which were less than 300 lux and greater than 3000 lux. It was concluded that the signs inside buildings should use white symbols on red background. However, the signs outside the building should use white symbols on blue background.

Jordan et al. [8] developed formulae to recommend the brightness level and hue differences for text colors and background combinations on websites. The results showed in the form of red, green and blue in the RGB color space. The results from the experiment are a formula that suggest the color pairs for reading text.

The standard for senior citizens of ISO / TR 22411 [9] make a proper color pairs for the elderly with 22 color pairs. (Figure 1)

background color	Sign color							
	Black	White	Purple	Blue	Cyan	Green	Yellow	Red
Black		+	+	-	+	+	+	-
White	+		+	+	-	-	-	+
Purple	+	+		-	-	-	-	-
Blue	-	+	-		+	-	+	-
Cyan	+	-	-	+		-	-	-
Green	+	-		+	-		-	-
Yellow	+	-	+	+	-	-		-
Red	-	+	-	-	-	-	+	

+ very suitable
- not suitable

NOTE: The color combination of black and purple in Table usually does not appear well in high contrast of luminance due to the age-related sensitivity loss for blue and purple lights for older people. Purple can used with higher luminance in this combination

Fig. 1 Reproduce from the standard for senior citizens of ISO / TR 22411 [9]

The Web Content Accessibility Guidelines (WCAG) 2.0 [10] which determines the contrast ratio. The AA level must have a minimum sharpen aspect ratio of 4.5:1 for normal text and 3:1 for large text. The AAA level must have a minimum sharpen aspect ratio of 7:1 for normal text and 4.5:1 for large text. (Figure 2)

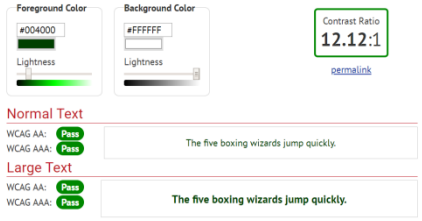

Fig. 2 The Web Content Accessibility Guidelines 2.0 [11]

And the third standard is the standard of the World Wide Web Consortium (W3C) [12] determines that it should be at least 125 (Brightness contrast >= 125) with a difference of two colors at least 500 (Tone difference >= 500). It is an acceptable contrast for reading.

From these literature reviews, the researchers designed a computer-based experiment. It is divided into two experiments.

The first experiment, the researchers displayed on six computer display screens with differing screen brightness levels at 20, 40, 60, 75, 95, and 120 lux. The research of Nareerat et al. [6] studied the ability of the elderly to see the color on warning signs under different bright. It was found out that different brightness environments affect the ability to see color pairs of symbol and background colors on warning signs differently. It is possible that the brightness level of the computer display screen affects the individual ability to see color pairs of text and background colors. Hence, the researcher had to experiment on a computer display screen with different brightness levels to study the results of the experiment.

And the color pairs that we used were based on from three standards. The first standard, The standard for senior citizens of ISO / TR 22411, The Web Content Accessibility Guidelines (WCAG) and The World Wide Web Consortium (W3C) standard

3. RESEARCH METHODOLOGY

This pilot study aimed to conduct an experiment to collect user preference on computer display screen brightness levels by controlling the text and background color pair and screen brightness.

The data collection of this work is based on qualitative research and we will collect it by ourselves through observation and interviews by letting the participants choose the color pair and display brightness choices that match with their preferences.

The researchers collected data from September to October 2018.

3.1 Sample population and selection

At the initial meeting with the prospective research participants, the objectives of the research were explained and discussed with the elderly and those who agreed to participate were screened for color blindness to check whether the they were qualified for color portion of this experiment. The participants were informed that no personal identifiable information would be collected and reported. Each participant was identified using a code and the research participation consent were obtained separately from the research data. After the initial meeting and screening, a date and time was scheduled for the experiment and interview.

The experiment was performed on two population groups: the elderly (over 60 years) and early adults (20 to 40 years). In this pilot study, 20 people were selected for each group.

For the elderly, the researchers started by meeting with the president of the elderly communities near the university to ask for cooperation and permission. After obtaining verbal agreement second meeting was set up to screen the participants and obtain written consent forms before beginning the experiment.

For the early adults, we approached employees and students from university and similarly obtained written consent forms before beginning the experiment.

Color-blindness test panel is used to screen research participants before starting the experiment to examine for color vision problems. Those who failed the screening were not included in the experiment.

Researchers have made color-blindness test panel based on Ishihara's tests designed by Shinobu Ishihara [13] for examining the color vision of the participants that is normal color visibility. By using determined proportion but reducing size to fit in the test.

Color-blindness test panel is an image with a diameter of 8.3 cm. There is one image per A5 page and the image in the test covers all five groups according to the design of the color-blindness test panel of Shinobu Ishihara.

3.2 Data collection

Basic demographic data about the participants was collected without personal identifiable information. This data includes gender, age, vision health and satisfaction with the use of brightness adjustment tools on computer display and mobile phones or tablets. Experiment results data was recorded was used to record the results describe the experiment procedures before starting the research data collection. Various forms were used for data collection as follow:

3.2.1 Personal data record form was used for collecting. Basic demographic information of the participants including gender, age, occupation, vision health, and color vision problems. The participants were assigned a participant ID for identifying the results of the experiment and to protect the rights of participants.

3.2.2 Experiment results data record form was used for collecting color pair and display brightness preference data. Experiment results data record were divided into two parts: the first part was a checklist that let the participants choose the brightness level which can be read in each pair of text and backgrounds colors and the computer display screen brightness levels checklist. And the second part was a checklist that let the participants choose the pairs of text and backgrounds colors which can be most clearly viewed and read.

The questionnaire is a Checklist question that is answered by selecting choices that match the opinions of the participants.

3.3 Research equipment

3.3.1 A light meter is used for data collection.

The instrument used to measure the brightness of light is a light meter made by Digicon LX-70 model LUX2. The units of measurement are foot-candle (fc) or lux (cd / m^2) units. In this study, the light meter was used instrument to measure the brightness level at the experiment room and the brightness of the computer display screens according to the conditions in the research study.

3.3.2 The type of computer display screen used in the experiment is an IPS LCD Lenovo ThinkVision LT2024. The brightness level can be adjusted in six steps at 20, 40, 60, 75, 95 and 120 lux.

3.3.3 The location of the experiment was at computer training rooms at university. The brightness in the room was determined to be between 300-500 lux. The brightness in the room is measured at 40 centimeters from each computer display screen at which is the same distance that the participants would sit during the experiment. The measurement was done using a light meter (Digicon LX-70). The room brightness is set in accordance with the Department of Science Service Journal by the Department of Labor Protection and Welfare [14] which recommends that the range of 300-500 lux as a guide for lighting in the work area.

3.4 Text and background colors

The text and background color pairs selected for the experiment are based on the related works discussed above.

3.4.1 The font used is 20-point TH Sarabun PSK as recommended by Ratanachote [15].

3.4.2 The color pairs are based on ISO / TR 22411 [10] , but the color pairs were reduced to seven based on WCAG recommended contrast ratio and sharpen aspect ratio[10], which states that the AA level must have a minimum sharpen aspect ratio of 4.5:1 for normal text and 3:1 for large text and the AAA level must have a minimum sharpen aspect ratio of 7:1 for normal text and 4.5:1 for large text. These were calculated using the tool [11]. Additionally, the selected color pairs also pass the W3C recommendation for reading which states that brightness contrast should be at least 125 with a tone difference of the two colors of at least 500.

Hence the pairs of text and backgrounds colors used in the experiments are cyan on black, yellow on black, white on black, black on white, black on yellow, white on navy, and white on green. (Table 2)

Table 1 Color code used in the experiments

Color	RGB color code			Hexadecimal color code
	Red	Green	Blue	
White	255	255	255	#FFFFFF
Yellow	255	255	0	#FFFF00
Green	0	100	0	#006400
Cyan	0	255	255	#00FFFF
Navy	0	0	128	#000080
Black	0	0	0	#000000

Table 2 Pairs of text and backgrounds colors used in the experiments

Background Color	Text color	Brightness contrast diff. >=125	Hue difference >=500	Contrast ratio
Black	Cyan	178.76	510	16.75
Black	Yellow	255.00	765	19.56
Black	White	221.14	551	21.00
White	Black	255.00	765	21.00
Yellow	Black	225.93	510	19.56
Navy	White	240.41	637	16.01
Green	White	196.30	665	7.44

3.5 Experimental procedure

In the experiment, the participants were shown text on six IPS type LCD screens of the same model. These screens were set up with differing screen brightness levels at 20, 40, 60, 75, 95, and 120 lux. The participants were instructed to read the text at a distance of around 40 centimeters at a height level within his/her visual field. During the experiment, the researchers used the light meter to measure the brightness of the screen periodically. The experiment was divided into two steps as follows:

3.5.1 First experiment: To study the screen brightness preference where each pair of text and backgrounds colors could be seen the most clearly. The six displays show the word 'ทดสอบ' in 20-point TH Sarabun PSK font one color pair at a time and the participants were asked to select their preferred brightness level. (Figure 3)

Fig. 3 First experimental setup

3.5.2 Second experiment: To study the preferred text and background color combination for reading. The brightness is fixed at 120 lux and all seven color pairs are shown together. The participants were asked to choose the pair of text and backgrounds colors they can most easily read. (Figure 4)

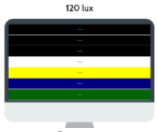

Fig. 4 Second experimental setup

4. RESULTS

4.1 Personal information of the participants

Group 1: Population over 60 years old.

There were 20 participants in this group. There were 17 females and 3 males. The average age was 68.6 years old. For vision health, the participants had a variety of conditions including, wearing glasses (90%), farsightedness (25%), dry eyes (10%), nearsightedness with farsightedness (10%), surgically removed cataracts (10%) and astigmatism (5%). Many people (40%) did not specify the reason to wear glasses. Half of the participants used mobile phone or tablets less than one hour per day. Most (70%) did not know the automatic brightness adjustment tool and the satisfaction in the use of the automatic brightness adjustment tool from the participants who knew it (four out of six people) was at moderate level.

Group 2: Early adults aged 20 to 40 years.

There were 20 participants in this group. There were 16 females and 4 males. The average age was 26.45 years old. For vision health, less than half (40%) wore glasses, nearsightedness (15%), nearsightedness with astigmatism (20%), astigmatism and dry eyes (5%). Nearly all (90%) of the participants use mobile phone more than four hours each day, most (85%) also knew the automatic brightness adjustment tool and less than half (41.18%) of those who knew of the tool indicated a high satisfaction level.

4.2 The results of the experiment

4.2.1 Experiment 1 This experiment asked 20 participants to choose the preferred brightness levels for seven text and background color pairs, resulting in a total of 140 responses. In the first participants group, more than half (57.86%) of the responses indicated the preferred brightness level of all pairs of texts and background colors on computer display screen at 95 or120 lux. Of these, 30.71% of the responses chose the preferred brightness level for each pair of texts and background colors on computer display screen at 120 lux. (Table 3)

Table 3 Elderly age group's preferred brightness levels for each color pair.

Pairs of text and background color	Brightness levels (lux)					
	20	40	60	75	95	120
	No. of elderly who preferred each brightness level					
Cyan on black	3	0	0	5	**7**	5
Yellow on black	1	2	3	4	3	**7**
White on black	1	1	0	4	**8**	6
Black on white	1	2	2	3	**8**	4
Black on yellow	1	3	5	2	1	**8**
White on Navy	1	0	1	5	**7**	6
White on green	1	0	4	4	4	**7**

In the second participants group, nearly two-thirds of the participants (61.43%) preferred the brightness level of all pairs of texts and background colors on computer display screen at 40 and 60 lux. Of these, 37.14% of the responses indicated preferred the brightness level for each pair of text and background colors on computer display screen at 60 lux. (Table 4)

Table 4 Early adults age group's preferred brightness levels for each color pair.

Pairs of text and background color	Brightness levels (lux)					
	20	40	60	75	95	120
	No. of early adults who preferred each brightness level					
Cyan on black	3	6	**7**	4	0	0
Yellow on black	5	6	**7**	2	0	0
White on black	3	4	**6**	5	2	0
Black on white	1	4	**9**	3	3	0
Black on yellow	1	**7**	6	3	3	0
White on Navy	2	5	**8**	3	1	1
White on green	0	2	**9**	6	1	2

4.2.2 Experiment 2

In the first participants group, it was found out that 35% of the participants specified that pair of black text on yellow background was the most easily read. And white on navy, yellow on black and white on green were 30%, 20% and 15% respectively. (Table 5)

In the second group of the participants, it was found out that 40% of the participants specified that pair of white texts on navy background was the most easily read. And yellow on black, black on white, white on green and white on black were 20%, 15%, 15% and 10% respectively. (Table 5)

Table 5 The number of elderly and early adults who preferred each text and background color at 120 lux.

Pairs of texts and background colors	No. of elderly	No. of early adults
Cyan on black	0	0
Yellow on black	4	4
White on black	0	2
Black on white	0	3
Black on yellow	7	0
White on Navy	6	**8**
White on green	3	3

6. DISCUSSION

From the results of the first experiment, more than half of the elderly preferred brightness levels of all pairs of texts and background colors at 95 and 120 lux. Whereas, the early adult group preferred brightness levels at 40 and 60 lux. This corresponds well to previous research that noted the deterioration of optic nerve and contrast sensitivity, which will worsen further at age 80. Of particular note is the decrease in color perception in the blue-green group [4]. The early adults group preferred much lower display brightness which corresponds to good health and fully developed senses such as visual acuity, hearing ability, smell, taste [16]. This is also consistent with [17], which showed that the visual ability to distinguish the darkness and brightness of early adulthood was different from the elderly.

In the second experiment, the elderly group chose black on yellow as the most easily readable color combination. This is consistent with the result of The Impacts of the Text and Background Color on the Screen Reading Experience [7], which reported that black text

on white background and black text on yellow background can be read easily. This choice can be explained by the vision problems article by Dr. Wittaya Manavanich [18], which described that elderly see the colors that are at the spectrum end which are red, orange and yellow easier than green, blue and purple. In contrast to the elderly group, no one in the early adult group chose black on yellow. Rather, this group chose white text on navy background to be the most easily read color combination. This choice difference may be explained by the results from the first experiment., When the early adults were presented with black text on yellow background, they preferred brightness level on the computer screen at only 40 lux, but in the second experiment the researchers had only tested the brightness level of the computer screen at 120 lux. Thus, it is likely that the screen brightness influenced the choice of preferred color combination. Further experiments could be further conducted to explore this possibility.

7. CONCLUSION

This pilot study provided empirical evidence that the clarity and legibility different text and background color combinations are influenced by the display brightness. Although the result is not unexpected, the experiment provided concrete values of preferred display brightness and color combination for two age groups. More than half (57.86%) of the elderly's responses indicated preference for brightness level at 95 and 120 lux. However, the brightness level that the early adults preferred was much different at xx lux. This implies that display brightness should be set differently for different age groups and auto-brightness algorithms of smartphones and computers should be customized to suit the age range and vision of the user.

The elderly group and the early adults group chose different color combinations (Black on yellow vs. white on blue) as the most easily read color pair. In the present, there are only a few software applications that can adjust the texts and background color to be suitable with the user's age ranges. This is especially important if the applications required a lot of reading such as news, chat, eBooks, and web sites. Additional functions could be added to automatically adjust (or allow the users to choose) combinations of texts and background colors to suit the age ranges.

8. FURTHER WORK

The study was conducted on the brightness levels on the IPS computer display screen only at 6 levels: 20, 40, 60, 75, 95 and 120 lux. So, further investigation could study in more brightness levels on computer display screens and on the other types of display screens. Additionally, this study investigated the data collected in the room brightness level of 300-500 lux, so doing a study in different environments to make the research more widely applicable. Other age groups could also be studied to provide more age specific results.

9. REFERENCES

[1] ชมพูนุท พรหมภักดิ์, 2556, การเข้าสู่สังคมผู้สูงอายุของประเทศไทย [Online], Available: http://library.senate.go.th/document /Ext6078/6078440_0002.PDF.

[2] The Department of Economic and Social Affairs Population Division United Nations New York, 2017, World Population Prospects [Online], Available: https://esa.un.org/unpd/wpp/publications/files/wpp2017_ keyfindings.pdf

[3] สำนักงานสถิติแห่งชาติ (2560), ประชากร60[Online], Available: http://www.nso.go.th//sites/2014/DocLib13/ด้านICT/เทคโนโลยีในครัวเรือน/2560/excel_ict_60.rar.

[4] จันทนา รณฤทธิวิชัย, 2553, การเปลี่ยนแปลงของร่างกายและจิตใจของผู้สูงอายุ [Online], Available: https://www.doctor.or.th/ article / detail/4930.

[5] Yun, Y., Lee, C. and Lim, H., 2016, Designing an intelligent UI/UX system based on the cognitive response for smart senior, Department of Computer Science and Engineering KOREA University, Page 281-284.

[6] นารีรัตน์ สังวรวงษ์พนา, รัชนีภรณ์ ทรัพย์กรานนท์, พรทวี พึ่งรัศมี, ชมนาด สุ่มเงิน และ โทโมโกะ โอบามา, 2558, ความสามารถในการมองเห็นสีของผู้สูงอายุภายใต้ระดับความสว่างที่ต่างกัน, วารสารคณะพยาบาลศาสตร์, ปีที่23, ฉบับ 1, หน้า 13-25.

[7] Anja, Z., Snježana, I.W., Mario, T. and Darijo, C., 2017, The Impacts of The Text and Background Color on The Screen Reading Experience, TECHNICAL JOURNAL, Vol. 11, No. 3., pp. 78-82.

[8] Jordan, K., David, B., Lyle, U., Ayaka, N. and Joshua W., Determining the Readability of Colored Text [Online], Available: http://www.seas.upenn.edu/~cse400/ CSE400_2012_2013/reports/01_report.pdf.

[9] International Organization for Standardization. ISO/TR 22411:2008 Ergonomics data and guidelines for the application of ISO/IEC Guide 71 to products and services to address the needs of older persons and persons with disabilities. Switzerland: n.p., 2008.

[10] The Web Content Accessibility Guidelines (WCAG) 2.0, C. Ben, W. Chisholm, C. Michael, G. Vanderheiden, Editors, W3C Recommendation 11 December 2008, https://www.w3.org/TR/WCAG20/

[11] Center for Persons with Disabilities, 2018, Color Contrast Checker [Online], Available: https://webaim.org /resources/contrastchecker/

[12] Techniques for Accessibility Evaluation and Repair Tools, R. Chris, C. Wendy, Editors, W3C Working Draft, 26 April 2000, https://www.w3.org/TR/AERT/

[13] Shinobu Ishihara, 1972, Test for colour-blindness by Ishihara [Online], Available: http://www.dfis.ubi.pt/~hgil /P.V.2/Ishihara/Ishihara.24.Plate.TEST.Book.pdf

[14] The Labor Protection Act, 2011, the Department of Science Service Journal by the Department of Labor Protection and Welfare [Online], Available: https://www. labour.go.th/th/doc/law/safety-statute-2554.pdf

[15] รัตนโชติ เทียนมงคล, 2560, The Study of Fonts Legibility for Elders: A contextual of Thai Alphabets on Tablet Screen, สาขามนุษยศาสตร์ สังคมศาสตร์ และศิลปะ, ปีที่ 10, ฉบับที่ 3, หน้า 1066-1082

[16] สุชา จันทน์เอ, 2536, จิตวิทยาพัฒนาการ, สถานที่พิมพ์: ไทยวัฒนาพานิชย์

[17] Schieber, F. (1992). Aging and the senses. In J.E. Birren, R. Sloan & G. Cohen (Eds.), Handbook of mental health and aging. New York: Academic Press. pp. 251-306.

[18] วิทยา มานะวาณิชเจริญ, 2006, ภาคที่ 4 จิตวิทยาผู้สูงวัย ตอนที่ 37: ปัญหาการมองเห็น [Online], Available: http://haamor.com/th/ th/จิตวิทยาผู้สูงวัย-37/

FATIGUE ANALYSIS OF SUNDRY I.C. ENGINE CONNECTING RODS

Ashwin Misra[1], Ghanvir Singh[1] and Mukul Tomar[]
[1] *Delhi Technological University, New Delhi, India*
Email: sghanvir@gmail.com

ABSTRACT: The connecting rod is a vital component in all Internal Combustion Engines. When subjected to alternative compressive and tensile stresses in a cycle of the engine the chances of fatigue failure in the connecting rod are higher. More over the connecting rod acts as a column which also leads to the development of buckling stress. Hence, it is necessary to determine the fatigue life of the existing connecting rod materials and also look for alternative materials. Using the output of a test, which was conducted on computerized variable compression ratio (V.C.R), Kirloskar Diesel Engine equipment provided with a pressure transducer, kinematic and dynamic analysis of a connecting rod was carried out at a compression ratio of 16.5. Further a Quasi-Dynamic stress model is used for analysis which was based on the results of the Dynamic analysis. We embarked on performing the kinematic and dynamic analysis of connecting rod using MATLAB at a compression ratio of 16.5, 17.5 and 18.5 and also at four different critical crank angles with the existing materials namely Forged Steel, Aluminum Alloy and Titanium alloy. Further, the analysis was performed by using ANSYS workbench for determining the Factor of safety, Von mises stresses and Deformations.

Keywords: Quasi-Dynamic ,Compression, Fatigue, Dynamic, Buckling

1. Literature Review

The connecting rod of an Internal combustion engine is subjected to a complex state of loading. It undergoes high cyclic loads of the order of 106 to 1010 cycles, which range from high compressive loads because of combustion, to high tensile loads because of inertia. Therefore, durability of this component is of high importance, because of these factors, the connecting rod has been the topic of research for different categories such as materials, production technology, performance experiential simulation, fatigue analysis, etc. Webster et al. [1] performed three dimensional finite element analysis of a high-speed Compression ignition engine connecting rod. For this analysis they used the maximum compressive load and the maximum tensile load which was experimentally calculated. The distributions of load on the crank end and piston pin end were determined experimentally. They modeled the connecting rod cap separately, and also modeled the bolt pretension with the use of beam components and multi point constraint equations.Yoo et al.[2] used variation of equations of material derivative idea of continuum mechanics, elasticity and an adjoint variable technique to calculate shape design stress sensitivities. The results were used as an input to an iterative optimization algorithm, descent algorithm with the highest gradient to numerically solve the optimal design problem. The main concentration was on shape design sensitivity analysis with application to a connecting rod of an internal combustion engine. The stress constraints were imposed on firing loads and principal stresses of inertia. The fatigue strength was still not addressed. The other constraint was the one on thickness to bind it away from zero. They could achieve a one fifth weight reduction in the neck region of the connecting rod.Folgar et al. [3] developed a fiber Metal matrix composite connecting rod with the help of FEA, and loads were obtained from kinematic analysis. Fatigue was not yet tended to at the design stage. However, prototypes were fatigue tested. The investigators identified design loads in terms of maximum engine speed, and loads at both ends. They performed static tests in which the crank ends and the piston pin end failed at different loads. Clearly, the two ends were designed to withstand different loads. Serag et al.[4] developed approximate mathematical formulae to define connecting rod weight and cost as objective functions and also the constraints. The optimization was achieved using a Geometric Programming technique. Constraints were imposed on the compression stress, the bearing pressure at the crank and the piston pin ends. Fatigue was not addressed. The cost function was expressed in some exponential form with the geometric parameters. El-Sayed and Lund [5] presented a method to consider fatigue life as a constraint in optimal design of structures. They also demonstrated the concept on a SAEkey whole specimen. In this approach a routine calculates the life of the specimen and in addition to the stress limit, limits are imposed on the life of the component as calculated by the FEA results. The most common types of manufacturing processes for Connecting rods are powder metallurgy, casting and forging. There are many different types of materials and production methods that can be used in the fabrication of connecting rods.

2. Analysis

2.1 Design Method of Connecting Rod

The connecting rod undergoes a complex motion, which is characterized by frequent bending stresses due to the inertial loads. In view of the aim of this study, which is analysis and optimization of the connecting rod, it is essential to determine the value of the loads on the connecting rod. Generally circular section is generally used for low speed engines whereas the I-section is used for high speed engines. So the connecting rods are designed generally of I-section to provide maximum rigidity with the least possible weight. On the basis of this design, a physical model is modelled in Solidworks 2018. Structural system of the connecting rod has been analysed using FEA. Numerical solutions to even very complex stress problems can now be obtained easily

using FEA, and the process is so vital that even introductory treatments of mechanics of materials such as these modules should outline its principal features. With the use of FEA, various stresses are calculated for a particular loading conditions using FEA software Solidworks Simulation

The most used materials which are being utilised for Connecting rods in the current global economy are Steel and Aluminium.

1. Small end called as Piston end which connects the piston with connecting rod through gudgeon pin.

2. The shank of I-Section.

3. Big end called as Crank end which connects the connecting rod with crank pin.

Thickness of I Beam	6.5
Thickness of crank and piston end	15.3
width at crank end	17.32
width at piston end	12.33
Height	134
Crank end diameter	34.9
Piston end diameter	24.6

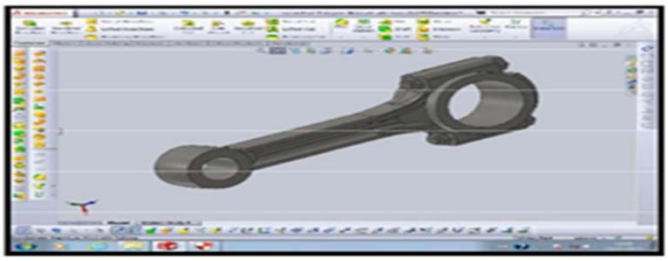

Fig.1 3D model of IC engine connecting rod

3. FACTOR OF SAFETY

Factor of safety is a ratio of maximum stress that a component can withstand by an object to applied stress. It is a measure of the load carrying capacity. The factor to which the design component can work without any failure. Whenever the Factor of safety is greater than or equal to 1, then the applied stress is less than or equal to the maximum stress so the object can bear the applied load. But when the ratio is equal to 1, the object is tough enough to withstand load. Whenever a Factor of safety is less than 1, the applied stress is greater than maximum stress then the object can't bear the stress applied, it leads to failure of the specimen under experimentation. In simple words, Strength is the ultimate load at which material can fail and Stress is the allowable load at which material cannot fail. FOS increases with increase in the life of its individual components. Formula for Factor of Safety (F.O.S) calculation- FOS =

1.Strength/Stress Fig. 6- F.O.S calculation for Forged Steel rod on application of 5kN at Piston end.

Yield Strength - 750 MPa

Max Working Stress- 338.6 MPa

F.O.S = Yield Stress / Working stress

=750 / 338.6

=2.22

2. F.O.S calculation for Aluminium Alloy rod on application of 5kN at Piston end.

Yield Strength - 505 MPa

Max Working Stress- 330.9 MPa

F.O.S = Yield Stress / Working stress

=505 / 330.9

=1.53

3. F.O.S calculation for Forged Steel rod on application of 5kN at Crank end.

Yield Strength - 750 MPa

Max Working Stress- 194.3 MPa

F.O.S = Yield Stress / Working stress

=750 /194.3

=3.9

In all the four cases the F.O.S comes out be more than 1, hence the connecting rods of both the material will bear the applied load without failure. Also we can depict the results obtained from F.O.S that the connecting rod has a good fatigue life of higher number of cycles

4. Finite Element Modeling of Connecting Rod

The figure 1 shows individual components in 3D spaces. Bush, connecting rod split members along with clamping bolts with nuts is shown. Material color codes are used to represent the problem in various color codes.The figure 2 shows Connecting rod modeled with Solidworks. Solidworks sketcher, part modeler and assemblers are used for building the geometry. Solidworks is a solid/surface modeling software in the industry and various modeling and assembly options are available to build the geometries of different components. Additionally, geometric dimensioning and extra tolerances can be provided for the modeled parts.

5. Results of Static Analysis

Initially contact analysis is carried out to appro ximate the contact pressure between the members bec ause of press fit bush. Geometric interference is provi ded between members. The results are as summarized below.

Figure 3 shows hoop stress. The inner bush is very close to the yield condition because of interference of 0.049mm. Tensile hoop stress can be observed in the outer small region. Both the tensile and compressive stresses are represented in different colors. Solidworks simulation style, plot-controls, style option is used to represent the axial-symmetric problem in three dimensional spaces. This provides to help the customer to understand the reality of the problem as axi-symmetric approach is technically right, but represents the problem in 2 dimensional spaces. Nonlinear material property of the bush allows plastic yielding of the problem and converges to the right solution.

The figure 4 shows contact pressure in the member. Maximum contact pressure is around 54.9812 Mpa at the interface. Contact elements are created to find the given contact pressure. This contact pressure is developed because of the interference of 0.059mm between the members for press fit. Higher the interference, contact pressure between the members is

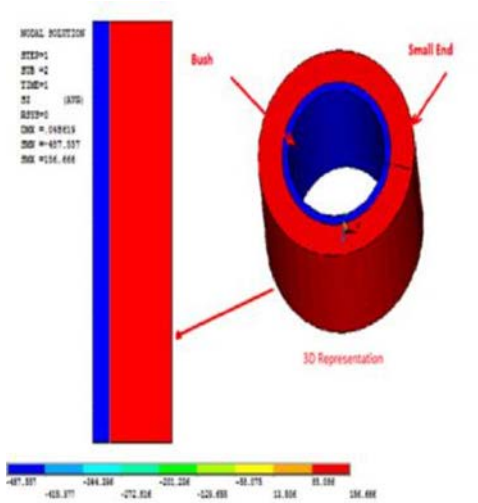

Fig 3: Hoop Stress plot

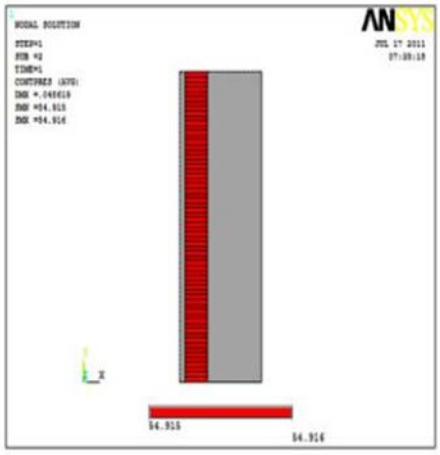

Fig 4: Contact pressure between the members

higher and the load carrying capacity will also be higher for the members. The fatigue life of the inner member increases with compressive stress on the structure. A fatigue failure generally starts with tensile stress on the surface. With compressive stress on the surface, fatigue life will increase. Shot peening is generally done to induce compressive stresses on the structure to prevent fatigue failure of the specified structure. This preloading also increases the holding strength of the members and helps in increasing the resonant frequency of the system.

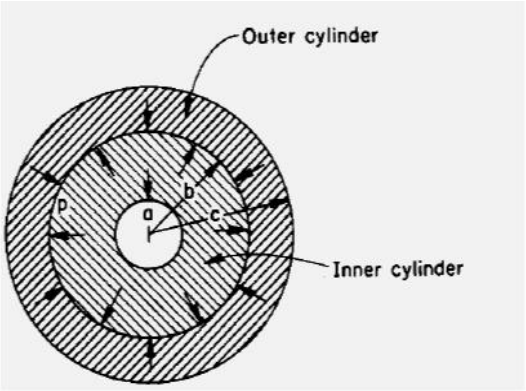

Fig 5: compound cylinder with shrink fit

Where 'P' is the contact pressure
'b' = Outer radius of inner cylinder
'a'= Inner radius of inner cylinder
'c;=Outer radius of outer cylinder
'δ'=Interference
Here δ=0.058mm
Eo= Young's modulus of outer cylinder
Ei= Young's modulus of inner cylinder
b=13mm, c=18.75mm, a=11.5mm
E0=2x105 N/mm2Ei=105x103 N/mm2.

On substitution of the values contact pressure equals to 50 N/mm2. Small deviation of results (10%) can be observed between theoretical and Finite element solutions (Theoretically 50 N//mm2 and 54.9 N/mm2 from FEM solution).

The figure 6 shows radial stress development in the problem in hand. Maximum radial stress in the compression cycle is represented by 55 N/mm2 at the interface. Both the materials steel and aluminium are subjected to decreasing stress from the interface. Higher radial stress is desirable at the interface for better load carrying capacity. Radial stresses are minimum at the extreme ends. Higher radial stress also indicates bond strength. Generally structures will not fail by radial stress as the extent of radial stress is less than the hoop stresses. Solidworks has the provision to have virtual view of three dimensional plot of two dimensional axisymmetric problems. This helps in imaging three dimensional joint.

The figure 7 shows von-mises stress in the given problem. Maximum von-mises stress is around 433.1 N/mm2 in the bush member. Almost 91 N/mm2 can be observed at the outer end of connecting rod specimen. The bush is subjected to maximum stress compared to the smaller end of connecting rod. The inner surface to the bush member is subjected to maximum von-mises stress. 91N/mm2 stress can be observed at the outer boundary or small end of the connecting rod. Von-mises is the stress is used to find the failure of the ductile components as it accounts all types of stresses in its calculation. Also von-mises stress failure is the most applicable theory based on literature review. Whereas the von-mises theory considers all 6 stress components of the problem.

The figure 8 shows sudden variation of stress at the interface from bush to outer small end of connecting rod. The stress is varying its sign from compression to tension at the interface. Maximum compressive hoop stress is around 488N/mm2 at the inner boundary to the maximum tensile stress of 157 N/mm2 at the small end interface and stresses are reducing to outer boundary. An Solidworks path operation helps in representing the graphical plot of the problem. Nodal coordinates are considered along the 'X' axis and stress is plotted along 'Y' axis.

The figure 9 shows radial stress variation in the geometry. A high slope reduction (increasing values in absolute system) can be observed in the graph. Maximum compressive stress of 55 N/mm2 can be observed at the interface and values are converging to minimum positive values (almost zero's) to the outer boundaries from the interface. This is also clear from thick cylinder concept where outer radial stress is taken zero for obtaining the stress relation in Lame's equations. Lame's equation helps in obtaining interference pressure for compound cylinders with radial interference

The figure 10 shows von-mises stress variation in the problem. Maximum von-mises stress is around 434 N/mm2 at the inner boundary and reducing to 91N/mm2 at the outer boundary. A steep drop of stress can be observed at the interface (This drop is from compression to tension on the smaller end). Generally interfaces are the stress raisers and also possible sources of crack or fault generations. The Heat also will generate because of frictional sliding of the members which is very difficult to analyse. Present algorithms are based on iterative techniques which consume considerable resources of computers and time and accuracy is mainly based on

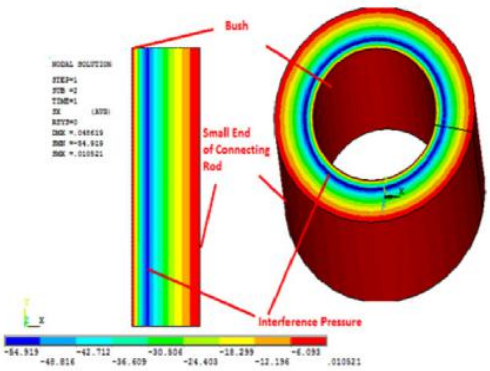

Fig6: radial stresses in members

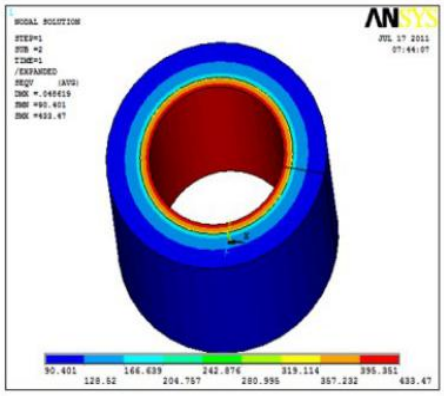

Fig7: vonmises stresses in joint

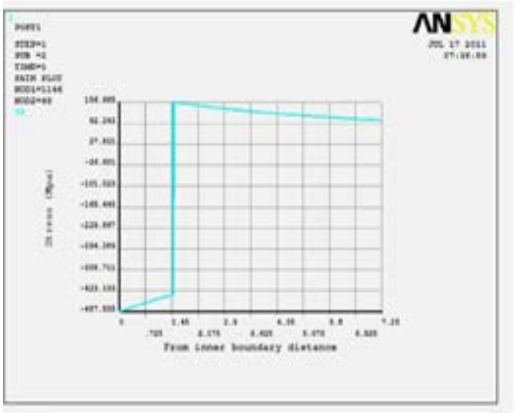

Fig 8: Hoop Stress variation

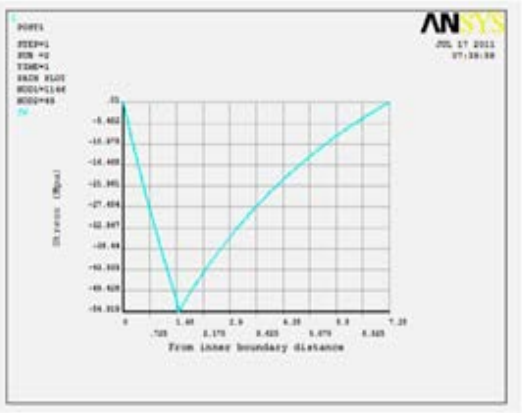

Fig 9 : Radial stress variation in the assembly

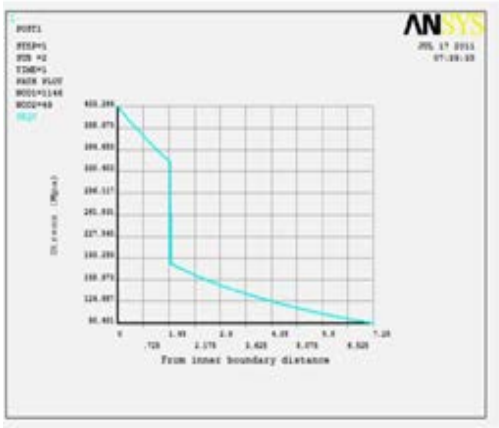

Fig 10: Vonmises stress variation

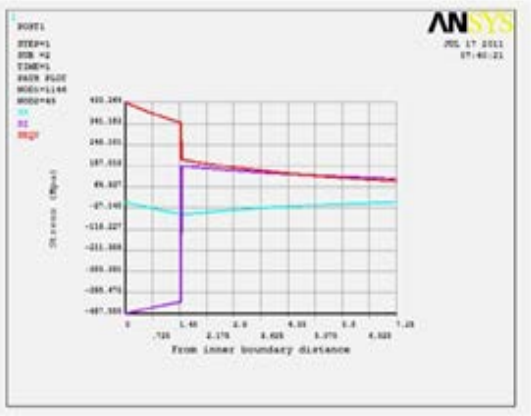

Fig 11: Vonmises, Hoop and Radial stress variation in the assembly

convergence levels. This also depends on the algorithm adopted and frictional values. Generally Lagrangian algorithms provides better quality analysis compared to the penalty approaches. In the present problem, augmented lagrangian methodology with standard contact algorithm is considered with Newton Raphson convergence technique.

This analysis is carried out with the initial pretension in the member. The pretension load is applied through the primary bolt elements. The results are as given. pretension load is calculated for the bolt diameter of 8.1 mm with pretension stress of 209Mpa applied through an axial element by coupling constraints to the connecting rod end. The bolt pretension helps in joining the split parts and also holds the bush in position The results are discussed as follows.

The figure 13 shows displacement in the connecting rod that because of bolt pretension. A displacement of 0.0049mm can be observed because of the clamping load shown with red colour. Other displacements of region are also shown in the status bar which shows change in displacement in the connecting rod. The values are shown in colour ranges. By default 9 colours are used for representation of the displacement variation. Maximum deflections in the red region and minimum deflections in the blue regions.

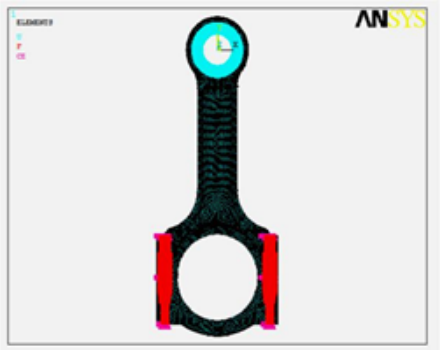

Fig 12: Pretension in the load in the connecting rod

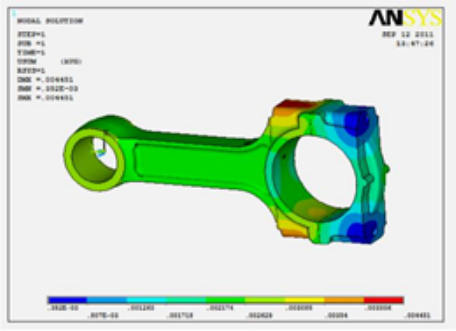

Fig 13: Displacement due to pretension load

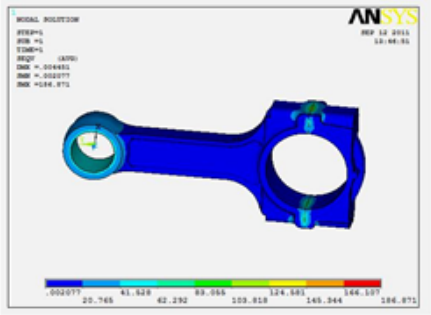

Fig 14: vonmises stress due to pretensionload

The figure 14 shows Von-Mises stress generation because of the clamping loads. Maximum stress points can be observed at the joint region of the specimen. Other region is relatively free from stresses. Maximum stress of 187 N/mm2 can be observed in the problem. The stresses are highest at the split parts where bolt pretension is applied. The shank region is almost free of stresses except at the constrained small crank pin end region.

7. Fatigue Analysis (Model A- Load Through Complete Contact)

The two dimensional analysis results are used to apply the loads on the small end and big end regions. The three dimensional mesh is imported to ansys in 'inp' file format and analysis is carried out. The inner nodes of small end are rotated to cylindrical system to ease load application. The interference loads are applied as radial coordinates at the small end to create the pretension effect through inner surface elements. At the big end, the contact loads are directly considered as uniformly distributed load at the inner surface. Two load steps are considered for fatigue analysis at the big end. In the first case, no external load is considered except the Assembly loads(Both pretension because of bolt loads and interference at the big end and small ends). And in the second case, all the loads (assembly and service loads) are considered. The boundary conditions are as follows The figure 15 shows boundary conditions for the fatigue analysis for the Assembly and service loads. Assembly loads are considered for load case 1 and assembly and service loads are considered for 2nd case. In the load case1 the shank region is constrained and the assembly loads obtained from the axisymmetric analysis is applied at the small and big end regions. Bolt pretension loads are also applied. In the load case 2 the constraint at the shank region is removed and small end nodes are rotated to cylindrical system and direct interference loads are applied.

8. Results for Assembly Loads (Case 1)

The figure 16 shows displacement in the connecting rod assembly. The symbol 'Mx' indicates maximum displacement location. Maximum displacement of around 0.028455mm can be observed at the big end. The figure4.16 shows varying displacement in the problem The contact pressure obtained from the axisymmetric analysis is applied through constraints at the inner boundary of the small end of connecting rod. Minimum displacements can be observed at the shank region as it is constrained. The displacements can be observed at both big end and small end due to interference loads. But maximum displacement is taking place in the bigger end as its dimensions are large compared to the smaller end.The figure 17 shows vonmises stress in the structure due to Assembly loads (bush interference and bolt tension) at small end and big end of connecting rod. Maximum stress is around 298.935N/mm2 is taking place at the big end split joint. The more stress can be observed at the joint region. Almost minimum stresses can be observed in the shank region as it is constrained. The fatigue analysis is carried out for assembly loads and service loads with assembly loads.

9. Results for Assembly Loads (Case 2)

The figure 18 shows maximum displacement in the connecting rod big end. The color red shows the maximum displacement location. Maximum displacement of around 0.11051mm can be observed at the big end. Minimum displacements can be observed towards the small end . Maximum variation of displacement also can beobserved at the big end. Elliptical shape can be observed in the big end due to the loading.The figure 19 shows vonmises stress in the structure due to assembly and service loads. Maximum stress is around 565.017N/mm2 is taking place at the big end joint. This tress raise can be attributed to the discontinuity of material at the joint region. Almost minimum stresses can be observed in the web region.

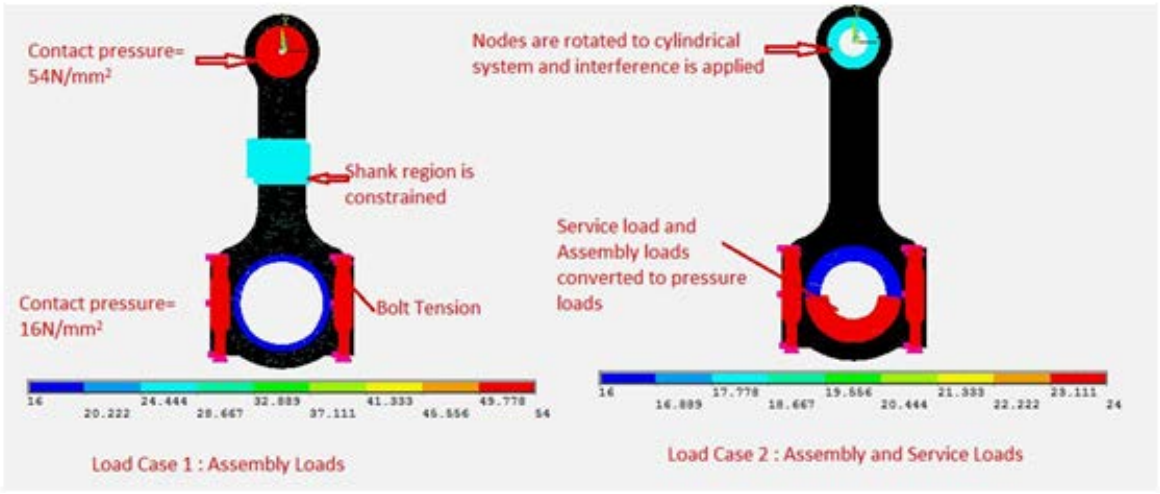

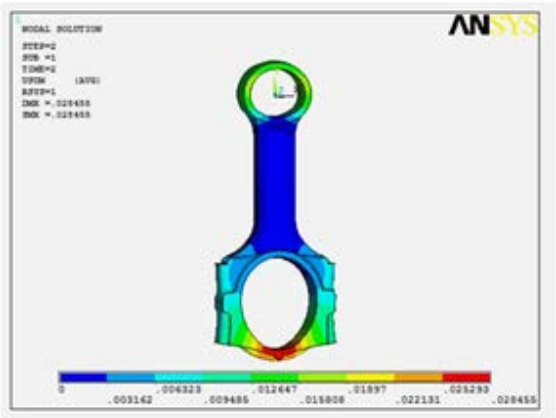

Fig 16: Displacement in the connecting rod due to Assembly loads

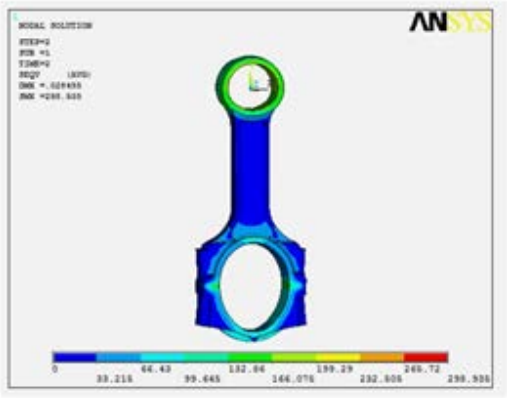

Fig 19: Vonmises stress due to Assembly and Service loads

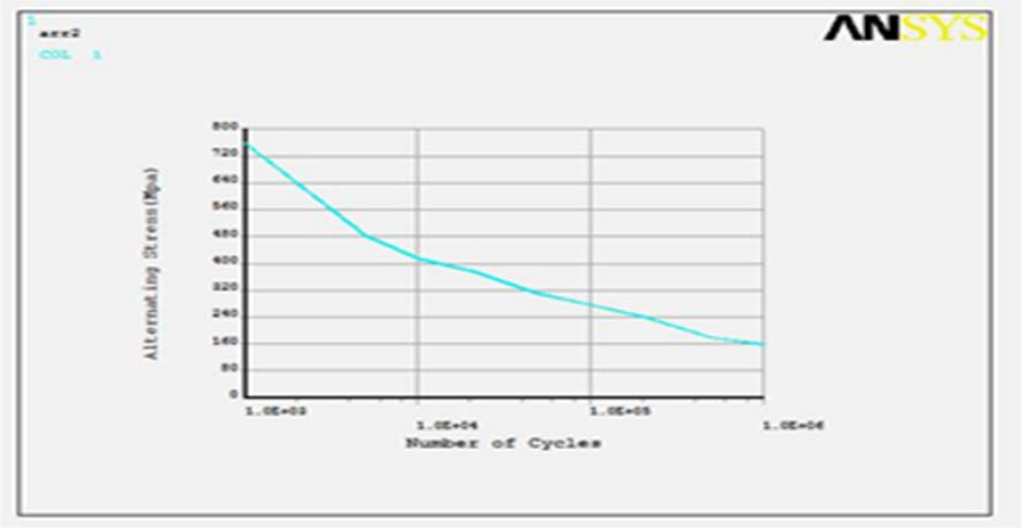

Fig 20: S-N curve for Steel 42

The figure 20 shows S-N curve data for the connecting rod material. The alternating stress value is reducing with number of cycles. Fatigue limit corresponding to one million cycles is represented by 160Mpa for the material. So fatigue analysis is carried out for this endurance limit. High cycle region is considered for the analysis. SN curves are obtained through experimentation for different material. The curve varies with alloying elements. Generally fatigue life is specified for one million cycles which is defined with endurance limit of the material under reversed loading.

The Table 2 and results shows developed stresses in the members. The alternating stress developed is around 139.58N/mm2 which is less than the fatigue limit of 160N/mm2 for one million cycles. If number of cycles is extended, then life of the member will reduce. But for

present consideration the structure with stands one million cycles for the assumed load transfer through complete contact and load transfer through the bush material**.**

Table 2. Stresses for the load cases

Load case	Sx	Sy	Sz	Sxy	Syz	Szx
1	-53.824	236.74	38.742	25.949	1.2019	0.28512
2	-95.309	471.81	75.336	-44.827	-0.7001	1.8273

Fatigue Summary:
Alternating stress =139.58 N/mm2.
Cycles used/allowed = 0.1000e+07/ 0.1000e+07
Cumulative fatigue usage =1.00000

10. Conclusions

This analysis of connecting rod is carried out to check the alternating stress development and fatigue life due to service and assembly loads with variation in load distribution. The results are summarized as follows. In initially the connecting rod is built to the actual dimensions using solidworks software.Axi-symmetric analysis is carried out to find interference effect on the stress behavior in the joint. 8 noded plane82 element with quadratic displacement variation is used for accurate results. The contact pair is created with Contac172 and Targe169 elements. Interference is created through geometric built up .The result shows contact pressure development at the interface and higher compressive stress in the bush and tensile stress development in the small end. The results are plotted for vonmises stresses, radial and hoop . Also a three dimensional views are obtained through Ansys axisymmetric options .Further three dimensional analysisis carried out to find the fatigue nature of the connecting rod with variation in load transfer. Two models of load nature (Model-A and Model-B) are considered with assembly and service loads to analyze the fatigue nature of the connecting rod.

11. References

[1] Webster, W. D., Coffell R., and Alfaro D., “A Three Dimensional Finite Element Analysis of a High Speed Diesel Engine Connecting Rod,” SAE Technical Paper Series, Paper No. 831322,1983,
[2] Yoo, Y. M., Haug, E. J., and Choi, K. K., 1984, “Shape optimal design of an engine connecting rod,” Journal of Mechanisms, Transmissions, and Automation in Design, Transactions of ASME, Vol. 106, pp. 415-419,1984.
[3]Folgar, F., Wldrig, J. E., and Hunt, J. W. “Design, Fabrication and Performance of Fiber FP/Metal Matrix Composite Connecting Rods,”
[4] Serag, S., Sevien, L., Sheha, G., and El-Beshtawi, I., “Optimal design of the connecting-rod”, Modelling, Simulation and Control, B, AMSE Press, Vol. 24, No. 3, pp. 49-63,1989.
[5] El-Sayed, M. E. M., and Lund, E. H., “Structural optimization with fatigue life constraints,” Engineering Fracture Mechanics, Vol. 37, No. 6, pp. 1149-1156,1990.
[6] Sarihan, V. and Song, J., “Optimization of the Wrist Pin End of an Automobile Engine Connecting Rod With an Interference Fit,” Journal of Mechanical Design, Transactions of the ASME, Vol. 112, pp. 406-412,1990.
[7] Athavale, S. and Sajanpawar, P. R. “Studies on Some Modelling Aspects in the Finite Element Analysis of Small Gasoline Engine Components,” Small Engine Technology Conference Proceedings, Society of Automotive Engineers of Japan, Tokyo, pp. 379-389,1991.
[8] Balasubramaniam, B., Svoboda, M., and Bauer, W. “Structural optimization of I.C. engines subjected to mechanical and thermal loads,” Computer Methods in Applied Mechanics and Engineering, Vol. 89, pp. 337-360,1991.
[9] Hippoliti, R., “FEM method for design and optimization of connecting rods for small two-stroke engines,” Small Engine Technology Conference, pp. 217-231,1993.
[10] Sonsino, C. M., and Esper, F. J , “Fatigue Design for PM Components,” EuropeanPowder Metallurgy Association (EPMA),1994.

Groundwater Flow Model of Bangkok and Vicinity Areas

Pee Poatprommanee[1)*], Schradh Seanton[1), 2)]
[1)]*Department of Geological Sciences, Faculty of Science, Chiang Mai University, Huay Kaew Road, Chiang Mai, Thailand 50200.*
[2)] *Environmental Science Research Center, Faculty of Science, Chiang Mai University, Huay Kaew Road, Chiang Mai, Thailand 50200.*

ABSTRACT: Bangkok and vicinity areas are located in the Chao Praya river floodplain which is in the lower part of central Thailand. The area is flat and low-lying landscape with an average elevation of about 1.5 m above mean sea level. The Chao Praya river basin was filled with the sequence of unconsolidated sediment that is alluvial sand and gravel interbedded with floodplain silt and clay grading to marine clay. The major aquifers of the Chao Praya basin can be divided into top clay layer and 8 major aquifers with approximate total thick 700 m depth. Each aquifer is about 50 m thick. The largest amount of groundwater has been extracted from Phra Pradaeng (PD), Nakorn Luang (NL), and Nonthaburi (NB) aquifers. Groundwater in upper aquifers cannot be used because of its high salinity due to seawater intrusion. The simulated domain covers 70×80 km^2 area of 6 provinces. The aquifer system is modeled using 3D finite-difference groundwater flow model (MODFLOW). The model is divided into 35 columns, 40 rows with 2×2 km^2 grid size, and 5 layers including top clay layer and four additional 4 aquifers. Both steady-state and transient responses were simulated and historical data of hydraulic heads was used as calibration target. The model was calibrated systematically and automatically using parameter estimation code (PEST). Spatially variable parameters such as hydraulic conductivity, storage coefficient, specific yield, recharge and evapotranspiration were calibrated based on the "pilot-points" technique in order to allow heterogeneity. The simulation results indicated that the flow model can successfully simulate transient behavior of aquifer systems with the most sensitive parameter is hydraulic conductivity. Groundwater usage in the modeled area have declined considerably in recent years resulting an increase, in general, of hydraulic heads. This calibrated model will be subsequently used to assess land subsidence or to predict the buoyancy effect to subway tubes.

1. INTRODUCTION

Bangkok is located in the Chao Phraya River flood plain which is the lower part of Central Thailand Plain. This area is of flat and low-lying topography with an average elevation of 1.5 m above mean sea level. Bangkok metropolitan covers an area of 1,500 km^2 with approximately 8.3 million population [1]. In Bangkok metropolitan area, more than 30% of consumed water was acquired from underlying groundwater aquifers.

Groundwater extraction in Bangkok and vicinity provinces in 1975 was 0.65 Mm^3/d and rapidly rose to over 1 Mm^3/d in 1980. During mid-1980s to early 1990s, the pumping rate has been reduced and stabilized but increased again after 1993. The highest pumping rate reached over 2 Mm^3/d in 2000 [2]. Since 2004, the pumping rate has decreased due to a strict control of groundwater use.

For a long period, exceedingly high groundwater extraction rate can cause environmental problems due to the lowering groundwater level. A large cone of depression whose center is located in the eastern Bangkok which is has high industrial and residential growth. The cone of depression covered the whole city area. The smaller cone occurred in southwest suburban area due to the lack of surface water supply. A decrease in piezometric head led to drastic land subsidence in a large scale. Nutalaya et al. [3] found that land subsidence affected Bangkok area more than 4,550 km^2 from 1960 to 1988 and maximum settlement was over 160 cm. During 1978 to 1981, the subsidence rate in the East of Bangkok was as high as 10 cm/year and the rate was 5-10 cm/year in central Bangkok. After the enforcement of groundwater using control, the subsidence rate decreased to less than 5 cm/year and reduced to less than 3 cm/year in 2008 [4].

JICA [5] investigated groundwater flow, land subsidence, and seawater intrusion in Bangkok and vicinity area and found that (1) groundwater pumping rate of 1.5 Mm^3/year, (2) groundwater level dropped about 30 m in Samut Sakhon, Pathum Thani, and Eastern Bangkok to Samut Prakarn, (3) land subsidence occurred in Bangkok, Samut Sakhon, Samut Prakarn, Nonthaburi, and Pathum Thani with a rate of more than 20 mm/year, (4) high chloride concentrations were found along the west side of Chao Praya River and near shore in Samut Prakarn.

The uncontrolled groundwater extraction in Bangkok and vicinity provinces has led to several environmental impacts including a decline of groundwater level, land subsidence, and seawater intrusion. Land subsidence can cause damage to buildings. Seawater intrusion make groundwater cannot be consume because high salinity. In recent years, the rising of groundwater level causes lower cohesive strength in clay that mean clay is more liquid and carry less weight. In addition, the buoyancy effect occur with subsurface structure.

2. OBJECTIVES OF THIS STUDY

This study will provide better understanding Bangkok aquifer system using groundwater modeling approach. The calibrated numerical groundwater flow model that can be used to plan groundwater management and assess land subsidence or predict the buoyancy effect to subway tubes in Bangkok and vicinity provinces. The study area is located in lower Chao Phraya basin and cover areas of six provinces that include Bangkok, Pathum Tani, Nakhonpathom, Samut Sakhon, Samut Prakan, and Phra Nakorn Si Ayutthaya. It is located in 13°27′25.6″N- 14°10′34.4″N and 100°11′30.2″-

100°50′38.0″E (Fig. 1).

Fig. 1 Study area (yellow line is cross-section line) (modified from Google Earth®).

3. BASIC INFORMATION OF STUDY AREA

3.1 GEOLOGY OF STUDY AREA

The basement structure of the Chao Phraya basin is not clearly understood. In late Pliocene-Pleistocene, the Chao Phraya basement that consists of granite and metamorphic rocks complex was pulled downward into graben [6]. The basin was buried continues in Tertiary to Quaternary with the sequence of fluvial gravel and sand sediment interbedded with floodplain silt and clay grading to marine clay sediment [7-8].

3.2 GEOHYDRAULOGY OF STUDY AREA

The unconsolidated soil in lower Chao Phraya basin can be divided into top clay layer and 8 layers of major aquifers. The upper most aquifer is Bangkok aquifer (BK, 50 m zone). The groundwater in BK cannot be consumed because it has high salinity. The main extracted aquifers are the Phra Pradaeng aquifer (PD, 100 m zone), Nakorn Luang aquifer (NL, 150 m zone), and Nonthaburi aquifer (NB, 200 m zone) because of good quality and yield. The Sam Khok aquifer (SK, 300 m zone) and Phaya Thai aquifer (PT, 350m zone) are lower potential because further depth and lack of quality. The deeper aquifers are Thon Buri aquifer (TB, 450m zone) and Pak Nam aquifer (PN, 550 m zone) can provide fresh water but only few wells in these layers [9]. Fig. 2 shows cross-section of lower Chao Phraya basin from N to S [5] along the yellow line in Fig. 1

4. METHODOLOGY

4.1 CONCEPTUAL MODEL

The groundwater conceptual model can be used to describe physical and hydrological properties of the groundwater system. The conceptual model of Bangkok and vicinity areas is conceptualized based on the geology, hydrogeology, topography, and groundwater extraction. The multi-layer aquifers of small and thin lenses were simplified to larger layer aquifer with heterogeneous properties. The conceptual model contained 5 simplified layers which are top clay layer and 4 aquifers including BK, PD, NL, and NB aquifers. The conceptual model was subsequently converted to numerical model for simulation and calibration. The conception model cross-section is shown in Fig. 3.

4.2 NUMERICAL MODEL AND CARIBRATION

A computer code MODFLOW [10-11], a three-dimensional finite difference groundwater model of the US. Geological Survey, was used to simulate and predict the behavior of groundwater system. MODFLOW simulates steady-state groundwater flow in lower Chao Phraya basin aquifer system based on the following equation:

$$K_x \frac{\partial^2 h}{\partial x^2} + K_y \frac{\partial^2 h}{\partial y^2} + K_z \frac{\partial^2 h}{\partial z^2} \pm W = 0 \qquad (1)$$

where K_x, K_y, and K_z are hydraulic conductivities along the x, y, and z coordinate axes, h is piezometric head or

hydraulic head, and *W* is source (positive) and/or sink (negative) of groundwater such as recharge, evapotranspiration, pumping well, river, and boundary conditions. The regional flow model size is 80-km long, 70k-m wide, and 310 m below ground surface. The 3D finite difference model has 35 rows, 40 columns, and 5 layers. The grids of the flow model are defined as 2×2 km^2.

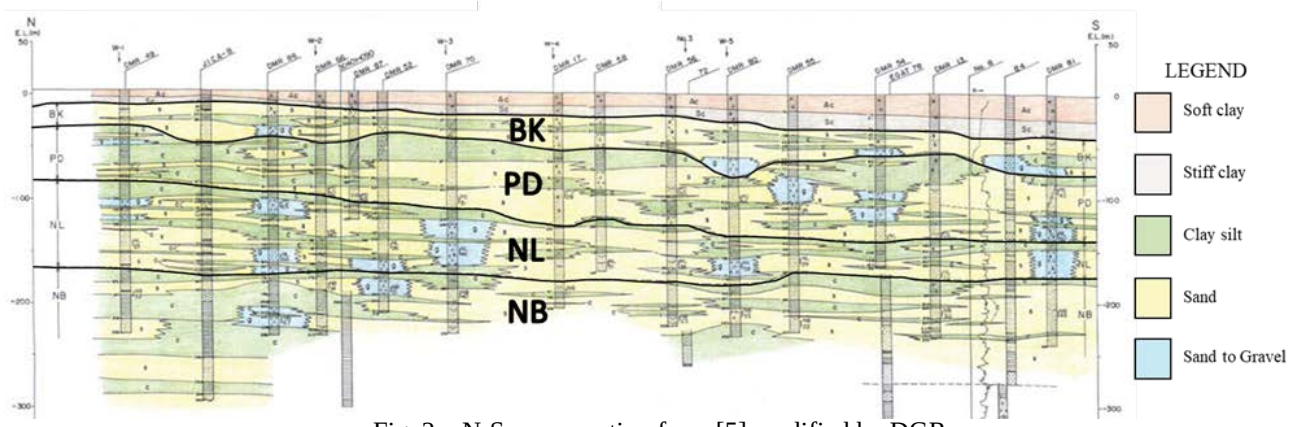

Fig. 2 N-S cross-section from [5] modified by DGR

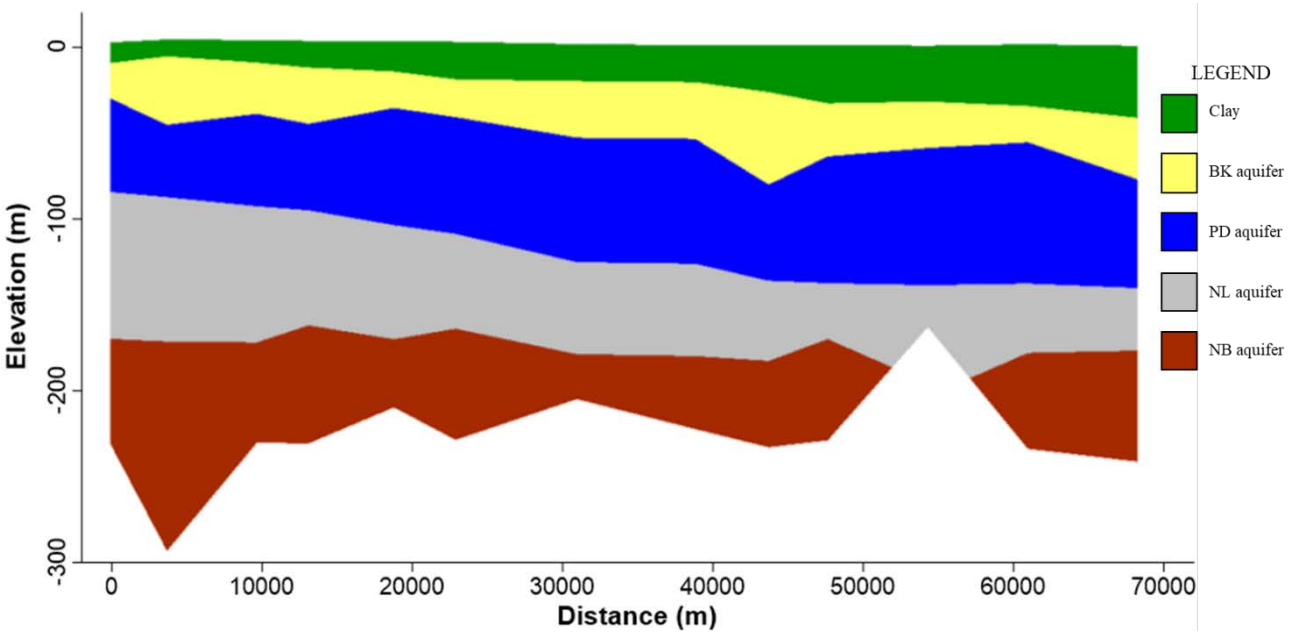

Fig. 3 N-S conceptual model cross-section.

The groundwater extraction rate and groundwater level are obtained from Department of Groundwater Resource (or DGR). The initial hydraulic conductivity is assumed about 1 m/day for aquifer and 0.001 m/day for aquitard although these parameters will eventually be calibrated to obtain heterogeneous hydraulic conductivity field.

The 3D numerical flow model was calibrated by using the automated parameter estimation that is PEST [12]. PEST systematically adjust the value of parameters until the output matches with hydraulic head (from 66 observation wells were used as calibrate target). The calibrated parameters consist of recharge, evapotranspiration, river-bed conductance, general head conductance, and hydraulic conductivity. The pilot point method is used with hydraulic conductivity instead zonation because heterogeneous properties of aquifers.

5. RESULT AND DISCUSSION

The steady-state flow model is executed and calibrated base on MODFLOW and PEST. The calibrated simulation head of is shown in Fig. 4. The computed head is not very different to each other. The mean squared error (MSE) is 4.43. The reported extraction rate must be multiplied by 1.5 in order to obtain a good model fit indicating that there must be an unreported amount of groundwater extraction in the study area. It was found that the simulated heads at some observation wells located near the shore line are high due to the assumption of constant head boundary where groundwater head actually fluctuates.

The calibrated head distribution of NL aquifer is shown in Fig. 5. The head distribution picture depicts the

cones of depression observed at Northeast (Pathun Thani) and Southwest (Nakhon Pathom and Samut Sakhon) zones which are highly industrialized and utilize a large amount of groundwater. The groundwater levels in this area are 30 m below mean sea level and may cause seawater intrusion.

6. CONCLUTIONS

Numerical groundwater flow model of the Lower Chao Phraya basin was conducted by using a finite-difference based MODFLOW program and the automatic calibration was achieved by using PEST algorithm. The regional model shows the groundwater extraction rate in study area is 1.5 times higher than report. The depression cones occur in Pathun Thani, Nakhon Pathom and Samut Sakhon.

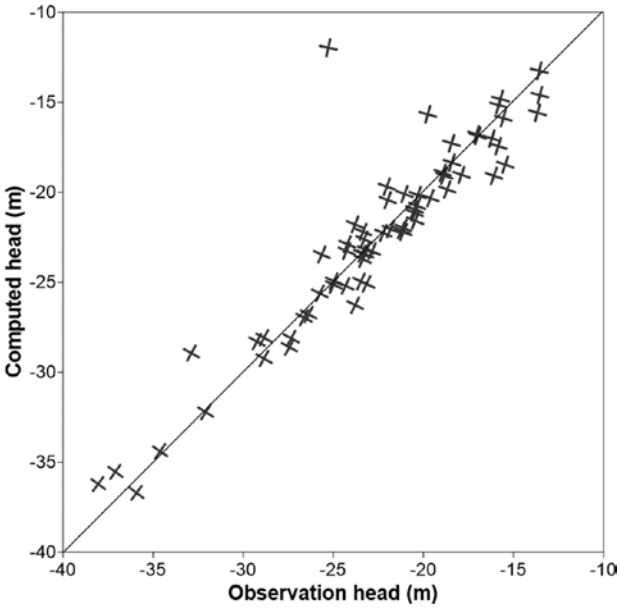

Fig. 4 computed head vs observation head

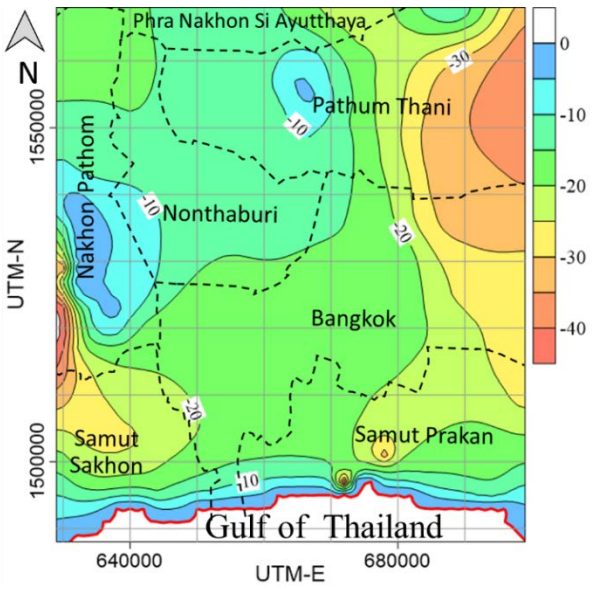

Fig. 5 Computed hydraulic head (5m contour interval)

7. ACKNOWLAGEMENTS

I wish to acknowledge the help provided by Department of Groundwater Resource for the support hydrogeological and piezometric head data.

8. REFERENCES

[1] National Statistics Office (NSO) (2010). Table 1. Population by sex, household by type of household, changwat and area, Statistic tables. Retrieved January 8, 2018, from http://www.nso.go.th.
[2] Phien-wej N., Giao, P.H., and Nutalaya, P., 2006. Land subsidence in Bangkok, Thailand. Engineering Geology, 82, 187-201.
[3] Nutalaya, P., Yong, R.N., Chumnankit, T., Buapeng, S., 1996, Land Subsidence in Bangkok during 1978–1988. Sea-Level Rise and Coastal Subsidence, (pp. 105–130). J.D. Haq, B.U. (Eds.), In: Milliman.
[4] Fornes, J., Pirarai, K., 2014, Groundwater in Thailand. Journal of Environmental Science and Engineering, B 3, 304-315.
[5] Japan International Cooperation Agency (JICA), 1995. The study on management of Groundwater and land subsidence in Bangkok metropolitan area and vicinity, Report submitted to Department of Mineral Resources and Public Works Department, Kingdom of Thailand, p.1-1 to p.11-5.
[6] Nutalaya, P., and Rau, J.L., 1984. Structural framework of the Chao Phraya basin, Thailand. Proceedings of Symposium on Cenozoic Basin Thailand: Geology and resources, Bangkok, Thailand, p. 106 to p.129.
[7] Asian Institute of Technology (AIT), 1981. Investigation of land subsidence caused by deep well pumping in Bangkok area, Research Report, vol. 91. Asian Institute of Technology, Bangkok, Thailand.
[8] Ramnarong, V., 1983. Groundwater Depletion and Land Subsidence in Bangkok. Proceedings of Conference on Geology and Mineral Resources of Thailand. Department of Mineral Resource, Bangkok, Thailand.
[9] Nguyen, A.D., 1999. Updating and Analysis of Bangkok Land Subsidence Caused by Deep Well Pumping with Emphasis on Shallow Soil Settlement. A Master of Engineering degree Thesis No. GE-28-1, Asian Institute of Technology, Bangkok, Thailand.
[10] Harbaugh, A.W., Banta, E.R., Hill, M.C., and McDonald, M.G., 2000, MODFLOW-2000, the U.S. Geological Survey modular ground-water model -- User guide to modularization concepts and the Ground-Water Flow Process: U.S. Geological Survey Open-File Report 00-92, 121 p.
[11] Harbaugh, A.W., 2005, MODFLOW-2005, the U.S. Geological Survey modular ground-water model -- the Ground-Water Flow Process: U.S. Geological Survey Techniques and Methods 6-A16.
[12] Doherty J.,1994, PEST-Model-Independent Parameter Estimation. Watermark Computing, Corinda.

STUDY OF VERTICAL, LATERAL AND LONGITUDINAL FORCES FOR A 4-WHEEL VEHICLE UNDER ALL-TERRAIN CONDITIONS

Varun Gupta, Vipul Sharma, and Mukul Tomar
Mechanical Engineering, Delhi Technological University, New Delhi, India

ABSTRACT: This article explains the kinematics and dynamics of a 4-wheel vehicle due to different road conditions more emphasis on "off-road conditions". The scope of the article is to only analyze the motion of the vehicle under different road profiles. Computer modeling of the Vehicle combined with different types of road profiles is very crucial aspect for developing simulation model for a Vehicle-Road system. In this Article, Simulation and Modeling software 'MATLAB & Simulink' has been used to model a Quarter-car model which shows the kinematics of corner mass of a vehicle under the effect of different road profiles.

1. INTRODUCTION

'Vehicle Dynamics' or the study of the motion and forces experienced by a vehicle as it traverses over a road profile is very crucial aspect of vehicle design and performance especially for Off-road vehicles. It is very important for every vehicle to maintain a contact with the road as the forces from the interaction of road and tire are solely responsible for keeping the vehicle on the ground [1].
However, this task of maintaining a continuous contact with the ground becomes quite difficult. For designing and manufacturing an off-road vehicle, it is essential to analyze the motion of the un-sprung as well as sprung masses under the effects of road irregularities (Bumps, pits, falls. turns, etc.). Lateral, Vertical and Longitudinal motions of the vehicle must be studied with the help of mathematical models like Quarter-car model, Bounce-pitch model [2]. Software like MATLAB can be used for simulating the mathematical model developed under the effect of different road-conditions [3].

1.1 VEHICLE AXIS SYSTEM

The conventional axis system is placed at the center of mass of the vehicle with the x axis pointing towards the front of the vehicle, the y axis pointing towards the right side of the vehicle, and the z axis pointing towards the bottom of the vehicle. The x axis is known as the longitudinal axis, the y axis is known as the lateral axis, and the z axis is known as the vertical axis. The rotation about the x axis is known as roll, the rotation about the y axis is known as pitch and the rotation about the z axis is known as yaw (Figure 1: Vehicle axis system).

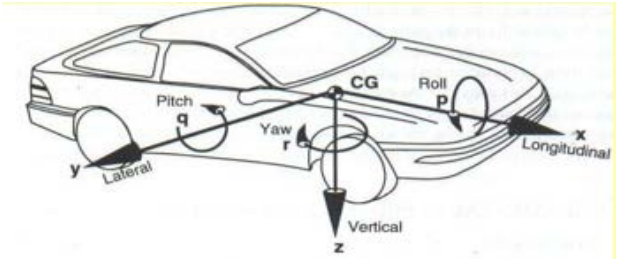

Fig 1: Vehicle Axis System

1.2 ROAD LOADS

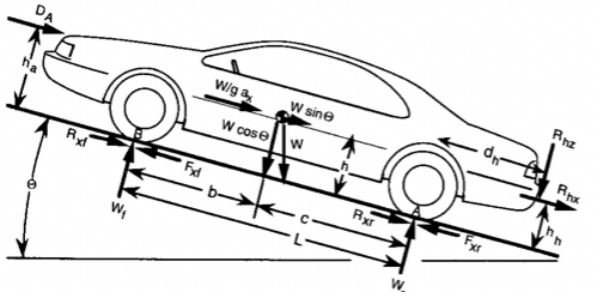

Fig 2: Loads acting on vehicle

Above figure completely shows all the types that may act on any vehicle. Given below is a description of these forces.

- W is the weight of the vehicle acting at its CG with a magnitude equal to its mass times the acceleration of gravity. On a grade it may have two components, a cosine component which is perpendicular to the road surface and a sine component parallel to the road.
- If the vehicle is accelerating along the road, it is convenient to represent the effect by an equivalent force known as a "D'Alembert force" denoted by W/g.ax acting at the center of gravity opposite to the direction of acceleration.
- The tires will experience a force normal to the road, denoted by Wf and Wr representing the dynamic weight carried on the front and rear wheels.
- Tractive forces Fxf and Fxr or rolling resistance forces, Rxf and Rxr, may act in the ground plane in the tire contact patch.
- Da is the aerodynamic force acting on the body of the vehicle.
- Rhx and Rhz are the horizontal and vertical forces acting at the hitch point when the vehicle is towing a trailer.

2. ANALYSIS-VEHICLE RIDE MODELLING

2.1 VERTICAL DYNAMICS: "QUARTER-CAR MODEL":

Mechanical vibrations in a vehicle represent a very complex field, and usually require multiple degrees of freedom to accurately predict the vertical performance of the vehicle. However, there exist two simplified models which when combined give an accurate approximation as to the ride quality of the vehicle. These include the quarter car model (corner model) (used to predict the motion of a single suspension unit) and the bounce/pitch model (used to predict the motions of the sprung mass of the vehicle). These models combined produce the half car model (four degrees of freedom model). The vertical performance of the vehicle is directly linked to the sprung mass, the unsprang mass, the pitch inertia, the suspension stiffness, the tire stiffness, the damping in the tires, the damping in the suspension units, and the excitation frequency. Before the half car model is introduced, the quarter car model and the bounce/pitch models will be introduced [4].
The quarter car model is a model that models the motion of a single suspension system (it models one corner of the car) (Figure 3: The quarter car model). The sprung mass in this model represents some portion of the total sprung mass of the system. The tire is excited because of the shape of the path it is following (the shape is not flat, especially for an off-road track). Applying Newton's 2nd Law of motion the equations of motion that govern the quarter car model are as follows (Equation 1:
The equations of the quarter car model).

$$Mz_1dd + C\,(z_1d - z_2d) + k\,(z_1 - z_2) = 0$$

$$M_uz_2dd + C_s(z_2d - z_1d) + k_s\,(z_2 - z_1) + C_tz_2 + k_tz_2 = C_tz_0 + k_tz_0$$

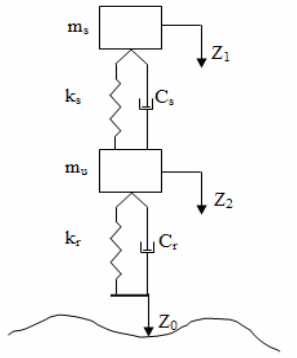

Fig 3: The Quarter Car Model

This is a two degree of freedom system, thus there will be two natural frequencies (the unsprung and sprung mass will each have a resonant frequency). The wheel hop frequency is the frequency associated with the unsprung mass it is usually around 10Hz. The body motion frequency is the frequency associated with the sprung mass and it is usually around 1 to 1.25 Hz. Note, the damping ratios in most suspension systems is relatively low, therefore the majority of the time the undamped natural frequency will be really close to the damped natural frequency thus the damped natural frequency is usually calculated by neglecting any damping in the system. The following equation can be used to calculate the natural frequencies of the system. Note the natural frequencies are calculated by neglecting damping in the system and neglecting any excitation (Equation 2: The natural frequencies of the unsprung and sprung mass).

$$f1 = \frac{1}{2pi}\sqrt{\frac{ks*kt}{\frac{ks+kt}{m1}}}$$

$$f2 = \frac{1}{2pi}\sqrt{\frac{ks+kt}{m2}}$$

2.2 LONGITUDINAL DYNAMICS ("BOUNCE-PITCH MODEL"):

The bounce/pitch suspension model models the vehicle motions separately from the wheel motions. The equations of motion that govern this system can be obtained by applying Newton's second law of motion in both pitch and bounce to the system (note damping will be first neglected so that the natural frequency can be obtained)
Equation 3: Bounce and pitch equations of motion (neglecting damping)

$$M_szdd + K_f\ (z - a*\theta) + K_r(z + b*\theta) = 0$$

$$M_sr_y^2\,\theta dd - K_f*a*(z - a*\theta) + Kr*b*(z + b*\theta) = 0$$

$$I = m_s*r_y^2$$

The above equations of motion can be solved to obtain the natural frequencies and amplitude ratios, as well as the amplitudes for a given frequency. This can be done by reducing the equations from second order to first order (Equation 9: Bounce and pitch damped natural frequency).

2.3 COMBINED MODEL "HALF-CAR MODEL":

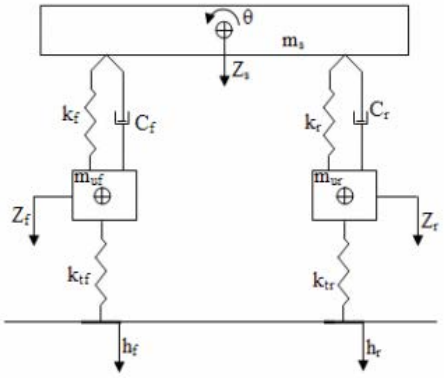

Fig 4: The Half Car Model

The bounce/pitch model and the quarter car model are two of the most powerful models to predict the vertical motion of the vehicle. These two models can be combined to create the half car model. This model couples the motions of the front and rear suspension through the motion of the sprung mass (both bounce and pitch). This model allows the wheel hop frequencies to be obtained for both the front and rear suspensions at the

same time. As well as the pitch and body motion frequencies can be obtained. The half car model predicts the motions of the both the front and both the rear suspension units at once. There are certain assumptions used in this model, and these include that the tires on either side of the vehicle have the same effect on the dynamics, and the width of the vehicle is assumed to be constant. Also, it is assumed that the springs are linear, and that the damping can be modeled as viscous dampers [6].

2.4 LATERAL LOAD TRANSFER WHILE CORNERING:

As a vehicle goes along a corner at a considerable speed, a force known as "Centripetal force" acts on the vehicle through its tire - road interaction keeping it on the curvature it traversing. Now, if we consider the vehicle moving along a turn in static equilibrium a pseudo force "Centrifugal force" acting in the opposite direction at the center of gravity. It is due to these two forces that a couple is produced which tends to rotate the sprung mass about an axis called the "Roll axis" and the phenomena is called "Body Roll". While cornering, it leads to a change in the normal loads at the left and right wheels.

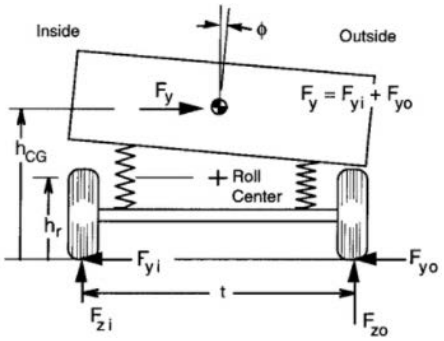

Fig 5: Force analysis

By writing Newton's Second law for moments on the axle, we can determine the relationship between Wheel loads and Lateral force and Roll angle. In addition to the vertical forces imposed on the tyros there is a net lateral force, F_y (the sum of the lateral forces on the inside and outside wheels), acting to the right on the axle at its roll center. The body roll angle acting through the springs imposes a torque on the axle proportional to the roll stiffness, Kθ times the roll angle θ. This results in an equation for the load difference from side to side of the form:

$F_{zo} - F_{zi} = 2*F_y*h_r/t + 2*K\theta*\theta/t = 2*Fz$

Where:
F_{zo} = Load on the outside wheel in a turn
F_{zi} = Load on the inside wheel in a turn
F_y = Lateral Force
h_f = Roll center height
t = Track width
Kθ = Roll stiffness of the Suspension

3. ANALYSIS MATHEMATICAL MODELING:

3.1 "QUARTER CAR MODEL":

Normally car is divided into three type of categories: full car model, half-car-model and quarter-car model [5,7,8]. Quarter-car models are extensively used in automotive engineering due to their simplicity and provide the qualitatively correct information, at least in the initial design stages of vehicle dynamics. The quarter car model of 2 DOF consists of wheel and its attachments the tire, the suspension elements, quarter portion of the chassis and rigidly connected parts.

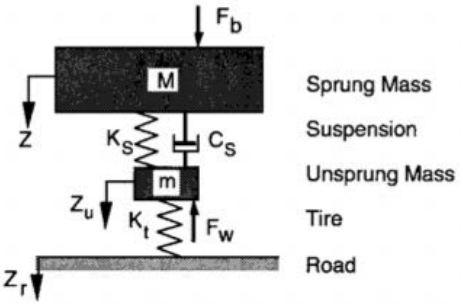

Fig 6: The Quarter Car Model

$$M\ddot{Z} + C_S\dot{Z} + K_S Z = C_S\dot{Z}_u + K_S Z_u + F_b$$

$$m\ddot{Z}_u + C_S\dot{Z}_u + (K_S + K_t)Z_u = C_S\dot{Z} + K_S Z + K_t Z_r + F_w$$

where:

Z = Sprung mass displacement
Z_u = Unsprung mass displacement
Z_r = Road displacement
F_b = Force on the sprung mass
F_w = Force on the unsprung mass

3.2 MODELING ROAD BUMP:

There are different types of road excitation i.e. circular, parabolic, trapezoidal. In this paper sinusoidal road ex-citations are used. For example, The sinusoidal road excitation derived by equation (3) as shown in Fig 7 can be used as input to the model in Simulink and the ride comfort, road holding and displacement of the system are computed. Bump width L with different vehicle velocity v. For an absolute time, frame t represents the simulation time when wheel is just approaching a bump with a distance d.

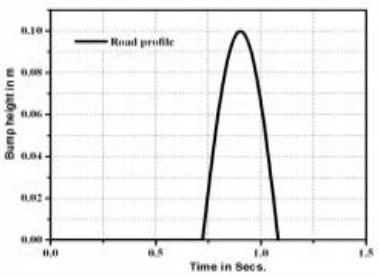

Fig 7: Road profile with bump height 0.1m

Similarly, any type of road profile can be mathematically modeling with the use of functions such as STEP function, Sine or Cos Function, Random function, etc. which can easily model the irregularities on the road surface over time.

3.3 SIMULINK MODEL FOR VEHICLE CORNER MASS:

Disturbance from the road: As defined in section 2. road can be modeled with use of sine and step functions over time. Hence, for modeling different road conditions we have used different functions as;

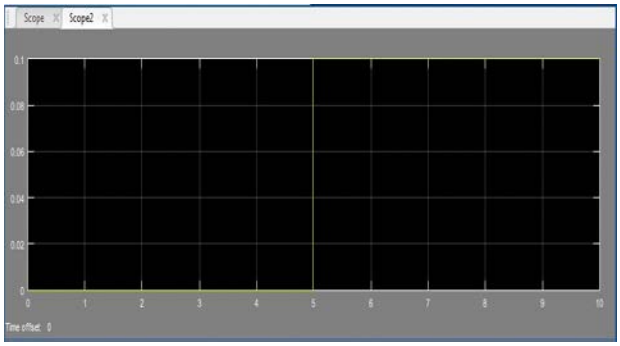

Fig 8: Zero Bumps Model

2 Sinusoidal Bumps over Road:

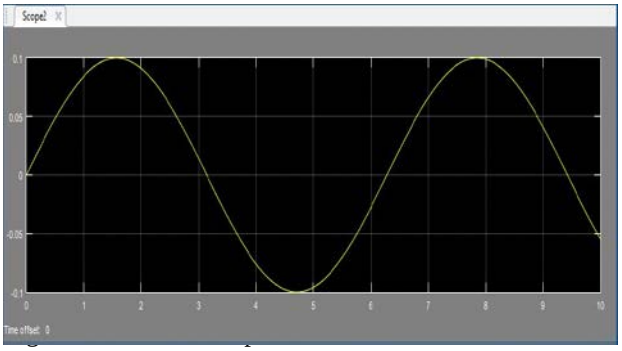

Following is the Simulink model based on the "Quarter Car Model" as defined in section 3.1. The model seems to be quite useful for studying the vertical dynamics of corner mass of a vehicle under the action of forces as well as road discontinuities.

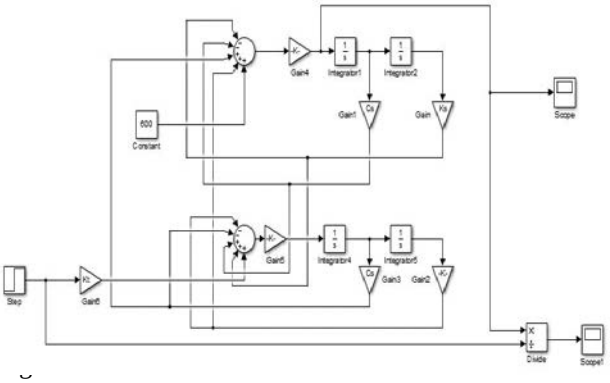

Results:

Above model is compiled and run for 10 s time. The displacement of the sprung mass is taken as output with the displacement of the point of contact of tire and road as input. The suspension variables which are also input in the model are;

Corner sprung mass = 60 kg
Corner Unsprung mass = 10 kg
Spring stiffness = 10,000 N/m
Damping Coefficient = 100 N/m/sec
Tire stiffness = 400,000 N/m

The scope of the Simulink model when the input is the "Platform" shows the result as;

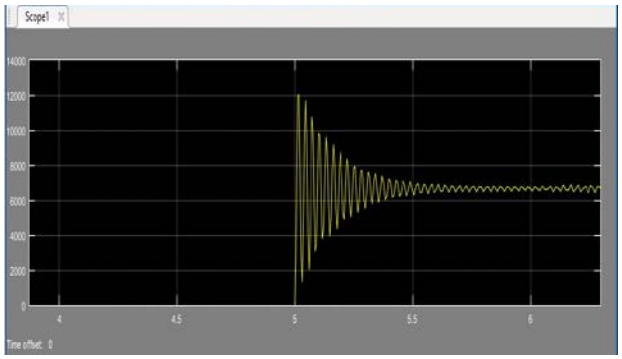

Fig 11: Scope of Simulink Model

4. DISCUSSION AND CONCLUSION

As seen from the output curve, the motion of the sprung mass of the vehicle can be studied as the tire hits a ' Platform 'like bump at t = 5s. The graph accurately shows the phenomena of damped oscillations experienced by the sprung mass which can be validated theoretically as well as experimentally.

The conclusion which can be drawn from this article is that all the forces acting on the vehicle whether longitudinal, lateral or vertical can be evaluated easily by the use mathematical models such as "Quarter Car Model", "Bounce-pitch Model", "Half car Model" , etc. Forces acting on the vehicle masses due to their interaction with the road can also be evaluated provided that the actual scenario that the vehicle can be modeled.

5. REFERENCES

(Book)
[1] Milliken, W.F. "Race Car Vehicle Dynamics", SAE International. Chapters- 3 and 5.
(Book)
[2] Gillespie, T.D, "Fundamentals of Vehicle Dynamics", SAE International, Chapters 2,5 and 6.

(Software)
[3] www.google.com/ Mathworks / MATLAB & Simulink / MATLAB & Simulink Racing Lounge.

(Paper)
[4] Phalke, T. P., & Mitra, A. C. (2017). Analysis of Ride comfort and Road holding of Quarter car model by SIMULINK. Materials Today: Proceedings, 4(2), 2425–2430. doi:10.1016/j.matpr.2017.02.093

(Technical Report)
[5] "WHO - Global Status Report on Road Safety - Time for Action", World Health Organization, Geneva, 2009.

(Book)
[6] M. Mitschke and H. Wallentowitz. Dynamik der Kraftfahrzeuge. Springer, Berlin, 2004.

(Published Paper)
[7] O. Gu ndogdu, International journal of Industrial Ergonomics 37, (2007) 327-332

(Published Paper)
[8] Anirban C Mitra, Gourav J Desai, Saaish R Patwardhan, Parag H Shirke, Waseem MH Kurne, Nilotpal Benerjee, Discovery, 2015, 29(112), 127-137.

(Published Paper)
[9] Anirban C. Mitra, Tanushri Sonia, Kiranchand G. R., ShaizamKhana, Nilotpal Banerjee, 4th International Conference on Materials Processing and Characterization, 2015

(Published Paper)
[10] Galal Ali Hassaan, International Journal of Computer Techniques -Volume 1 Issue 2, 2014

(Published Paper)
[11] Mr. Sushant S. Patole, Prof. Dr. S. H. Sawant, International Journal of Advance Research In Science And Engineering, JARSE, Vol. No.4, Special Issue (02), February 2015.

(Published Paper)
[12] Anirban C Mitra1, NilotpalBenerjee, National Institute of Technology Durgapur, India, Vol. 2 No. 1 January 2014.

(Published Paper)
[13] Galal Ali Hassaans, International Journal of Scientific Research Engineering & Technology (IJSRET), ISSN 2278 – 0882 Vol.4, Issue 4, April 2015.

(Book)
[14] International Organization for Standardization ISO 2631-1. Mechanical Vibration and Shock – Evaluation of Human Exposure to Whole – Body Vibration. Part 1: General Requirements. Geneva, 1997.

A STUDY ON THE SHAFT SURFACE DAMAGE OF THE HATCH SHAFT USED BY TANK PILOTS

Dae Un Kim[1], Kyung Seob Kuem[1], In Taek Oh[1], Sang Deuk Kim[1], Byeong Jae Moon[1]
[1]Consolidated Maintenance Depot Republic of Korea Army, Changwon P.O.BOX92 57 Sangnam-dong Seongsan-gu Changwon-si Gyeongsangnam-do Republic of korea.
Email: akdong48@nate.com

ABSTRACT: This study in about the damage of the shaft surface of the hatch used when the pilot enters and exits the cockpit. We will investigate the cause of the surface damage of the hatch shaft and how to improve it. Due to frequent opening and closing of the hatch shaft, frictional force is generated by the contact of the two sleeve bearings installed inside. This damages the surface of the shaft and causes uneven wear of the shaft during long-term use. As a result of the study, structural problems were observed due to the concentrated load of the ball bearing on the contact surface of the shaft. A surface contact bearing is proposed as a countermeasure to disperse the concentrated load of the bearing. As a result, surface damage to the shaft is expected to be reduced.

Keywords: Shaft surface damage, Damage protection, Surface treatment, Contact bearing, Finite element method, Failure analysis.

1. INTRODUCTION

The tank`s pilot hatch serves as the gate of the pilot. The shaft of the opening and closing device is an important part which enables the opening and closing of the pilot hatch and the vertical movement and rotation of the hatch smoothly. The shaft is installed in the opening and closing device and consists of two sleeve bearings. Grease is used to reduce the frictional force of the bearings. The surface of the shaft is treated with S.F.L(Solid Film Lub) to prevent smearing and abrasion. However, due to the long use of the hatch, the coating of the shaft due to the bearing ball is damaged. In addition, due to the generation of rust due to the inflow of water during the field operation of the tank, the uneven wear of the shaft occurs, and the shaft is discarded and replaced with a new one.

Hardness of bearing is lower than HRC 60 because hardness of shaft of shaft is HRC 54~58. Therefore, during operation for a long period of time, the punching due to the static load of the bearing occurs, and the discarding rate of the shaft becomes higher. These problems shorten the exchange period of the opening and closing device axis and have the possibility of increasing the risk of accident of the pilot in the operation of the tank. Therefore, the purpose of this study is to find the solutions to the cause of damage of the shaft of the opening and closing device.

First, the function and properties of the surface treatment of the shaft were examined and it was confirmed whether the surface treatment affected the shaft damage. Then, the structural analysis was carried out to confirm the damage caused by the friction and static load of the ball bearing. Before the structural analysis, the stress distribution due to the bearing shape was compared and analyzed. In order to confirm the boundary condition, the surface analysis and the outer diameter of the shaft damaged part were measured. The purpose of this study is to identify the causes of shaft damage by confirming the surface treatment of the shaft, and to analyze the cause of direct damage to the shaft surface and to propose a solution.

First, it was confirmed that the surface of the shaft of the opening and closing device was the cause of the damage caused by the surface treatment. In addition, the cause anslysis of the damage caused by the friction and static load of the ball bearing was carried out by structural analysis and the difference of the stress distribution due to the bearing shape was compared and analyzed. In order to present the boundary conditions for F.E.A(Finite Element Analysis), the surface analysis and the outer diameter of the shaft damaged part were measured and the solution of the stress distribution and deformation of the shaft surface was suggested.

2. SHAFT OF OPENING AND CLOSING DEVICE

The shape of the opening and closing device of the pilot hatch is shown in Fig. 1 Vertical and rotary operation is performed during opening and closing operation to directly engage in opening and closing the door. In addition, when the trainer crosses the river by blocking the entrance of the tank, the inside of the cockpit is closed to prevent the inflow of water.

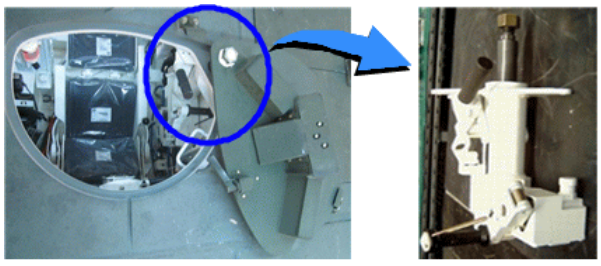

Fig. 1 Opening and closing device & Shaft

The material of the shaft is heat treated steel with surface hardness HRC 54~58 and it is treated with S.F.L. The basic properties are shown in Table 1.

Table 1. Material properties of shaft

Standard	ASTM A332
Density	7.85g/cc
Modulus of elasticity	205Gpa
Hardness, Rockwell C	54 ~ 58

3. S.F. L TREATING CHARACTERISTICS OF A SHAFT

S.F.L treating research has begun to address the problem of high temperature lubrication in the gas turbines of US navy aircraft in the 1950s. Since then, S.F.L treating has been actively researched and developed as applied to the space development plan since the 1960s. And it was put into practical use in advanced countries around this time. A representative example of this is as follows.

Unexpected damage occurred to 155mm flat springs of behind the battery at the time of the Vietnam War, and interest in application of the coating treatment was emerged. The reason for this was the rapid progress of corrosion and over abrasion in high-humidity tropical climates. The problem of corrosion and wear was a serious concern in the Navy. The shells on the shore are required to have new coating techniques due to the abrasion and corrosion caused by the salt contained in the air.

In order to solve all of these problems, we studied and analyzed the most effective surface treatment during water resistant surface treatment through corrosion test based on protective coating considering economy and compatibility. As a result, S.F.L treating has been proven to be the most effective coating treatment and has been used up to now.

To understand S.F.L treating, you first need to know the process. In order for this coating treatment to exhibit the best properties, the coating treatment process should be carried out after an appropriate pretreatment process. A suitable pretreatment film differs depending on the material and is a process for chemically and electrically forming a stable porous film on the surface of the material. S.F.L improves adhesion and adhesion life extension by increasing adhesion area. The process of S.F.L treating is shown in Table 2. As can be seen from the process of Table 2, the corrosion resistance is improved by the S.F.L treating after the phosphate coating treatment.

Table 2. Process of S.F.L treating

Basic Process (Steel Products)	Solvent Cleeaning → Masking → Sand air blow → P.C(Phosphate Coating) → Rinsing → Drying → S.F.L treating → Drying → Heat treatment

The characteristics of P.C and S.F.L treating are shown in Table 3.

Table 3. Comparative analysis of characteristics

	P.C (Phosphate Coating)	S.F.L (Solid Film Lub)
Wear Resisting Quality	The first friction is peeled off	Abrasion resistance, Smooth friction
Use & Storage	Wearing during use and storage, repairing rust-oil remeval parts and application of antirust oil can be used for a long time.	It can be used for a longer time than P.C because it has its own waterproof and anti-rust effect.
Moisture content of surface	If water remains on the surface, water and rust preventive oil are separated and partial corrosion occurs.	Even if water remains on the surface, corrosion and waterproof effect are pervented and corrosion does not occur well.

4. INSPECTION OF SHAFT SURFACE DAMAGE

In order to precisely measure the surface state of the damaged shaft and the thickness of the surface film, a coating thickness test method(Eddy current test method) of KS D 0246: 2001 standard was applide; The reference surface is the portion without the coating.

As shown in Table 4, the thickness of the coating in the operating range of the bearing was measured to be less than the reference value, and it was confirmed from the precision measurement that the friction damage occurred.

Table 4. Measure the surface thickness of the damaged shaft

	Surface thickness measurement result		
Measuring section	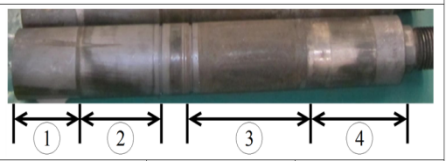		
Standard thickness (6 ~ 12㎛)	①,② 10.3 ~ 14.7㎛	③ 0 ㎛	④ 3.23 ~ 5.67㎛
Precision measurement of surface			

As a result of confirming the coating process of the shaft, it was confirmed that there was no problem in the S.F.L treating process. However, due to the long field operation, we could confirm the damage of the coating as shown in Fig. 2, and we could guess that the sleeve bearing was damaged due to ball damage. The cause of the surface damage of the shaft was supposed to be due to the ball stop load of the sleeve bearing.

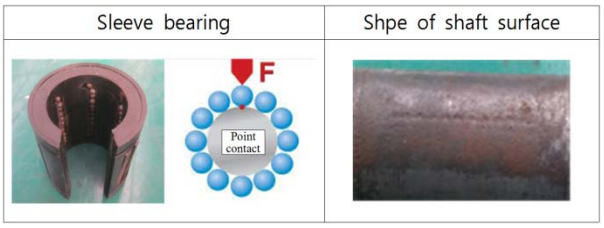

Fig. 2. Shape of shaft surface

5. SHAFT MODELING AND MECHANICAL PROPERTIES

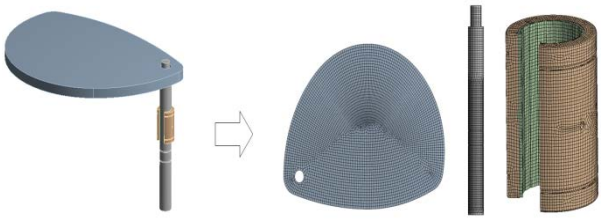

Fig. 3 3D Modeling of the opening and closing device.

Fig. 3 is a simplified representation of the actuator shaft of the pilot hatch, which is modeled in 3D with the shaft and bearing assembled. The position of the bearing is when the hatch is opened and the surface damage of the actual axis is serious. The material of the shaft is the SNCM 220 specified in the National Defense Code. This is nickel chromium molybdenum steel. The mechanical properties are shown in Table 5.

Table 5. The mechanical properties of shaft

Tensile Strength(Mpa)	1,226
Yield Strength(Mpa)	957
Quenching Temperature(°C)	843
Tempering(°C)	149
Carburizing(°C)	927

6. 3D MODELING FOR STRUCTURAL ANALYSIS

As shown in Fig. 4, the hexagonal and tetrahedral elements were used for grid generation to improve the convergence of the analysis. To increase the accuracy of the contact between the bearing and the shaft, the element was created with a size of 2mm.

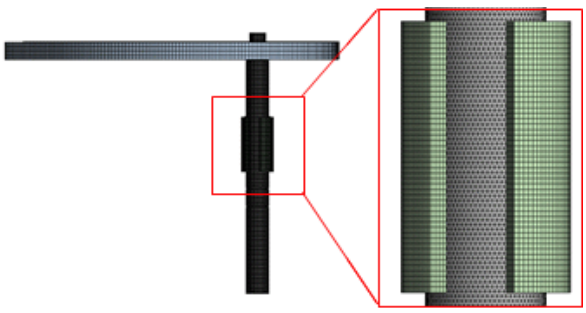

Fig. 4 3D modeling for structural analysis

7. STRUCTURAL ANALYSIS BOUNDARY CONDITION

The weight of the hatch is about 120kg, and an external force due to eccentricity exists. Because of this external force, we applied gravity and measured two axes diameters as shown in the Fig. 5 to simulate the shape of the surface impression of the shaft. For the minimum mean value of 0.02mm, forced displacement using a cylindrical coordinate system is applied and the model is simplified to shorten the analysis time.

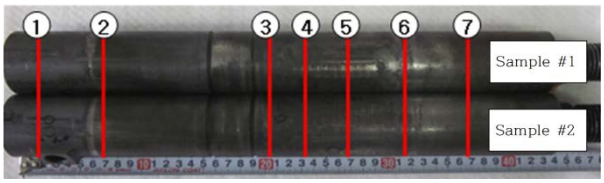

Fig. 5 Outer diameter measurement position

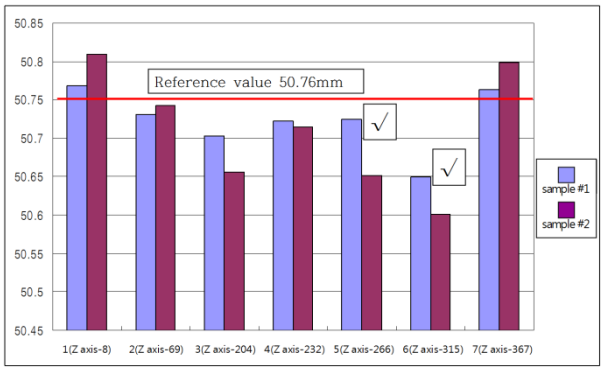

Fig. 6 Outer diameter measurement result value

A total of 7 external diameters were measured using CNC COORDIN ATE MEASURING. As a result, the measured value as shown in Fig. 6 was shown, and it was confirmed that the outer diameter was below the reference value in the measurement parts 5 and 6. It is confirmed that this is the contact area of the sleeve bearing due to the operation of the opening and closing device and that it is damaged by the concentrated load of the bearing ball. In the measurement part 3, damage by the ring and packing was confirmed.

However, this study does not cover ring and packing damage as a study of shaft surface damage by the opening and closing device operation. Fig. 7 shows the boundary conditions.

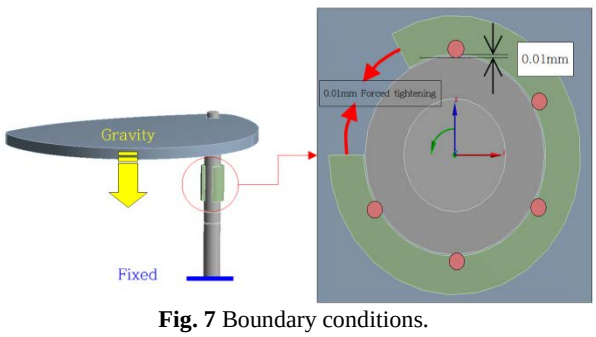

Fig. 7 Boundary conditions.

8. STRUCTURAL ANALYSIS RESULT

Fig. 8 shows the contact pressure value through the stress analysis of the sleeve bearing. The contact pressure after applying the forced displacement of the sleeve bearing was calculated as 1764 MPa at maximum. As a result of comparing the analysis result with the damaged axis where the actual dent occurred, it is confirmed that the damage type is well simulated as shown in Fig. 9. The average stress was taken into account for the alternating loads and Goodman Equation was applied for the life calculation.

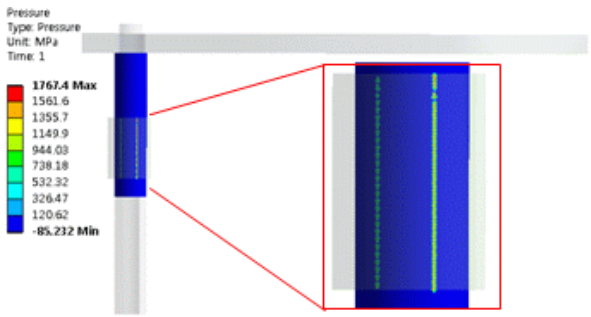

Fig. 8. Sleeve bearing contact pressure result

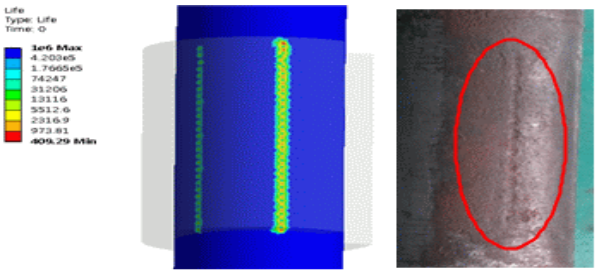

Fig. 9 Damage type simulation

$$\frac{\sigma_a}{S_e} + \frac{\sigma_m}{S_u} = 1$$

S_e is the fatigue limit, σ_m is the mean stress, and S_u is the tensile strength. The fatigue life of the shaft was predicted by the forced displacement analysis using the cylindrical coordinate system. It is estimated to be about 41000 ~ 42000 Cycle, which is a good reference for life prediction when considering the operating time of 10 years.

9. STRESS AND LIFE OF SLEEVE BEARING

Fig. 10 shows the curve for fatigue evaluation conditions, the alternating load was applied to the load. Actual experimental data tend to show between Goodman curve and Gerber curve, where Goodman is applied in fatigue life evaluation.

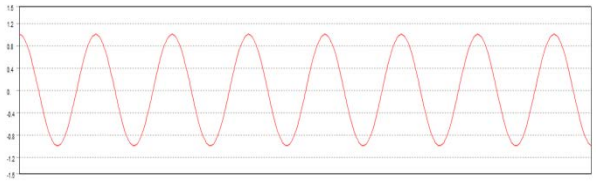

(a) Constant amplitude load fully reversed

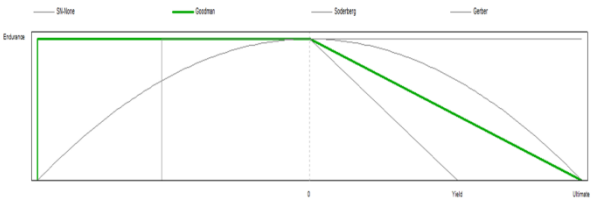

(b) Mean stress correction theory

Fig. 10 Fatigue evaluation condition

10. STUDY FOR PREVENT CONCENTRACTED LOAD

In order to reduce the stress, surface contact bearings were applied to the structural analysis under the same conditions. Fig. 11 shows the part where the surface contact bearing comes into contact with the shaft.

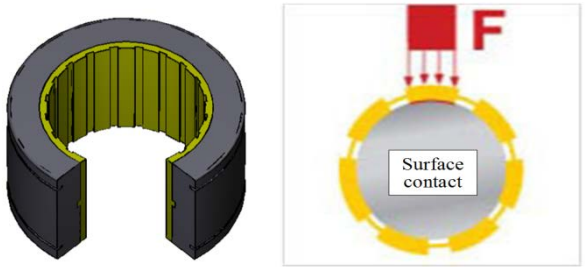

Fig. 11 Surface contact bearings

Fig. 12 shows the structural analysis results of the surface contact bearings, confirming that the stress is reduced. As a result of the structural analysis under the same condition as the sleeve bearing, it was found that the contact pressure of the region of interest was about 4MPa. It is confirmed that the stress reduction effect is about 400% higher than that of the conventional sleeve bearing. Through this structural analysis, the fatigue life and stress below the fatigue limit were predictive of the infinite life.

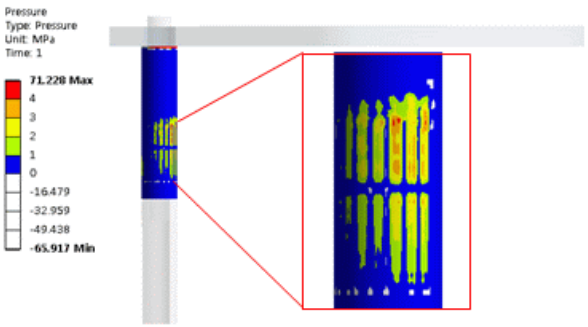

Fig. 12 Structural analysis results of surface contant bearings

11. CONCLUSION

We studied the causes of damages on the shafts of the opening and closing devices used by the trolleys and how to improve them. As a result of the study, it was found that there are many differences in the contact pressure due to the structural difference between the sleeve bearing and the surface contact bearings.

Surface damage of the hatch shaft is expected to be reduced by using surface contact bearings to prevent damage due to concentrated loads. In addition, chrome plating or spraying is applied to reuse of damaged shaft to improve the regeneration rate of surface treatment and to improve the problem of shaft damage in the case of water. This study will continue to carry out further research to prevent shaft damage.

12. REFERENCE

[[1] The report of surface treatment application for BIHO Gun ass'y in field condition, 2008.
[2] KS D 0246: "Method of Plating Thickness test(Eddy Current Type), 2001.
[3] Song,, S. H., Kim, S. D., Kim,, K. W., Stress Analysis at the Contact Boundary between the Work Roll and the Back-up Roll for a SmartCrown Roll Profile Shape, Transactions of Material Processing, Vol.24, No.3,2015.
[4] Bae,, M. W., Park, B. H., Jung,, H., A Study on Durability Characteristics for Plungers of Conventional Ceramic and Surface Modification by Power Coating Using High Velocity Oxygen Fuel Thermal Spary, Transactions of KSASE, Vol.24, No.3, pp.285-293, 2016.
[5] ANSYS, Theory Reference for ANSYS

UNCERTAINTY ESTIMATION OF PH MEASUREMENT BY ISFET SENSOR

A Vijittumrongsuk1), N Jinuntuya1)And S Leasen2*
1) Department of Physics, Faculty of Science, Kasetsart University, Bangkok, Thailand
*2)*Science Programme, Faculty of Science and Technology, Rajamangala University of Technology Suvarnabhumi, Nonthaburi, Thailand*
suthisa.l@rmutsb.ac.th

ABSTRACT: The uncertainty of pH measurement by Ion Sensitive Field-Effect Transistor (ISFET) is determined. Due to its small size and simple integration in measuring instruments, the sensor is suitable for pH measurement on the field. However, the uncontrolled environment can interfere the accuracy of the measurement. In this work, the uncertainty analysis of pH measurement that involve with environment such as light, temperature and standard uncertainty sources on the sensor is considered. Preliminary results reveal that the average responses of the sensor (Volt/pH unit) in dark environment slightly increase with temperature. The temperature coefficient determining can be used to correct the temperature-dependent of the measured pH. In lighting environment, the sensing responses are fluctuated and the temperature coefficient cannot be calculated. These results suggest that the measurement should perform in the dark. In conclusion, uncertainty of pH varies with the temperature and rms of pH differences have minimum value about ± 0.03 pH unit at 25 oC which correspond to mathematical model.

Keywords: ISFET, pH measurement, uncertainty, analysis

1. INTRODUCTION

ISFET, or Ion-Sensitive Field-effect Transistor, is a field-effect transistor used for measuring selective ion concentrations in a solution. In this kind of transistor, the gate electrode is replaced by the reference electrode. When the ion concentration in the solution changes, the current through the transistor will change accordingly. A voltage between substrate and oxide insulator layer arises due to an ion sheath against reference electrode [6, 8]. From this structure we can use the device to measure the proton concentration that is pH of the solution. The advantage of using ISFET as a pH meter is due to its structure decreased to small size and easily integrated to electrical instrument [1, 7]. However, the sensor is quite sensitive to the measuring environment such as light and temperature, are the main sources that interfere the accuracy of the measurement.
In order to précising the measurement, the uncertainty of pH [2, 4, 5] transduced by ISFET sensor is examined. A routine three-point calibration is used to obtain the sensor response. The measurements are performed in the both normal lighting and dark environment to see the effect of light on the sensor. The calibration at various solution temperatures are performed to estimate the temperature coefficient as the implicit parameter in slope that will be used to correct the temperature-dependent of the measured pH [3]

2. METHODOLOGY

Basic principle of ISFET is that the surface hydrolysis of Si–OH groups of the gate materials varies in solutions due to its pH value. This effects the surface gate oxide potential. The sensor was connected to an amplifier with a feedback control to obtain a constant drain-source current. By this configuration the surface potential can be measured from the gate-source voltage (VGS). Thus measure the change of VGS as a result of pH changing.

The measured VGS can be calibrated with standard pH buffers. Three-point calibration was utilized to obtain calibration lines. Slopes or sensitivities of the sensor and their corresponding uncertainties are obtained by spread sheet program using standard procedures.

A commercial ISFET sensor is used, bundle with an amplifier constant current circuit, in our study. An Agilent U1242B, calibrated with HP/Agilent Universal Source 3245A, with u(V) = ±0.0003 V, is used to measure VGS. Ajax Finechem “NIST traceable” buffers with pH 4.00±0.02, 7.00±0.02, and 10.00±0.02 at 20°C are used as calibration standards. The temperature is controlled to be ±1°C during the experiment

The calibration processes are performed at various temperatures to obtain the temperature coefficient of the slope. The sensitivity of the systems are also investigated under different lighting environment to see the effect of light to our system.

3. RESULTS AND DISCUSSION

1. Sensitivity of the system at various temperatures in the dark environment.

Following the suggestion of sensor manufacturer, a calibration process is started at 25°C in the dark environment. Table 1 shows the experimental data of VGS versus pH. Figure 1 shows the plot of data and the calibration line. The fitted parameters, the corresponding uncertainties and the R-square value are calculated by standard procedures using LINEST command in Excel software. Then repeat the calibration at different temperatures. The results are shown in table 2.

From the results in table 2. we plot the slope vs temperature in figure 2. Linear least square fitting is applied to determine the temperature coefficient of the slope. Again, the fitted parameter and its uncertainties

are calculated by standard procedures using LINEST command in Excel software. The results is α = -0.021 ± 0.002 V/(pH K)

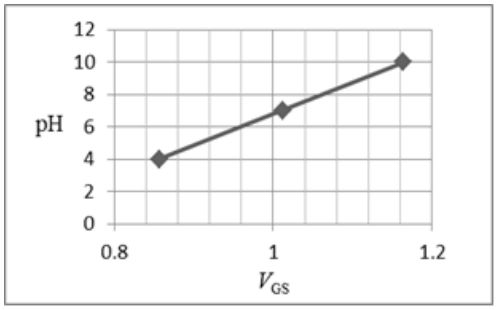

Fig. 1 Graph of VGS vs pH @ 25°C

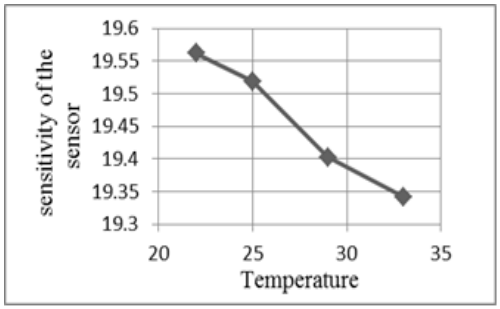

Fig. 2 Graph of the slope or sensitivity of the sensor vs temperature without light.

Table 1 VGS vs pH @ 25°C

pH	V_{GS} (Average)	Standard Deviation of V_{GS}
4	0.8564	0.0004
7	1.0121	0.0006
10	1.1638	0.0008

Table 2 Slope of the graphs of VGS vs pH at various temperatures, together with the corresponding uncertainties and R-square values.

T°	Slope	Uncertainties	R-square value
22	19.6	0.4	0.9996
25	19.5	0.1	0.9999
29	19.4	0.2	0.9999
33	19.3	0.2	0.9999

From above results we can write the mathematical models for the measured pH from our sensor and its uncertainty u(pH) as following,

$$\mathrm{pH}(V,T) = \mathrm{pH}_{is} + [k_0 + \alpha(T - T_0)](V - V_{is}) \quad (1)$$

$$\begin{aligned}[u(\mathrm{pH})]^2 = {} & u^2(\mathrm{pH}_{is}) + [Vu(k_0)]^2 + [k_0u(V)]^2 + [V_{is}u(k_0)]^2 + [k_0u(V_{is})]^2 + [(TV)u(\alpha)]^2 \\ & + [\alpha Tu(V)]^2 + [\alpha Vu(T)]^2 + [T_0Vu(\alpha)]^2 + [\alpha T_0u(V)]^2 + [\alpha Vu(T_0)]^2 + [(TV_{is})u(\alpha)]^2 \\ & + [\alpha Tu(V_{is})]^2 + [\alpha V_{is}u(T)]^2 + [T_0V_{is}u(\alpha)]^2 + [\alpha T_0u(V_{is})]^2 + [\alpha V_{is}u(T_0)]^2\end{aligned} \quad (2)$$

Here k_0 is the slope at 25°C, T_0 = 25°C, V_{is} and pH_{is} are the voltage and pH at intersection point of the calibration lines at different temperatures.

To estimate the working temperature of the sensor, the minimum of the rms of pH difference is calculated from each calibration temperature. The results are shown in table 3. We obtain the minimum value of ± 0.03 pH unit at 25°C. This is the working temperature, as also suggested from the manufacturer.

Table 3 The rms of pH difference from each calibration temperature.

T°	Uncertainties
22	0.08
25	0.03
29	0.05
33	0.05

2. Effect of the light

To see effect of light, we repeat the experiments in 3.1 with normal laboratory lighting. Slopes of calibration lines are plotted in figure 3. Large fluctuations of the sensitivity are occurred. Obviously, the temperature coefficient cannot be calculated. We may suggest that the sensor should be used in the dark environment.

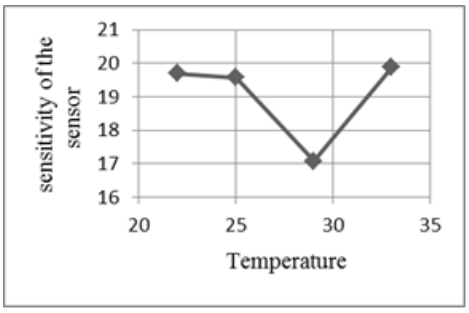

Fig.3 Graph of the slope or sensitivity of the sensor vs temperature with light.

4. CONCLUSION

The response of ISFET sensor is examined for various temperatures, with and without light, to estimate the uncertainty and proper condition for pH measurement. Light strongly effects the sensor

sensitivity then suggest to do measurement in the dark environment. Uncertainties of measurement parameters are obtained, which can be used to estimate the uncertainty of pH measurement. The working temperature is estimated to be 25°C, in which the rms of pH difference has minimum value. This result agree well with the manufacturer suggestion.

5. ACKNOWLEDGEMENT

The authors would like to sincerely thank the Department of Physics, Faculty of Science, Kasetsart University for the financial support and Dr. Sutisa Leasen from Faculty of Science and Technology, Rajamangala University of Technology Suvarnabhumi for her comments and support.
I would also like to extend my thanks to Winsense Co., LTD. for their professional guidance and valuable support and to ISFET product.

6. REFERENCES

[1] Rani, R. A. and O. Sidek. 2004. ISFET pH Sensor characterization: towards Biosensor Microchip Application. IEEE. 660–663.

[2] Buck, R. P., S. Rondinini, A. K. Covington, F. G. K. Baucke, C. M. A. Brett, M. F. Camõems, M. J. T. Milton, T. Mussini, R. Naumann, K. W. Pratt , P. Spitzer and G. S. Wilson. 2002. Measurement of pH. Definition, Standards, and Procedures. Pure Appl. Chem. 74(11): 2169–2200.

[3] Leito, I., L. Strauss, E. Koort and V. Pihl. 2002. Estimation of uncertainty in routine pH measurement. Accred Qual Assur. 7: 242–249.

[4] PetrÍk, J., J. KadukovÁ, P. Palfy, D. IvÁnovÁ and H. HorvÁthovÁ. 2013. The quality of pH measurement process. ACTA TECHNICA CORVINIENSIS – Bulletin of Engineering. 91-965.

[5] Degner, R. 2002. Measurement uncertainty in the pH measurement procedure. Anal Bioanal Chem. 374: 831–834.

[6] Péreza, J. F. V., M. M. M.Velascoa, M. E. M. Rosasa and H. L. M. Reyesa. 2012. ISFET sensor characterization. Procedia Engineering. 35: 270-275.

[7] Jimenez-Jorquera, C., J. Orozco And A. Baldi and K. Coale. 2010. ISFET Based Microsensors for Environmental Monitoring. Sensors (Basel). 10(1): 61-83.

[8] Manlises, C. O., F. R. Cruz , W.-Y. Chung and A. Paglinawan. 2017. Characterization of an ISFET with Built-in Calibration Registers through Segmented Eight-Bit Binary Search in Three-Point Algorithm Using FPGA. J. Low Power Electron. Appl. 7(19).

A CONSTRUCTION AND FINDING THE EFFICIENCY OF AUDIO SIGNAL PROCESSING INSTRUCTIONAL PACKAGE IN DIGITAL SIGNAL PROCESSING

Saranyaras Tongsawai[1)]
[1)]*Faculty of industrial education, Rajamangala university of technology Suvarnabhumi Suphanburi, Thailand*

ABSTRACT: The purposes of this research were 1) to construction of audio signal processing instructional package in Digital Signal Processing. 2) find the efficiency validation of audio signal processing instructional package in Digital Signal Processing. The method of operation are construction of instructional package included labsheets and activity learning and the research tools using find the efficiency validation are achievement test and suitability assessement form evaluation from 5 experts, satisfaction assessment form and finding the efficiency validation by sample group, 15 student of Industrial Technology in Telecommunication Technology, Rajamangala University of Technology Suvarnabhumi Suphanburi in semester 2 of the academic year 2018. The result showed average score from the experts is 4.34, high level. The means of satisfaction from the sample group is 4.40, high level. The efficiency were 82.33/88.67 which is higher than standard set. Overall, the instruction package is suitable for use in the teaching activities of digital signal processing and other courses related effectively.

1. Introduction

Teaching and learning in the content course or teaching activities are a practice model theory alongside practice, teacher need to have management activities for teaching in the classroom to be eligible by the should take into account, students, environment and situation for consideration. The appearance of which must be plain but should use the technique teaching methods integrated with teaching, it is appropriate, such as in some subjects as a practice. Teacher should not be taught a lecture alone or in some cases, teaching it is necessary and important in the learning process of the students, including the activity may be required, appropriate teaching, coupled with.

The Learning pyramid with the knowledge of the learning activities in the classroom, where students have the opportunity to practice listening, rather than alone. The students have to learn from reading, writing, and interactive analysis [1] In addition, students have been using advanced processes that include analysis, synthesis and Valuation It also can motivate and stimulate learning to the student attention to the practice as well. Which course Bachelor of Industrial Telecommunications Technology Rajamangala University of Technology suvarnabhumi Suphanburi. Digital Signal Processing code 105-43-07 in a basic course. The lesson in course study on the analysis of the audio signal. This requires the implementation and results of the trial proved that. If the student does not have a basic understanding of the principles of sound and signal analysis. It is impossible to develop the knowledge and solve problems in processing signals and can not see clearly the results or cause errors.

From the background and significance of the problem. To encourage students to apply knowledge from theory to practice, In this research, the researcher choose the topic audio signal processing. Which is the basic knowledge in the course of digital signal processing part the application in various aspects, such as the electronic and telecommunications. However, the measurement is one of several tools that aid in the development of quality education in various educational levels, because the results of various studies from the measurement will be fundamental in the decision of the Executive to improve instruction and teaching methods and course evaluation. [2], the research design instruction package for use in teaching activity in Digital Signal Processing course code 105-43-07 of practice for audio signal processing, as well as stimulate the learning process of students.

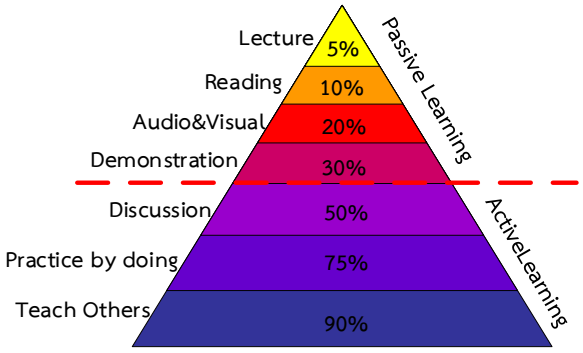

Fig. 1 Learning pyramid

2. Methodology

The purposes of this study aims to construction and finding the efficiency of audio signal processing instructional package in Digital Signal Processing course. To create a instructional package in Digital Signal Processing which consists of labsheets and learning activities, The research tools including a achievement test, suitability assessment form for 5 experts and a satisfaction assessment form for the sample group. Research methodology as follows:

2.1 The research plan

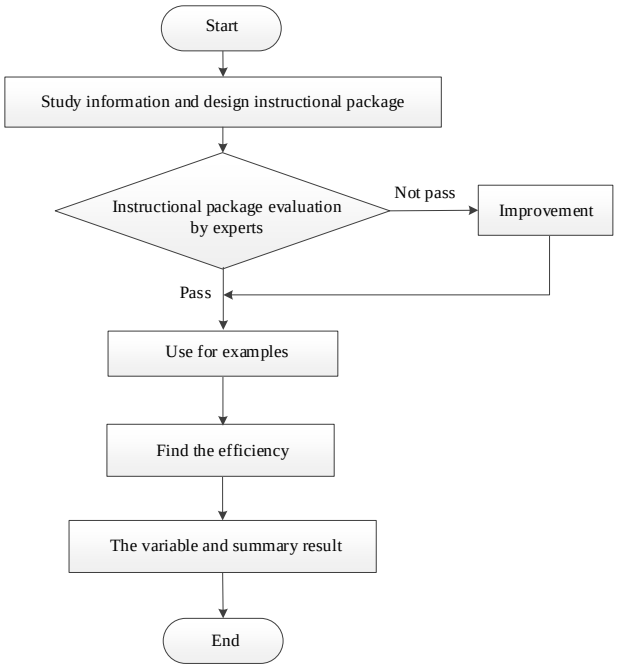

Fig. 2 The research plan

1) Study information and create the instructional package by studying the relevant information, including details such as related research or related documents for research and then gather the knowledge that has been produced. The technique of create the labsheets must be clear and easy to understand for the user or the educator.

2) Evaluate instructional package by experts. Using the instructional package suitability assessment form include labsheets and learning activity about audio signal processing instructional package in Digital Signal Processing course by 5 experts. From the evaluation results, if any part is incomplete or errors, then the results have been revised to be complete and accurate, according to expert advice.

3) Apply to sample group, 15 students.

4) Find the efficiency and satisfaction form the sample group.

5) The results from the efficiency and effectiveness of the satisfaction assessment form to translate and summarize the results.

2.2 Sample group

This research, researchers have determined the sample group is the undergraduate students are enrolled in the second semester of 2017. Digital Signal Processing course code 105-43-07. The first year of sample group in bachelor of Industrial Telecommunications Technology Rajamangala University of Technology suvarnabhumi Suphanburi, 15 students.

2.3 Research tools.

The purposes of this study aims to construction and finding the efficiency of audio signal processing instructional package in Digital Signal Processing course. Research tools as follows:

1) Instructional package include labsheets for laboratory about audio signal processing instructional package in Digital Signal Processing course. [3] Labsheets as follows:

- Labsheet 1 Creating a tone phone.
- Labsheet 2 Recording audio signals.
- Labsheet 3 Sub-sampling signals.
- Labsheet 4 Quantitation signals

2) Suitability assessment of Labsheets.

3) Achievement test

4) Satisfaction assessment for sample group.

2.4 Experimental Data.

After the researcher has created a instructional package include labsheets about audio signal processing instructional package in Digital Signal Processing course is completed. The experts assessed the instructional package to be appropriate and then apply to the sample group to find out the efficiency of the instructional package and evaluate the satisfaction of the students using for instructional package. To experiments and collect data from instructional package include labsheets and learning activity about audio signal processing in Digital Signal Processing course is completed. Were assessed by 5 experts and evaluated by 15 students and then evaluated for the efficiency of the labsheets. The statistics used in the analysis of data, the researcher selected the statistics used to analyze the data as follows:

2.4.1 Basic statistics [4]

1) Mean Statistic is given by:

$$\overline{X} = \frac{\sum X}{N} \qquad (1)$$

when

$\overline{X}$ = Mean average.

$\sum X$ = Sum of all scores in the sample group .

N = Number of people in sample group.

2) Standard Deviation is given by:

$$S = \sqrt{\frac{N\sum X^2 - (\sum X)^2}{N(N-1)}} \qquad (2)$$

when

S = Standard Deviation.

X = Score.

$\sum X$ = Sum of all scores in the sample group .

N = Number of people in sample group.

2.4.2 Statistical values used to find tools quality. [5]

ltem discrinination is the value between -1.00 to 1.00

- Positive discriminant value (0.01 to 1.00) means that the question has the power to distinguish. That is the question is measured exactly. The question can be used.

- Negative discriminant value (-1.00 to- 0.01) means that the question does not have a discriminating power. That is the question can not be measured exactly. Should cancel this test.

- Zero discrimination power means no power classification. This question should not be used further or

if it is to continue to be revised.

2.4.3 Determine the content validity of the achievement test and the attitude test is given by:

$$IOC = \frac{\sum R}{N} \quad (3)$$

when

IOC = Index of item objective congruence
$\sum R$ = Sum of experts opinion scores.
N = Number of experts.

2.4.4 Performance statistics E_1 / E_2

Method of data analysis by using a benchmark that determines the level of application of knowledge (Applied knowledge : A) 80/80 and the level of knowledge transfer (Transferred knowledge : T) 80/80 given by 80, first as a percentage of the test after the class, the accuracy of the performance of the process, and 80, the latter is the percentage of test who measure accurately the performance of the results.

Benchmark E_1 / E_2 the criteria used to compare the scores obtained from the assessment in the learning process with the scores from the final exam, after graduation or expected learning outcomes. If a good student should set the criteria 90/90. The relatively weak students should use the criteria 70/70 or 80/80 depending on the difficulty of the subject matter.

E_1 Percentage of average scores of all students collected from activities such as labsheets, exercises, and quizzes during the class is given by:

$$E_1 = \frac{\overline{X_1}}{N_1} \text{ X } 100 \quad (4)$$

when

E_1 = Efficiency of teaching process
$\overline{X_1}$ = Average scores during class of all students
N_1 = Full score collected during class.

E_2 Percentage of average score after the test or the final exam of expected learning outcomes for that purpose is given by:

$$E_2 = \frac{\overline{X_2}}{N_2} \text{ X } 100 \quad (5)$$

when

E_2 = Efficiency of teaching and learning after graduation.
$\overline{X_2}$ = Average final score of all students.
N_2 = Full score of final exam.

Fig. 3 Activities in class.

3. RESULTS

3.1 Experts Evaluation Results.

This research utilizes the instructional package evaluation for the audio signal processing instructional package in Digital Signal Processing course is completed by 5 experts, 5 points were rated based on Likert scale rating [6], which is the highest, high, medium, low, and lowest score.

4.50 – 5.00 means highest
3.50 – 4.44 means high
2.50 – 3.44 means medium
1.50 – 2.44 means low
0.00 – 1.44 means lowest

The results of the suitability assessment form by the experts found that the average score of 4.34 was appropriate at the high level, details of the results are shown in table 1.

Table 1 Instructional package evaluation from experts.

List	$\overline{X}$	S.D.	Results
1. Appropriate Instructional package design for students.	4.40	0.55	High
2 .Instructional package can skills supplement use for Digital Signal Processing.	4.20	0.45	High
3 .Interesting instructional package.	4.20	0.45	High
4 .Instructional package according to objective.	4.20	0.84	High
5 .Gramma corrected.	4.60	0.55	Most
6 .Correct pattern instructional package.	4.00	0.71	High
7 .Instructional package appropriate pattern.	4.20	0.45	High
8 .Clear describes from instructional package.	4.20	0.45	High
9. Instructional package urge learning process student	4.60	0.55	Most
10 .Sequence appropriate instructional package.	4.80	0.45	Most
Means total	4.34	0.54	High

3.2 Results of the analysis the efficiency of instructional package.

Determining the performance of the instructional package by applying a design labsheets to the sample group, 15 peoples, Then the scores from the results using the instructional package to analyze for efficiency based on the learning achievement of the sample group using the efficiency of the instructionla package, which is collects scores from the progress of learning from the labsheets ((E_1) = 82.33), the The achievement of the achievement test ((E_2) = 82.19). It appears that the created labsheets are effective 82.33/88.67 which is higher than the standard criteria. The Following is the example for table 2.

Table 2 Labsheets learning progress (E_1)

Labsheets	ΣX	$\overline{X}$	*S.D.*	(E_1)
Lesson 1	110	7.33	0.90	73.33
Lesson 2	122	8.13	0.64	81.33
Lesson 3	132	8.80	0.68	88.00
Lesson 4	130	8.67	0.62	86.67
$\overline{X}$	82.33			

The means of score from achievement test of the sample group was high level than the standard criteria (E_2 = 88.67). The Following is the example for Table 3.

Table 3 Achievement test (E_2)

Labsheets	ΣX	$\overline{X}$	*S.D.*	(E_1)
Achievement test	133	8.87	0.74	88.67
$\overline{X}$	88.67			

3.3 Student satisfaction assessment results.

Researchers have released a instructionla package to sample group is the undergraduate students are enrolled in the second semester of 2017. Digital Signal Processing course code 105-43-07. The first year of sample group in bachelor of Industrial Telecommunications Technology Rajamangala University of Technology suvarnabhumi Suphanburi, 15 students. After learning, the student were able to improve their learning and the student's satisfaction with the instructionla package was 4.40, high levels. The results of the assessment are shown in Table 4.

Table 4 The performance instruments.

List	$\overline{X}$	S.D.	Results
1. Appropriate Instructional package design for students.	4.40	0.51	High
2 .Instructional package can skills supplement use for Digital Signal Processing.	4.53	0.64	Most
3 .Interesting instructional package.	4.13	0.64	High
4 .Instructional package according to objective.	4.47	0.52	High
5 .Gramma corrected.	4.40	0.63	High
6 .Correct pattern instructional package.	4.40	0.63	High
7 .Instructional package appropriate pattern.	4.47	0.52	Most
8 .Clear describes from instructional package.	4.53	0.52	Most
9. Instructional package urge learning process student	4.33	0.49	High
10 .Sequence appropriate instructional package.	4.33	0.49	High
Means total	4.40	0.56	High

4. CONCLUSION

Based on the results, it is found that construction and finding the efficiency of audio signal processing instructional package in Digital Signal Processing course, can enhance the development of knowledge and stimulate the students learning process by training, experiment, practical experience and students can their own intelligence. The researchers collected the scores form results of the learning progress and achievement tests in classes. The result of the achievement of the study is effective 82.19/88.75 which is higher than the standard criteria (80/80).

5. DISCUSSION

This research presents the construction and finding the efficiency of audio signal processing instructional package in Digital Signal Processing course, The results are as follows:

5.1 Results of the suitability assessment of the instructional package by the experts.

This research used the suitability assessment for instructional package of the audio signal processing instructional package in Digital Signal Processing course, by 5 experts, the scores was based on the characteristics of the Likert scale. The scores were 5, which is the highest, high, medium, low, and lowest score. The average score of 4.34 which is high levels.

5.2 Results of the analysis efficiency of instructional package.

The effectiveness of the instructional package was applied to 15 peoples, based on the learning

achievement of the sample group. The results of the analysis of the progression scores from labsheets 1-4, with the average score is 82.33 and the achievement score from the achievement test, were 88.67 percent.

5.3 Student satisfaction assessment results.

Students are satisfied with the instructional package in audio signal processing instructional package in Digital Signal Processing course. After being used, average score of 4.40 which is high levels.

6. REFERENCES

[1] Active Learning ,2018, “http://www.aksorn.com/active-learning/ ”[20July 2018].

[2] "Measurement and evaluation of education", Technical Education Technology. King Mongkut's University of Technology North Bangkok.

[3] Lunchakorn, W. et al. ,2008, “MATLAB”. Chulalongkorn University Printing House, Bangkok. [3] Jantima, S.,201 8,“ Creating and Finding a Quality Learning Measurement Center,”. "http://www.slideshare.net/kaew393/ss-3956137 [20 July [5] Saranyaras, T., 2017, Application using filter circuits to design signal generator in Analysis and Design Using Software Engineering.

[6] Boonsom, P., 2018, “How to conduct an assessment,” https://www.gotoknow.org/posts/253663 [20 July 2018].

DESIGN AND CONSTRUCTION OF INSTRUCTIONAL MATERIAL DEVELOPMENT

Pitichon Piamboriboon*[1)]

*[1)] *Technical education department, Faculty of industrial education, Rajamangala university of technology Suvarnabhumi Suphanburi, Thailand*

ABSTRACT: The design and construction of instructional material development, Bachelor of Science in Technical Education (B.Sc.Tech. Ed.) Program in electronics and Telecommunication Engineering, Program in Mechanical engineering, Program in Industrial Engineering (Improvement of 2554) consists of the teacher's book and teaching materials, including the teaching plans, worksheets, post-lesson exercises, and the tests. In the teaching kit, there are teaching contents as following, types and the importance of Industrial engineering's teaching-assisting materials, types of printed media, the analysis of teaching-assisting material development, the document analysis forms, the performance evaluation, the progressive record of learning and project. All teaching materials mentioned above are designed and implemented in the form of Microsoft Power Point. After assessed by 3 specialists, the teaching kit of Teaching Material Development has been proved that these materials are good for implementing in authentic teaching. The instructional materials development helps teach the use of sampling. The total evaluation results in good teaching material development teaching instruction can considerably. The research of water.

Keywords: including the teaching plans, the importance of Industrial engineering's teaching-assisting materials, the document analysis forms

1. INTRODUCTION

At present, the education has developed far and wide, the modern technology adapted to the studying . Teachers are more comfortable teaching. Bachelor of Science in Technical Education (B.Sc.Tech.Ed.) Program in electronics and Telecommunication Engin eering, program in mechanical engineering, program in industrial engineering (Improvement of 2554) has course of the instructional materials development (107-33-01). Course description, type and importance of industrial teaching aids, print document type, professional analysis for teaching material developme nt, create and develop teaching materials in accordan ce with learners. Practice writing documents, knowle dge sheets, and practice projects.

According to studies, it has been found the teacher's manual and teaching materials are not yet complete. In the present study, technology has been incorporated into the teaching media, such as static media. This is a great way for students to learn about their imagination. If the learner does not understand, can take the media learn more by yourself. Therefore, the instructor create the instructional materials development (107-33-01). Bachelor of Science in Technical Education (B.Sc.Tech.Ed.) Program in electronics and Telecommunication Engineering, Program in Mechanical engineering, Program in Industrial Engineering (Improvement of 2554), using the Microsoft Power Point software, displays slide content that will make the teaching process more effective. Meet the set objectives with the same standards.

1.1 Objectives

The construction of instructional material development, Bachelor of Science in Technical Education (B.Sc.Tech. Ed.) Program in electronics and Telecommunication Engineering, Program in Mechanical engineering, Program in Industrial Engineering (Improvement of 2554)

1.2 Scope

The Instructional Package of The Instructional materials development (107-33-01) was created to meet the Bachelor of Science in Technical Education (B.Sc. Tech.Ed.) Program in electronics and telecommunication engineering, program in mechanical engineering, program in industrial engineering (Improvement of 2554) consists of 3 parts.

1.2.1 The lesson plan consists of syllabus, content, teaching activities and after the unit, all units are 4 multiple choice.

1.2.2 The achievement test is multiple choice 4 options.

1.2.3 The teaching materials used are: Microsoft Power Point.

1.3 Method of operation

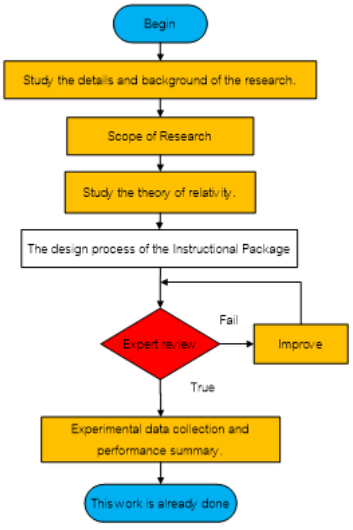

1.4 Expected benefits

1.4.1 The Instructional Package of The Instructional materials development (107-33-01) was created to meet the Bachelor of Science in Technical Education (B.Sc.Tech. Ed.) Program in electronics and Telecommunication Engineering, Program in Mechanical engineering, Program in Industrial Engineering (Improvement of 2554)

1.4.2 Instructors are confident in teaching and reduce the time to prepare the teaching.

1.4.3 There is a clear use of teaching materials and there is a corresponding understanding between the teacher and the learner.

1.4.4 The instructional process is objective and meet the scheduled time.

2. METHODOLOGY

2.1 The theory and basic principles

Meaning of Instructional Package in Thailand and abroad are defined as follows.

Instructional Package means a set of teaching and learning materials and instructional systems. The media is consistent and appropriate with the subject. Any heading and the purpose is to help the learner get the learning activities to gain knowledge. Experience with the purpose or purpose. And to change the behavior of learning efficiency (Surakiat Sanit, 2006).

The Instructional Package is a complete collection of instructional materials to achieve the purpose of teaching the instructional package is a multimedia system. Teachers do not have to prepare other media or new teaching plan the instructional package includes media and instructional methods. Teachers should be able to use the instructional package appropriately (Ladda Sook Pridit, 1979).

The instructional package is a multimedia system that is consistent with the content and the experience of each unit to help change the learning habits to be more effective. The instructional package is usually arranged in a box or envelope. With the instruction manual, use the instruction set. Teaching materials that are consistent with the content and experience such as pictures, slides, tapes, films, lectures, materials, etc. (Chaiyong Promvong, 1978)

The instructional package is a multi-media instructional package that is organized into a package called Multi-Media for students to learn effectively. (boonchum srisaad 1998)

The instructional package refers to the systematic production and use of multimedia in a systematic manner. Unit and topic to help students learn effectively (Chalilya Limprasert, 1993). From the meaning of the teaching set that many students have given meaning and say it.

The instructional package is a process of organizing the content of the course to the students in a systematic way the media used to mix. Consistent with the subject matter, the teaching and learning activities have been achieved.

Steps to produce a teaching set

1) Content classification and experience.
2) Teaching unit
3) Set subject
4) Define concepts and principles.
5) Objectives
6) Define learning activities.
7) Set evaluation form
8) Select and produce teaching materials.
9) Find out the performance of the instruction set.

2.2 Types and composition of instructional packages

The Instructional package Individual It is a teaching system designed to help students learn independently. In the order specified there are special classrooms called. "Individual Classroom" with booths provided. The instructor will use the instruction set in the booth when there are problems during the course, students will be able to discuss them. Instructors are available to provide immediate assistance as coordinators the student may bring this kind of instructional package. At home or anywhere individualized instructional packages can train and promote the habits of the individual. Learn in pursuit. Knowledge is very good. This individual instructional package focuses on the sub-unit, so it is commonly referred to as the "module" or the programmed lesson (programmed lesson) in the form of print media, audio visual material or computer.

Element of teaching set

1) Manual and Practical for teachers.
2) Orders or assignments.
3) Content.
4) Evaluation
   - Pre-test
   - Introduction to the lesson.
   - Activities instructional packages.
   - Summarize and test after class to know.

2.3 Course Structure

2.3.1 Meaning of the course

Course means a plan designed to demonstrate the purpose. Organizing content, activities and mass experiences in each educational program to develop students in various fields the purpose.

2.3.2 Course Syllabus Include:

1) Course Description
2) Unit / Lesson / Topic
3) Teaching Objectives
4) Tea Evaluation
5) Teaching schedule
6) References

2.4 Development of course curriculum

Course Syllabus If the teaching objectives are clear the instructor was able to easily prepare the instruction. However, if the course syllabus does not have an exact teaching purpose. Teachers also need to gather information. In terms of teaching and learning in the course to analyse to design the teaching objectives of course curriculum can be summarized as follows.

2.4.1 Study the topics or characteristics of the subjects.

2.4.2 The study compiled the topic.

2.4.3 Assess the importance of the topic.

2.4.4 Analyze key contents of the topic.

2.4.5 Analyze knowledge for important content items.

2.4.6 Define the behavioral objectives of all subtopics.

2.5 Creating Quizzes

The test is one of the instruments used to measure performance of students at all levels of education to measure with the test The test will be accurate or reliable, depending on the quality of the test. Therefore, writing the correct test is a very important consideration, because

it will affect the quality of the test directly.

2.5.1 Characteristics of good exam authors.
2.5.2 General principles in writing the test.
2.5.3 Creating Subjective Tests
2.5.4 Creating multiple-choice tests

2.6 Introduction to Microsoft Power Point

Microsoft Office Power Point is an application created specifically for presentations, with the ability to create quick and easy presentations. Customize and customize your presentation. It attracts viewers more than the original presentation.

2.6.1 Getting Started with Microsoft Office Power Point
2.6.2 Program screen components
2.6.3 Creating a new presentation
2.6.4 Documentation
2.6.5 Using new tools and effects to create presentations.
2.6.6 Creating text by using literal characters
2.6.7 Picture Creation (Picture / ClipArt)
2.6.8 Animation Assignment
2.6.9 Define audio and speed while changing slides.
2.6.10 Slide Transition Timer
2.6.11 Exiting Microsoft Office PowerPoint to create this tutorial.

Create the Instructional Package of the Instructional materials development (107-33-01) was created to meet the Bachelor of Science in Technical Education (B.Sc.Tech. Ed.) program in electronics and Telecommunication Engineering, program in Mechanical engineering, program in Industrial Engineering (Improvement of 2554). The framework is structured by studying the data and problems to set goals or scope of creation Know the scope of the instructional packages the creators have created the tool consists of 3 parts: the lesson plan, the test of achievement and the teaching media.

- Lesson plans include lesson plans, units after class, all units are 4 multiple choice options.
- The achievement test is 4 multiple choice.
- Instruction media Includes Microsoft Power Point.

2.7 Course Analysis

Course Analysis the Instructional Materials Development It's an important step to obtain the important topics and behavioral objectives that students have expressed. There is a need for teaching. It is a guide to the choice of content, teaching methods, learning levels of learners. Instruction media and evaluation in summary the process of analysing the course is as follows.

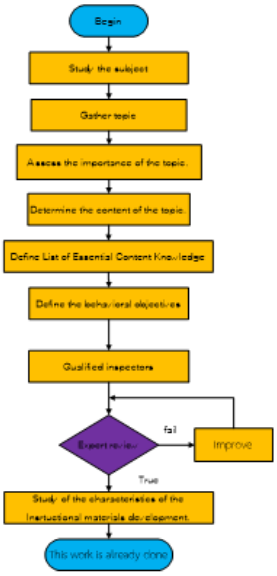

Figure 1 Steps to analyze the course characteristics.

2.8 The Instructional package in course the Instructional Materials Development.

The tools used in the implementation of the instruction set. The organizer is created by the details and steps in the implementation of each section. Teaching Materials Development this is a set of teaching a lecture or instructional package for the instructor to use in the teaching process. There are steps in creating the instruction set.

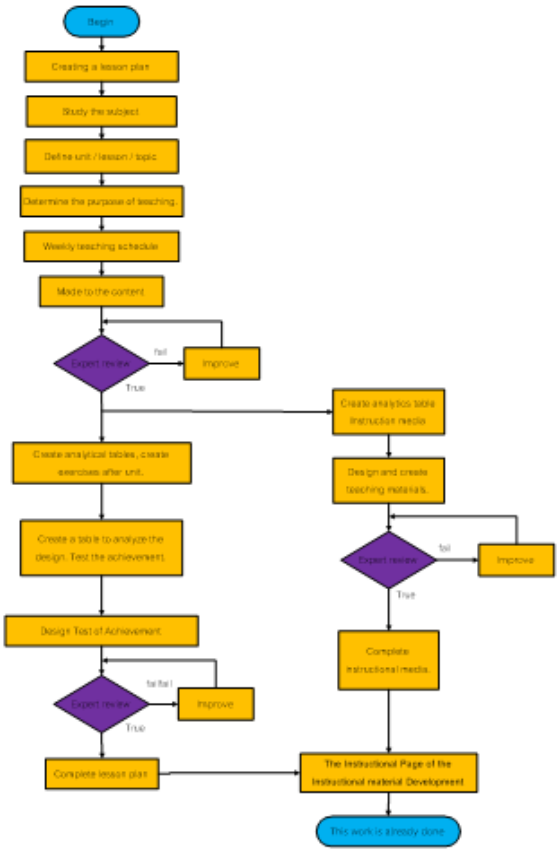

Figure 2 Step of construction of Instructional material Development

2.9 Assessment of Teaching Quality

Creating a learning achievement model the organizer is organized into four multiple-choice tests, with the steps of creation as shown in Figure 3

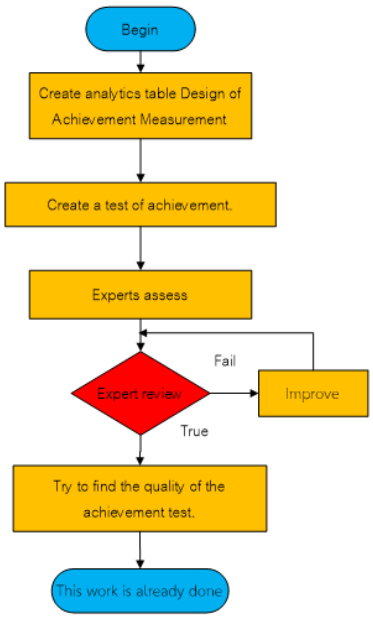

Figure 3 Steps to Create Achievement

A questionnaire to assess teaching quality for the opinions of the experts about teaching aids. The organizers created by compiling and referring to the teaching materials (Pisit and Teerapol) on "Media Quality Assessment".

Episode 1 is the evaluation form of the opinion. Qualified Instructional page of Instructional Materials Development Create a questionnaire for valuation by dividing the opinion level into 5 levels as follows:

Level 4 means agree.
Level 3 means moderate.
Level 2 means disagree.
Level 1 means strongly disagree.

Episode 2 Comments and other suggestions from the opinions of the experts when evaluating, the mean value derived from the average formula is then taken into account (Chaiyot Ruangsuwan).

Score 4.50 - 5.00 means very good.
Score 3.50 - 4.49 means good.
Score of 2.50 - 3.49 means at a moderate level.
Score of 1.50 - 2.49 means at the moderate level
Score 1.00 - 1.49 means that the level must be updated / corrected. The score obtained is based on the formula.

$$\bar{\bar{x}} = \frac{\sum (A \times B)}{N_1} \quad (1)$$

When

$\bar{\bar{x}}$ = Mean average.
A = Number of assessors.
B = Rating level.
N_2 = Total number of assessors.

$$\text{Average total} = \frac{\sum (\bar{\bar{x}})}{N_2} \quad (2)$$

When

$\bar{\bar{x}}$ = Average total
A = Number of assessors.
B = Rating level.
N_1 = Number of questions

Take the value of the calculated number into the table to evaluate the whole quality of the instruction set of the Instructional Materials Development.

3. RESULTS

The Instructional Package of the instructional materials development. Bachelor of Science in Technical Education (B.Sc.Tech. Ed.) Program in electronics and Telecommunication Engineering, Program in Mechanical engineering, Program in Industrial Engineering (Improvement of 2554) Rajamangala University of Technology Suvarnabhumi It consists of a teacher manual and the teaching media. The teacher's manual consists of a lesson plan, a lesson plan, a lesson plan, and a lesson plan. Achievement test there are 5 units of study units, types and importance of industrial teaching materials, types of printed materials, occupational analysis for teaching aids, leaflet analysis and measurement and evaluation, worksheets, progress notes, and instructional programs and divided into lesson plans 17 lesson plans for Instructional media make a media for learning, teaching with Microsoft Power Point.

Researcher a questionnaire was used to evaluate the quality of teaching materials three teachers were selected to evaluate the quality of teaching materials the results of the evaluation of the quality of the instructional package. As shown in Table 1

Table 1 Table of results of the qualification submission

At.	Questions Answered	Level					
		5	4	3	2	1	Avg.
	1. Commments on the lesson plan.	**Total level**					**4.30**
1	Objective covers topics.	3					4.60
2	Determining the necessary basic knowledge to teach.		3				4.00
3	The duration of instruction is appropriate for the purpose.		3				4.00
	2. Content Comments	**Total level**					**4.19**
1	Course content covers objectives.		3				4.00
2	Course content is sufficiently detailed with the leaner the level	1	2				4.33
3	Course content is accurate		3				4.00
4	Course content is sorts appropriately	1	2				4.33
5	The language used appropriate and readable.		4				4.00
6	Images are related to subject matter.	1	1	1			4.00
7	Description of the image is clear.	1	2				4.33
	3. Feedback on unit exercise	**Total level**					**4.38**
1	Post-test after unit covered purpose.		3				4.00
2	Post-test after unit correspond to the content of each subject.	3					5.00
3	Post-test after unit classes appropriate to the level.		3				4.00
4	Post-test after unit of study appropriate to the ability of the student.	1	2				4.33
5	The questions and answers are clear and clear.		3				4.00
6	Easy and convenient answering.	5					5.00

At.	Questions Answered	Level					
		5	4	3	2	1	Avg.
	4. Feedback instruction package Microsoft power point.	**Total level**					3.70
1	The picture is clear.		3				4.00
2	The size of the letter is clearly visible.		3				4.00
3	Color used in the picture and the text is clear.	1	2				4.33
4	Appropriate to the content and objectives.		3				4.00
5	Create a stimulating learning experience.	3					5.00
6	Encourage student activities.	1	2				4.33
7	The design is easy to produce.		2	1			3.66
8	It is convenient to prepare teaching equipment.		3				4.00
9	It is easy to teach.		3				4.00
	5. Feedback on the achievement test.	**Total level**					**4.40**
1	The test covers the intended purpose.	3					5.00
2	Quizzes are consistent with the content in each topic.		3				4.00
3	Test of the ability of the students.		3				4.00
4	The questions and answers are clear and clear.	3					5.00
5	The answer is easy.		3				4.00
	Total level						4.27

4. DISCUSSION

The results of the evaluation of the instruction al media were good. The teaching materials were ta ught by Microsoft Power Point. The test scores for the achievement tests were at a good level. Quizzes are consistent with the content in each topic. Test of the ability of the students, the questions and ans wers are clear and clear. The results of the evaluati on were good. Can be used in the teaching of the objectives of the research.

5. CONCLUSION

The content in some units is quite difficult, so the preparation of the lesson plan is delayed. The research was delayed. For example, Unit 2, type of publication. The content in this section is quite difficult. And it is difficult to choose the appropriate content for teaching at the undergraduate level to meet the objectives and duration of the teaching.

6. ACKNOWLEDGEMENT

Researcher would like to thank Department of Electronics and Telecommunication Engineering, Mechanical Engineering, Industrial Engineering, Faculty of Industrial Education Rajamangala University of Technology Suvarnabhumi SuphanBuri Center for Research and Development Tools and equipment. The research was successful.

7. REFERENCES

[1] Chaliya Limpiyakorn. 1993, Educational Technology. Bangkok : Phisit Printing,.
[2] boonchom srisaad. 1998, Teaching Development . Bangkok : Children's Club,
[3] Ladda sookpridee. 1979, Teaching Technology . Bangkok : Pikanesh Printing,
[4] Surakiat Sanitmuch. 2006, Principles and methods of teaching technical education for industrial teachers. Rajamangala University of Technology Lanna Tak.
[5] Suawanee sitkabaandit. 1985, Educational Technology. Bangkok : Printing house King Mongkut's Institute of Technology North Bangkok,
[5] Nipon reungwariyanan. 2012, Teaching of the Instructional Material Development. Rajamangala Institute of Technology Tak ,
[6] Instructional Media .Didactic for Technical Training . Rajamagala University of Technology Suvarnabhumi Suphanburi, 2011
[7] Instructional Media .Educational Measurement and Assessment . Rajamagala University of Technology Suvarnabhumi Suphanburi, 2011
[8] Instructional Media .Principles and Methods of Teaching . Rajamagala University of Technology Suvarnabhumi Suphanburi, 2011
[9] Instructional Media .Didactic for Technical Training. King Mongkut's Institute of Technology North Bangkok ,2007
[10]Chaiyong Promvong .Creating a instructional package (Online), 5November 2013.
[11]Chanamete Mee Thong Lang .Introduction to print media (Online), 2July 2014.

ESTIMATION OF TOTAL PHENOLIC CONTENT, IN-VITRO ANTIOXIDANT AND ANTI-TUMOR ACTIVITY OF FLOWERS OF BOSCIA VARIABILIS (KURZ) COLLECT & HENS

San San Aye, Zin Thu Khine, Ni Ni Than
Department of Chemistry, University of Yangon, Myanmar

ABSTRACT: Tumor and cancer are the major causes of death all over the world. Bioassay offers special advantages to know about the biological activity of plant extracts and provide information to isolate active compounds which is a preliminary key step for drug discovery system. Several bioassays such as total phenolic content, antioxidant and anti-tumor activities were determined. Acute toxicity of 70 % ethanol and watery extracts of the flowers were also evaluated by the method of OECD guidelines. The main aim of the present research was to evaluate the biological properties of Boscia variabilis flowers. Total phenolic contents were studied using a spectrophotometric technique, based on the Folin-Ciocalteu reagent and calculated as gallic acid equivalents. B.variabilis flowers of ethanol and water were found to contain 17.54 and 13.44 µg/mg gallic acid equivalent of total phenol. In-vitro antioxidant capacity of 70 % ethanol and watery extract was determined by DPPH assay method. The antioxidant activity of ethanol extract of B.variabilis possessed higher potency than watery extract. The antitumor activity of flavonoid extract, 70 % ethanol and watery extracts of the flowers was investigated by using Potato Crown Gall (PCG) test with Agrobacterium tumefaciens. Ethanol extract of B.variabilis flowers was good in preventing the crown gall formation with the dose of 0.05 g/disc in-vitro potato disc assay. The anti-tumor and antioxidant activities of the extracts were positively associated with the total phenolic contents of the extract. In conclusion, 70 % ethanol extracts of the flowers, possess significantly anti-tumor activity and antioxidant activity. Therefore, B.variabilis flowers may be used for preventing cancer.

Keywords: Agrobacterium tumefaciens, Tumor, Potato Crown Gall, antioxidant, total phenol

1. INTRODUCTION

Plants have a significant role in maintaining human health and improving the quality of human life. The world health organization (WHO) estimated that 80 % of the people rely on traditional medicine.
Boscia variabilis Collect & Hens belongs to the family Capparaceae and also known as Tha-mon in Myanmar. The plant locally known as Tha-mon (Thamar-mone), become the focal point of the study with regard to the anti-tumor because it has not been reported elsewhere. Tha-mon (B.variabilis) is one of the oldest edible flowers and is widely grown in many tropical and subtropical countries. In upper Myanmar, the flowers of B.variabilis is used as medicine for eye diseases and the flowers are famous for making salad.
B.variabilis flowers contain a number of beneficial antioxidants including polyphenols. Antioxidants protect against free radicals, which are by products of cell oxidation. Free radicals are associated with causing a number of health problems, including breast, prostate and lung cancers [1].

2. MATERIALS AND METHODS

4.1 Sample

The flowers of B.variabilis were collected in flowering season (February, 2017) from Myingyan Degree College Campus, Myingyan Township, and Mandalay Region. The flowers were left in the open air till they were completely dried. The dried sample was ground in a grinding machine. The drug powder was then stored in air-tight containers.

4.2 Preparation of Crude Extracts

Dried powders of flowers were extracted with 70 % ethanol and water using Soxhlet apparatus. Extraction time with each solvent was six hours. After removing each solvent by rotary evaporator, crude extract was dried and kept in desiccator.

4.3 Procedure

(1) Determination of Total Phenolic Content by Folin-Ciocalteu Reagent Method

One of the anti-oxidative factors, total phenolic content (TPC) was measured by spectrophotometrically according to the Folin-Ciocalteu method. The sample solution was prepared by dissolving 1mg of respective crude extract in 1 mL of distilled water. To this 5 mL of F-C reagent (1:10) was added and incubated for 5 minutes. To each tube, 4mL of 1M sodium carbonate was added and the tubes were kept in room temperature for 15 minutes and the UV absorbance of reaction mixture was read at □max 765 nm. The blank solution was prepared as the above procedure by using distilled water instead of sample solution. Total phenolic content was estimated as □g Gallic acid equivalent (GAE)/ mL of different extracts [2].

(2) Determination of Antioxidant Activity of Both 70 % Ethanol and Watery Extracts by DPPH Assay Method

DPPH radical scavenging activity of 70 % ethanol and watery extracts of B.variabilis flowers was determined by UV-visible spectrophotometer [3].The control solution was prepared by mixing 1.5 mL of 0.002 % DPPH solution and 1.5 mL of the ethanol in the brown bottle .The sample solution was also prepared by mixing 1.5 mL of 0.002 % DPPH solution and 1.5 mL of tested sample solution. These bottles were incubated at room temperature and were shaken on shaker for 30 minutes. After 30 minutes, these solutions were measured at 517 nm and the percentage of radical scavenging activity (% RSA) was calculated. The antioxidant power (IC50) (50 % inhibition concentration) values were calculated by linear regressive excel program.

(3) Anti-agrobacterium tumefaciens Activities of Extracts on Potato Crown Gall (PCG)

In this study, the efficiency of Agrabacterium tumefaciens was used as a tool in antitumor study. The sample (0.05 g) was dissolved in dimethyl sulphoxide (DMSO) (2 mL) and filtered through Millipore filters (0.22 µm) into sterile tube. This solution (0.5 mL) was added to sterile distilled water (1.5 mL) and broth culture (2 mL) of A.tumefaciens strain. Control was made in this way; DMSO (0.5 mL) and sterile distilled water (1.5 mL) were added to the tube containing broth culture (2 mL) of A.tumefaciens strain. By using a sterile disposable pipette, one drop (0.05 mL) from the test tube was used to inoculate each potato disc spreading it over the disc surface. After inoculation, petri dishes were sealed by paraffin and incubated at 27-30 ºC for 14 days [4].

(4) Acute Toxicity Study of Both 70 % Ethanol and Watery Extracts on Albino Mice

To determine the consequent of the plant and to determine the nature and degree of toxicity produced by these extracts and to find out the medium lethal doses (LD50) of the extracts, acute toxicity test was done. In this study, acute toxicity effect of 70 % ethanol and watery extracts of B.variabilis flowers were determined on albino mice. Acute toxicity of different doses of the extracts was evaluated by the methods of OECD (Organization for Economic Cooperation and Development) Guidelines. They were fasted for 18 hrs before giving the extracts. Group (A) mice were orally administrated with ethanol extract of 2000 mg/kg dose. Group (B) mice were given orally with ethanol extract of 5000 mg/kg dose. Group (C) mice were orally administrated with watery extract of 2000 mg/kg dose. Group (D) mice were also given orally with watery extract of 5000 mg/kg dose. Group (E) mice performed as a control group and they were treated with clean water and normal animal food. All groups of mice were kept in the three mouse cages in the separated room at the room temperature of 26 ± 1º C. After administration of extract on each group of animals were observed first 6 hrs continuously for mortality and behavior changes. Then check the animals each 24 hrs for fourteen days. The mortality during this period was noted [5].

4. RESULTS AND DISCUSSION

4.1 Total Phenolic Content

Total phenolic content of B.variabilis flowers was estimated by Folin-Ciocalteu method. According to the experimental results, the total phenolic content (TPC) (µg / GAE / mg) of ethanol extract (19.67± 1.96) was higher than that of watery extract (18.97 ± 1.25). The greater the total phenolic content, the higher the antioxidant activity. Therefore, the ethanol extract of B.variabilis flowers has more antioxidant activity than watery extract. In addition, there was a positive correlation between total phenolic content and antioxidant activity in the plant sample (Table 1).

4.2 **Antioxidant Activity**

In this study the antioxidant potential of ethanol and watery extracts of B.variabilis flowers was evaluated by DPPH assay method. According to the result of antioxidant activity, the IC50 values of ethanol and watery extracts are 27.19 mg/mL and 71.08 mg/mL, respectively. So the antioxidant activity of ethanol extract possessed higher potency than watery extract. Their antioxidant activity are compared with standard ascorbic acid (IC50 = 8.40 mg/mL). The lower the IC50 value, the higher the antioxidant activity (Figure 1 & 2).

4.4 Anti-Tumor Activity

The ethanol extract of B.variabilis flowers bears on extremely high content of polyphenolic compounds. It could be used as an anti-tumor activity. The anti-agrobacterium tumefaciens activity of flavonoid extract, 70 % ethanol and aqueous extracts of B.variabilis flowers was investigated by using Potato Grown Gall (PCG) test with A.tumefaciens. From the experimental result, it was found that all extracts of B.variabilis flowers were good in preventing the crown gall formation with the dose of 0.05 g/disc in- vitro potato disc assays (Figure 3).

4.5 Acute Toxicity

Acute toxicity screening of 70 % ethanol and watery extract of B.variabilis flowers were done with the dosage of 2000 mg/kg and 5000 mg/kg body weight in each group of albino mice. The condition of mice groups were recorded after fourteen days administration. The results showed no lethality of the mice was observed up to fourteen days administration. Each group of animals were also observed still alive and did not show any visible clinical symptoms of toxicity like restlessness, respiratory disorders, convulsion, aggressive activities, coma and death. Even with the dose up to 2000 mg/kg and 5000 mg/kg body weight administration, there was no lethality at the day of fourteen.

5. CONCLUSION

From the present research work on "Estimation of Total Phenolic Content, In-vitro Antioxidant and Anti-tumor Activity of Flowers of Boscia variabilis (Kurz) Collect & Hens'', the following conclusions can be drawn.

The antioxidant activity of 70 % ethanol extract of flowers showed higher potency than watery extract. It is noticed that the highest concentration of phenolic compound will be present in 70 % ethanol extract. Therefore, it is required to isolate the phytoconstituents

of the plant that showed a broad spectrum of pharmacological activity. From the anti-tumor experiment, all the extracts (flavonoid, 70 % ethanol, water) showed anti-agrobacterium tumefaciens. Even with the dose up to 2000 mg/kg and 5000 mg/kg body weight administration, there is no lethality at the day of fourteen.

B.variabilis flower is an important food crop and medicinal plant with immense pharmacological potential, such as antioxidant and anti-tumor activities. The result of this research revealed that this drug can be used as an anti-tumor agent and a natural source of antioxidant to prevent the progression of many diseases.

5. ACKNOWLEDGEMENTS

The authors would like to express their profound gratitude to the Department of Higher Education (Yangon Office), Ministry of Education, Yangon, Myanmar, for provision of opportunity to do this research. We also wish to express my grateful thanks to Dr Maung Maung, Principal of Myingyan Degree College.

6. REFERENCES

[1] Bhowmik, M. and Lombardi, P., 2014, Recent advances in anti-tumor berberine. *J.Cancer Sci Ther*, Vol. **7** (10), pp. 11-15.
[2] Sheikh, J.H., and Tsujuyama, M.T., 2008, A total phenolic content, antioxidative, anti-amylace, anti-clycosidase and anti-histamine release activities of Bangladesh fruits, *Food Sci. Technol. Res*, Vol. 14, pp 261 - 268.
[3] Marinova, G.L and Batchvarov, V., 2011, Evaluation the free radical scavenging activity by DPPH, *Agricultural Science*, Vol. 17, pp. 11-24.
[4] Galsky, A. G., Wilsey, J. P. and Powell, R.G., 1980, Crown – gall tumor disc bioassay a possible aid in the detection of compound with anti-tumor activity, *Plant Physiol.*, Vol. 65, pp 184 - 185.
[5] OECD (2000). "Guidance Document on Acute and Toxicity". Environmental Health and Safety Monograph Series on Testing and Assessment, No 24 (Organization for Economic Cooperation and Development).

Table 1 Total Phenolic Content of Ethanol and Watery Extracts of Flowers of *B.variabilis*

No.	Extracts	TPC (µg GAE / mg ± SD)
1.	Ethanol	19. 67 ± 1. 96
2.	Water	18.97 ± 1.25

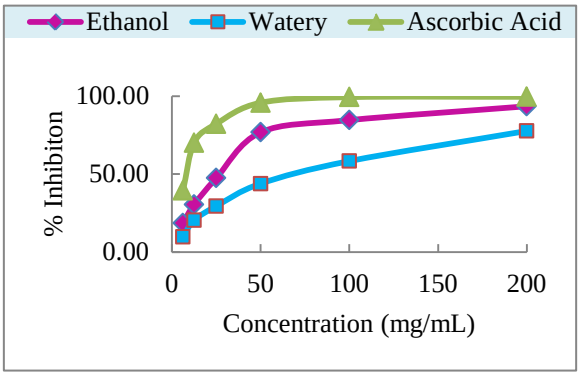

Figure 1. Average inhibition % of crude extracts from flowers of *B.variabilis*

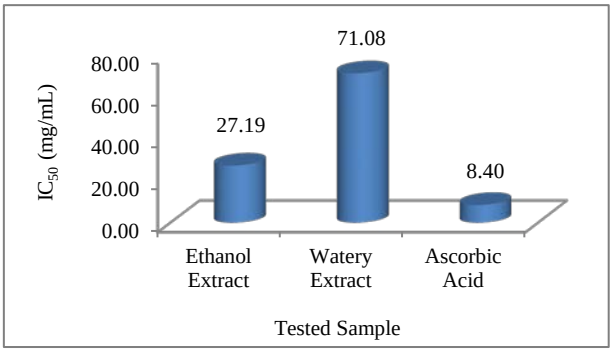

Figure 2. IC_{50} values of crude extracts from flowers of *B.variabilis*

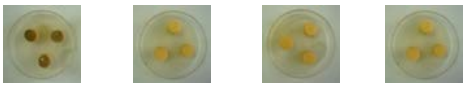

Control Flavonoid 70 % EtOH Water

Figure 3 The crown gall formation with flower extract s of *B. variabilis*

Authors Index

R

S

T

V

W

Y

Z

List of Sponsors

Sponsors:

Platinum sponsor

Gold sponsor

สมาคมผู้ปกครองและครู
มหาวิทยาลัยเทคโนโลยีราชมงคลสุวรรณภูมิ
ศูนย์นนทบุรี

สมาคมศิษย์เก่า
มหาวิทยาลัยเทคโนโลยีราชมงคลสุวรรณภูมิ
ศูนย์นนทบุรี

Organizer:

RUS - Rajamangala University of Technology Suvarnabhumi

Office of the President (Huntra Campus)

60 Moo 3 Asian Highway, Phranakhon Si Ayutthaya 13000
Tel. : +66(0) 3570 9103
Fax : +66(0) 3570 9105
https://www.rmutsb.ac.th